TECHNISCHE UNIVERSITÄT WIEN
VIENNA UNIVERSITY OF TECHNOLOGY

Dissertation

ANALYSIS OF MUSCLE COORDINATION IN CROUCH-GAIT OF CHILDREN WITH CEREBRAL PALSY

Ausgeführt zum Zwecke der Erlangung des akademischen Grades eines Doktors der technischen Wissenschaften unter der Leitung von

ao Univ. Prof. Dipl.-Ing. Dr.techn. Margit Gföhler

E307
Institut für Konstruktionswissenschaften und Technische Logistik

eingereicht an der Technischen Universität Wien
Fakultät für Fakultät für Maschinenwesen und Betriebswissenschaften
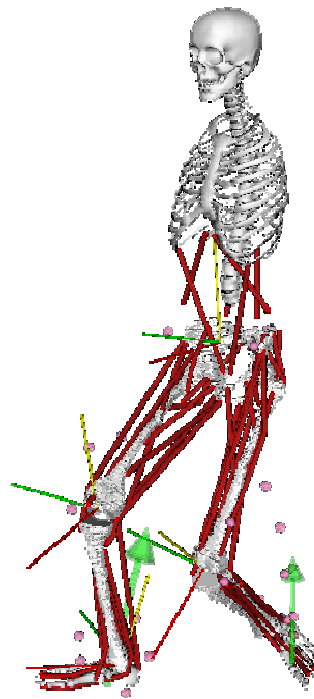
von

Dipl.-Ing. Reinhard Hainisch

Matrikelnummer: 9431312
Getreidemarkt 9, 1060 Wien, Österreich

Wien, am 05. March 2015

Diese Dissertation haben begutachtet:

………………….. ………………..

Children are one third of our population
and all of our future

Abstract

The most common cause for childhood disability in Europe is cerebral palsy (CP). Permanent disturbances of movement, gait and posture are caused by this non-progressive neurologic disorder. Surgeries that correct deformities of muscles and bones of the lower limbs are a common treatment. The mobility of patients after these interventions can improve even more, if the individual muscle functions of a patient are known in advance.

Goal of this dissertation is to investigate the crouched gait of children with CP on a level of individual muscle analyses according to biomechanical calculations using individual models based on radiology data. A secondary goal of this thesis is the development of methods that can help to pave the way for using muscle specific biomechanical analysis in clinical routine.

Musculoskeletal lower-limb models of two children with cerebral palsy were created together with five models of a control group of normally developing children. Here a newly developed method was applied that facilitates the generation of models that incorporate of individual subject's geometry with the appropriate parameterization of the modelled muscles. The method and the generated models are validated by comparing simulated maximum isometric joint moments to dynamometric measurements. Additionally a combination of the data of the control group is used to describe the first available generic biomechanical model for children.

The individual models are used to calculate the time histories of leg-muscle forces and their contribution towards joint moments as well as to joint and centre of mass accelerations. These results provide insight into muscle coordination during gait of normally developing children and of crouch gait in children with cerebral palsy. Analysis of particular muscle functions show the capability of such simulation methods to provide additional diagnostic information that can help to improve the treatment of children with cerebral palsy.

Kurzfassung

Die häufigste Ursache für Behinderungen von Kindern in Europa ist Zerebralparese. Dieser nicht progressive neurologische Defekt verursacht unter anderem Störungen im Bewegungsapparat, dem Gang und der Körperhaltung. Mittels Operationen wird nach derzeitigem Stand der Medizin versucht, die auftretenden Deformierungen von Muskeln und Knochen der unteren Extremitäten zu korrigieren. Die Mobilität der Patienten nah solchen Eingriffe ließe sich weiter verbessern, sollten die individuellen Funktionen der Muskeln in der Diagnose erfasst und zur Operationsplanung herangezogen werden können.

Ziel dieser Dissertation ist es den Scherengang von Kindern mit Zerebralparese auf muskelspezifischer Ebene anhand biomechanischer Berechnungen und mittels Modellen welche auf radiologischen Daten basieren, zu untersuchen. Ein weiteres Ziel dieser Arbeit ist die Entwicklung von Methoden welche die Einführung von muskelspezifischen Analysen in der klinischen Routine erleichtern.

Individuelle biomechanische Modelle von zwei Kindern mit Zerebralparese und einer Kontrollgruppe von fünf normal entwickelten Kindern werden erstellt. Hierfür kommt eine neu entwickelte Methode zu Einsatz, welche die Erstellung von Modellen mit individueller Geometrie und entsprechender Parametrisierung der modellierten Muskeln ermöglicht. Die Methode und die erstellten Modelle werden durch den Vergleich von simulierten maximalen Gelenksmomenten zu dynamometrischen Messdaten validiert. Eine Kombination der anatomischen Daten der Kontrollgruppe dient als Grundlage für das erste bekannte generische biomechanische Modell der unteren Extremitäten von Kindern.

Anhand von Bewegungsdaten und mittels der individuellen Modelle werden die zeitlichen Verläufe von Muskelkräften und deren Beitrag zu Gelenksmomenten sowie zu auch Beschleunigung der Gelenke und des Massenschwerpunktes berechnet. Diese Ergebnisse erlauben Einblick in die Muskelkoordination bei normalem Gangbild als auch bei Scherengang von Kindern mit Zerebralparese. Eingehende Analysen muskulärer Funktionen in Scherengang zeigen das Potential solcher Berechnungen als diagnostisches Instrument, um in Zukunft das Behandlungsergebnis von Kindern mit Zerebralparese zu verbessern.

Declaration

This is to certify that:

(i)   the thesis comprises only my original work towards the PhD except where indicated in the Preface,

(ii)   due acknowledgement has been made in the text to all other material used,

(iii)   the thesis is less than 50000 words in length, exclusive of tables, maps, bibliographies, appendices and footnotes.

_____

Reinhard Hainisch   March 5, 2015

Preface

Magit Gföhler and Marcus G. Pandy were involved in the study design and the preparation of the manuscript. R. Hainisch was responsible for the remainder of the work.

Used experimental data was based on work of Mohammad Zubayer-Ul-Karim who coordinated and documented isometric joint moment measurements and gait experiments that provided the gait data used in this study. He was also was mainly responsible for the manual segmentation of the radiology images that were recorded for this project.

Andreas Kranzl was overseeing all gait experiments in the gait lab at Orthopaedic Hospital in Speising and provided medical and technical expertise during most experimental tasks and data interpretation.

Dr. Morgan Sangeux from the Royal Children's Hospital in Melbourne) contributed the program-code needed to access and modify the XML-structure of the used biomechanical models in OpenSim via Matlab.

Acknowledgements

Contents

CONTENTS

Abbreviations

ACSA	Anatomical cross sectional area
AT	Adult template model
avCh	Average model of ND-children
BMI	Body mass index
BW	Body weight (force)
CE	Contractile element in muscle model
CoM	Centre of mass
CP	Cerebral palsy
CT	Children's template model
DoF	Degrees of freedom
EMG	Electromyogram
GRF	Ground reaction force vector (direction and location)
HAT	Model segment representing head arms and trunk
MA	Moment arm
MR	Magnetic resonance
ND	Normally developing (control group)
ND	Normally developing
PCSA	Physiological cross sectional area
PE	Passive parallel elastic element in muscle model
scAd	Child model based on average scaled adult model
SEE	Serial elastic element in muscle model

Symbols

AT	Indicating: from adult template (superscript ^{AT})
av	Indicating average of several models (superscript ^{av}).
G	Indicating: from generic model (superscript ^{G})
J	Indicating: rotational centre of a joint (superscript ^{J})
sAT	Indicating: from scaled adult template (superscript ^{sAT})
sG	Indicating: from scaled generic model (superscript ^{sG})
sM	Indicating: from mass-length scaled model (superscript ^{sM})
z	Indication: at zero degrees joint angle (subscript $_z$)
$\dot{q}$	Vector of joint velocity
$\ddot{q}$	Vector of joint acceleration
$\vec{L}$	Vector between points along a muscle path
F_{CE}	Force of contractile element
F_m	Muscle force / Matrix of muscle forces
F_{max}	Peak isometric force
F_{PE}	Force of parallel elastic element
g	Generalized force due to gravity
l_{0m}	Optimal muscle fibre length at optimal joint angle
l_m	Muscle fibre length
l_m	Muscle fibre length
$l_{m.z}$	Muscle fibre length at zero degrees joint angle
l_{mT}	Muscle-tendon length
$l_{mT.z}$	Muscle-tendon length at zero degrees joint angle
l_{sT}	Tendon slack (or rest) length, at optimal joint angle
l_T	Tendon length
$l_{T.z}$	Tendon length at zero degrees joint angle
$l_{T.z0}$	Tendon elongation: zero degrees to optimal angle
$m,\ m_m$	Mass/Mass matrix
M, M_m	Moment, Moment matrix
MA, MA_m	Moment arm of a muscle, Matrix of moment arms
m_{body}	Total body mass of a subject
$m_{body}{}^{av}$	Average body mass of normally developing children
M_m	Moment of a particular muscle
P	Generic coordinate of a point on a muscle path
P_{dis}	Point on muscle path that is distal to via-point
P_{pro}	Point on muscle path that is proximal to via-point

P^s	Subject specific point on a muscle path
P_{via}	Via-point on muscle path
q	Vector of joint displacement
v	generalized force due to centripetal and coriolis effects
V_m	Muscle Volume
V_m	Volume of muscle in individual child model
$V_m{}^{av}$	Volume of muscle in average child model
α	Pennation angle
ε_m	Elongation factor for muscle fibre
ε_T	Elongation factor for each tendon
ν_m	maximum contraction velocity of a muscle fibre
σ	Muscle stress factor
ρ	Specific weight

List of tables

LIST OF TABLES

List of figures

xxiii

1

Introduction and Background

CONTENTS

INTRODUCTION AND BACKGROUND

1.1 Introduction

Human walking is the result of a quite complex interaction of numerous skeletal muscles, sensors and neural interlinks. Injury or chronic disorders can affect this sensitive system and lead to difficulties in walking or make autonomous daily-life activities almost impossible. Cerebral palsy (CP) affects neuromuscular control and musculoskeletal structure and many children with this impairment show restrictions in the functional performance of the muscles in the lower limbs. Surgical interventions, which correct deformities of bones and modify characteristics of muscles, are a common treatment to improve the patients ability to walk. To help the patients in an optimal way, a deep understanding of the functional roles of the muscles in gait is essential.

1.1.1 Objectives

The overall goal of this thesis is to combine individual musculoskeletal modelling with optimization theory to assess lower-limb muscle function when healthy children walk at their natural speeds, and when children with cerebral palsy walk with a crouch gait. This is done to gain insight into the roles of muscles, such as contributions to forward progression and vertical acceleration to support the body against gravity as well as angular joint accelerations and influences on lateral stability.

A secondary goal of this thesis is the development of methods that can help to pave the way for using individual biomechanical analysis in clinical routine. Practicability will be given, if applied modelling techniques lead to accurate models and their analysis while keeping the manual work in a reasonable moderate time span.

1.1.2 Contribution of this Dissertation

This thesis aims to investigate the gait of children with CP on a level of individual muscle analyses. The main contributions of this work are as follows:

(i) Development of comprehensible methods for generation of musculoskeletal models based on radiology data that can incorporate individual subject's geometry and are able to accurately parameterize the muscle model.

(ii) Detailed musculoskeletal model descriptions of the lower limbs of two children with cerebral palsy together with 5 models of a control group of normally developing children from 7 to 9 years of age, that include individual bone and joint geometry as well as individual muscle model parameterization of 52 muscles.

(iii) Evaluations of models and methods by means of dynamometric measurements that confirm the approach of using radiology based individual models for muscle function assessment in CP.

(iv) A detailed description of a biomechanical child model based on averaged radiology data of five normally developing children. A majority of the biomechanical analyses of children are based on a scaled adult-model. The provided specific model for biomechanical analysis of children can reduce scaling errors, such as misplaced joint centres or divergent peak muscle forces and hence can improve the outcome of simulations and studies.

(v) Computational simulations utilizing MR-based biomechanical models provide insight into muscle coordination during gait of normally developing children and of crouch gait in children with CP in two cases. Particular muscle functions, such as contributions to joint moments or towards joint or centre of mass acceleration in severe crouched gait, are analyzed.

1.2 Cerebral palsy

CP is one of the most common disorders of the developing brain, second only to mental retardation. There are currently from 1.5 to more than 4 new cases of CP per 1000 live births in both Europe and the United States, and this rate continues to increase (CDC, 2013; Krägeloh-Mann et al., 1995; Pakula et al., 2009). CP is a condition that is caused by a prenatal (~36%), peri/neonatal (~42%), or post-neonatal brain injury (Himmelmann et al., 2010) and results in paralysis of various motor areas and sensory functions. The injury is normally a lesion occurring in the upper motor pathways, which

are responsible for controlling muscle activity and limb movement. Brain lesions can cause abnormalities of the nerve connections and of muscle tissue itself (Dietz and Berger, 1995). These abnormalities result in weakness or paresis of limbs, which prevents development of a mature gait pattern and can go along with disturbances of sensation, cognition and perception as well as behaviour and communication plus epilepsy and secondary musculoskeletal problems (Rosenbaum et al., 2007). Paresis can affect all the upper and lower limbs (quadriplegia, ~7%), just the lower limbs (diplegia, ~32%), or the limbs on only one side of the body (hemiplegia ~38%) or it can be a diskynetic CP (~17%) or ataxia (~5%)(Himmelmann et al., 2010).

The most common form of CP is spastic cerebral palsy (~85%), which primarily affects the lower limbs (McManus et al., 2006). In normal development, muscles are stimulated to grow by regular stretching as the child learns to move and walk. Spastic cerebral palsy as primary impairment hinders movement and activity of children from birth, thereby obstructing the mechanisms necessary for proper muscle growth. Muscle contracture or "short muscles" occur as secondary impairment when the muscles cannot keep pace with the growth of the bones, or if the muscles develop in a constant shortened position. Muscles shortened by contracture, particularly biarticular muscles, act to limit joint range of motion and produce skeletal deformities such as tibial torsion, femoral anteversion, or foot deformities. Skeletal deformities, in turn, can produce abnormal muscle lever arms, which alter joint moments. (Gage and Schwartz, 2002; Gage, 2004, 1990).

1.3   Crouched Gait in CP and its treatment

One of the most common movement abnormalities among children with cerebral palsy is crouch gait (Rodda et al., 2004). Crouch gait is characterized primarily by excessive flexion of the knee during stance, although exaggerated flexion, adduction, and internal rotation of the hips are also often observed (Figure 1.1). Most cases of crouch gait are attributed to spastic or contracted hamstrings muscles, but hip flexion contracture and
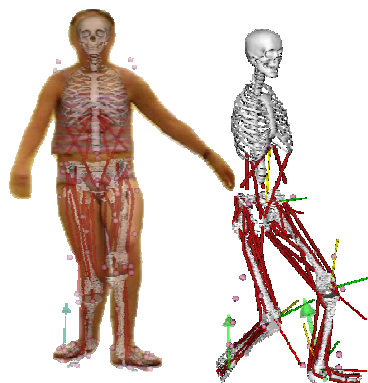
Figure 1.1 Characteristic posture in crouch gait

weakness of the ankle plantarflexors are also believed to contribute. Damiano et al. (2006) suggest that there might be some degree of causality between spasticity and movement speed.
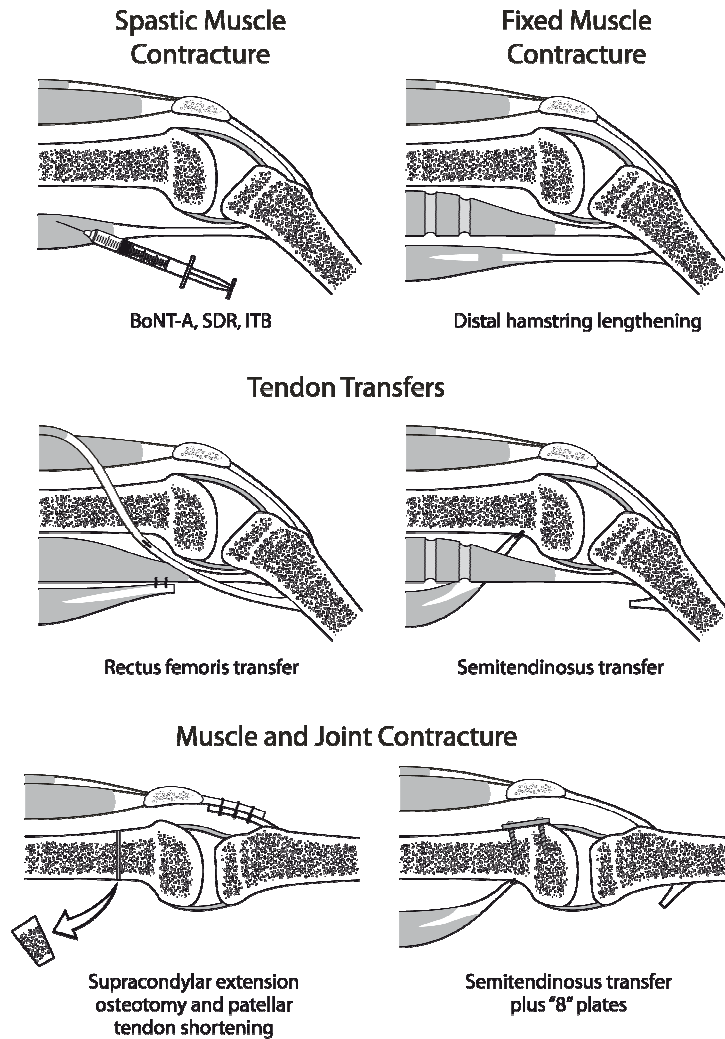
Figure 1.2 Knee interventions in spastic dilegia - For spastic muscle contracture, spasticity management may include Botulinum Toxin type A (BoNT-A), selective dorsal rhizotomy (SDR), and occasionally intrathecal baclofen therapy (ITB). Fixed muscle contractures are addressed by medial distal hamstring lengthening. Useful tendon transfers include a rectus femoris transfer or semitendinosus transfer. Fixed knee flexion contracture may be addressed by supracondylar extension osteotomy and patellar tendon shortening. When growth is remaining, guided growth can be used, applying eight-Plates across the anterior distal femoral physis. Reprinted from Orthopaedic Clinics of North America 41 (4), Young JL, Rodda J, Selber P, Rutz E, Graham HK, Management of the knee in spastic diplegia: what is the dose?, 561-577, Copyright (2010), with permission from Elsevier.

Introduction and Background

In order to adjust the characteristic ability of a muscle to generate force throughout the range of motion of the spanned joint, surgeons perform adjustments to muscle or tendon length (Figure 1.2). The standard procedures in orthopaedic surgery for the treatment of cerebral palsy can include derotation osteotomy to correct excessive torsion of the femur or tibia as well as the correction of deformities such breaching of the mid-foot. Relocation of the attachment point of a muscle is also a common procedure, which changes moment arm, force transmission or even the functional role of a muscle

Surgical lengthening of the hamstrings is typically indicated for the patient who walks with at least 20-30° of knee flexion during stance, a popliteal angle (i.e., the angle between the femur and tibia when the hip is flexed to 90°) that is greater than 45°, and evidence of prolonged hamstrings activity as determined from a dynamic electromyogram (EMG) (Rab, 1992). Lengthening the hamstrings usually decreases knee flexion in stance, but it also leads to other movement abnormalities, including decreased knee flexion in swing and increased hip flexion in stance (Arnold et al., 2005; Damiano et al., 2006; Gage, 1990; Gage et al., 1984; Granata et al., 2000)

The indication and outcome of the surgical treatment is dependent on a precise identification of the underlying causes of the specific gait deviation. Different impairments are interacting and it is often not clear to identify what is the reason and what is the effect of muscle degeneration or bone deformities. The observed impaired movement can be affected by motions that are made to cope with some other problems (Gage, 2004). Gait abnormalities on one end of the kinematic chain can affect movements of other joints instantly or for future actions (Brunner et al., 2008; Kerrigan et al., 2001).

1.4 State of clinical gait biomechanics

1.4.1 Gait analysis by direct measurements
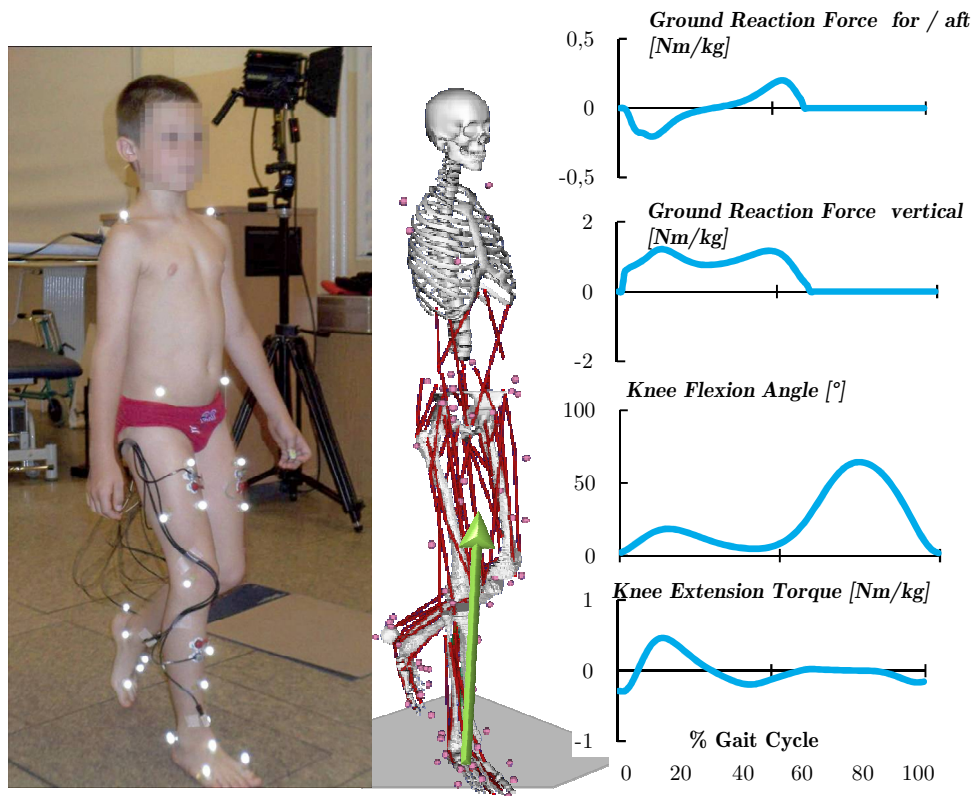
Figure 1.3 Gait analysis in laboratory - Child with skin mounted motion tracking markers and EMG-electrodes is stepping on a force plate. The recorded marker tracks and kinematic data are processed by means of models matching the subjects scale. The displayed graphs show vertical and horizontal ground reaction forces (GRF) as well as exemplary data of knee joint angles and knee joint moments in a full gait cycle.

Gait analysis techniques have led to a more objective assessment of movement abnormalities in children with cerebral palsy. Joint kinematic, force plate, and dynamic EMG continue to be widely used in planning orthopaedic surgeries and in evaluating their outcomes (Bleck, 1990; DeLuca et al., 1997; Dhawlikar et al., 1992; Gage, 1991; Gage et al., 1984; Park et al., 2009; Thometz et al., 1989; Westwell et al., 2009). In particular, joint kinematic and force plate data have been combined with the inverse

dynamics method in mechanics to estimate and compare the net moments exerted about the lower-limb joints pre- and postoperatively (Gage, 1991; Zwick et al., 2002).

The limb motion can be measured in a motion capture setup that is typical for gait laboratories: reflective markers are fixed on the skin and reflect the light of infrared illumination (Figure 1.3). The marker positions during motion are tracked by combining the images of several infrared cameras via triangulation algorithms. A matching virtual marker set can be added to the model and serves as guide for the positions of the model-limbs and joint angles according to the skin-mounted marker traces. The ground-reaction forces (GRF) can be measured via force plates. A combination of the GRF with appropriate joint angles allows a bottom-up calculation of the joint moments by applying the Second Law of Newton to the model.

Gait analysis has been helpful in assessing net muscular moments exerted about hip, knee, and ankle in normal and pathologic gait. While these data provide quantitative descriptions of kinematics and kinetics of joint movement, this approach cannot provide necessary information about actions of particular muscles during walking, that my help to identify the cause of a walking disorder such as CP-related crouch gait. There are several reasons for this:

(i)   Muscular moments derived from inverse dynamics analysis describe the net action of all the muscles crossing a joint. However, because there are mostly more muscles that span each joint, than there are degrees of freedom prescribing joint movement, an infinite number of muscle force combinations can produce the net joint moment.

(ii) Optional muscle EMG recordings determine only whether a muscle is active or not. There is no known correlation between the level of a measured EMG signal and the amount of force, which the muscle might be producing during dynamic activity.

Insights into particular muscle function in gait cannot be obtained by analyzing joint moment and muscle EMG data alone. Alternatively, detailed models of the musculoskeletal system can be combined with limb motion, ground reaction forces, and muscle EMG data to determine muscle action during movement.

1.4.2 Musculoskeletal models for biomechanical calculations

Mathematical models of the musculoskeletal system are commonly used to estimate muscle forces non-invasively, as a direct measurement of muscle force in vivo is currently not practical. Simulations utilizing such computational models allow a characterization of muscle function during movement and can give insight into muscle contributions to acceleration of joints and the mass centre. These methods can help to develop new methods for treating patients with movement disorders (Pandy and Andriacchi, 2010).

Detailed computer models of the human body have been used to study the biomechanics of standing (Kuo and Zajac, 1993), rising from a seated position (Pandy et al., 1995), vertical jumping (Anderson and Pandy, 1999; Pandy et al., 1990; van Soest et al., 1993) and cycling (Gföhler and Lugner, 2000; Gföhler, 2004; Neptune and Hull, 1998). The actions of individual leg muscles have been analyzed for a number of activities such as normal walking (Anderson and Pandy, 2003, 2001a; Anderson et al., 1999; Neptune et al., 2001) and running (Dorn and Tjio, 2006; Dorn et al., 2012b) using a variety of computational algorithms (Erdemir et al., 2007). Recent studies aim to investigate the muscle function in impaired movement (Correa et al., 2012; Krogt et al., 2009; van der Krogt et al., 2012, 2008).

1.4.2.1 The muscle model
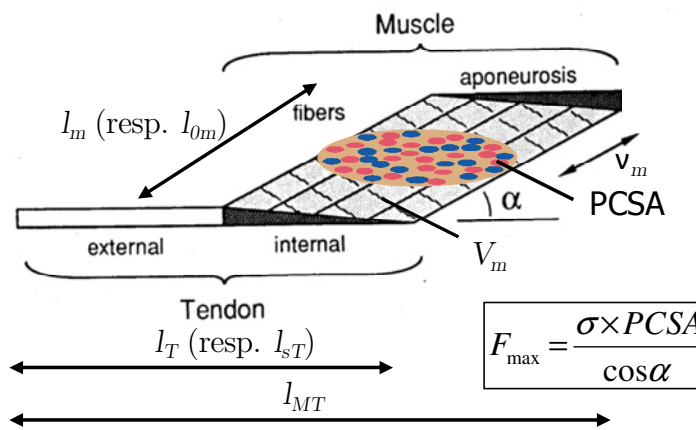
Figure 1.4 Model for muscle fibres and tendons with model parameters - (modified picture of orignial by Zajac, 1989).

INTRODUCTION AND BACKGROUND

Figure 1.4 shows a representation of macroscopic muscle architecture according to Zajac (1989). Muscle fibres lie in parallel at muscle-specific pennation angle α. As the total muscle volume V_M is constant α changes when the total muscle-tendon length l_{MT} is changed during motion. Physiological cross sectional area (PCSA) is used together with the muscle stress factor σ to calculate the Peak isometric muscle force F_{max}. Maximum shortening velocity of the muscle fibres is denoted by ν_m. Tendon slack length l_{sT} defines the tendon length l_T when the muscle fibre length l_m equals optimal muscle fibre length l_{0m}.
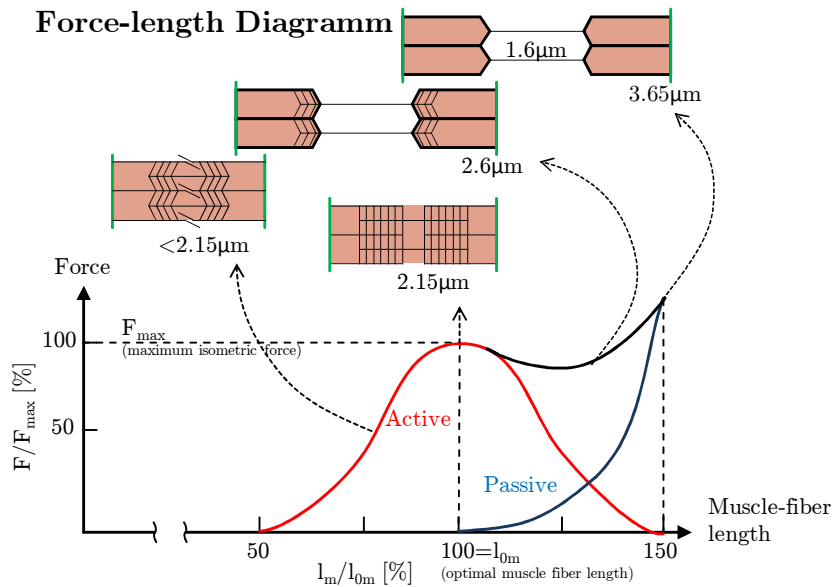
Figure 1.5 Force-length-diagramm Red line: Maximum active contractile force of a muscle, Blue line: passice elastic force when lenghening a muscle (modified image, original by Paulev and Zubieta-Calleja, 2004)

The physiological characteristic of a muscle to actively generate force is defined by the microanatomy of a muscle fibre and is shown in a force-length-diagram in Figure 1.5. Length of a muscle fibre in the body when at rest is called optimal fibre length l_{0m}, corresponding to a sarcomere length of 2,15 μm. At this length there are a maximum number of active cross-bridges and the muscle can generate its maximum active contractile force, which is shown in the red curve. Active force declines at muscle fibre lengths less than l_{0m} due to collision of the filaments with the Z-discs and when muscle fibres length increases above l_{0m} due to decreased overlap between thin and thick

filaments. The blue curve reflects the properties of the elastic, connective tissue, which becomes less compliant or stiffer with lengthening.

Musculotendon actuators are typically modelled as a Hill-type muscle model as illustrated in Figure 1.6. This model includes five parameters according to Zajac (1989), which are needed to describe force-generating properties of each musculotendon actuator: F_{max}, l_{0m}, α, v_m, and l_{sT},

The mechanical behaviour of the muscle fibres is represented by a Hill-type contractile element (CE) which models the muscle's active force-length-velocity characteristic. This model incorporates the dependency of the force-length relationship on variations of the shortening velocity v_m, where the active force of the contractile element, F_{CE}, is dependent on l_m, v_m and the state of muscle activation $a_{(t)}$. Some models include an optional series-elastic element (SEE).
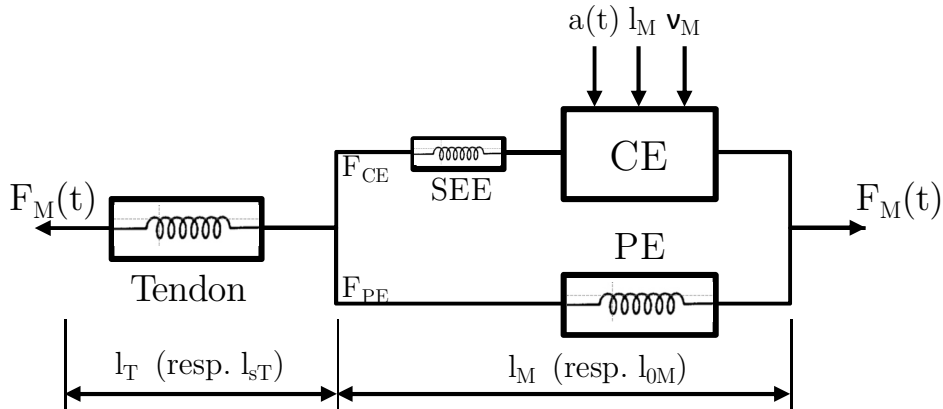
Figure 1.6 Commonly used Hill-type model -

The muscles passive force F_{PE} is caused by the muscles stiffness, which is modelled by the passive parallel-elastic (PE) element, and acts in parallel to F_{CE} (Pandy, 2001; Pandy et al., 1990; Zajac, 1989). F_{PE} and F_{CE} sum up to the total muscle force F_M that is transferred via the elastic tendon with length l_T.

Tendon is assumed to be elastic and is modelled with an elastic element in series to the muscle. Its mechanical behaviour is represented by a nonlinear force-length curve (Butler et al., 1978).

1.4.2.2 Available methods for biomechanical simulations

Generic models of the musculoskeletal system have been developed from anatomical and biomechanical studies of cadaveric specimens (Arnold et al., 2010; Blemker et al., 2007; Klein Horsman et al., 2007; Pandy, 2001; Ward et al., 2009). Several of these models have been published along with commercial packages such as AnyBody (www.AnyBodyTech.com), SIMM (Delp et al., 1990) or the open source biomechanics platform OpenSim (www.simtk.org) (Delp et al., 2007; Seth et al., 2011) for a broad range of applications and analyses of 3D movement. The most detailed full body models available contain up to 86 degrees of freedom, 117 joints and 344 muscle-tendon actuators (Delp and Loan, 1995).

These generic models have been applied in many previous studies, but skeletal and musculotendon parameters are different for each individual, resulting in the unique capability of each muscle to generate joint moment profiles. A widespread method for individual customisation of a generic model is to scale a template according to individual anthropometry and with that are muscle model parameters scaled in relation to limb segment dimensions.

The scaling of such template models, which are mainly based on data obtained from a normal healthy adult male (Delp, 1990), to the size of children might lead to biased shapes of the pelvis, the long bones and the paths of the muscles (Scheys et al., 2008). However, accurate biomechanical calculations require exact modelling of individual moment arms, maximum isometric muscle forces and muscle physiology.

Model customisation can be enhanced if individual musculoskeletal computer models embody more details of a subject's anatomy: the body dimensions and weight, the lengths and masses of the limb segments, exact locations of the joints and even muscle volumes, attachments and muscle paths. Scheys et al. (2009) published a deformable model whose geometry can be adapted according to individual anatomy based on radiology data.

1.4.3 Muscle function assessment in normal gait

Estimates of muscle force are needed to understand how a muscle contributes to the accelerations of the body joints and the acceleration of the mass centre during gait. However, muscles can accelerate body segments that they do not actually touch, because the segments are dynamically coupled. Thus, muscles can accelerate joints they do not span. This follows from the fact that the equations of motion are coupled (Pandy and Zajac, 1991; Pandy, 2001; Zajac and Gordon, 1989; Zajac, 1993).

For example, the soleus muscle exerts only an extensor moment at the ankle, yet it can accelerate the knee into extension with more vigor than it accelerates the ankle into plantarflexion (Raasch et al., 1997; Zajac and Gordon, 1989). Another example is the gluteus maximus, a uniarticular muscle spanning the hip, whose potential to accelerate the knee toward extension is similar to that of as vastus, which directly spans the knee (Arnold et al., 2005a). Furthermore, biarticular muscles can produce accelerations of the joints that oppose their applied moments. For example, hamstrings can accelerate the knee toward extension, even though it applies a flexion moment at this joint (Piazza and Delp, 1996; Anderson et al., 2004). Thus, conclusions regarding muscle function derived solely based on anatomy and muscle EMG data may well be erroneous.

Muscle potentials of individual mass-length scaled models of healthy children to accelerate the body was evaluated by Correa and Pandy (2012). Here only relative capacities of muscles to generate whole-body motion were described rather than the manner in which these muscles are actually used.

Static and dynamic optimization theory provide means to calculate the pattern of muscle activations and muscle forces during movement using musculoskeletal models combined with kinematic, kinetic, and muscle EMG data. Several optimization criteria can be used to solve the optimization problem over one complete cycle of gait such as minimizing force, stress, activation or metabolic energy (Y.-C. Lin et al., 2011). Computed muscle control, a muscle actuated simulation algorithm by (Thelen et al., 2003), is another known method to compute muscle activations according to recorded motion patterns, but less robust than static optimization (Mokhtarzadeh et al., 2014).

A concept called induced accelerations has been formulated to quantify how each muscle contributes to the accelerations of all the joints at each instant during a task (Zajac and Gordon, 1989). This concept allows to investigate the muscle coordination of a variety of movements, including walking (Anderson and Pandy, 2003; Liu et al., 2008, 2006; Neptune et al., 2004; Pandy, 2001; Zajac et al., 2003)

1.4.4 Analysis of muscle function in crouch gait

With an increase in the degree of impairment and the associated deviations in muscle and bone anatomy, it is of crucial importance to use models that simulate the subjects as accurately as possible. While calculations of muscle-tendon length may indicate, which muscles may be too short during walking (e.g., tight hamstrings in crouch gait), they do neither provide information about muscle force nor specify where on its force-length curve (Figure 1.5 at page 10) a muscle may be actively operating during the gait cycle.

A number of studies (Arnold et al., 2005; Delp and Arnold, 1996; Krogt et al., 2009; Schutte et al., 1997) have calculated the lengths of the hamstrings muscles during crouch gait. Delp and Arnold (1996) also calculated the lengths of the psoas and found that these muscles were shorter than normal in all patients, suggesting that the psoas rather than the hamstrings was the cause of the crouch gait. Whilst these studies have provided much insight into how the hamstrings and/or the psoas muscles can limit knee extension during stance, additional information is needed to understand more fully the role of each muscle in abnormal gait. Accurate knowledge of muscle forces enables more quantitative analyses to be undertaken to assess muscle function during walking.

Analyzes of muscle potentials of models of children with cerebral palsy (Correa et al., 2012) and the effects of spasticity in conjunction to muscle lengthening velocity in crouch gait (Krogt et al., 2009; van der Krogt et al., 2010) have been reported in literature. Correa et al. (2012, 2011) investigated the accuracy of scaled generic models in comparison to MR-based models of children with mild CP by predicting the functional roles of individual muscles in gait. Substantial differences in moment arms were found, but the potentials of the muscles to accelerate a joint or the centre of mass were

consistent in both scaled generic models and MR-based models of the CP-children. Studies, which investigated muscle contributions to support and progression during crouch, applied scaled versions of a generic adults model, without taking into account the disability related alterations in musculature (Steele et al., 2013, 2012, 2010).

Gait-based biomechanical simulations provide information on movement kinematics and can give insight into muscle coordination patterns. Especially when investigating gait abnormalities, results get more precise when used models incorporate individual force generating properties such as force-length relationship or peak isometric force. Computational outcome can be even more accurate when measured neural activation patterns from EMG are included in calculations or abnormal muscle activations are simulated (Krogt, 2009).

However, all results of computational biomechanical simulations depend highly on the accuracy of the used models. Therefore plays the method how such models are generated an important role when medical decisions are based on mathematical calculations.

1.5 Biomechanical modelling

Individual musculoskeletal models are used for the assessment of muscle properties and analysis of muscle function during motion. The generation of such models based on radiology data is very time consuming.

As a trade-off between modelling effort and accuracy of calculation results, researchers use generic template models that are adapted to subject specific properties. To obtain such patient specific configurations, the generic models are typically customized by scaling with respect to body dimensions. The application of gait-marker-scaled generic musculoskeletal models provides a quick method to estimate a subject's musculoskeletal geometry, but this approach does not account for individual geometry (Hainisch et al., 2010; Scheys et al., 2008).

A large number of generic models used for biomechanical calculations are based on a single anatomical cadaver study by Wickiewicz et al., (1983), where no details on the subject's age, weight or size were denoted. Arnold et al. (2010) developed a lower limb model that aggregates experimentally measured architectures of 21 adult cadaver subjects. As this model of the

lower limb was based on MR image data of subjects aged 82.5 ± 9.42 years acquired by Ward et al., (2009), the age related decrease in muscle mass was compensated by muscle specific exaltation of the muscle stress factor. Virtually no data is available up to now to describe the geometric and architectural properties of leg muscles either in healthy children or in children with CP.

Computer-generated 3D reconstructions from computed tomography or magnetic resonance images provide a more accurate, non-invasive method to quantify musculoskeletal anatomy in living subjects. If high accuracy in modelling is required radiology data can be used to generate individual biomechanical models although this process is very time consuming.

1.5.1 Modelling based on radiology data

Magnetic resonance imaging has been applied to the development of individual biomechanical models of normal and CP subjects, that integrate individual details (Blemker et al., 2007; Correa, 2011; Murray et al., 1998; Scheys et al., 2006). Bone structures can be identified from MR images for more accurate modelling of body segments, their connecting joints and wrapping surfaces that define the path of a muscle spanning a joint. Muscle and tendon structures as well as their attachment sites can be identified and muscle moment arms derived.

Several groups have investigated the accuracy of muscle moment arms, muscle-tendon lengths and muscle volumes determined from MR images. For example, Murray et al., (1998) developed a 3D reconstruction of an upper extremity from MR images in one position. Estimated moment arms from the model were compared to moment arms measured from the same specimen. In five of the six muscles studied, the model predicted 84-94% of the variation in the experimental data. Spoor and van Leeuwen (1992) compared knee muscle moment arms of 9 muscles from MR images and from tendon travel, and found good agreement with a few exceptions over small ranges of joint angulations. Arnold et al. (2000) investigated the accuracy of muscle moment arms estimated from MR-based musculoskeletal models of the lower extremity. The moment arms were compared with experimentally determined moment arms from the same specimens, and results showed that errors in the moment arms calculated with the models were less than 10% of the

experimental values. In contrast, several approaches for rescaling generic models fail to accurately estimate absolute values for muscle–tendon lengths and moment arms in comparison to MR-based models (Scheys et al., 2008). However, Correa and Pandy (2011) found that scaled models of adults, whose muscle parameters are estimated through mass–length scaling of a generic model, generate similar predictions of lower-limb muscle function as individual MR-based models in normal gait.

Results of such studies suggest that MR-based modelling provides a more accurate representation of individual specimen compared to the generally accepted literature standard of scaling template models. Hence, combining MR imaging and musculoskeletal modelling can provide accurate and efficient means to estimate muscle-tendon lengths and moment arms in vivo (Arnold et al., 2000).

The outcome of the time consuming generation of MR-based models highly relies on the diligence during a mainly manual segmentation process. A model's ability to reproduce real kinematic and kinetic functionality is largely determined by the accuracy of geometric relations and muscle-model parameters. In the commonly used Hill-type muscle model (Hill, 1938), these parameters are tendon rest length, optimal muscle-fibre length, physiological cross section area (PCSA) and pennation angle (Weijs and Hillen, 1985; Zajac, 1989).

A number of studies have examined the sensitivity of model calculations to variations in body anthropometry (Lenzi et al., 2003; Pataky et al., 2003), and muscle-tendon properties (Ackland et al., 2012; R. Brand et al., 1986; Herzog, 1992; Raikova and Prilutsky, 2001; Redl et al., 2007; Scovil and Ronsky, 2006). Variations in PCSA, tendon rest length, and muscle moment arms have been found to show the highest influence on model estimates of muscle force. Hence, it is important to derive these parameters carefully.

However, the determination of tendon rest length and optimal muscle-fibre length from MR-images is challenging due to the difficulty of distinguishing the aponeurotic part of tendon from the muscle belly, and because the muscle is usually not at its optimal length during imaging. Arbitrary human decisions during modelling can lead to high variations in models and simulation results.

1.5.2 Biomechanical Models of children

Models with musculoskeletal geometry (i.e. bone geometry, joint locations and muscle paths) for healthy children as well as for children with movement disorders have been reported in the literature. These models were used to estimate the lengths of a few leg muscles during gait (Delp et al., 1996; Eames et al., 1997; Schutte et al., 1997), but no information is given where on its force-length curve a muscle may be operating during the gait cycle. Also, the shapes of the long bones and the paths of the muscles were based on data obtained from a normal healthy adult male (Delp et al., 1990) and do not reflect differences in body-segment anthropometry and muscle paths.

Very few data is available to describe skeletal geometry in combination with muscle architecture of the lower-limb muscles of children (Arnold et al., 2001; Correa and Pandy, 2012). O'Brien et al. (2010) found that the fascicle, muscle and tendon lengthen proportionally during maturation, and that differences in maximum joint moment are mainly due to changes in PCSA.

The practicability of adult models is limited when they are used as template for generating individual models of children via a scaling. One reason for this is, that body-segment anthropometry and muscle paths are likely to be different in children and adults (Lebiedowska and Polisiakiewicz, 1997), and both groups have a different body composition. Further, according to anthropometrical data of Eek et al. (2006) children have a mean body mass index (BMI) of 15-20, which is much lower than the value commonly used in generic template models based on adult subjects. For example, the model developed by Arnold et al. (2010) is based on subjects with an average BMI of 29. If a children's model were built by means of mass length scaling of a generic adult's template model, large scaling factors might be problematic. Such differences can lead to errors in mass-length scaled models and to errors when performing computational simulations to investigate muscle function.

1.6 Scientific approach

1.6.1 Primary objective

Primary objective of this study is the assessment of muscle function in crouched gait caused by CP. Musculoskeletal models based on radiology data currently provide the best reproduction of individual musculoskeletal geometry and are therefore the first choice for analysis of muscle function during motion. To the best of my knowledge no study has attempted to calculate leg-muscle forces during walking in children with cerebral palsy, using individual models based on MR-data. Further, no study has quantified individual muscle contributions to joint motion or to movement of the mass centre during CP affected crouch-gait using MR-based models.

The lower the degree of human decisions in modelling the better comparable models and their simulation outcome will be. Especially radiology-based modelling of subjects with biased musculoskeletal structure requires as starting point a reliable and repeatable workflow for the basic model generation.

Therefore primarily, a comprehensible way of modelling needs to be developed that considers subject specific geometry. Further should the method provide reproducible means of setting the muscle model parameters, so that individually modelled particular muscles can approximately operate in the similar region of their force-length curve.

This modelling technique will be tested on a normally developing control group of children with similar age as the investigated CP-subjects and will be evaluated by comparing simulation results to experimentally measured maximum isometric joint moments. If the modelling method delivers reliable results, it will be applied to model the subjects with cerebral palsy.

These models will then be used to assess lower-limb muscle function to gain insight into the roles of particular muscles during gait, as contributions of muscle forces to joint moments or to accelerations of centre of mass and joint angles.

INTRODUCTION AND BACKGROUND

Simulation results will be used to specifically investigate the functional role of the hamstrings in hip extension and knee flexion as well as the effect of iliopsoas, soleus, gastrocnemius, rectus femoris and vastus throughout the stance as well as the swing phase of crouch gait. These specific questions for identifying abnormal muscle functions in CP were addressed in this thesis:

(i) Which muscles contribute most significantly to the net moments exerted about the hip, knee, and ankle in normal and crouch gait?

(ii) Which muscles contribute most significantly to the angular accelerations of hip, knee, and ankle in normal and crouched gait?

(iii) Which muscles contribute most significantly to the vertical, lateral and fore-aft accelerations of the centre of mass of the body in normal and crouched gait?

(iv) Are lengths of identified main contributors different during normal and crouch gait?

(v) Where on their force-length curves do the main contributing muscles operate during normal and crouch gait?

Information obtained from static optimization solutions and induced acceleration analysis for the two CP-patients will lead to a better understanding of muscle function in crouch gait. Several factors typically contribute to crouched gait, and determining whether an individual's gait abnormality is due to hamstrings contracture, spastic hip flexors, weak ankle plantarflexors, or some other source is not straightforward. Whilst modelling results alone may not be sufficient to identify the cause of crouch gait in a specific patient, quantification of contributions of individual muscles to joint and mass centre accelerations can be a necessary first step toward this goal.

Based upon the results obtained from normal gait in adults (Anderson and Pandy, 2003; Liu et al., 2006) and CP-gait analysis (Gage, 1991; Lin et al., 2000; Sutherland and Cooper, 1978), it was hypothesized for CP-gait that:

(i) Excessive passive forces are generated in tight hamstrings, which cause lower-than-normal forces to be generated in gluteus maximus.

This hypothesis is based on results of gait analysis studies, which have shown that there is a marked increase in the net extensor

moment exerted about the hip during early stance in crouch gait (Gage, 1991; Lin et al., 2000). This may be caused by increased passive forces in hamstrings.

(ii)   Hamstrings act to accelerate the knee toward flexion with more vigor during the stance phase of crouch gait than during the stance phase of normal gait.

It is assumed that the excessive passive forces in hamstrings strongly accelerate the knee toward flexion during stance. The hypothesis will test positively if the activation level predicted for hamstrings is low, yet the force developed by this muscle is high. Large forces in hamstrings can only be due to excessive passive stretch of the muscle.

(iii)   Vastus is the major contributor to accelerating the knee toward extension throughout stance, and therefore, this muscle dominates vertical support and forward progression in crouch gait.

Gait studies have shown that an increase in knee flexion during stance is accompanied by an increase in the net extensor moment exerted about the knee. Specifically, knee extension moment is normal in early stance but progresses to pathologically high levels in late stance. These studies have also shown that an increase in ankle dorsiflexion is accompanied by a significant decrease in the net plantarflexion moment exerted about the ankle (Gage, 1991; Lin et al., 2000; Sutherland and Cooper, 1978). These results suggest that, unlike normal gait, soleus and gastrocnemius do not contribute significantly to vertical support and forward progression during the second half of stance (Anderson and Pandy, 2003; Liu et al., 2006). Instead, by virtue of an increasing extensor moment at the knee during stance, it would appear that vasti contributes most significantly to accelerating the knee toward extension. It is proposed, therefore, that vasti generates the majority of vertical support and forward progression throughout the stance phase of crouch gait.

1.6.2 Secondary objective

So far, no averaged children's model is available that can be quickly customized to establish individual models of children. An assumption was that by generating individual models of children based on scaling of adult's models, the mismatch between model and real anatomy is high due to different body structure of adults and children. This may lead to misinterpretation of muscular function in further calculations that can be lowered if the template model is more similar to the desired subject's model. For example, if musculoskeletal models to study crouch gait of children with mild forms of cerebral palsy were based on an average children' model, these errors might be reduced while still having the benefit of quick modelling.

Therefore, the second aim of this study was twofold:

(i) To generate an average musculoskeletal model of children based on musculoskeletal parameters of a group of normally developing children that where obtained from *in vivo* MR images.

(ii) To investigate the functional behaviour of CP-models based on a mass-length scaling of either a generic adult's template model or the average child model in comparison to results from CP-models based on MR-data. This analysis can also provide information about the gain that the extra effort of using MR-based models may provide.

The average children's model shall be available as template for scaling towards individual models of healthy children as well as in cases of children with mild cerebral palsy, if MR-based modelling would be too time consuming.

1.6.3 Non goals

Methods that are more efficacious may be needed to reliably identify which factors contribute an individual's abnormal gait. This would include both pre-operative and post-operative analysis of muscle-tendon lengths, velocities, and forces in the same patient. Analyses of post-operative gait patterns are beyond the scope of this initial investigation.

2

Methodology

CONTENTS

2.1   Methodical Outline

Major tasks in this study to provide functional muscular analysis of individual musculoskeletal models included medical image data processing, biomechanical modelling, gait-data processing as well as application of tools and data analysis techniques for multi-body-system dynamic studies.

Two groups of subjects were studied: a control group of 5 healthy subjects with no previous history of musculoskeletal injury or disease, and case studies on two CP patients with a clinical diagnosis of crouch gait. Bone and joint structure, muscle paths, and the architectural properties of 52 leg muscles were individualized on a prior defined generic model on basis of MR-data, which was measured and pre-processed for each child. A universal method for defining individual muscle-model parameters was developed, tested and applied for all MR-based models, such that the average static response of all models could be validated against average maximum isometric, joint moment-angle data recorded from hips, knees, and ankles of all subjects.

Several models of CP-children and normally developing (ND) controls were generated, using much quicker scaling techniques for model generation, to highlight the potential modelling errors of such quick procedures.

Gait analyses were performed on each CP patient and each subject of the control group to obtain joint kinematics and ground force. Time histories of forces of all modelled actuators during a gait cycle could be calculated with these data using a static optimization approach. Further particular muscular contributions to joint moments and, by applying a concept known as induced acceleration analysis, their effects towards CoM and joint accelerations were calculated.

2.2 Experimental Methods and Records

Selected subjects underwent a series of examinations that provided data for individual model generation and muscle function assessment in gait. Maximum isometric joint moments at hip, knee and ankle were measured using a dynamometer, motion and GRF were recorded in a gait laboratory and several series of MR-images of their lower limbs were recorded.

2.2.1 Human subjects and selection criteria

The study was designed to assess muscle function in children with CP in comparison to a control group of normally developing children. Inclusion criterion for the CP-children, was a clinical diagnosis of crouch gait resulting from diplegic spastic cerebral palsy, that is corresponding to Level II according to the "Gross Motor Function Classification System" (Palisano et al., 1997). In order to recruit patients who best fulfil requested criteria, subjects underwent a complete, multidisciplinary (i.e., physician and physical therapist) clinical exam at the Orthopaedic Hospital in Speising.

Subject	Height [cm]	Weight [kg]	Age	BMI
ND1	133,0	31,4	9,0	17,8
ND2	124,0	24,0	9,0	15,6
ND3	140,0	33,0	11,0	16,8
ND4	129,2	27,8	7,9	16,7
ND5	126,5	28,5	7,0	17,8
ND Average	130,5 ± 6,3	28,9 ± 3,5	8,8 ± 1,5	16,9 ± 0,9
CP1	140,0	30,7	12,0	15,7
CP2	146,0	37,0	11,0	17,4

Table 2.1 Body properties of subjects - Height, weight, age and body mass index (BMI) of the investigated normally developing subjects (ND1-ND5), are compared to averaged data (ND Average) and to parameters of the two children with cerebral palsy.

The selected two CP-patients, denoted CP1 and CP2, were 11 years, 140 cm, 28.9 kg and 12 years, 146 cm, 37 kg respectively. Results from clinical gait analyses showed, that each of the CP patients walked with a minimum of 20° of knee flexion in both limbs throughout the stance phase, had a popliteal angle greater than 40-45°, and showed prolonged or premature hamstrings EMG activity (Gage, 1991; Sutherland and Davids, 1993).

CP-Diagnosis	CP1				CP2			
	R		L		R		L	
Hip joint								
Extension/Flexion		120°		110°	10°	110°	10°	110°
Abduction/Adduction	25°	30°	20°	30°	30°	30°	30°	30°
External-Internal rotation	45°	80°	40°	75°	50°	30°	40°	30°
Popliteal angle at hip 90°	40°		45°		80°		85°	
Popliteal angle at hip 0°	40°		50°		70°		75°	
Hip abductor power	5		5		5		5	
Hip adductor power	5		5		5		5	
Hip flexor power	4		4		5		5	
Ankle joint								
Dorsal/Plantar Knee at 90°	0	50°	10°	50°	20°	30°	20°	30°
Dorsal/Plantar Knee at 0°	0	50°	15°	50°	10°	30°	10°	30°
Dorsiflexion power	4		3		4		4	
Planterflexion power	-4		-4		3		3	
Rectus spasm	present		higher		higher		higher	
Hamstring spasm	present		higher		none		none	
Triceps surae klonus	present		present		higher		higher	
Knee joint								
Extension-flexion		160°	0	160°	20°	130°	15°	130°
Femur rotation	50		40		40		40	
Tibia rotation	15		50		20		20	
knee extensor power	-5		-5		5		5	
knee flexor power	4		4		5		5	
Standing posture								
Trendelen burg sign	no		no		no		no	

Table 2.2 Medical report of children with cerebral palsy - Data provided bythe Orthopaedic Hospital in Speising, Vienna.

Other inclusion criteria for the patients were:

(i)   first, they must be able to walk without orthotic equipment or other assistance;

(ii)   second, not any fixed contractures in lower extremities;

(iii)   third, no history of orthopaedic surgery or rhizotomy;

(iv)   forth, no previous local treatments for spasticity (e.g., Botulinum toxin injection, phenol injection, etc.)

(v)   and fifth, they do not show compensatory toe-walk.

The five normally developing subjects of the control group, denoted ND1 to ND5, had no previous history of musculoskeletal injury or disease. Their mean age was 8,8±1,5 years, they had a mean height of 130,5±6,3 cm and a mean weight 28,9±3,5 kg. Subject's details are shown in Table 2.1 for the body parameters and Table 2.2 for the detailed CP diagnosis.
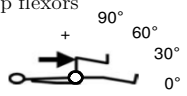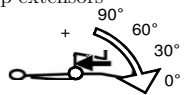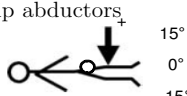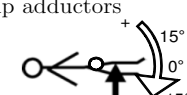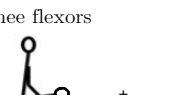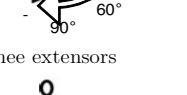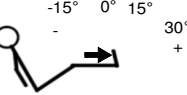
The study was approved by the Local Human Ethics Board of Vienna and the parents of the children gave informed consent prior to participation.

2.2.2 Measurement of maximum isometric joint moments

Maximum joint moments were measured at the ankle, knee, and hip during maximum voluntary isometric contractions for each healthy subject and each CP patient. These experiments were conducted in the Neurological Hospital Rosenhügel in Vienna using a Biodex dynamometer. Two isometric contractions were measured at the selected joint angle, and the average was taken to represent the maximum joint moment. To minimize the effects of fatigue, subjects were encouraged to rest between the contractions.

Hip flexor and extensor moments were measured in increments of 30° from 90° of flexion to full extension. These data were recorded with the knee flexed to 90° and the hip in neutral abduction and rotation. Hip abductor and adductor moments were measured in increments of 15°, from 15° abduction to 15° adduction. For the knee, maximum isometric flexor-extensor moments were recorded from 90° of flexion to 30° of flexion in 30° increments with the ankle in neutral position and the patient sitting such that the hip had approximately 60° flexion. Maximum isometric ankle plantar- and dorsiflexion moments were recorded in increments of 15° from 30° of plantarflexion to 15° of dorsiflexion, while the patient was sitting with knee flexed 60°. Table 2.3 displays the measurement setup and body positions.

Muscle Group	Position	Stabilisation	Resistance
Hip flexors	Supine, knee flexed 90°, hip joint flexion angle 0°, 30°, 60°, 90°	Belt around hip, hold on bench	Femur distally
Hip extensors	Supine, knee flexed 90°, hip joint flexion angle 0°, 30°, 60°, 90°	Belt around hip, hold on bench	Femur distally
Hip abductors	Lying on either side, streched legs, lower leg is stabilized, upper leg is measured, hip joint adduction angle -15°,0°,15°	Hold on bench, stabilization of the other leg	Femur distally
Hip adductors	Lying on either side, streched legs, lower leg is stabilized, upper leg is measured, hip joint adduction angle -15°,0°,15°	Hold on bench, stabilization of the other leg	Femur distally
Knee flexors	Sitting, hip position approximately 80°	Belt around hip, hold on bench	Shank distally
Knee extensors	Sitting, hip position approximately 80°	Belt around hip, hold on bench	Shank distally
Ankle dorsiflexors	Sitting, shank at measured leg set to horizontal position which results in a hip angle of aproximately 60° and a knee angle of 30°	Belt around hip, hold on bench, thigh fixed with belt	foot fixed on plate
Ankle plantarflexors	Sitting, shank at measured leg set to horizontal position which results in a hip angle of aproximately 60° and a knee angle of 30°	Belt around hip, hold on bench, thigh fixed with belt	foot fixed on plate

Table 2.3 Positions when measuring maximum isometric joint moments Description of position and stabilization of subject, joint angle definitions on the dynamometer and arrows to show the position of the dynamometer's resistance to the body movement

Maximum hip flexion moment

Maximum hip extension moment
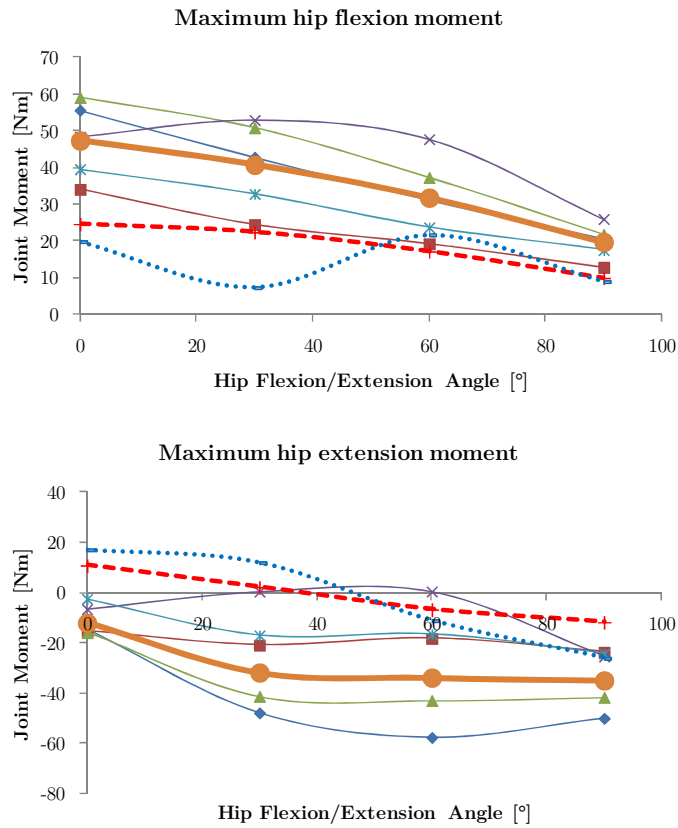
Figure 2.1 Measured maximum isometric hip flexion/extension moment - Position: Supine, knee flexed 90°, isometric moment measured at hip joint angle of 0°, 30°, 60°, 90°; body fixation with belt around hip and subject holding on bench; resistance force applied at femur distally.

Maximum hip abduction moment

Maximum hip adduction moment
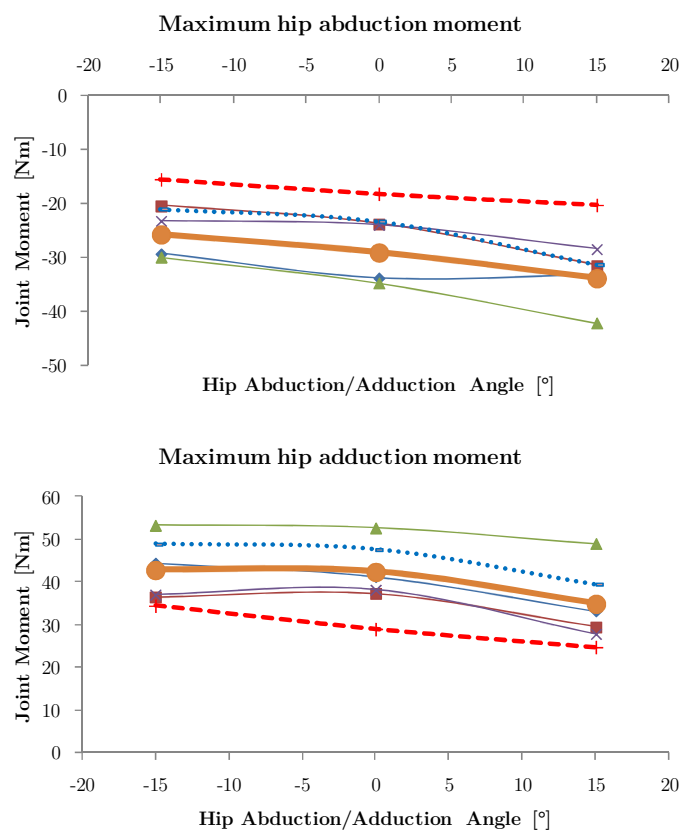
Figure 2.2 Measured maximum isometric hip ab-/adduction moment - Position: Supine, knee flexed 90°, isometric moment measured at measured at hip joint flexion angle of 0°, 30°, 60°, 90°; body fixation with belt around hip and subject holding on bench; resistance force applied at femur distally.
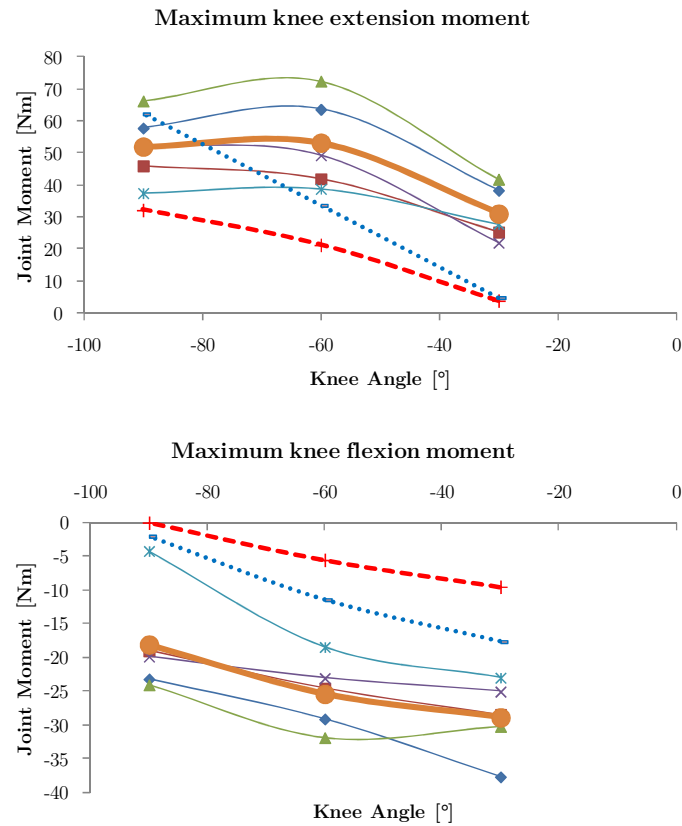
Figure 2.3 Measured maximum moment at knee extension and flexion - Position: Sitting, with hip position approximately 80°;°; body fixation with belt around hip and subject holding on bench; resistance force applied at shank distally

Segment	Definition	% of body weight	Segment-CoM in % of body height
Foot	Lateral malleolus to head matatarsal II	1,5%	2,0%
Leg	Femoral condyles to medial malleolus	4,7%	10,7%
Thigh	Greater trochanter to femoral condyles	10,0%	10,6%
Foot and Leg	Femoral condyles to medial malleolus	6,1%	17,3%
Total Leg	Greater trochanter to medial malleolus	16,1%	23,7%
Foot	From ankle (vertical)	1,5%	5,1%

Table 2.4 Anthropometric relations of limb segments Limb segments and estimated weight and position of the centre of mass (CoM) from the proximal joint centre in relation to the total body weight and total body height based on data by Winter (2009)

31
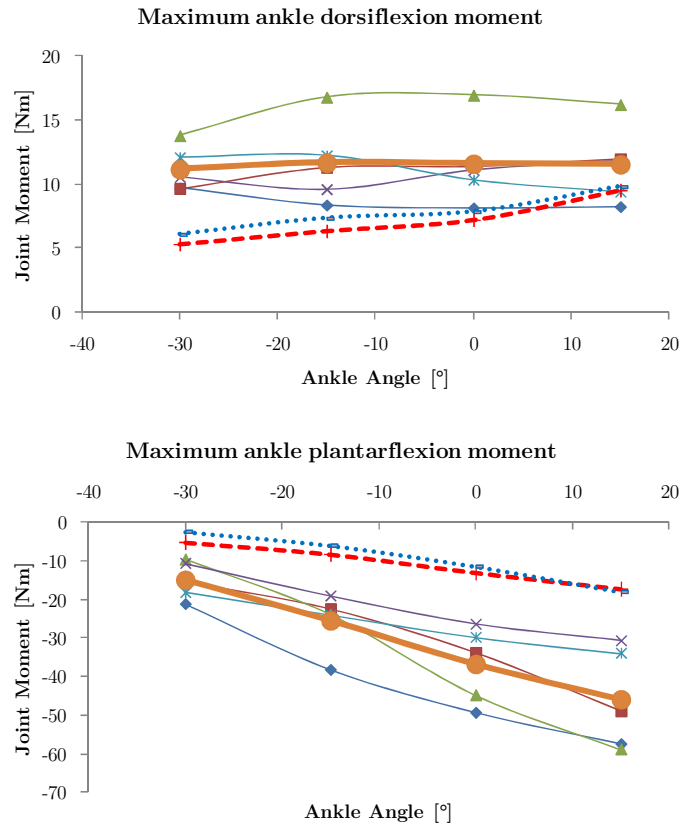
Figure 2.4 Measured maximum dorsiflexion and plantarflexion moment - Position: Sitting, shank at measured leg set to horizontal position which resulted in a hip angle of approximately 60° and a knee angle of 30°; body fixation with belt around hip and thigh fixed with belt; resistance force on foot that was fixed on a plate.

The passive moment due to gravity effects on the measured limb was estimated from the subject's anthropometric data and the limb posture at each measurement position (Table 2.3). To obtain the maximum active joint moment generated by muscles this passive gravity-based joint moment was depending on the measured direction either added or subtracted from the measured moment. Mean recordings of both legs of each subject were included in displayed data of Figure 2.1 to Figure 2.4.

2.2.3 Gait recordings

All subjects underwent a clinical gait analysis at the Gait and Movement Analysis Laboratory at the Orthopaedic Hospital in Speising. Kinematics, and ground reaction force (GRF) were recorded simultaneously for each subject. As a warm-up, each normal subject walked 10 times and each CP patient 3 times up and down a 10 m level walkway in the lab. All subjects were instructed to march in place at the beginning of the walkway and then begin forward progress at a time of his or her own choosing and in at his or her self-selected speed and cadence.
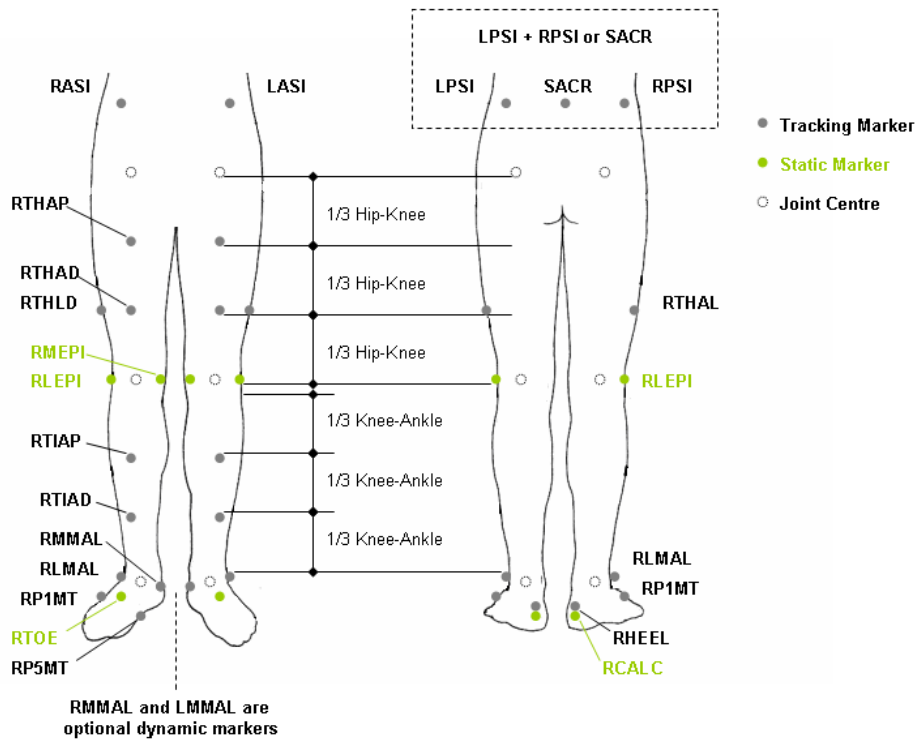
Figure 2.5 Applied Marker set - Two not displayed markers (RSHO and LSHO) were placed on the shoulders to record the motion of the upper body segment including head arms and torso (HAT)

Movement data was recorded by capturing marker positions with 60Hz using a 6-camera, opto-electronic, motion measurement system (Motion Analysis Corporation, CA). A set of twenty-nine passive retro-reflective markers, were placed on both the left and right sides of the body. Details of the applied marker set, which was based on the Cleveland Clinical marker

set, are shown in at shown in Figure 2.5, Table 2.5 and Dorn et al. (2012b). Hence, the three-dimensional positions of 10 body segments: forefoot, hindfoot, shank, and thigh of each leg, plus pelvis and one segment including head, arms and torso could be measured. Ground-reaction forces and moments were measured using two six-component, strain-gauge force plates (AMTI Advanced Mechanical Technology, Inc., MA) with 500Hz.

marker name	description	attached body segment
RSHO	Right shoulder marker (placed on the Acromio-clavicular joint)	HAT
LSHO	Left shoulder marker (placed on the Acromio-clavicular joint)	HAT
RASI	Right ASIS (directly over the right anterior superior iliac spine)	Pelvis
LASI	Left ASIS (directly over the left anterior superior iliac spine)	Pelvis
SACR	Sacral wand marker (skin mid-way of post. and sup. iliac spines)	Pelvis
RTHAP	Right proximal anterior thigh marker	Right Thigh
RTHAD	Right distal anterior thigh marker	Right Thigh
RTHLD	Right distal lateral thigh marker	Right Thigh
RLEPI	Right lateral epicondyle knee marker	Right Thigh
RTIAP	Right proximal anterior tibial marker	Right Shank
RTIAD	Right distal anterior tibial marker	Right Shank
RMMAL	Right medial malleolus ankle marker	Right Shank
RLMAL	Right lateral malleolus ankle marker	Right Shank
RHEEL	Right proximal calcaneus	Right hind foot
RP1MT	Right proximal 1st metatarsal head	Right hind foot
RP5MT	Right proximal 5th metatarsal head	Right hind foot
RTOE	Right toe (junction of 2nd and 3rd proximal metatarsals)	Right toes
LTHAP	Left proximal anterior thigh marker	Left Thigh
LTHAD	Left distal anterior thigh marker	Left Thigh
LTHLD	Left distal lateral thigh marker	Left Thigh
LLEPI	Left lateral epicondyle knee marker	Left Thigh
LTIAP	Left proximal anterior tibial marker	Left Shank
LTIAD	Left distal anterior tibial marker	Left Shank
LMMAL	Left medial malleolus ankle marker	Left Shank
LLMAL	Left lateral malleolus ankle marker	Left Shank
LHEEL	Left proximal calcaneus	Left hind foot
LP1MT	Left proximal 1st metatarsal head	Left hind foot
LP5MT	Left proximal 5th metatarsal head	Left hind foot
LTOE	Left toe (junction of 2nd and 3rd proximal metatarsals)	Left toes

Table 2.5 Positions of gait markers on the lower limbs - List of reflective gait markers which were attached to the subjects pelvis and legs during the gait recordings

A minimum of five gait trials was collected from each control subject and from each CP patient, with video and force-plate data recorded simultaneously during each trial. One representative trial that was closest to

the mean of all trials was selected, to be used in all subsequent analyses. Marker traces and force plate data, together with manually identified gait phase events of the selected gait were processed to a .c3d-file, as this is a standard format for representation of 3D biomechanical motion lab data. By using the Gait Extraction Toolbox by Dorn (2008) for MatLab (Mathworks) the gait data was further prepared for use in the biomechanical simulation platform OpenSim (Delp and Loan, 2000; Reinbolt et al., 2011; Seth et al., 2011).

2.2.4 Magnetic resonance imaging

To determine bone and muscle geometry, MR images were collected from the five normal subjects (controls) and the two CP patients at the MR/CT Institut Schmidt GmbH&Co KEG, using a Siemens Symphony Maestro Class 1.5 Tesla scanner. Scanning parameters were selected to enhance the brightness of fatty tissue in order to make the boundaries of the muscles more visible.

Voxel size was set to 0.9x0.9x3.0mm for axial images and 1.8x1.8x8.0mm for sagittal images. The axial layer thickness of 3mm was comparable to what Spoor and van Leeuwen (1992) and Arnold et al. (2000b) used for investigations on the lower limb as well as to what Murray et al. (1998) applied for modelling of the upper limb.

Each subject was placed in the prone position in the MR scanner with hips and knees extended as far as possible and ankles in neutral position. Four series of transverse images were recorded using a body coil. The first series was obtained from the lower lumbar vertebrae down to the lesser trochanter of the femur to define the muscle and bone surfaces of the pelvis. Two series of were then obtained along the shaft of the femur and tibia from the lesser trochanter down to the calcaneus. Two series of sagittal images with slice thicknesses of 8 mm were obtained for additional information when combining the image sets.

As the four series of data overlapped, the positions of nitro capsules mounted on the skin during imaging were used as markers to identify the corresponding images for subsequent alignment of the image sets. These combined image sets were used to manually segment the musculoskeletal geometry of the thigh and both legs as described in Chapter 2.4.1.

2.3   Basic generic biomechanical model

A generic model based on data of adult subjects, denoted in this study 'adult template' or short 'AT', was used as starting point for detailed individual musculoskeletal computer models for each of the five healthy subjects and two children with cerebral palsy. Model structure was formulated in extended mark-up language (XML) for use in OpenSim, a biomechanical simulation platform (Delp and Loan, 2000; Reinbolt et al., 2011; Seth et al., 2011).
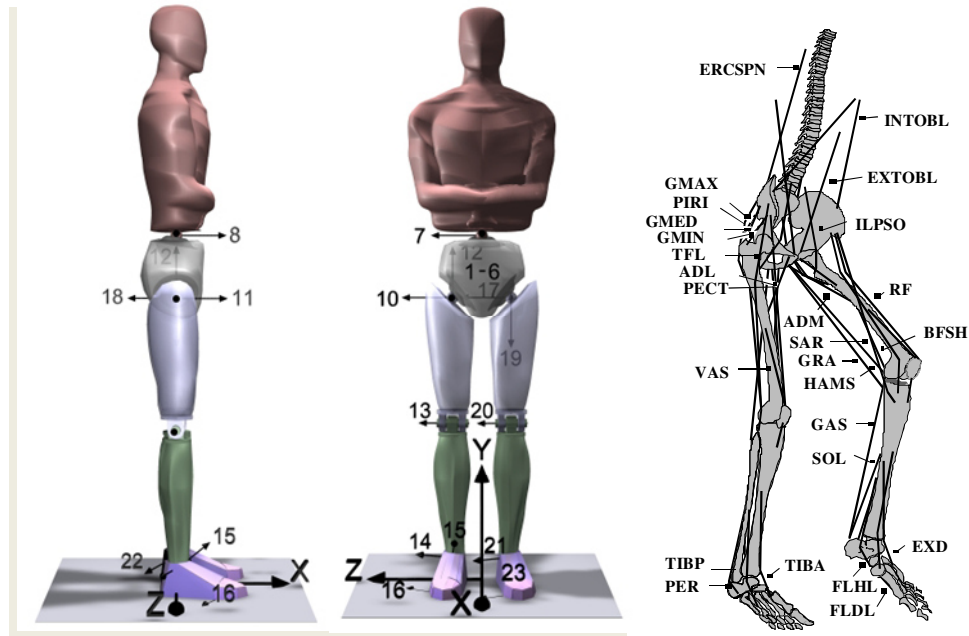
Figure 2.6 Model structure - Structure of a biomechanical model with joint coordinate systems and modelled muscles (modified image, original by Pandy, 2001).

The applied model had the same kinematic structure (Figure 2.6) as one previously used to simulate normal walking in healthy adults (Anderson and Pandy, 2001a; Arnold et al., 2010; Delp et al., 1990). The skeleton was represented as a 10-segment, 23 degree-of-freedom (DoF) articulated chain. Head, arms, and trunk were lumped together and represented as a single rigid body in the model (HAT segment). The pelvis had six DoF and was linked with the upper body by means of a three DoF back joint placed at the

3rd lumbar vertebra. Each hip was modelled as a three DoF ball-and-socket joint. Each knees was modelled as a three DoF hinge joint with its centre of rotation moving on trajectory in the sagittal plane, according to data by Beynnon et al. (2003). Each ankle was modelled as a two DoF universal joint. Each foot was represented as two separate bodies: a hind foot fibula and a toes segment connected by a one DoF metatarsal hinge joint.

All geometric model parameters defining the structure of the model skeleton were denoted in the local coordinate system of the realted body segment. The origin of each body segment was defined as the proximal joint centre where the segment is connected to the next proximal segment. For example, all coordinates of the thigh (reference body femur) are given in a coordinate system placed and pivoted in the hip joint centre. Further details of the template model skeleton are given by Anderson and Pandy (1999), Delp and Loan (2000) and Arnold et al. (2010).

The skeleton-model was actuated by 52 muscles, of which 23 actuated each leg and 6 abdominal and back muscles controlled the relative movements of the pelvis and upper body. Hill-type muscle model parameters were set according to a model published by Arnold et al. (2010), which was developed based on data obtained from 21 cadaver specimens and included 88 muscle–tendon compartments.

The number of model actuators was reduced from 88 in the underlying model of Arnold et al. (2010), which was developed on basis of data obtained from 21 cadaver specimens, to a set of 52 muscles by lumping some muscles into single actuators. This was done because individual compartments of some muscles were difficult to identify separately in the MR-image datasets when generating individual models as described in the following sections. For example, the three compartments of gluteus maximus were combined into a single muscle-actuator, having the sum of all three maximum isometric forces. Muscle attachment sites of new combined muscle as well as optimal muscle-fibre length and tendon slack length were manually adjusted to obtain similar joint moment-angle behaviour as the muscle group in Arnold's model.

Values of pennation angle, α, for all major muscles in the lower limb were based on data reported in the literature (e.g., (Friederich and Brand, 1990). Assuming that all lower-limb muscles have mixed fibre type, intrinsic maximum contraction velocity, v_m, was set to 10 muscle-fibre lengths/sec (Zajac, 1989).

2.3.1 Adjustments of the generic model based on measurements

Exceptions in reproducing the maximum isometric joint-moment angle characteristics of Arnold's model were made for hamstrings and gastrocnemius. Comparisons of the simulated maximal in knee extension made it necessary to adapt l_{0m} and l_{sT} of hamstrings to reproduce the decline in knee extension the more the hip is flexed. This was done in combination with a slight change of the via point path of rectus femoris and vastus at the knee, in order to reproduce the measured knee extension capability of the model while preserving the hamstrings effect on hip extension. Further, l_{sT} of gastrocnemius was changed so that its optimal joint angle was shifted from 10° dorsiflexion to 0°. Additionally, l_{sT} of tensor fasciae latae was shortened by 5cm to avoid errors in CP-gait calculations due to short muscle fibres caused by the gait posture.

2.4 MR-based biomechanical models

The semi-automatic method described in the following chapters was developed in order to provide a reproducible workflow when generating individual models based on MR-data that helps to reduce human error in this process. The method was implemented in Matlab (1994 Mathworks, Inc., Natick, MA, USA) and utilized the XML-based model definition of the biomechanical simulation software platform OpenSim (Delp et al., 2007).

Individual models of typically-developing children as well as children with cerebral palsy were generated by this workflow based on a generic model of an adult. The generic model was first scaled with subject-specific geometric parameters derived from a manually segmented set of MR-images. Subsequently muscle paths were extracted from the MR-data set of each subject by using a computational algorithm and values of all required Hill-type muscle-tendon parameters were set appropriately.

2.4.1 Image data processing and segmentation

Recorded MR-image series were processed using the commercial software package AMIRA (Visualization Sciences Group). MR-data were imported in DICOM-format (standard for Digital Imaging and Communications in Medicine) into the application. In a first step, image series where aligned according to anatomical landmarks as well as to position of nitro capsules, which were placed on the skin during imaging. Secondly, the aligned image sets were merged using a build-in function of AMIRA to obtain a single full dataset, which included all muscle and bone structures of the pelvis and legs.

Within each slice of the combined MR-data set, cross sections of pelvis, femur, tibia and 46 major muscle groups with corresponding tendons in the lower limb were then manually identified and segmented. Three-dimensional representations of bones, muscles, and tendons were subsequently created from identified 2D areas by adding voxels within each particular cross section to a specific muscle's volume point cloud. Details for segmentation of the main anatomical structures are given by Stingeder (2009)

Virtual marker location	Definition an application
Anterior superior iliac spine (ASIS)	Midpoint of left and right gives pelvis-centre
Posterior superior iliac spine (PSIS)	Midpoint for calculation of pelvis orientation
Hip Joint Centre (HIP)	Centre of femur head
Greater trochanter (TROC)	Used for calculation of femoral anteversion
Medial epicondyle of femur (EPIM)	Midpoint is identified as knee joint centre at 0°
Lateral epicondyle of femur (EPIL)	
Medial malleolus of the tibia (MALM)	Midpoint is identified as ankle joint centre
Lateral malleolus of fibula (MALL)	

Table 2.6: Virtual markers on anatomical landmarks - Location of virtual markers at anatomical landmarks in MR-images and intended application

Single voxels representing anatomical landmarks as indicated in Table 2.6 were labelled as virtual markers to prepare for subsequent semi-automatic processing of the segmented data. Those landmarks were also used to define the joint axis for the knee in neutral position (stretched leg) on the trans-epicondylar line that connects the medial and lateral femoral epicondyles.

2.4.2 Correction of biased limb orientations in MR

Subjects, and especially CP-patients lying in an MR machine do not always have their joints exactly in a neutral position, with 0° for all joint angles (Figure 2.7). To extract desired features like locations of the joints, muscle attachment points and muscle paths from the segmented MR-dataset, the limb positions must be taken into account. Scheys et al. (2009) published an atlas-based method for defining muscle paths from MR images, which also considers biased limb positions.
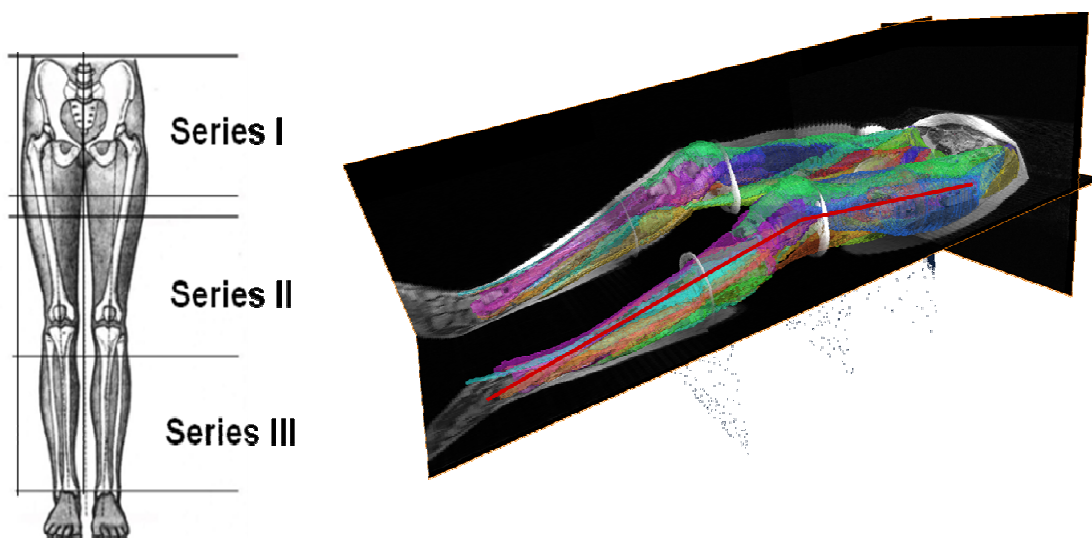
Figure 2.7 Reconstructed structure of the lower limbs - Reconstructed three-dimensional structure of bones, muscles, and tendons of an 11 year old child with cerebral palsy based on three sereies of MR images. The red line indicates the biased limb position

To obtain the limb positions during MR-recordings, first the virtual markers (Table 2.6) placed at a number of anatomical landmarks were used to derive the joint centres of the hip, knee, and ankle joints as well as the centre of the pelvis in global (MRI-series) coordinates. The origin of the global coordinate system in the MR-image data was defined at centre of the pelvis. The medial/lateral axis was oriented to the right virtual ASIS marker and the anterior/posterior axis to the midpoint of the two virtual PSIS markers.

Based on the global coordinates of the joint centres the orientation of each segment was calculated in relation to the adjacent proximal segment. For this, transformation matrices were defined that described orientations and positions of the limb segments with respect to the coordinate system of the proximal located body. These transformation matrices were combined to a kinematic chain, and so it was possible to virtually retransform all joint angles to a neutral position. In this way, all locations of desired model features from the MR images were obtained in both a global reference coordinate system and the local coordinate system of the segment in question.

2.4.3 Extraction of muscle geometry from MRI-data

To obtain a muscle's path, the centroid throughout the segmented volume of each muscle was calculated by connecting the geometric centres of the slices and smoothing the resulting line with a running average filter using a window size of three slices.

Joint centre locations and muscle centrelines were determined for the neutral standing position. Muscle paths were reproduced by defining all points proximal to a joint in the coordinate system of the proximal body. All points distal to a joint were primarily expressed in the original slightly rotated coordinate system of the distal body segment and were then transformed (rotated) to neutral standing position.

Muscle volume, V_m, was determined by adding up the volumes of the transverse muscle slices defined by the MR-images. The volume of a slice was computed as the product of the distance between images and the anatomical cross-sectional area (ACSA) of the muscle within the image.

2.4.4 Models with individual anthropometry and bone shapes

Detailed individual musculoskeletal computer models of five normally developing children were generated based on the adult's template model, which was customized by using information from MR-imaging as described in 2.4.1 to 2.4.3. First the models where scaled to subject specific dimensions. Further, real bone geometry of the subjects was integrated into the model to

improve graphical representation of the model and to inspect and correct muscle paths and attachment sites.

In a previous study (Hainisch et al., 2010) it was shown that a scaled model based on scaling according to joint centre locations better reproduces a subjects anthropometry than a model that was customized by scaling via skin mounted gait markers. Hence, joint centres defined by the virtual MR marker set described in Table 2.6 served as mask for the body-segment anthropometry of each subject's lower limbs. These virtual markers were likewise placed on the defined locations of the generic model. The ratio of the virtual MR-marker distances to the corresponding virtual marker distances defined in the generic model was used to scale the generic adult template model to the individual size and proportions of each child.

Voxels of the marked volumes for pelvis, left and right femur, tibia and fibula were converted into polygon surface volumes (VTP file format) by using the open-source data analysis and visualization application ParaView (Kitware Inc., New York). Hence they could be integrated into the scaled models and the real bone geometry could be displayed in the OpenSim graphics user interface. The location of the hip-joint rotation centre was identified in the femur geometry as centre of the spherically shaped voxel point cloud that represented the femoral head.

Values for mass and mass moments of inertia of each body segment were approximated by using scaled values from the generic model, with body mass as scaling factor.

These scaled models included a simply scaled version of the template model's muscle path as well as original maximum isometric forces from the adult template. Further had these models altered optimal joint angles due to direct proportional scaled values for tendon slack length and optimum muscle fibre length. Therefore, the model's muscle parameters needed to be customized according to data derived from MRI as described in the following sections.

2.4.5 Muscle path modelling

The origin and insertion sites of each muscle were defined in the model by using the centroid line of the muscle derived from the MR images. For each muscle the most proximal marked point of the centroid was defined as the origin and the most distal point as the insertion.
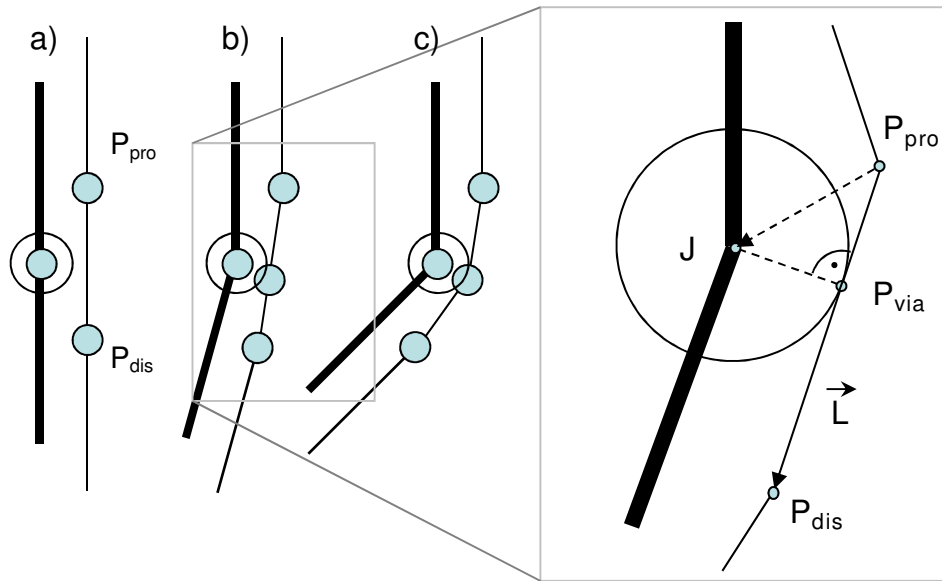
Figure 2.8 Determination of via point locations Schematic drawing of a muscle that illustrates, how a via-point is used to wrap the muscle path around the joint. Beginning at a defined joint angle: a) joint position where no via point is necessary because the muscle does not touch the wrapping surface, b) muscle path comes in contact with wrapping surface, c) path of the muscle with a via point wrapping around the joint. Right panel: Detailed diagram showing how the location of a via-point is obtained.

Via-points (Pandy and Andriacchi, 2010; Pandy, 2001) are commonly used in biomechanical simulations to model the manner in which a muscle wraps around other muscles and/or bones within a defined range of motion of the joint. If a joint angle was still outside a specified joint range of motion as shown in Figure 2.8a, a straight line connected a proximal point (P_{pro}) and a distal point (P_{dis}) of the modelled muscle's path. If the joint angle increases above a specified position (Figure 2.8b+c), the muscle's path was defined by an additional via-point (P_{via}). Because the coordinates of the proximal point, distal point and via-point are mainly related to reference frames of different limb segments, the via-point coordinates were found as follows:

First, the locations of the proximal and distal points of the muscle's path were transformed into a local coordinate system with its origin in the processed pivot joint centre (J) and with one axis matching the rotation axis of the joint, thus:

$$P_{pro} \Rightarrow P^J_{pro}, P_{dis} \Rightarrow P^J_{dis}$$

The distal point (P^J_{dis}) was then rotated about the pivot joint centre (J). The joint angle range specified in the generic model was applied. Let $\vec{L}$ be the connection vector between the proximal point (P^J_{pro}) and rotated distal point ($P^J_{dis.rot}$) as follows:

$$\vec{L} = \overrightarrow{P^J_{pro} P^J_{dis.rot}} \tag{2.1}$$

The via-point was placed on $\vec{L}$ at the shortest distance to the joint centre, J. To compute the shortest distance, let P_{via} be the base of the perpendicular extending from J to $\vec{L}$ as shown in Figure 2.8. Here the vector P_{pro} to P_{via} is the projection of the vector from P_{pro} to J onto $\vec{L}$. The global coordinate of the via-point is then given by:

$$P_{via} = \frac{\overrightarrow{P^J_{pro} J} \circ \vec{L}}{\vec{L} \circ \vec{L}} * \vec{L} \tag{2.2}$$

Alternatively, computational algorithms used in other simulation platforms can be applied to calculate the necessary muscle wrapping paths (Garner and Pandy, 2000).

2.4.6 Setting of muscle model parameters

The maximum isometric joint moment over the joint range of motion depends on the maximum isometric force of the muscle, which is related to the muscle volume (determined from MR data), the moment arm, which can be determined from the muscle path and joint centres as well as the muscle model parameters.

When a model is scaled in OpenSim, muscle-fibre lengths and tendon slack lengths are scaled uniformly, such they remain the same percentage length of the total actuator length. However, it has been shown that tendon rest length

and optimal muscle-fibre length do not scale linearly with bone length (Ward et al., 2005).

If a muscle's attachment sites and path are changed e.g. according to MRI-data, the length of the muscle-tendon unit is altered. Changing the muscle's attachment sites will change the muscle's joint moment-angle behaviour because 1) the muscle's moment arms are altered, and 2) if optimal muscle-fibre length and tendon slack length are not changed, the muscle no longer operates on the same portion of its force-length curve. This results in an unwanted shift of the optimum joint angle for the muscle, i.e., the joint angle at which the muscle fibre has its optimum length. Studies by Redl et al., (2007) on the sensitivity of muscle force estimates to changes in musculotendon properties emphasize the importance of obtaining accurate estimates of tendon slack length and muscle-fibre length.

2.4.6.1 Individual setting of optimal muscle fibre length

Due to the fact, that the joint angle trajectories during gait are similar for adults and children who are nine years and older (Sutherland et al., 1980), it could be assumed, that muscles in normally developing children generally operate on flat portions of their force-length curves during waking (Figure 1.5), similar to adults as reported by Anderson and Pandy (2001a). Winby et al. (2008) evaluated different approaches for individual scaling of musculotendon parameters and suggested proportional scaling of the muscle's normalized fibre length (fibre length divided by optimal fibre length). Hence, in the approach described below, the optimal muscle-fibre lengths and tendon slack lengths were derived so that the optimal joint angle remains identical with that given by the generic model.

As the shape of the muscle force-joint angle curve is assumed to be the same in a healthy child as in an average adult, also the relation of muscle-fibre length to the optimal fibre-length is assumed to be the same at any joint angle. Consequently, optimal muscle fibre lengths, l_{0m}, were set to the values, the result from the scaling process.

2.4.6.2 Individual calculation of tendon slack length

Individual muscle attachment sites in MR-based models usually result in changes of the total muscle length compared to that of a scaled generic model. Proportional scaling of muscle related limb segments can be used to derive the optimal muscle fibre length, l_{0m}, but this method is not suitable to estimate tendon slack length, l_{sT}. Therefore, a method for derivation of l_{sT} was suggested that is based on the assumption that relative length change of muscle fibre and tendon is similar for the same motions in adults and children. This method takes individual muscle attachment sites, muscle paths and moment arms into account.

Winby et al. (2008) showed that the geometric parameters generated via scaling of a model differed only slightly when two different postures were selected for evaluation. Consequently the absolute length changes in different joint positions could be used as operands that are independent of the total length of the muscle-tendon compartment, but dependent on the muscle path. The geometric muscle parameters l_{0m} and l_{sT} for the MR-based model were therefore evaluated on basis of muscle-fibre and tendon lengths with the template model and the MR-based model in different positions. One position was a reference position with all joints at zero degrees and the second position was the particular position that defined the optimal joint angle for each muscle. By assuming similar proportions of geometric muscle parameters in adults and children the resulting elongation ratios were then used to estimate l_{sT}, of each individual musculotendon actuator.

First, relative elongation of muscle fibre and tendons was derived from the generic model by calculating the length ratio of muscle fibres and tendons respectively in neutral limb position and at the muscle specific optimal joint angles. Relative elongation of the muscle fibre in the generic model was then used to calculate muscle fibre length in the MR-based model at neutral position. This allowed, based on measured total muscle-tendon length of the MR-based model, to calculate tendon lengths in neutral position.

2.4.6.3 Workflow for setting individual muscle model parameters

According to the described approach, the following steps were used to generate a MR-based musculoskeletal model of each subject, based on a template model, by using results from MR-data processing and to determine appropriate muscle parameters for the 46 muscles of the lower limb:

(i) From the generic model (superscript ^{G}), muscle-fibre length , $l^G_{m.z}$, and tendon slack length, $l^G_{t.z}$, need to be extracted for each muscle, with the model positioned in an erect reference standing position, i.e., with the hip, knee and ankle joints positioned at 0 degrees, which is in denoted by subscript $_{.z}$ (for zero degrees). For subsequent calculations, also the model's parameters for optimal muscle fibre length, l^G_{0m}, tendon slack length, l^G_{sT}, are required for all muscles.

(ii) For the generic model, calculate the elongation factor, ε_T, for each tendon, which is defined as the ratio between tendon slack length and the tendon length calculated with the model placed in the reference position, thus:

$$\varepsilon_T = l^G_{sT} / l^G_{T.z} \tag{2.3}$$

(iii) For the generic model, calculate the elongation factor for each muscle-fibre length (ε_m), defined as the ratio between the optimal muscle-fibre length and the muscle-fibre length calculated with the odel placed in the reference position, thus:

$$\varepsilon_m = l^G_{0m} / l^G_{m.z} \tag{2.4}$$

(iv) Scale the generic template model to individual anthropometry. When using the scaling function of OpenSim, all geometric muscle parameters are usually scaled uniform in proportion to the scaled size of the related limb segments. Obtain optimal muscle-fibre lengths for MR-based model, l_{0m}, model directly from this scaled model.

(v) Set all muscle-path coordinates in the model according to the acquired centreline of a muscle based on MRI-data. These coordinates are mainly muscle's proximal and distal attachment points and optional path defining points and via points.

(vi) Set optional via points according to the method described in section 2.4.5 to the optimal position along the derived muscle path.

(vii) Determine muscle-tendon length of the individual model, $l_{mT.z}$ in reference position, that means all joints set to zero degrees (subscript $_{.z}$). This is best done by summing up the segment lengths of each muscle path in the model.

(viii) Compute the muscle-fibre lengths for all muscles in the MR-based model in reference position, $l_{m.z}$, by multiplying the optimal muscle-fibre length in the individually scaled model by the elongation factor for each muscle, thus:

$$l_{m.z} = l_{0m} * \varepsilon_m \tag{2.5}$$

(ix) The tendon length in the reference position, $l_{T.z}$, is derived by deduction of the muscle fibre length, $l_{m.z}$, from the total length of the muscle-tendon compartment, $l_{mT.z}$, with taking the pennation angle, α, into account

$$l_{T.z} = l_{mT.z} - l_{m.z} * \cos(\alpha) \tag{2.6}$$

(xi) The absolute tendon length alteration, when changing a joint angle from optimal joint angle to reference position, is independent of the total tendon length. As l_{sT} and l_{0m} are scaled uniformly, the length change of the tendon when a joint in the MR-based model is changed from neutral to optimal joint angle can be derived based on scaled results from the generic model by:

$$\Delta l_{T.z0} = l_{sT}^{G} * \frac{l_{0m}}{l_{0m}^{G}} * \left(\frac{1}{\varepsilon_T} - 1 \right) \tag{2.7}$$

(xii) The tendon slack length for the MR-based model, l_{sT}, can finally be calculated by deduction of the changed length from the total tendon length in the reference position.

$$l_{sT} = l_{T.z} - \Delta l_{T.z0} \tag{2.8}$$

Hence, the equation for determining l_{sT} can be re-written as:

$$l_{sT} = l_{mT.z} - l_{0m} * \frac{l_{0m}^{G}}{l_{m.z}^{G}} * \cos(\alpha) - l_{sT}^{G} * \frac{l_{0m}}{l_{0m}^{G}} * \left(\frac{l_{T.z}^{G}}{l_{sT}^{G}} - 1 \right) \tag{2.9}$$

(xiv)   Maximum isometric muscle force, F_{max}, can be obtained by dividing the muscle's volume, V_m, by the optimal muscle-fibre length, l_{0m}, what leads to the value for the physiological cross sectional area of a muscle, PCSA. and then by multiplication of the PCSA with the value of maximum muscle stress, σ, which was set to 33 N/cm² (Weijs and Hillen, 1985). The equation for calculating the maximum isometric force is:

$$F_{\max} = PCSA \;*\sigma = \frac{V_m}{l_{0m}}*\sigma \qquad\qquad (2.10)$$

(xv)   The values for F_{max}, l_{0m} and l_{sT} of all muscles need than to be updated for all muscles in the MR-based model. Values for pennation angle, α, and maximum shortening velocity, v_m, can be retained from the scaled template model.

With the described method, the parameters for 46 muscles, which have been segmented in the MR-images could be set. Maximum isometric forces, for muscles that are connecting pelvis and torso, erector spinae, internal obliques and external obliques were set via mass-length scaling (Correa and Pandy, 2011) as described later on in Chapter 2.5.1, according to individual body weight and height.

Individual models of five normally developing children were created by applying the described method and are denoted ND1 to ND5. All model details and parameters are listed in Appendix A.

2.4.7 Modelling of children with cerebral palsy

The strength of the method described in Chapter 2.4 is that it is capable of dealing with effects from biased limb positions during MR-recording, incorporating bone deformities such as femoral rotation or biased pelvis shapes as well as individual muscle attachment points.

The best achievable neutral position when the CP subjects lay on their back during MR-recordings was for CP1 with the left leg rotated inward by 37° and for CP2 on both sides a minimum knee angle of about 26° and a minimal hip extension angle of 19°. To achieve muscle path coordinates for a neutral limb position these position errors were corrected by applying appropriate coordinate transformation matrices as described in Chapter 2.4.2.

Main difference in modelling the children with cerebral palsy compared to the control group was the incorporation of bony deformities. Femoral anteversion (Figure 2.9) or tibial rotation are relatively common in CP patients with crouch gait (Laplaza et al., 1993). Accounting for such changes in musculoskeletal geometry in our MR-based models was important, because femoral anteversion, in particular, is known to have a significant effect on moment arms of muscles crossing hip and knee (Arnold et al., 2000; Schutte et al., 1997). The rotations of joint axes in the models is shown in Table 2.7.

Subject	Left femur	Right femur	Left tibia	Right tibia
ND	20°	20,1°	0°	0°
CP1	44,6°	45,4°	10°	-10°
CP2	21,5°	22,1°	40°	-25°

Table 2.7: Femoral anteversion and tibial rotation angles -Values based on MR-data. The orientations of the angles are denoted as rotation of the distal joint around the reference coordinate system of the proximal joint according to the right hand rule.

In case of tibial rotation these abnormalities were reproduced by rotating the ankle joint axes. The necessary rotation angle was measured via manually selected anatomical landmarks in the MR images on medial and lateral epicondyles and malleolus.
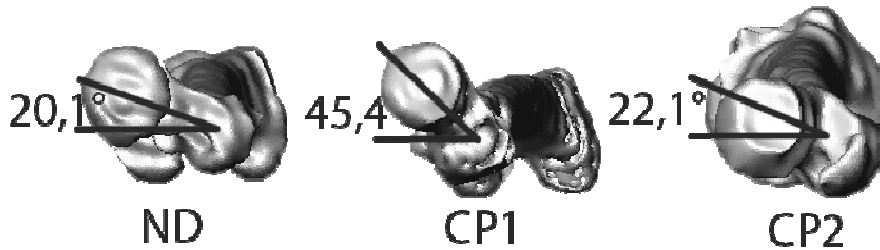
Figure 2.9 Femoral Anteversion - In the normally developing control group (ND) and the patients with cerebral palsy (CP1, CP2).

A correction of anatomical femoral rotation was not required as muscles attachment points and paths were obtained on correct anatomical positions of the greater trochanter from the MR analysis by using the described methods of Chapter 2.4. In this manner, significant changes in moment arms of muscles crossing the hip could be reproduced.

Muscle model parameters were set individually based on MR data and geometric model properties. Investigations of muscle fibre lengths in several models showed, that it was feasible to assume, that the joint angle for a muscle where it can generate its maximum isometric force (optimum joint angle for a muscle) to be similar in children with CP and normally developing subjects. The noticeable biased limb position in CP actually puts the major leg muscles close to their optimal length. Hence, model parameters such as optimal muscle fibre lengths, l_{0m}, and corresponding optimal joint angles were assumed to be similar in both, the CP subjects and normally developing subjects. Consequently, and in accordance to the method in Chapter 2.4.6 for normally developing children, values for these parameters, which resulted from scaling of the template model using OpenSim, were conserved.

Also similar to the method used in the control group geometrical relations were used to estimate tendon slack length, l_{ts} of each individual musculotendon actuator. As described in Chapter 2.4.6 this process took individual muscle attachment sites and muscle paths into account. Values for α and ν_m in MR-based models were set to same values as in the generic adult template model.

MR-based models for the two children with cerebral palsy are denoted CP1 and CP2. All model details and parameters are listed in Appendix A.

2.4.8 Average model of normally developing children

Based on the MR-based models of five children, an average children's model (superscript ᵃᵛ) of the corresponding age group was compiled. For that, lengths of main segments representing the lower body (*pelvis, thigh, shank, foot*) together with positions of joint centres were defined by averaging the dimensions of the individual children's models. The adult template model was then proportionally scaled to these average dimensions, using the scaling function in OpenSim (Seth et al., 2011). Optimal muscle fibre lengths, l^A_{0m}, as well as pennation angle, α, and maximum shortening velocity, ν_m, were retained from the template model after scaling.

To obtain averaged locations of muscle points for the averaged children's model, P^{av}, first all model segments of the normally developing children's

models were scaled to the size of the average children's model, by using OpenSim. Then coordinates of the muscle attachment points and via points on each muscle path in these individual scaled models, P^{Si}, were averaged:

$$P_{(x,y,z)}^{av} = \frac{1}{n}\sum_{1\to n}^{i} P_{(x,y,z)}^{Si} \tag{2.11}$$

A similar body composition in all normally developing children was assumed, with an average BMI of 17±1. To calculate the average muscle volumes (V^{av}_m), first the volume of each muscle in each subject specific model (V^{S}_m) was multiplied with the ratio of average to subject specific body mass ($m_{body}{}^{av}/m_{body}$), and then volumes for each muscle were averaged over all models:

$$V_m^{av} = \frac{1}{n}\sum_{1\to n}^{i} V_m^{Si} \times \frac{m_{body}^{av}}{m_{body}} \tag{2.12}$$

By using the method described in Chapter 2.4.6, the tendon slack length, l^{av}_{ts}, for each muscle was calculated for average muscle-tendon geometry. To obtain the averaged maximum isometric force for each muscle, F^{av}_{max}, the average muscle's volume of individual models, V^{av}_m, was divided by the appropriate l^{av}_{0m} This resulted in the mean PCSA^{av}, that was further multiplied with the maximum muscle stress, (σ=33 N/cm^2), to get F^{av}_{max}.

$$F_{max}^{av} = PCSA^{av} \times \sigma = \frac{V_m^{av}}{V_{0m}^{av}} \times \sigma \tag{2.13}$$

Detailed descriptions, geometric and physiologic model parameters of the average child model, which is denoted 'avCh' in this dissertation, are listed in Appendix A.

2.5 Modelling by mass-length scaling

A compromise between accuracy and time effort has to be made when biomechanical models are to be generated for clinical applications. Model calculations are sensitive to variations in body anthropometry (Lenzi et al., 2003; Pataky et al., 2003), and muscle-tendon properties. Deviations in muscle PCSA, tendon rest length, and muscle moment arms have been reported to show the highest influence on model estimates of muscle force (Ackland et al., 2012; R. Brand et al., 1986; Herzog, 1992; Raikova and Prilutsky, 2001; Redl et al., 2007; Scovil and Ronsky, 2006).

If the process of mass-length scaling presented by Correa and Pandy (2011) is used to generate a children's model based on a generic adult template model, high scaling-factors and different body composition of adults and children might lead to substantial errors especially in peak isometric forces and moment arms (see results in Chapter 3.1 p.70ff).

The following chapters describe the generation of several mass-length scaled models. These models were used either for evaluation of the modelling method, as literature-reference models or for testing modelling results based on different template models.

2.5.1 Child model by mass-length-scaled adult model

To investigate the average child model (avCh) as well as the gain of the extra effort that the generation of MR-based models might mean, the kinetic trajectories were compared to that of a model, which was generated in by the much quicker mass-length-scaling method published by Correa and Pandy (2011). Hence the adult template model (superscript ^{AT}) was mass-length scaled (superscript ^{sAT}) to proportions of the average child model, by using the joint centre locations as scaling reference. Muscle model parameters in this model were set according to the mass-length-scaling method (Correa and Pandy, 2011):

The maximum isometric muscle force, F^{sG}_{max}, of each muscle is expressed as:

$$F^{sAT}_{max} = PCSA \times \sigma = \frac{V^{sAT}_m}{l^{sAT}_{0m}} \times \sigma = \frac{m^{sAT}_m}{\rho \times l^{sAT}_{0m}} \times \sigma \qquad (2.14)$$

with muscle mass m_m^{sAT} and specific muscle density ρ. Consequently, as proposed by Correa and Pandy (2011), the maximum isometric force of a muscle of a scaled model, F_{max}^{sAT}, can be determined from the maximum force in the original model, F_{max}^{AT}, and relations of muscle masses and optimal fibre lengths (2.15).

No more detailed anatomically information (limb segment weights etc.) is usually recorded when models are mass-length-scaled. Therefore it was assumed that body compositions for the original and the individual subject's models are similar. Hence, the relation of total body masses, m_{body}, could be used instead of the relation of explicit muscle masses to calculate F^{sAT}_{max}: (2.17)

$$F^{sAT}_{max} = F^{AT}_{max} \times \frac{m^{sAT}_m}{m^{AT}_m} \times \frac{l^{AT}_{0m}}{l^{sAT}_{0m}} \qquad (2.15)$$

$$F^{sAT}_{max} \approx F^{AT}_{max} \times \frac{m^{sAT}_{body}}{m^{AT}_{body}} \times \frac{l^{AT}_{0m}}{l^{sAT}_{0m}} \qquad (2.16)$$

The child model, which was generated by mass-length-scaling of an adult template model using average body properties of the control group in this study, was denoted 'scAd' in the following chapters.

2.5.2 CP-models based on mass-length scaling

The MR-based models of the two children with cerebral palsy (CP1 and CP2) were compared to models that were generated by mass-length scaling (see Chapter 2.5.1) of two different template models each. These four additional models where created, to investigate, if the method of mass-length scaling of template models is feasible to generate individual models of children with cerebral palsy and further to examine the influence of the used template on functional characteristics of the generated model.

One template model was the generic adult model (AT) with 75 kg body weight, which was also the base for the individual MR based models and is described in detail in Chapter 2.3. This model is a modified version of a generic model that is available in OpenSim (Delp and Loan, 2000; Seth et al., 2011) and incorporates muscle parameters of a model published by Arnold et. al. (Arnold et al., 2010). The second template was the average child model (avCh) as described in Chapter 2.4.8 that was generated using MR data of five normally developing children and was denoted for this investigation as children's template model (CT).

Each of the template generic models was scaled to match the geometry of each of the CP-children using OpenSim. The scaling was based on gait marker positions (see Chapter 2.2.3) that were measured from the standing trial. This is a common practice:

- distance of anterior superior iliac spines markers (RASI, LASI) in combination with sacrum for pelvis;

- distance of RASI/LASI markers to the markers on the matching lateral epicondyles of the femur (RLEPI,LLEPI) for thigh

- and distance of RLEPI/LEPI to markers on the lateral malleolus (RMMAL/LMMAL) for shank.

The mass-length scaling law proposed by (Correa and Pandy, 2011) allowed to estimate the maximum isometric force, $F_{max}{}^{sM}$, of each muscle in the scaled individual model, without the necessity of radiology data. In this method, the maximum force of the particular generic model $F_{max}{}^{G}$ and its relations of muscle masses $m_m{}^{G}$ and optimal fibre lengths $l_{0m}{}^{G}$ were used to calculate $F_{max,}{}^{sM}$ (2.17). As the subject specific explicit muscle masses $m_m{}^{sM}$ are usually unknown when no radiology data is available the relation of total body masses, $m_{body}{}^{G}$ for the generic model and $m_{body}{}^{sM}$ for the subject-model, was used.

$$F_{\max}^{sM} = F_{\max}^{G} \times \frac{m_m^{sM}}{m_m^{G}} \times \frac{l_{0m}^{G}}{l_{0m}^{sM}} \approx F_{\max}^{G} \times \frac{m_{body}^{sM}}{m_{body}^{G}} \times \frac{l_{0m}^{G}}{l_{0m}^{sM}} \qquad \textbf{(2.17)}$$

The mass-length scaled, models of the child CP1 based on AT is denoted as CP1AT and the CP1 model based on CT is referred to as CP1CT. Analogously for CP2: the mass-length scaled models are labelled CP2AT and CP2CT.

2.6 Summarized Model Overview

Summarized are the abbreviations of all used models in this study and their generation technique given in Table 2.8.

Model name	Description of modelling technique
ND1 - ND5	MR-based models of normally developing control group
CP1, CP2	MR-based models of CP-children
avCh	Average child model based on data of ND1 - ND5
scAd	Scaled model of generic adult model (AT)
AT	Generic adult template model
CT	Generic children's template mode, equals avCh
CP1AT, CP2AT	Scaled models of CP-children based on AT model
CP1CT, CP2CT	Scaled models of CP-children based on CT model

Table 2.8 Overview of generated and used models

2.7 Method and Model evaluation

First, the functional characteristics of models in different workflow steps (see Chapter 2.4.6.3) and modelling approaches (MR-based and mass-lengthscaled) were compared on behalf of joint moment calculations of two exemplary joints. Second, the model behaviour was investigated by simulations of maximum isometric joint moments of all degrees of freedom that were compared to experimental results and literature data.

2.7.1 Comparison of modelling methods

Figure 2.10 illustrates different modelling methods and shows the change when adjusting model parameters according to the method described in section 2.4.6. Graphs labelled 'scaled generic muscles 1' show the resulting maximum isometric net joint moments over the range of motion for the generic model scaled according to the mass-length scaling as proposed by Correa and Pandy, (2011). This model was roughly scaled to the height of an average nine-year-old child (~75% of an adult) with maximum isometric forces were set to around ~56% of that of the adults model.

Figure 2.10 Joint moments during modelling steps - Hip-flexion (left) and knee extension (right) maximum isometric moment-angle curve calculated in different models and modelling steps when setting muscle model parameters.

When a model is scaled in OpenSim, the resulting uniform scaling of via-point coordinates is unsuitable as this can result in a snap-action function as best seen in the graph labelled 'Specific Model 1' of Figure 2.10a. In the graph titled 'scaled generic muscles 2', the via-point of the mass-length scaled model was additionally corrected according to the new muscle path after scaling. Here also the tendon slack length was set to the correct value, what is required even if small changes of in the muscle path are made, as described in section 2.4.6.3, equation (2.9).

The graph titled 'Specific Model 1' was obtained once the subject-specific muscle attachment points were adjusted to the data derived from the MR images and maximum isometric muscle forces were then set to subject-specific values obtained from the MR data. The discontinuities observed at a hip flexion angle of 50° and at a knee flexion angle of -15° in Figure 2.10a were caused by incorrectly positioned via-points. After adjusting the position of these via-points and correcting l_{sT}, the final joint moment-angle curve labelled 'Specific model 2' shows again a similar shape to the 50%-joint moment-angle curve computed for the template 'Generic adult model'.

Measured subject-specific attachment points for vasti lie about 10 cm more proximal than in the generic model after scaling. This leads to an unusual joint moment profile for knee extension, as shown in the graph titled 'Specific Model 1' (Figure 2.10b). After adjusting the via points and tendon slack lengths in 'Specific Model 2' a reasonable match was obtained to the shape of the joint moment-angle curve computed in the scaled generic model. The discontinuity observed at a knee flexion angle of -80° is model-specific and resulted from an incorrectly positioned attachment site for the vasti on the patella, which was not corrected after scaling.

2.7.2 Model evaluation and generic model adaption related to maximum joint moment behaviour

To evaluate the modelling method and the applied generic model magnitudes and overall shapes of maximum isometric joint moment-angle curves of the MR-based models were compared to results obtained from the scaled generic adult model, experimentally measured joint moment-angle data (see Chapter 2.2.2) and results from literature (Eek et al., 2006) in Figure 2.11 and Figure 2.12. This procedure served to verify the method for setting muscle model parameters (i.e., peak isometric muscle force, optimum muscle-fibre length, muscle pennation angle, and tendon rest length) that were acquired by using a method described in detail in chapter 2.4.6 for all major muscle groups in the models.

For means of better comparability the generic model was scaled to average size of the subjects (~75%) and maximum isometric forces were adjusted to muscle strengths corresponding to a reduced body mass (56%).

To calculate the net maximum joint moment, only the 'positive' contributing sections of the joint moment angle curve of each active muscle over the range of joint motion were summarized and the passive moments of the antagonistic muscles were deducted.

Results in Figure 2.11 and Figure 2.12 show, that magnitudes and overall shape of joint moment-angle curves in MR-based and scaled-generic models were very similar for the joints examined in this study. However, some differences can be observed between simulated joint moments and experimental measurements.
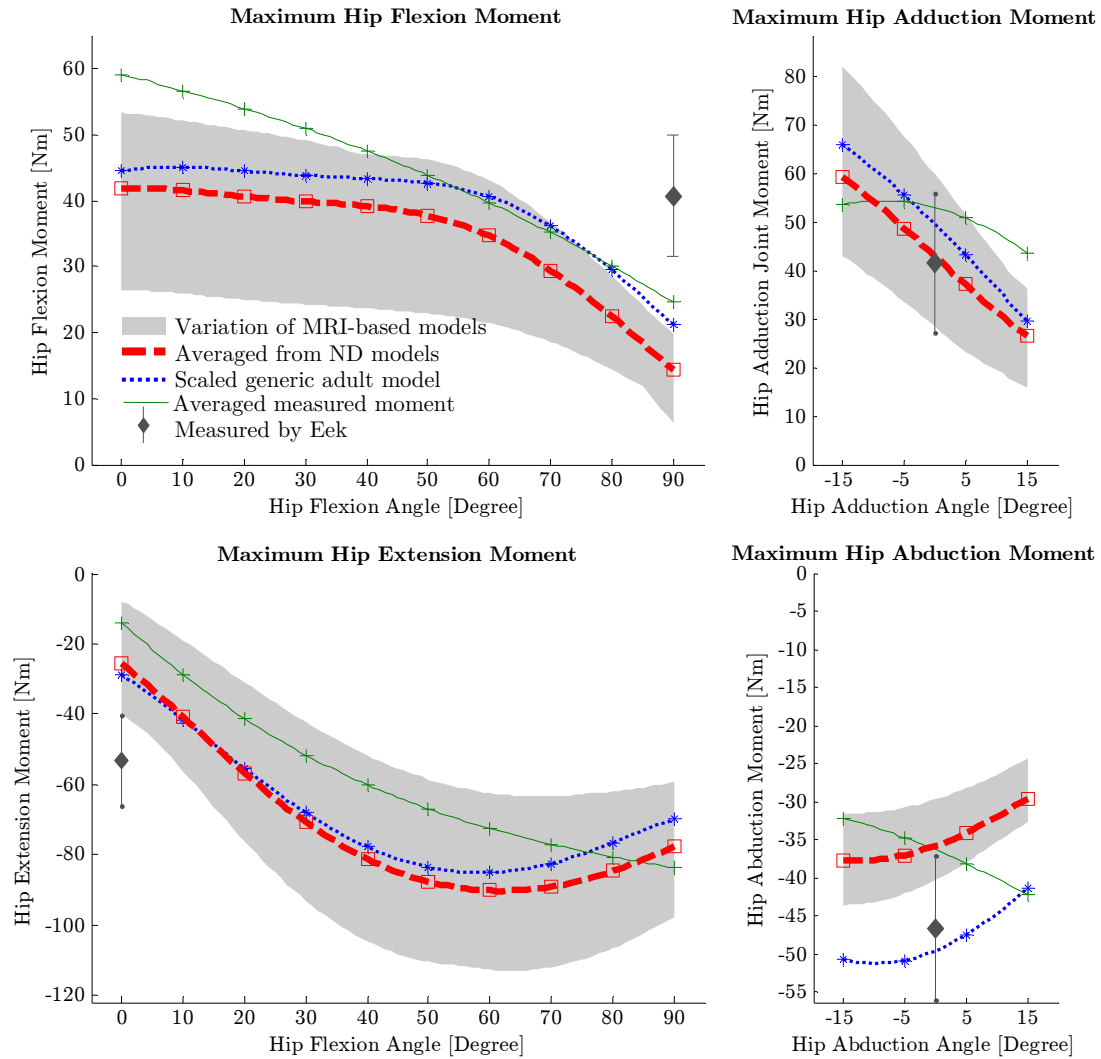
Figure 2.11 Model evaluation by maximum isometric hip joint moments - Hip flexion-extension with knee flexed to 90° and adduction-abduction. Thick dotted line: Average result of MR-based models with variation indicated by the gray area; Thin dotted line: Result obtained from scaled model of adult model based on data of Arnold et al. (2010) with scaling of 75% in geometry and 56% peak muscle force); Thin line: average measurements of hip flexion and extension with subjects and hip extension results as reported by (Anderson and Pandy, 1999) and normalized by method of Eek et al. ,(2006); Dot with error bar: Result from (Eek et al., 2006), manual dynamometry on children
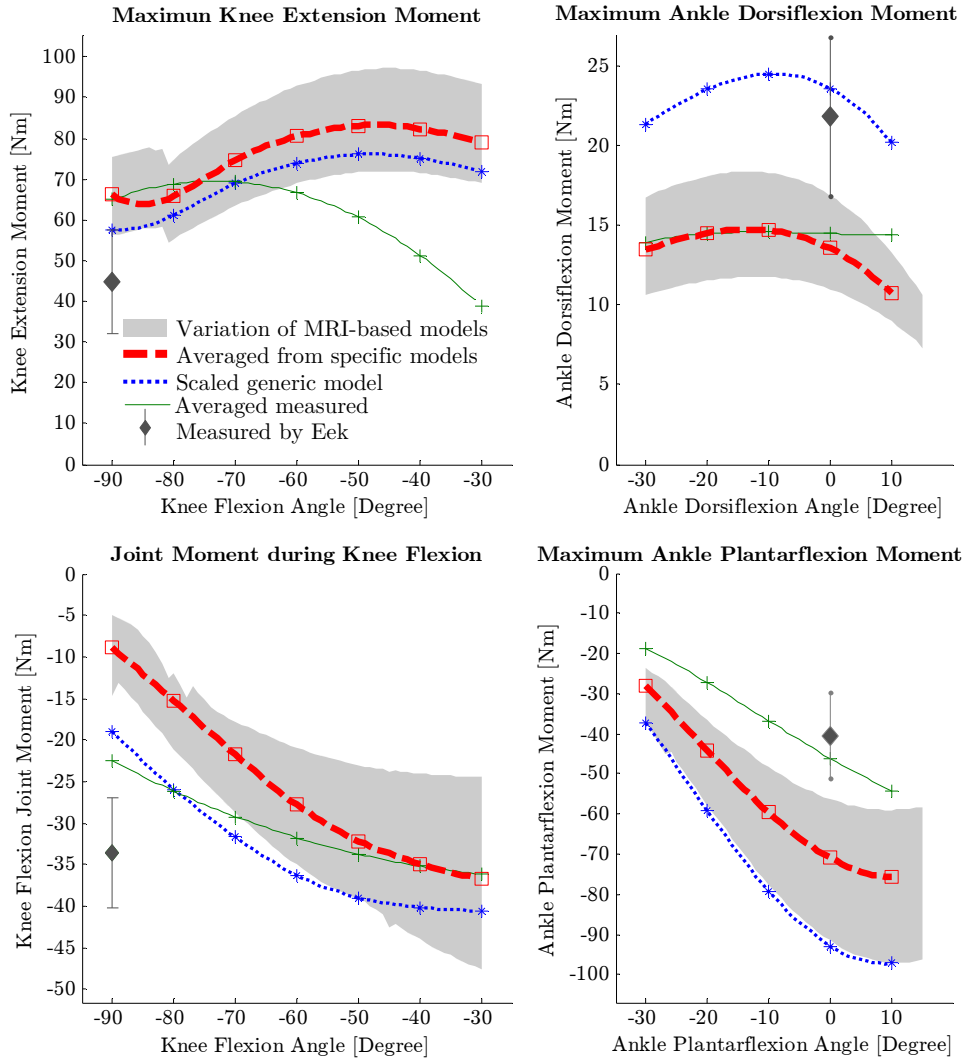
Figure 2.12 Model evaluation by max. isometric knee and ankle moments - Knee results with hip flexed to 60° and ankle results with knee flexed to -60°. Thick dotted line: Average result of MR-based models with variation indicated by gray area; Thin dotted line: Result obtained from scaled model of adult model based on data of Arnold et al. (2010) with scaling of 75% in geometry and 56% peak muscle force); Thin line: Result from average measurements obtained on subjects; Dot with error bar: Result from (Eek et al., 2006), manual dynamometry on children

Compared to result of Eek et al. (2006) in Figure 2.11, a reduction in hip flexion moment could be observed both in the model and our experimental data. Eek measured the data with a hand dynamometer with other degrees of freedom of the measured leg not completely locked. To examine the effect of

this limitation, maximum hip flexion moment in the model was calculated with a slight hip adduction of 10° that might have helped the subject to stabilize and a possible knee angle of greater than 90° that shortens the hamstrings tendon and therefore reduces the hamstrings passive joint moment during hip flexion. With this configuration, results of Eek could be reproduced as the maximum joint moment computed in the model was up to 30% higher, particularly when the hip flexion angle was increased.

All computational models showed a decreasing potential for hip abduction the more the hip is adducted (Figure 2.11). Contrary to this our experiments show increased hip abduction when the hip is adducted. However, the underlying generic model was not revised regarding this issue.

Measurements for knee extension were performed in a sitting position of the test person where the hip was flexed to approximately 60°. In this posture, the knee flexors that also cross the hip joint (e.g. hamstrings) are stretched. This leads to a rising resistive moment when extending the knee, what in consequence lowered the measured total knee extension moment. Decreasing tendon slack length for the hamstrings by around 5 cm generated strong passive joint moments at smaller knee angles. This in turn reduced the net knee extension moment in a way that the shape of joint moment calculated in the model more closely resembled results measured for the subjects. Hence the generic adults model was revised by shortening the tendon slack length of hamstrings by 5cm compared to values given by Arnold et al. (2010).

It can be concluded, that the applied modelling method to modify the used generic model leads to reasonable functional characteristics of the control group models. The modelling process results in replicable and comparable models and can also be applied to generate models of subjects with special anatomical characteristics like children with CP.

If dynamometry results shall be used to verify a biomechanical model it will be important to either record the exact body posture during measurement or to even adapt the protocol that is given by the dynamometer manufacturer Biodex to measure the maximum joint moments.

2.8 Biomechanical Simulations

Joint kinematics (positions, velocities, accelerations) and ground-reaction forces obtained from the gait experiments were used as input to the computer model of each healthy subject or CP-patient. Inverse dynamics and static optimization theory were used to determine the time histories of all joint moments and leg-muscle forces during walking. This data was finally used to calculate the individual contributions of all muscles to joint accelerations as well as forward, vertical and lateral acceleration of the centre of mass.

2.8.1 Functional model characterisation by maximum isometric joint moments

Joint moment-angle curves were used to assess the static response of the musculoskeletal models. Comparisons of maximal joint moment over joint angle between models, literature data and experimental results were made for hip flexion, extension, abduction, and adduction, for knee flexion and extension as well as for plantarflexion and dorsiflexion of the ankle.

The maximum isometric joint moment at a specific joint and orientation was calculated as the sum of all active moments generated by fully activated agonistic muscles deducted by passive moments which originate from stretching of the antagonistic muscles. Explicit joint moment progressions were calculated by multiplying the muscle moment arm along the motion range of a joint with the maximum isometric muscle force according to the muscles force-length characteristic. At the same joint orientation, passive muscle forces and moments from antagonistic muscles where calculated for corresponding muscle length and moment arm. Moment arms were determined as function of to the joint angle by measuring the shortest distance between a muscle's line of action and the corresponding joint axis.

The functional role of some muscles, e.g. the adductors, can change depending on hip flexion angle so they can contribute to hip flexion as well as to hip extension. Therefore, only the 'positive' contributing sections of the joint moment-angle curve of each active muscle (agonist) were added and passive moments of antagonistic muscles were deducted when determining

the maximum isometric joint moment.. Joint moment results were normalized for better comparability by division with subject specific body weight force and body height, giving [Nm/(N*m)], multiplied by 100 for percentage values.

Results for evaluating the functional characteristics of the ND-models and the accuracy of the average child model are given in Chapter 3.1.2, Figure 3.1 to Figure 3.4 (p.72ff). These figures show a comparison of average maximum joint moments of ND with results from the average child model, with literature data and with results from the scaled generic adult model.

A comparison of maximum joint moments of the two CP-models to the ND control group as well as results depending on the applied modelling method is given in Chapter 3.2.3, Figure 3.6 and Figure 3.7 (p.83ff).

Particular characteristics of moment arm and maximum joint moment of 46 muscles of the lower limb are shown in Appendix chapter B.1 (p. B-3) and may help to understand individual deviations of the CP-child models.

2.8.2 Determination of muscle forces in normal and crouch gait

The marker positions recorded during the gait experiments were low-pass filtered using a Butterworth 2nd order filter with a cut-off frequency of 6 Hz (Anderson, 1999). Similar to the gait recording markers were virtual gait markers placed in the computational models on the positions defined in Table 2.5 (p.34). A weighted least square optimization of distance from the virtual gait markers to the gait recording markers was used, to determine via joint angle adaption in each period of the gait recordings. This resulted in the 3D angular displacements of each metatarsal joint, each ankle, each knee, each hip, and the back joint. For this, built-in functions of the Software OpenSim were used (Anderson and Pandy, 2001a; Davis et al., 1991; Lu et al., 1999).

A mismatch between model and experimental data is usually caused by model simplifications and experimental errors. To keep the required dynamic consistency for subsequent force calculations, residual forces and moments were added to the model at each joint and on the defined pelvis centre (PC) (Kuo, 1998). A residual reduction algorithm form OpenSim (Delp et al., 2007) was used to optimize the motion pattern by minimizing the necessary residual forces.

Methodology

The inverse dynamics function of OpenSim was then used to compute net joint moments acting at the ankle, knee, and hip using the motion data in combination with the GRF-vector that was applied to the centre of pressure of the stance foot. Joint angles as well as joint moments during gait are shown in Chapter 4.1 (p.97ff).

A net joint moment can be produced by an infinite combination of muscle forces. To get results for individual muscle forces a static optimization problem was defined. The optimization criterion was to minimize the muscle activation (R. A. Brand et al., 1986). Static optimization does not take into account the dynamics of muscle activation and deactivation, as other approaches like forward-dynamics do, but provides considerably faster calculations. The OpenSim environment provides a built-in function for deriving forces with static optimization:

At each time step throughout one full gait cycle, and not concerning the model states in the previous or subsequent period, the forces are calculated, which are developed by each of the modelled leg muscles (Anderson and Pandy, 2001b). The performance criterion was to minimize activation squared, summed across all muscles in the model (Anderson and Pandy, 2001b; Crowninshield, 1983; Kaufman et al., 1991; Seth and Pandy, 2007) for both, the control group as well as for the CP patients, in order to account for the force-length-velocity properties of the muscles.

The applied function in OpenSim solved the static optimization problem by minimizing the sum of the squares of all the muscle activations depending on two constraints:

(i) The sum of force outputs are constrained to produce the net muscular joint moments estimated from inverse dynamics;

(ii) Muscle operate according to their force-length-velocity property.

The optimization solution produced time histories of all muscle activations and muscle forces in the model consistent with the measured gait pattern.

The particular muscular forces in gait of the CP-patients in comparison to the ND control group is shown in Figure B.2.1 to Figure B.2.30 Appendix B.2 with index 'b)'. The force graphs have been normalized to the body weight of the subjects so that they are comparable and useful to understand individual deviations of modeled CP-children.

2.8.3 Joint moments in gait and particular muscle contributions

Total joint moments in gait were calculated directly based on the kinematic data in combination with GRF data. Contributions to the joint moments in gait of specific muscles were calculated according to the derived muscle forces, F_m, in gait in combination with the displacement (q) dependent moment arm, $MA_{(q)}$.. Particular muscle's moment arms in gait were obtained by applying the "MuscleAnalysis Tool" of OpenSim. Hence was the particular joint moment contribution of single muscles, $M_{m(q)}$, calculated via multiplication of F_m and $MA_{m(q)}$ in gait:

$$M_{m(q)} = F_m * MA_{m(q)} \tag{2.18}$$

All joint moment results shown in Chapter 4.2 (p.100ff) for hip, knee and ankle of ND, CP1 and CP2 in

Figure 4.4 to

Figure 4.7 have been normalized to values matching the average body height and weight of ND (1,34m 30,4kg) according a method published by Eek et al. (2006). The dimensionless, relative values displayed in these figures were calculated by dividing the resulting joint moments with the average body height and weight to provide better means of comparison with results in literature or future research results. Results for the control group are averaged values. Variations of ND are not indicated in the ND-results to obtain a better recognition of relevant information. Particular muscle contributions including variation of ND are shown in Figure B.2.1 to Figure B.2.23 of Appendix Chapter B.2 (p.B-22ff)

METHODOLOGY

2.8.4 Induced acceleration analysis

A muscle can contribute to the motion of a body segment without physically touching it. This is a consequence of the fact that the skeleton is comprised of a number of segments, all coupled by joints. A muscle force applied to one segment affects the motion of all the other segments because reaction forces are transmitted up and down the system by the joints.

For the applied method of induced acceleration analysis, equations of motion for the skeletal linkage system are expressed in second-order form as:

$$\ddot{q} = \frac{g_{(q)} + v_{(q,\dot{q})} + GRF_{(q,\dot{q})} + MA_{m(q)}F_m}{m_{m(q)}} \qquad (2.19)$$

In equations (2.19) to ((2.21) q, $\dot{q}$ and $\ddot{q}$ are $n*1$ vectors of joint displacements, velocities and accelerations, respectively. Mass and inertial properties of the body segments are specified in m_m, an $n*n$ system mass matrix, g is the generalized forces due to gravity. The generalized force due to centripetal and coriolis effects is the $n*1$ vector v. The vector of ground reaction forces is GRF, and MA_m is the $n*k$ matrix of muscle moment arms that transforms a k*1 vector of into individual muscle forces F_m. Into generalized forces (Y. Lin et al., 2011; Zajac et al., 2003). The contribution that each muscle force adds to the joint accelerations is given by:

$$\ddot{q}_f = \frac{MA_{m(q)}F_m}{m_{m(q)}} \qquad (2.20)$$

Similarly, gravity's contribution to the joint accelerations is given by:

$$\ddot{q}_f = \frac{g_{(q)}}{m_{m(q)}} \qquad (2.21)$$

Each muscle force, as well as gravity, contributes to the acceleration of each joint in the model. The reason is that the mass matrix $m_{(q)}$ is not diagonal (Zajac and Gordon, 1989). Equation (2.20) can be used to compute muscle contributions to the joint accelerations, because the time histories of all the muscle forces will be available from the optimization solutions obtained for normal and crouch gait.
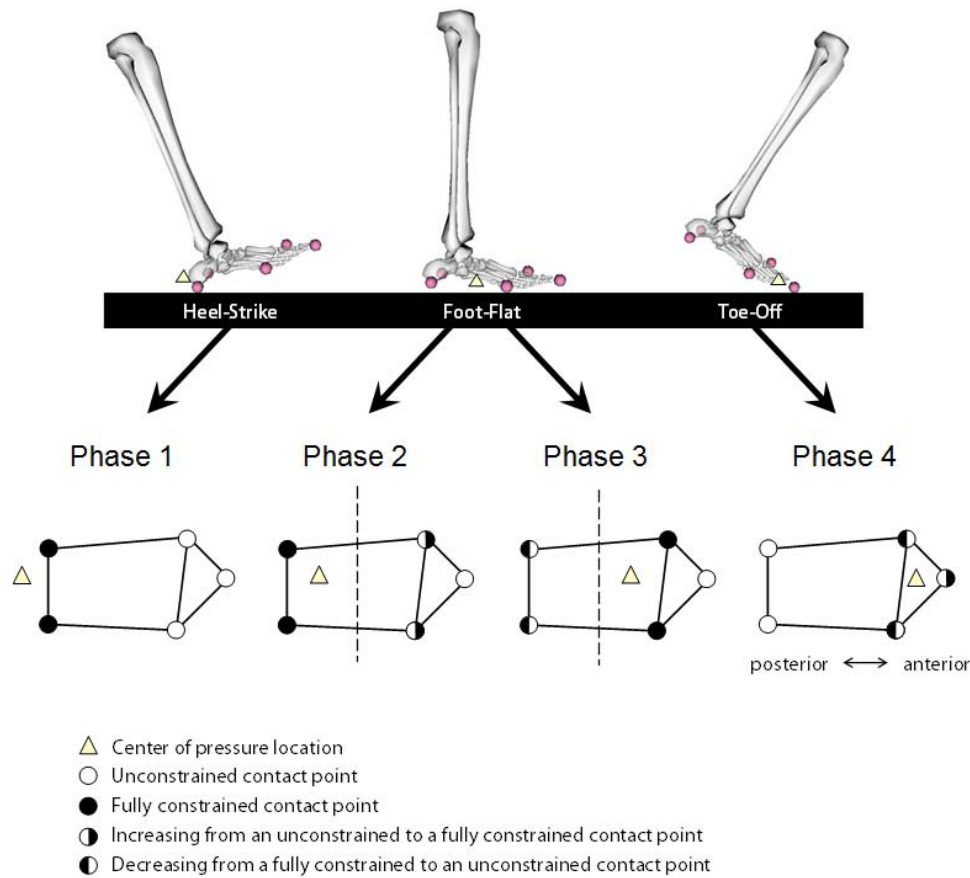
Figure 2.13 Foot ground contact model - A smooth transition between the phases of heel-strike (Phase 1), foot-flat (Phase 2 and 3) and toe-off (Phase 4) was possible by applying weighting coeffcients at each of the five discrete contact points. The contact model depends on the phase of the gait cycle: Phase 1 is depicted during heel strike, Phases 2 and 3 are depicted during foot flat. Phase 4 is depicted during toe off. (Dorn et al., 2012a; Y. Lin et al., 2011)

By using the muscle forces resulting from the static optimization and applying the foot-ground contact model (Figure 2.13) proposed by Dorn et al. (2012a) the induced acceleration analysis in this study was done for all models using the OpenSim plug-in "IndAccPI" by Tim Dorn (Dorn et al., 2012a, 2012b; Y. Lin et al., 2011). This method was selected as it applies a pseudo-inverse matrix operator to analytically compute induced-accelerations and is hence several orders of magnitude faster than solving numerical forward-integrations that are required for the perturbation method. Further, the five-point ground contact model replicates the foot contact on the sole of the foot more realistically than the available methods with just one centre of

pressure. By calculating the induced accelerations could be quantified how each muscle, as well as gravity, contributes to the acceleration of each joint in the model during normal and crouch gait in the stance phase.

Total angular joint and CoM accelerations with particular muscular contributions are given in Chapter 4.3 (p.106ff) and Chapter 4.4 (p.119ff) respectively. Detailed comparisons for joint and CoM accelerations of all modelled muscles between the two CP-children and the control group in gait are shown in Appendix B.2.

3

Modelling Results

Contents

3.1 Models of normally developing children

3.1.1 Model parameters of ND-models

Segment lengths and hip joint centre locations of the normally developing children in Table 3.1 show standard deviations around 4% for most, with body height normalized, values. The highest difference can be seen for posterior distance of hip joints to pelvis centre with a standard deviation of about 25,7%, what may be caused by deviations in pelvis tilt during MR-imaging.

PC to Hip Joint - lateral	6,1 cm ± 2,7%
PC to Hip Joint - posterior	3,1 cm ± 25,7%
PC to Hip Joint - distal	5,9 cm ± 5,3%
Thigh length	31,5 cm ± 4,0%
Shank length	30,2 cm ± 1,7%
Foot (ankle to toe joint)	13,9 cm ± 3,0%

Table 3.1 Segment dimensions of normally developing children - Location of hip joint centre and segment lengths in the average children's model plus standard deviation values of normally developing subjects, that were normalized with body heigth. The pelvis centre (PC) is defined as the midpoint of the connection line between left and right anterior superior iliac spines.

Average musculotendon parameters of the five normally developing children were incorporated to the average child model (avCh) and are compared to values of a mass-length scaled adult model (scAd) in Table 3.2. Children had much smaller muscles on the outer surface of the pelvis (gluteus medius and gluteus min -43%) and smaller dorsal hip muscles (iliopsoas -30%) but a stronger rectus femoris (+45%).

	PCSA [cm²]		V_m [cm³]		F_max [N]		l_mt [cm]		l_0m [cm]		l_sT [cm]		Moment Arm [cm]		Major Motion
	avCh	scAd	avCh	scAd	avCh	scAd	avCh	scAd	avCh	scAd	avCh	scAd	avCh	scAd	
Adductor longus	6,0	10,3	49,0	84,9	198	340	16,8	11,9	8,2	8,2	8,6	3,7	4,95/3,66	5,12/2,16	Hip Add/Flex
Adductor magnus	19,3	15,2	215,3	169,2	637	500	21,8	21,9	11,1	11,2	11,1	11,2	4,46	4,47	Hip Adduction
Biceps femoris short head	4,3	4,7	37,5	40,6	143	155	17,0	15,5	8,7	8,7	8,5	7,1	2,05	2,66	Knee Flexion
Extensor digitorum	6,9	7,7	37,6	42,0	227	253	37,3	33,4	5,5	5,5	31,9	28,0	2,35	2,86	Dorsiflexion
Flexor digitorum longus	4,3	4,2	14,6	14,3	143	139	38,6	32,0	3,4	3,4	35,3	28,7	0,51	0,76	Plantarflexion
Flexor hallucis longus	7,2	6,7	29,2	27,0	239	221	39,6	31,8	4,0	4,0	35,7	27,9	1,13	1,20	Plantarflexion
Gastrocnemius	31,7	29,3	135,4	125,1	1048	968	34,8	33,9	4,3	4,3	30,6	29,7	3,55/2,19	3,58/1,21	P-Flex/Knee Flex
Gluteus maximus	23,1	26,4	320,6	367,5	764	873	22,2	18,6	13,9	13,9	9,3	5,7	4,63	4,20	Hip Extension
Gluteus medius	17,5	29,5	112,1	188,1	579	975	9,4	11,6	6,4	6,4	3,4	5,6	3,44	3,45	Hip Abduction
Gluteus minimus	4,3	7,9	21,7	40,3	142	262	6,8	7,3	5,1	5,1	1,8	2,3	3,36	3,38	Hip Abduction
Gracilis	2,2	2,1	39,4	36,5	74	68	29,1	30,3	17,6	17,6	11,6	12,9	4,67	3,93	Hip Adduction
Hamstrings	28,4	32,5	210,7	240,5	939	1072	32,7	31,9	7,4	7,4	25,4	24,6	4,07/2,23	3,45/2,39	Hip Ex/Knee Flex
Iliopsoas	11,4	15,5	100,0	141,2	377	513	15,5	17,2	8,7	9,1	7,0	8,3	2,59	2,53	Hip Flexion
Pectinius	5,3	2,7	52,2	27,5	175	90	13,8	10,2	9,9	10,1	4,0	0,1	2,65	1,55	Hip Flexion
Peroneus	11,3	16,1	43,5	62,1	372	531	36,2	29,7	3,9	3,9	32,4	26,0	1,06	0,86	Plantarflexion
Piriformis	7,6	4,4	14,8	9,0	251	147	9,5	10,9	1,9	2,0	7,5	8,9	1,04	1,74	Hip Abduction
Rectus femoris	17,7	12,3	108,7	75,3	585	406	33,4	33,8	6,1	6,1	27,4	27,9	2,84/2,94	2,57/2,96	Hip Flex/Knee Ex
Sartorius	1,9	1,7	59,6	53,4	61	55	39,8	40,9	32,0	32,1	7,7	8,8	2,66/1,20	2,84/0,71	Hip Fl/Knee Fl
Soleus	46,9	55,0	156,8	184,1	1547	1817	26,9	26,5	3,3	3,3	24,0	23,6	3,41	3,52	Plantarflexion
Tibialis anterior	8,8	10,3	45,9	53,7	292	341	30,9	26,4	5,2	5,2	25,8	21,3	3,69	3,38	Dorsiflexion
Tibialis posterior	16,0	13,9	44,9	39,1	527	459	30,4	26,6	2,8	2,8	27,6	23,9	0,68	0,79	Plantarflexion
Tensor fasciae latae	3,0	2,2	22,9	17,2	98	74	38,1	40,0	7,7	7,7	30,4	32,3	2,77/3,56	2,81/3,62	Hip Flex/Abd
Vastus	74,6	69,2	588,1	545,5	2460	2282	30,2	28,3	7,9	7,9	22,7	20,7	3,02	3,12	Knee Extension

Table 3.2 Musculotendon parameters in child models -. 'avCh' is the averaged children's model based on MR-data of 5 normally developing children; 'scAd' is the, to average child size mass-length scaled adult template model. Prior to averaging muscle volumes (V_m), maximum isometric forces (F_{max}) and PCSA values were normalized to average body weight of the normally developing children. All length parameters (l_{mt}, l_{0m}, l_{ts} and moment arms) were normalized to average body height of the normally developing children. Children had much smaller muscles on the outer surface of the pelvis (gluteus medius and gluteus min -43%) and smaller dorsal hip muscles (iliopsoas -30%) but a stronger rectus femoris (+45%). Marked parameters show significant differences between the two modelling methods

As consequence of different muscle strengths, contributions of involved muscles in children to joint torques are shifted compared to the scaled adult's model. Iliopsoas (F_{max} -26%) contributes less and rectus femoris (F_{max} +45%) more towards hip flexion and a stronger rectus femoris also contributes more to hip abduction, while the role of gluteus medius (F_{max} -41%) was decreased for hip abduction. Adductor longus (F_{max} -41%) contributed lower, while adductor magnus (F_{max} +27%) had a higher contribution on the maximum hip adduction moment. Longer moment arms (MA) compensated the lower strength of gluteus maximus (F_{max} -12%, MA +10%) and hamstrings (F_{max} -12%, MA +18%) for hip extension. Due to decreased strength of hamstrings they were also less contributing to knee flexion, but gastrocnemius (F_{max} +8%) contributed more to this motion. Increased knee extension moment of the average children's model mainly resulted from a stronger vastus (F_{max} +8%). Increased strength of rectus femoris showed no impact on knee extension as the muscle was too short at the selected hip position during knee extension moment calculation and measurement. Decreased plantarflexion ability in the average children's model is mainly caused by a weaker soleus (F_{max} -15%).

3.1.2 Maximum isometric joint moments of ND-Models

The total maximum isometric joint moment in Figure 3.1 to Figure 3.4 looks similar in scaled adults and average children's models, with largest differences of approximately 20%. However, according to Table 3.2, the contributions of some of the involved muscles are quite different due to specific differences in maximum isometric muscle force and moment arm.

Calculated joint moment-angle curves agreed at large with literature results, except for hip extension and ankle plantarflexion, where two to three times larger maximum isometric joint moments are generated by the models. For hip flexion and abduction as well as ankle dorsiflexion are the simulated results for maximum isometric joint moments corresponding with the experimental results. Slightly higher values than measured were calculated in the average children's model for hip adduction as well as knee flexion and extension. Significant difference can be seen for hip extension and ankle plantarflexion between simulated and measured results.

72
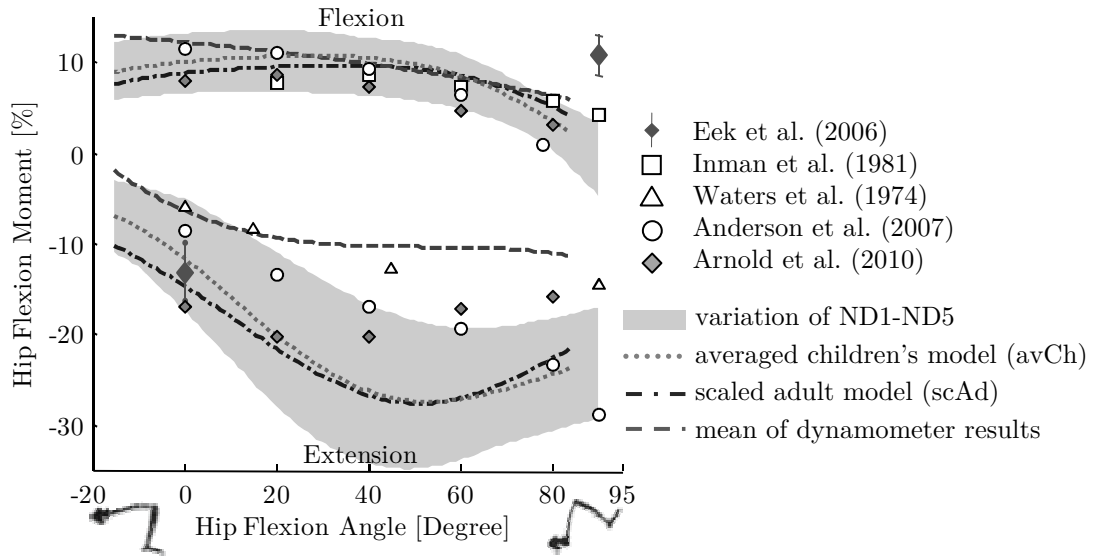
Figure 3.1 Normalized maximum isometric hip flexion/extension moments - Comparison of models of normally developing children (ND), the average children's model (avCh), the mass-scaled adult model (scAd), exerimental results and literature data. Knee was flexed 90°. Joint Moment Unit: Moment[Nm]/BW[N]*ht[m] in %
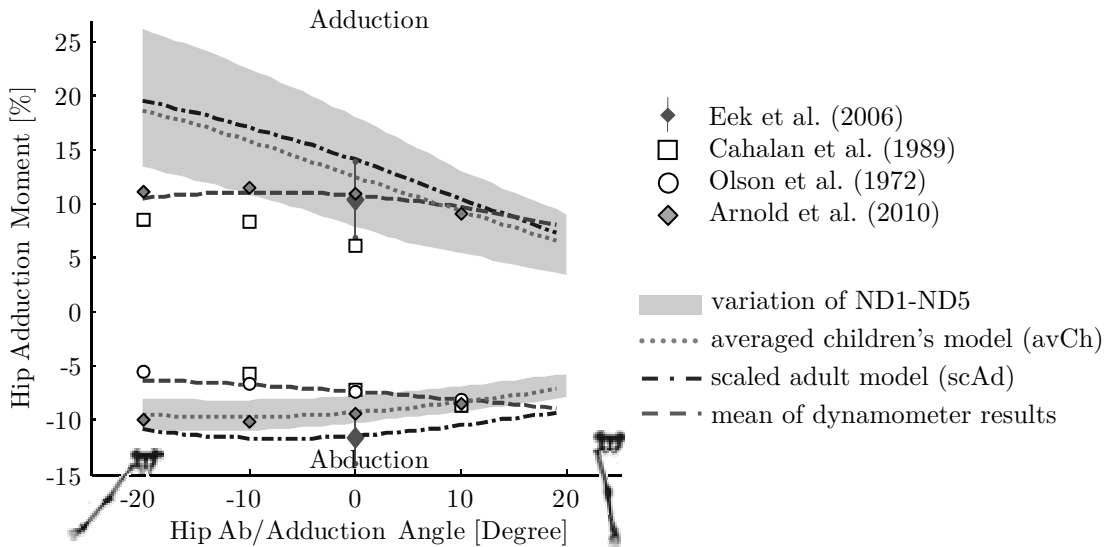
Figure 3.2 Normalized maximum isometric hip ab/adduction moments - Comparison of modles of normally developing children (ND), the average children's model (avCh), the mass-scaled adult model (scAd), exerimental results and literature data. Supine with straight leg. Joint Moment Unit: Moment[Nm]/BW[N]*ht[m] in %

73
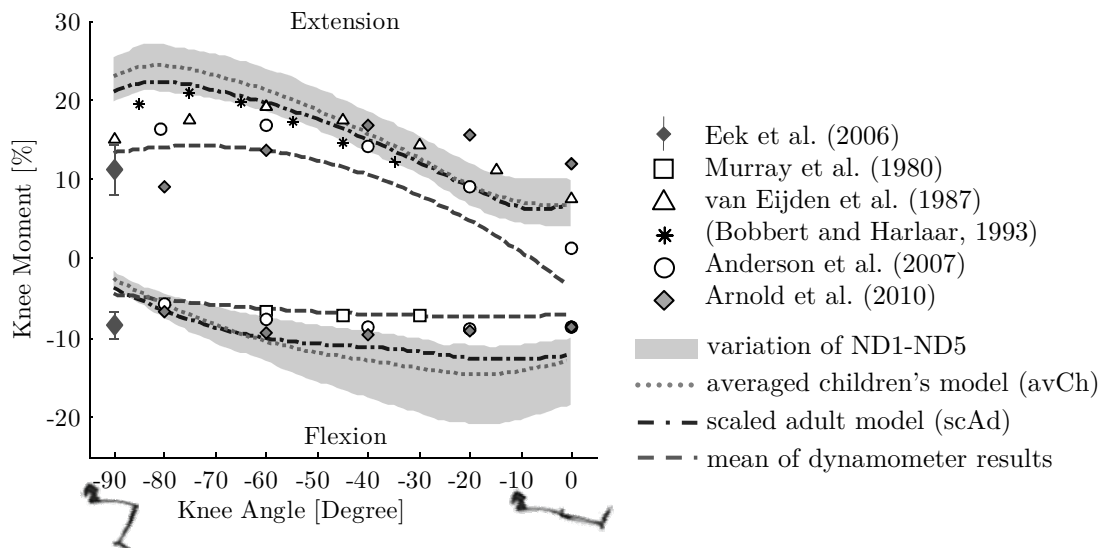
Figure 3.3 Normalized maximum isometric knee moments - Comparison of models of normally developing children (ND), the average children's model (avCh), the mass-scaled adult model (scAd), exerimental results and literature data. Seated position with 80° hip flexion. Joint Moment Unit: Moment[Nm]/BW[N]*ht[m] in %
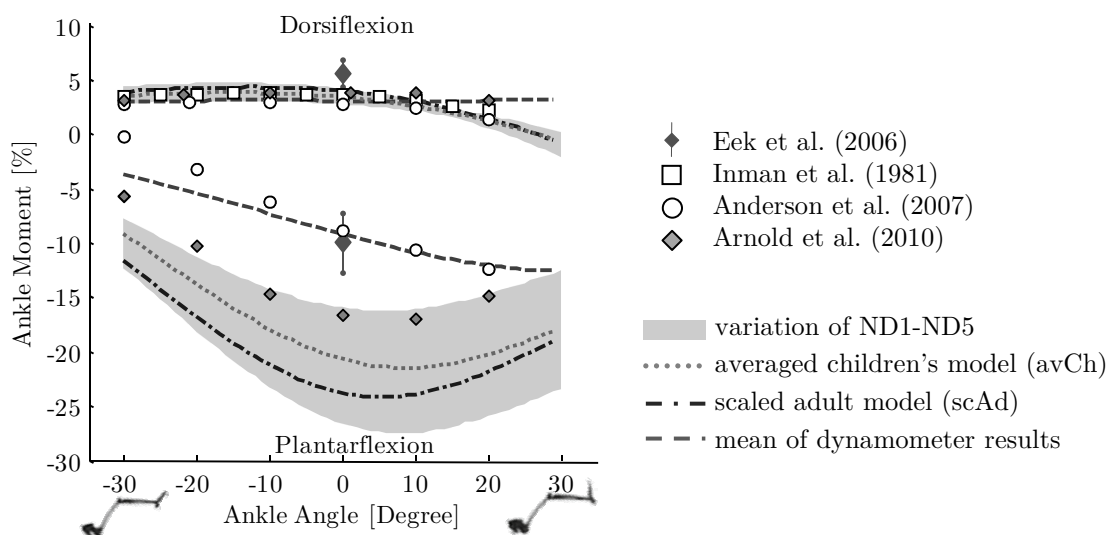
Figure 3.4 Normalized maximum isometric ankle moments - Comparison of models of normally developing children (ND), the average children's model (avCh), the mass-scaled adult model (scAd), exerimental results and literature data. Seated position with hip and knee flexed 60°. Joint Moment Unit: Moment[Nm]/BW[N]*ht[m] in %

74

3.1.3 Summary ND modelling

All individual models (ND1 –ND5) had similar characteristics of their maximum isometric muscle moment – joint angle curves, with individual variations due to subject specific muscle paths and moment arm progression.
5   Detailed model descriptions including all geometrical and physiological model parameters of the five ND children are shown in Appendix A.

3.2 Models of children with CP

3.2.1 Model parameters of CP-models

Table 3.3 shows the normalized musculotendon parameters of the 23 leg
10   muscles in the two MR-based models of CP1 and CP2 and corresponding mean values of ND. Muscle moment arms were calculated as minimal distance of a muscle's path to the related joint centre, averaged over the typical range of joint motion during gait (kinematics see Chapter 4.1, p.97).

CP-children had averaged 18% less total muscle volume (V_m) compared to
15   average of the ND control group, but with very individual differences. CP2 had a 17% enhanced volume of adductor magnus, but smaller moment arm and almost similar muscle volumes for adductor longus, gluteus medius and vastus compared to ND. Muscle volume for gluteus medius and iliopsoas in CP1 were in the area of control group. Gluteus Maximums MA and gluteus
20   medius MA hip abduction were around 35% smaller in CP-children. Hamstrings in both CP-children were around 27% weaker.

Anthropometry of the CP-children to the ND control group is compared in Table 3.4. Displayed segment dimensions of the two CP-children are normalized with the proportion of a models body height to average body
25   height of the ND control group. In comparison to ND had CP1 a 1,2cm (38%) more posterior and 1,1cm (19%) more distal hip joint while CP2 had an almost similar pelvis shape as the normally developing controls. The posterior placed hip joint in CP1 and the gait posture directly affect moment arms of gluteus maximus (-40%) and rectus femoris (+55%).

Modelling Results

	PCSA [cm²]			V$_m$ [cm³]			F$_{max}$ [N]			l$_{mt}$ [cm]			l$_{0m}$ [cm]			l$_{sT}$ [cm]			Moment Arm[cm]			Major Motion
	ND	CP1	CP2	ND	CP1	CP2	ND	CP1	CP2	ND	CP1	CP2	ND	CP1	CP2	ND	CP1	CP2	ND	CP1	CP2	
Adductor longus	6,0	5,1	4,7	49	44	48	198	170	157	16,8	17,7	18,1	8,2	8,1	9,0	8,6	9,7	9,1	4,95/3,66	5,00/2,46	5,20/2,78	Hip Add/Flex
Adductor magnus	19,3	14,3	18,1	215	164	252	637	473	597	21,8	22,7	24,3	11,1	10,7	12,5	11,1	12,4	12,3	4,46	4,30	2,43	Hip Adduction
Biceps femoris short head	4,3	3,6	3,5	37	33	36	143	118	114	17,0	17,6	15,6	8,7	8,7	9,2	8,5	9,0	6,6	2,05	1,47	2,16	Knee Flexion
Extensor digitorum	6,9	4,9	4,7	38	29	29	227	163	155	37,3	37,5	36,0	5,5	5,6	5,4	31,9	32,0	30,7	2,35	3,17	2,20	Dorsiflexion
Flexor digitorum longus	4,3	1,9	2,9	15	7	11	143	63	95	38,6	36,9	37,6	3,4	3,4	3,4	35,3	33,5	34,3	0,51	0,38	0,33	Plantarflexion
Flexor hallucis longus	7,2	5,2	3,5	29	23	15	239	170	114	39,6	40,7	36,6	4,0	4,1	4,0	35,7	36,8	32,8	1,13	0,75	0,73	Plantarflexion
Gastrocnemius	31,7	16,8	12,6	135	79	60	1048	553	415	34,8	36,1	34,4	4,3	4,4	4,2	30,6	31,8	30,2	3,55/2,19	3,23/2,65	3,16/2,65	P-Flex/Knee Flex
Gluteus maximus	23,1	17,1	13,7	321	274	218	764	565	451	22,2	23,5	20,2	13,9	14,9	14,3	9,3	9,6	7,0	4,63	2,77	3,78	Hip Extension
Gluteus medius	17,5	15,1	16,3	112	118	115	579	499	539	9,4	9,7	7,5	6,4	7,3	6,3	3,4	2,9	1,6	3,44	2,39	2,33	Hip Abduction
Gluteus minimus	4,3	2,7	3,0	22	16	17	142	88	99	6,8	7,2	5,1	5,1	5,7	5,0	1,8	1,6	0,2	3,36	2,68	2,24	Hip Abduction
Gracilis	2,2	2,2	1,2	39	40	26	74	71	39	29,1	27,8	30,6	17,6	17,3	19,1	11,6	10,7	11,7	4,67	4,21	4,14	Hip Adduction
Hamstrings	28,4	20,4	16,3	211	159	147	939	675	539	32,7	32,5	32,5	7,4	7,3	8,1	25,4	25,3	24,5	4,07/2,23	4,44/2,51	4,65/1,48	Hip Ex/Knee Flex
Iliopsoas	11,4	9,4	6,3	100	101	61	377	310	208	15,5	13,8	12,1	8,7	10,0	8,7	7,0	4,0	3,7	2,59	2,89	2,71	Hip Flexion
Pectinius	5,3	5,3	1,6	52	56	19	175	174	53	13,8	13,9	11,2	9,9	10,0	10,8	4,0	3,9	0,4	2,65	2,23	1,43	Hip Flexion
Peroneus	11,3	7,3	4,9	43	31	21	372	239	161	36,2	36,7	31,9	3,9	3,9	3,8	32,4	32,9	28,2	1,06	0,73	0,71	Plantarflexion
Piriformis	7,6	4,6	5,8	15	11	13	251	153	192	9,5	8,4	9,8	1,9	2,2	2,0	7,5	6,3	7,8	1,04	0,62	-0,05	Hip Abduction
Rectus femoris	17,7	11,4	8,7	109	76	64	585	376	289	33,4	34,6	35,8	6,1	6,2	6,6	27,4	28,6	29,4	2,84/2,94	4,45/3,19	2,99/3,44	Hip Flex/Knee Ex
Sartorius	1,9	2,0	1,8	60	69	69	61	65	60	39,8	39,8	42,5	32,0	32,8	33,8	7,7	7,0	8,7	2,66/1,20	5,92/1,69	3,84/1,85	Hip Fl/Knee Fl
Soleus	46,9	32,1	26,1	157	119	97	1547	1061	862	26,9	28,2	26,5	3,3	3,4	3,3	24,0	25,2	23,6	3,41	3,00	2,95	Plantarflexion
Tibialis anterior	8,8	6,9	4,0	46	39	23	292	228	131	30,9	29,1	29,2	5,2	5,3	5,1	25,8	23,9	24,1	3,69	4,12	3,80	Dorsiflexion
Tibialis posterior	16,0	12,9	12,4	45	40	39	527	425	410	30,4	28,7	30,4	2,8	2,9	2,8	27,6	26,0	27,7	0,68	0,57	0,42	Plantarflexion
Tensor fasciae latae	3,0	2,9	2,5	23	24	22	98	94	82	38,1	37,6	39,7	7,7	7,9	8,1	30,4	29,7	31,6	2,77/3,56	4,95/2,38	3,82/2,52	Hip Flex/Abd
Vastus	74,6	56,8	61,7	588	479	594	2460	1874	2036	30,2	29,5	31,8	7,9	7,9	8,6	22,7	22,0	23,6	3,02	3,26	3,45	Knee Extension

Table 3.3 Musculotendon parameters of models of children with CP - Compared are the resuls of models of the children with cerebral palsy (CP1,CP2) to average parameters of normally developing children (ND) of the same age group that were incorporated in the children's template model (CT). For better comparibility were values for physiological cross sectional area (PCSA), the muscle volume (V_m), and the maximum isometric force (F_{max}) normalized to the average body weight of the normally developing children. The muscle-tendon length (l_{mt}), optimal muscle fibre length (l_{0m}), the tendon slack length (l_{ts}) and the moment arms were normalized according to the average body height of the normally developing children. The moment arms are averaged values of over the typical range of joint motion during gait. Maximum isometric forces and moment arms with significant deviations between control group and CP-children are marked.

3.2.2 Influence of modelling method on CP-models

As mass-length scaling in combination with bone model rotations provides a relatively quick method to create individual models of CP-children, the question raises whether such models based either on a generic adult model or a generic children's template model, can be an adequate substitute to MR-based individual models.

Therefore two additional mass-length-scaled models each of the two CP-children, one based in an adult template (AT) and one based on a child template (CT) were established and compared to MR-based models. As child template model the average children's model (scCh) from Chapter 2.4.8 was used.

Additionally, for investigation of possible geometric errors due to gait marker based scaling of healthy children, the experimental model - a gait marker based scaled version of the AT-model (scAd) as described in Chapter 2.5.1, was generated and added to the comparison.

	scAd	CT	CP1(n)	CP2(n)	CP1AT	CP2AT	CP1CT	CP2CT
PC to Hip Joint - lateral [cm]	5,9	6,1	6,4	6,7	-15,2%	-15,7%	-15,2%	-15,7%
PC to Hip Joint - posterior [cm]	5,0	3,1	4,3	3,1	6,8%	54,6%	-37,3%	-9,2%
PC to Hip Joint - distal [cm]	4,7	5,9	7,0	5,6	-39,0%	-20,1%	-25,7%	-2,7%
Thigh length [cm]	31,6	31,5	31,4	34,1	4,8%	-0,3%	2,9%	-2,0%
Shank length [cm]	32,6	30,2	31,3	30,4	4,0%	6,4%	4,4%	6,6%
Foot (ankle to toe joint) [cm]	13,9	13,9	13,4	13,9	5,9%	3,3%	5,2%	2,6%

Table 3.4 Segment dimensions of models - Mean (L/R) distances of the hip joint centre to the pelvis centre (PC) as well as length of thigh, shank and foot. Values for scaled AT (scAd) and CT and the subject-specific models and of the two children with cerebral palsy (CP1 and CP2) are given in [cm]. Values for the corresponding four mass-scaled based models (CP1AT and CP2AT as well as CP1CT and CP2CT) are given in percentage compared to the MR-based results. Values in the columns marked (n) are normalized to the average body height of the normally developing children for means of better comparability.

The four left columns in Table 3.4 show mean (L/R) distance from pelvis centre (midpoint between anterior iliac spines, PC) to hip joint centre as well as thigh, shank and foot lengths of scAd-model, CT-model and MR-based CP-models (CP1 and CP2).

Modelling Results

The comparison of hip joint centres in scAd and CT indicates that the characteristic shape of the pelvis differs in the two template models. A reason for this is, that the pelvis of the experimental scAd-model was uniformly scaled from the AT shape. Typically this scaling is done by using gait markers, in particular the mean distance of left and right anterior superior iliac spine (ASIS) and posterior superior iliac spine (PSIS) markers. This resulted in a similar lateral dimension of the scAd-pelvis as in the CT-model, but the distal position of the hip joint in the scAd-model was 1,2cm (21%) more proximal and 1,9cm (64%) more posterior.

For means of comparability, the four columns on the right side of Table 3.4 are for mass-length scaled models (CP1AT, CP2AT and CP1CT, CP2CT) and show percentile deviation of joint centres compared to the MR-based results. The hip joint positions in these models were derived similarly to sAT by uniformly scaling the pelvis according to the marked anterior superior iliac spine (ASIS) and posterior superior iliac spine (PSIS) position.

Maximum isometric musce force per kg body weight [N/kg] and deviation of mass-length scaled models

	Model Data [N/kg]				Bias to MRI based results [%]			
	AT	CT	CP1	CP2	CP1AT	CP2AT	CP1CT	CP2CT
Adductor magnus	13	22	16	21	-11,8%	-35,0%	18,7%	-12,5%
Gluteus maximus	25	26	20	16	59,4%	84,3%	30,0%	50,4%
Gluteus medius	29	20	17	19	126,8%	93,1%	18,8%	1,0%
Hamstrings	29	32	23	19	36,8%	60,3%	25,5%	46,0%
Iliopsoas	15	13	11	7	82,4%	150,0%	23,3%	69,0%
Rectus femoris	11	20	13	10	-0,9%	19,3%	42,6%	72,2%
Vastus	63	85	65	70	8,4%	-7,9%	18,9%	1,5%
Gastrocnemius	26	36	19	14	59,0%	109,2%	83,1%	126,8%
Soleus	48	53	37	30	55,6%	89,4%	41,6%	61,9%
Tibialis posterior	12	18	15	14	-2,1%	0,0%	20,3%	15,7%

Table 3.5 Muscle force per kg body weight - Comparison for major muscles of the lower limb for template models and MR-based CP models, as well as percentage of deviation in mass-scaled, template-based CP models to MR based results. Forces for the child-template (CT) and two models for children with cerebral palsy (CP1 and CP2) are calculated from the values in Table 3.3 that were divided by the body mass of the subjects. Values for adult-template model (AT) are divided by a body mass of 75kg.

The observed offset of the hip joint position effects moment arms of related muscles in the template-based models. For example, the highly biased position of hip joint in CP1 leads to a 33% longer moment arm for gluteus maximus and a 30% shorter moment arm for rectus femoris in both, CP1AT and CP1CT, compared to individual MR results (Table 3.1 and Table 3.7). Errors in moment arms are consistent to findings of Scheys et al. (2008) or Correa et al. (2011).

The inference to the notional muscle volume for the mass-length scaled models and the adult template model as shown in Table 3.6 was done by expressing V_m from the equation for the maximum isometric force F_{max}:

$$F_{\max} = PCSA * \sigma = \frac{V_m}{l_{0m}} * \sigma \qquad \rightarrow: \ V_m = \frac{F_{\max}}{\sigma} * l_{0m} \qquad \textbf{(3.1)}$$

Musce volume per kg body weight [cm³/kg] and deviation of mass-length scaled models

	Model Data [cm³/kg]				Devition to MRI based results [%]			
	AT	CT	CP1	CP2	CP1AT	CP2AT	CP1CT	CP2CT
Adductor magnus	5,86	7,44	5,67	8,71	3,0%	-32,9%	31,3%	-14,5%
Gastrocnemius	4,33	4,68	2,71	2,06	59,2%	109,6%	72,6%	127,2%
Gluteus maximus	12,72	11,08	9,46	7,53	34,2%	68,7%	17,2%	47,4%
Gluteus medius	6,52	3,87	4,08	3,96	59,3%	64,3%	-4,9%	-2,0%
Hamstrings	8,33	7,28	5,50	5,09	51,1%	63,1%	32,6%	43,1%
Iliopsoas	4,89	3,45	3,48	2,11	40,3%	130,7%	-0,5%	63,6%
Rectus femoris	2,61	3,76	2,63	2,23	-1,0%	16,7%	43,2%	68,8%
Soleus	6,37	5,42	4,10	3,35	55,3%	90,1%	32,5%	62,1%
Tibialis posterior	1,35	1,55	1,37	1,34	-1,5%	1,0%	13,4%	16,2%
Vastus	18,89	20,32	16,55	20,52	13,9%	-8,1%	23,0%	-0,8%

Table 3.6 Muscle volumes per kg body weight - Comparison for major muscles of the lower limb for template models and MR-based CP models, as well as percentage of deviation in mass-scaled, template based CP models to MR-based results. The volumes for the average children (CT-model), and the two models for children with cerebral palsy (CP1 and CP2) are calculated from the values in Table 3.3 that were divided by the body mass of the subjects. The values for the adult template model (AT) are divided by a body weight of 75kg.

MODELLING RESULTS

Moment arm (normalized to average body height of control group) and deviation of template based, gait marker scaled models (CPxAT, CPxCT) to MRI based results

Muscle	Function	Model Data [cm]				Bias to MRI results [%]			
		AT	CT	CP1	CP2	CP1AT	CP2AT	CP1CT	CP2CT
Adductor magnus	Hip Adduction	4,47	4,46	4,30	2,43	-10,4%	86,7%	-9,1%	97,5%
Gluteus maximus	Hip Extension	4,20	4,63	2,77	3,78	33,7%	2,4%	26,5%	-3,1%
Gluteus medius	Hip Abduction	3,45	3,44	2,39	2,33	38,8%	61,4%	20,3%	35,5%
Hamstrings	Hip Extension	3,45	4,07	4,44	4,65	-12,1%	-12,7%	-2,1%	-2,8%
Iliopsoas	Hip Flexion	2,53	2,59	2,89	2,71	-1,3%	9,4%	-13,5%	-4,1%
Rectus femoris	Hip Flexion	2,57	2,84	4,45	2,99	-30,4%	7,7%	-31,8%	5,4%
Vastus	Knee Extension	3,12	3,02	3,26	3,45	2,3%	6,3%	-22,0%	-20,5%
Gastrocnemius	Plantarflexion	3,58	3,55	3,23	3,16	2,5%	-1,2%	-20,6%	-23,0%
Soleus	Plantarflexion	3,52	3,41	3,00	2,95	5,6%	-0,3%	-20,7%	-25,3%
Tibialis posterior	Plantarflexion	0,79	0,68	0,57	0,42	11,7%	31,4%	-27,5%	-18,1%

Table 3.7 Moment arms in CP-models - Moment arm of major muscles of the lower limb for template models (AT and CT) and MR-based CP-models (CP1, CP2), as well as   percentage of deviation in gait marker scaled, template based CP models to MR-based results. The distances for the child-template model (CT), and the two MR-based models for children with CP are calculated from values of Table 3.3 divided by the corresponding body weight. Values for the adult-template model (AT) are normalized to body heigh of CT. Deviations shown for template-based models (CPxAT and CPxCT) depict the relation of model specific values in relation to the corresponding value in the corresponding MR-based model.

Different modelling techniques resulted in models with diverging model parameters. The bar graphs in Figure 3.5 show the difference in maximum isometric muscle forces per body weight of nine major lower-limb muscles of the two template models (AT and CT). Figure 3.5a illustrates the difference in body composition of adults and children by contrasting AT and CT. Figure 3.5 (b&c) show the muscle force per body weight of the two MR-based CP-models (CP1 and CP2) compared to the results of the mass-scaled equivalent CP-models based on AT ac CT.
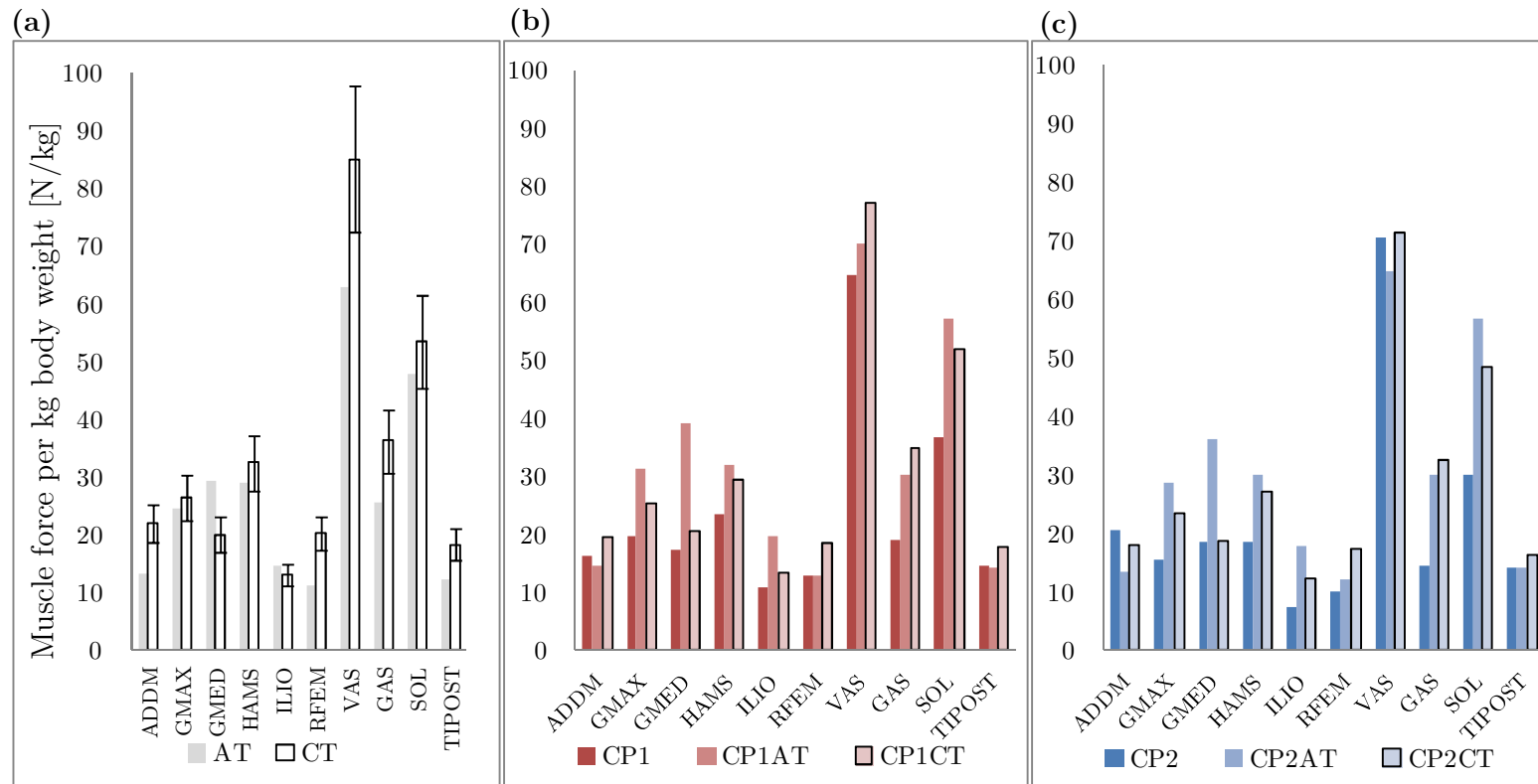
Figure 3.5 Maximum isometric force depending on modelling method - The maximum isometric muscle force per body weight of nine major muscles of the lower limb highligths differences of the diverse modelling approaches. A comparison of the template models (one based on adult's data (AT) and the average children's model (CT=avCh), including variations of the control group), are shown in (a). The modelling results of the two children with cerebral palsy CP1 (b) and CP2 (c) are shown with three modelling approaches applied: MR-based, based on mass-length scaling of AT and of CT

Muscle forces per body weight in Figure 3.5 (b&c) of mass-length scaled models were similar to those of the corresponding template models (a). Individually scaled optimal muscle fibre lengths cause small differences of F_{max} between mass-length-scaled models of each CP-child to its template. Consequently, the models CP1AT, CP2AT as well as CP1CT, CP2CT show similar muscle forces per body weight as corresponding template models. However, these results for maximum isometric muscle force are deviant for some muscles by more than 100% compared to MR-based results.

As forces in mass-length-scaled models were estimated via a modified version of the mass-length scaling law of Correa and Pandy (2011), by using total body mass as described in Chapter 2.5.2 (p.54), the models' body composition was characterized by those of the used template model. Therefore, the total muscle volume per kg body weight for mass-length scaled CP-models, averaged over all muscles, was 28% higher for AT-based models and 22% higher for CT-based models (see Table 3.6 for deviations to MRI-based results). Hence, the maximum isometric forces in mass-length scaled CP-Models were higher compared to MR-based CP- models (see Table 3.5 for bias to MRI-based results). These enhanced maximum muscle forces propagate, similar to deviations in moment arms, to particular muscle contributions to joint moments.

3.2.3 Maximum isometric joint moments in CP

Maximum isometric joint moment-angle characteristics at hip, knee and ankle resulting from the three different modelling techniques were compared. Model postures for joint moment calculations were: for hip flexion/extension: knee flexed 90°; for knee flexion/extension: hip flexed to 60°, and for ankle plantar/dorsiflexion: hip and knee flexed to 60° (see Chapter 2.2.2). Total joint moments were determined at each position by summing up maximal contributions of all agonist muscles and subtracting passive moments of antagonistic muscles. Including counteracting moments was particularly important when calculating the knee extension moment, as passive forces of hamstrings generated a considerable knee flexion moment because these muscles were nearly fully stretched.

Figure 3.6 and Figure 3.7 show maximum joint moments over a range of joint motion for hip, knee and ankle in several models. To compare the joint moments of different models the CT-model was selected as norm. First, results of all CP-models were normalized with respect to age and weight of the CT-model by using a method proposed by Eek et al. (2006). Dimensionless values were calculated in a second step by dividing the resulting joint moment with weight and height of the CT-model (1,34 m, 30,3 kg) for better comparability with published results in literature. Computed average results of ND were similar to those for the average child template model (CT).

Summarizing, MR-based CP-models could generate around 50% lower joint moments compared to the normally developing control group. Template based CP-models could generate higher joint moments at all degrees of freedom with mostly around 30% increase, but in some cases to up to 100% higher values compared to MR-based CP-models. Only for hip flexion of CP1 higher maximum joint moments in the MR-based model (Figure 3.6a) were observed, what is caused by a longer moment arm of rectus femoris with regard to anatomically inferior positioned hip joint centres (see Table 3.4 and Table 3.3). Both MR-based CP models show a decreased ability to generate ankle plantarflexion while the template based models predict results that are in the range of normally developing children (Figure 3.7 c&d).
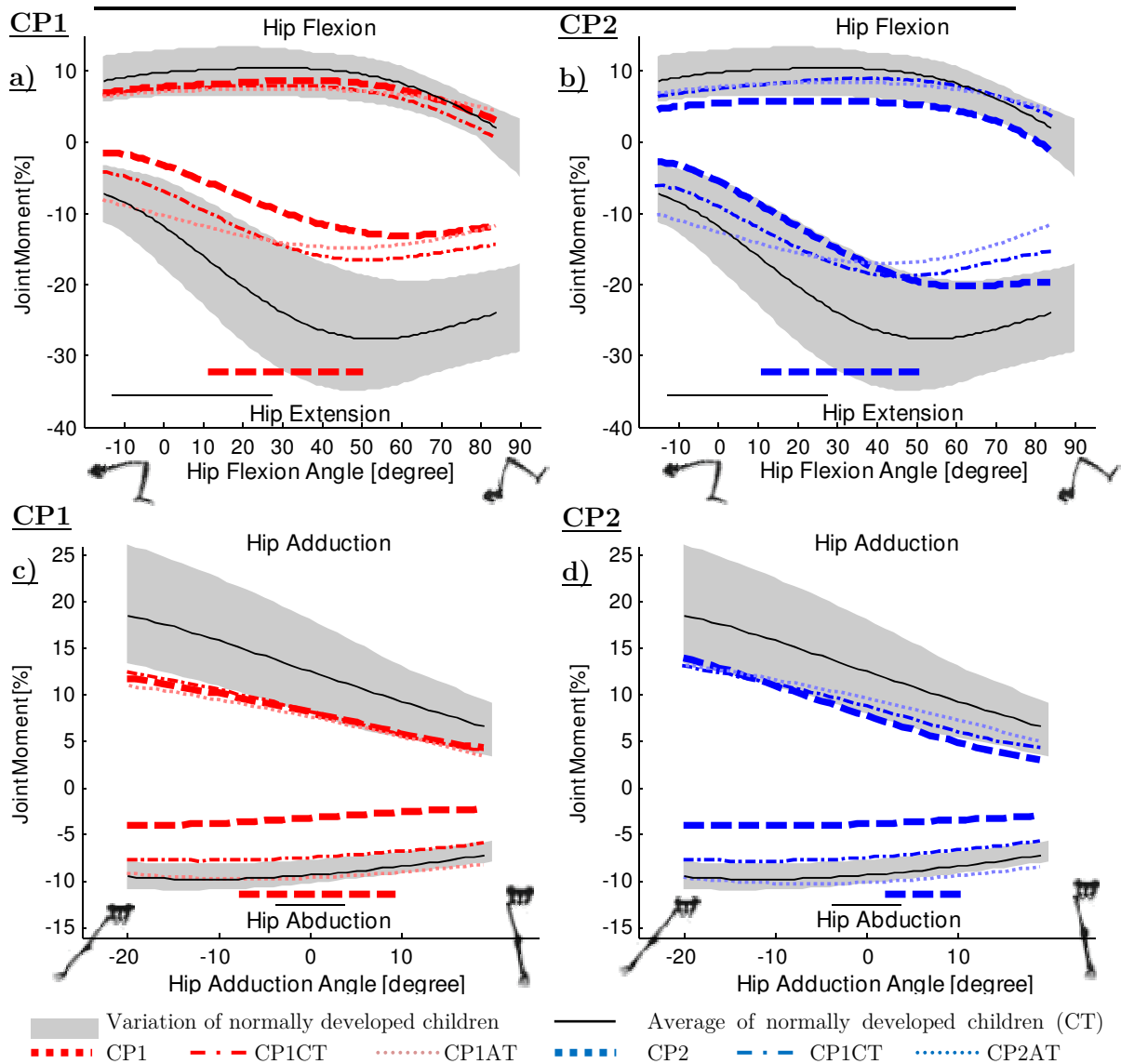
Figure 3.6 Normalized maximum isometric joint moments at hip - Results for CP1 left and CP2 right with different modelling techniques. The horizontal bars at the bottom mark the joint angle range, during gait for CP children and the control group. This interval was used to calculate the mean moment arms of the muscles. Maximum hip flexion and hip adduction moments for CP1 are shown in (a) and (c) and for CP2 in (b) and (d) respectively. Joint moments were normalized to ND-average age and weight with a method proposed by Eek et al. (2006). Dimensionless values were obtained by dividing the resulting moments by the average body weight (30.3kg) and average body height (134cm) of the normally developing children.

Figure 3.7 Normalized maximum isometric knee and ankle moments - Results for CP1 left and CP2 right with different modelling techniques. The horizontal bars at the bottom mark the joint angle range, during gait for CP children and the control group. This interval was used to calculate the mean moment arms of the muscles. Maximum hip flexion and hip adduction moments for CP1 are shown in (a) and (c) and for CP2 in (b) and (d) respectively. Joint moments were normalized to ND-average age and weight with a method proposed by Eek et al. (2006). Dimensionless values were obtained by dividing the resulting moments by the average body weight (30.3kg) and average body height (134cm) of the normally developing children.

3.2.3.1 Comparison of contributions to maximum isometric joint moments of selected muscles in CP-models

Figure 3.8 to Figure 3.16 show the detailed contributions to the maximum isometric joint moments of selected major lower limb muscles of the MR-based models of the CP-children compared to results of mass-length scaled CP-models based on an adults template model (AT) and on a children's template model (CT).

The selected muscles are:

(i)   Hip flexion: rectus femoris, iliopsoas
(ii)   Hip extension: gluteus maximus, hamstrings, adductor magnus, gluteus medius
(iii)   Hip adduction: adductor magnus, hamstrings
(iv)   Hip abduction: gluteus medius, rectus femoris
(v)   Knee extension: vastus, rectus femoris
(vi)   Knee flexion: Hamstrings, gastrocnemius
(vii)   Ankle dorsiflexion: tibialis anterior
(viii) Ankle plantarflexion: gastrocnemius, soleus
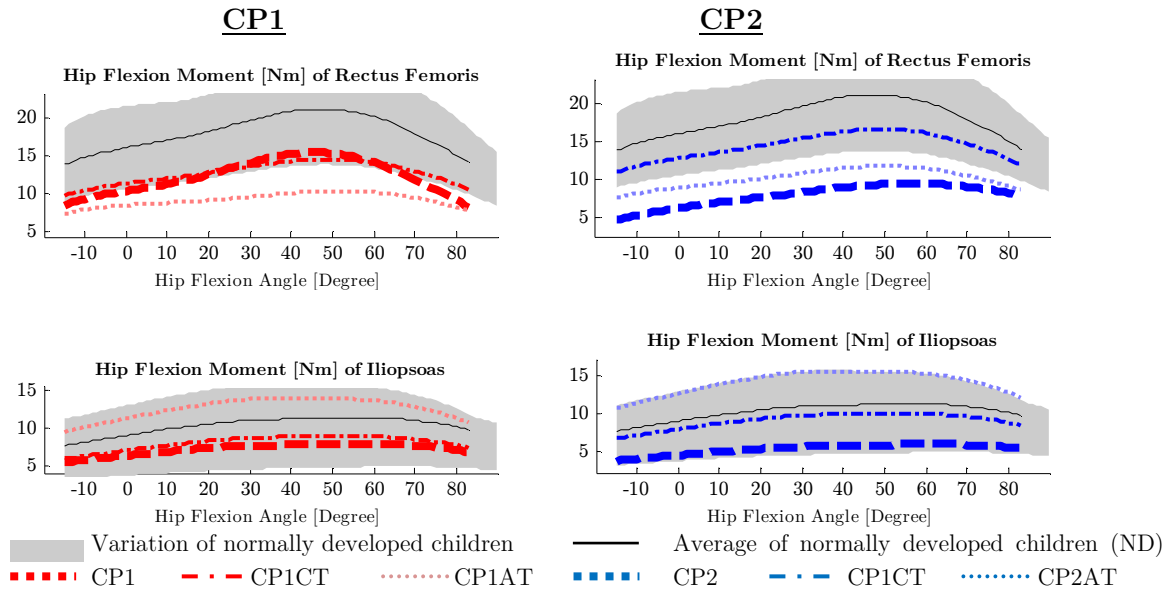
Figure 3.8 Contributions to maximum isometric hip flexion - generated by rectus femoris and iliopsoas of the CP-children (CP1 left, red; CP2 right, blue) determined with different modelling approaches, in comparison to ND.

CP1

CP2

Hip Extension Moment [Nm] of Gluteus Maximus

Hip Extension Moment [Nm] of Gluteus Maximus

Hip Extension Moment [Nm] of Hamstring

Hip Extension Moment [Nm] of Hamstring

Variation of normally developed children — Average of normally developed children (ND)

CP1 — · — CP1CT ·········· CP1AT ▪▪▪▪▪ CP2 — · — CP1CT ·········· CP2AT
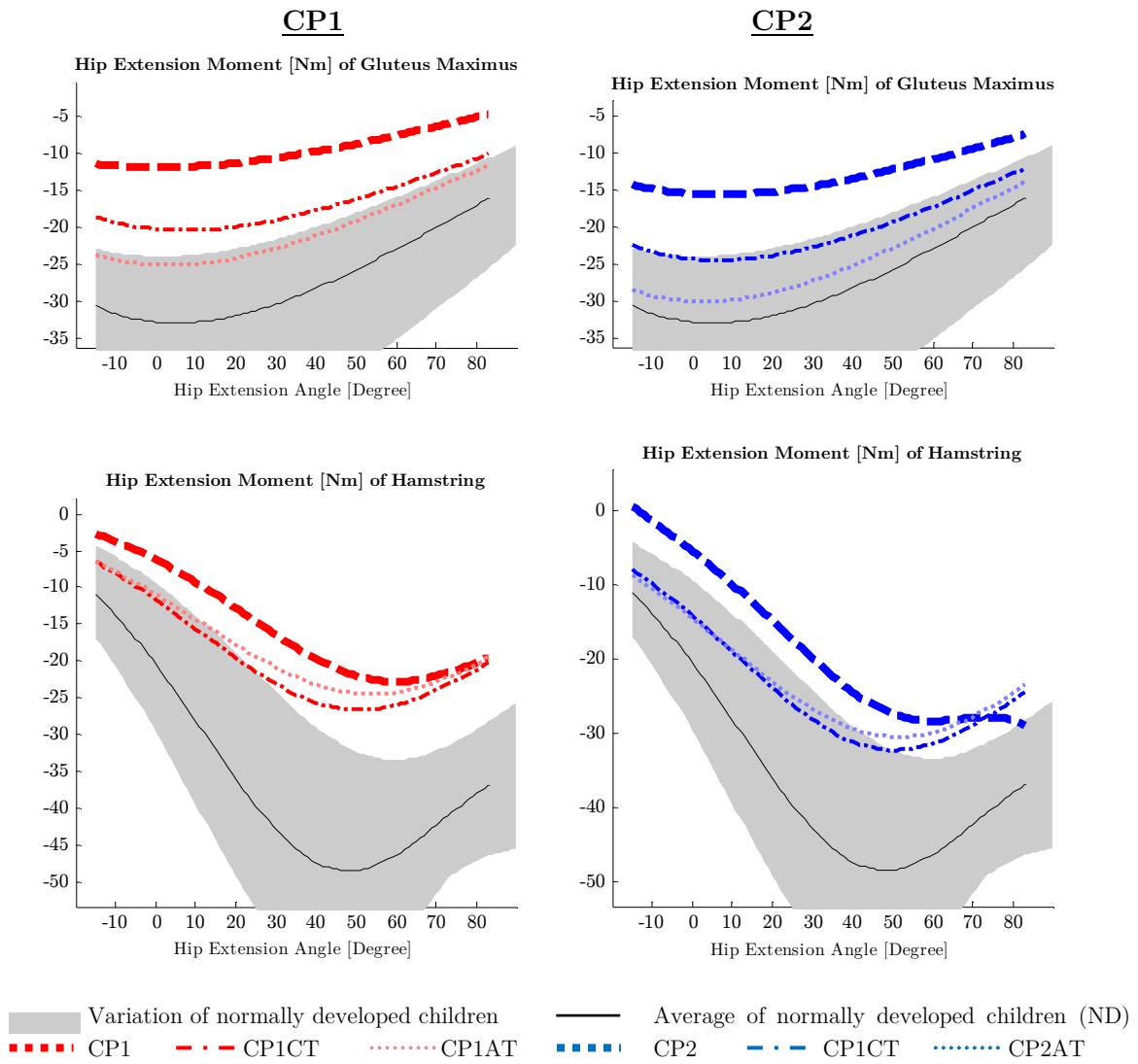
Figure 3.9 Contributions to maximum isometric hip extension - generated by gluteus maximus and hamstrings of the CP-children (CP1 left, red; CP2 right, blue) determined with different modelling approaches, in comparison to ND.

CP1   CP2
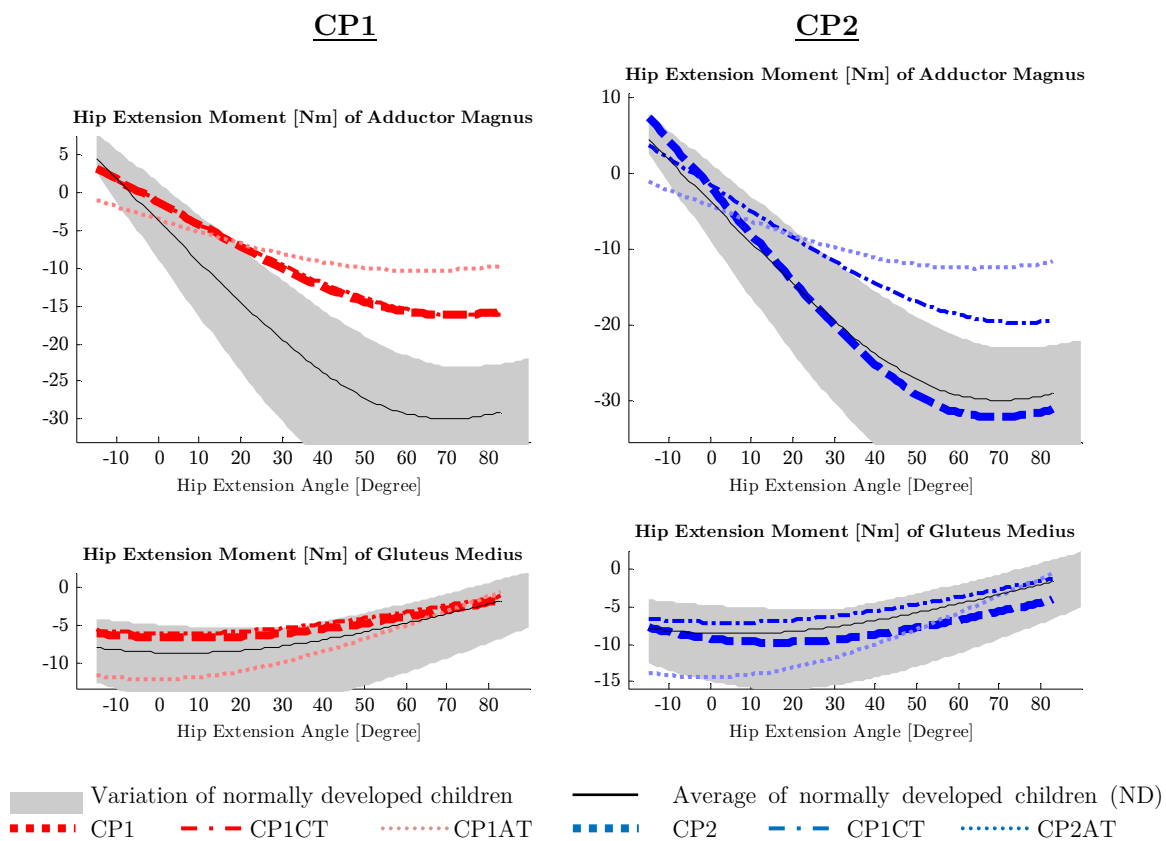
Figure 3.10 Contributions to maximum isometric hip extension - generated by adductor magnus and gluteus medius of the CP-children (CP1 left, red; CP2 right, blue) determined with different modelling approaches, in comparison to ND.

CP1

CP2
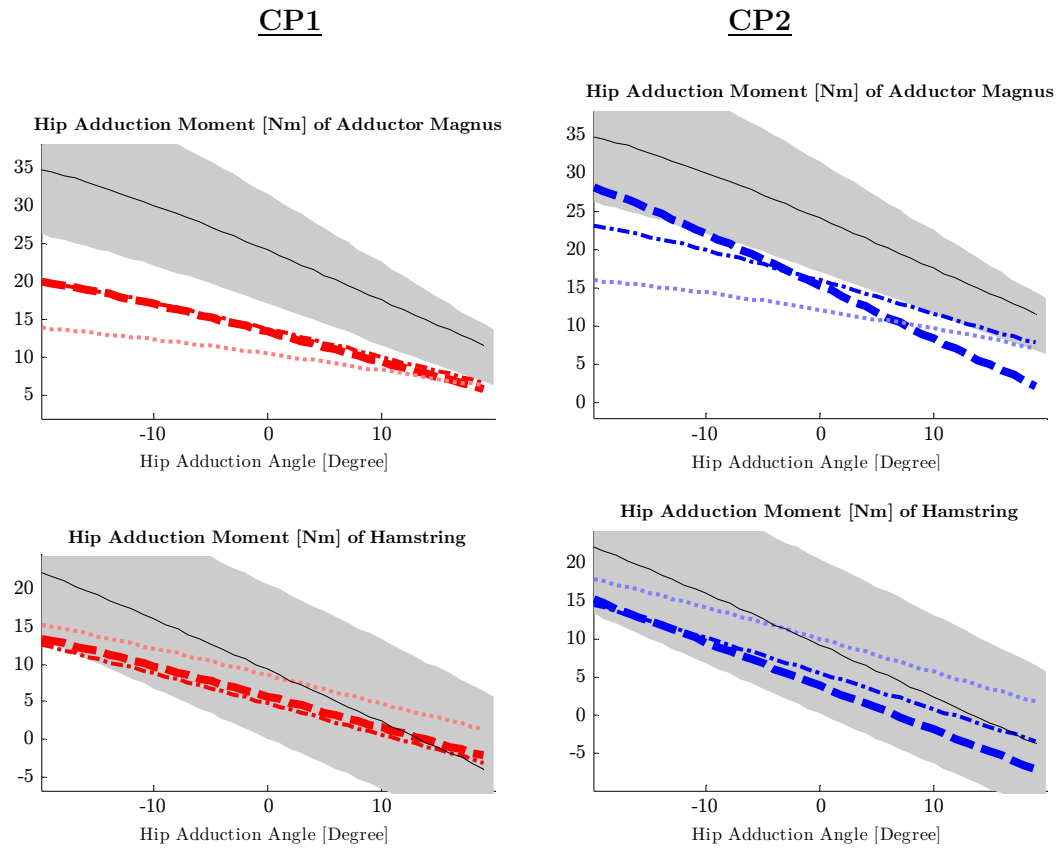
Figure 3.11 Contributions to maximum isometric hip adduction generated by adductor magnus and hamstrings of the CP-children (CP1 left, red; CP2 right, blue) determined with different modelling approaches, in comparison to ND.

Figure 3.12 Contributions to maximum isometric hip abduction - generated by gluteus medius and rectus femoris of the CP-children (CP1 left, red; CP2 right, blue) determined with different modelling approaches, in comparison to ND.

CP1

CP2

Knee Extension Moment [Nm] of Vastus

Knee Extension Angle [Degree]

Knee Extension Moment [Nm] of Vastus

Knee Extension Angle [Degree]

Knee Extension Moment [Nm] of Rectus Femoris

Knee Extension Angle [Degree]

Knee Extension Moment [Nm] of Rectus Femoris

Knee Extension Angle [Degree]

| | Variation of normally developed children | | Average of normally developed children (ND) |
| CP1 | CP1CT | CP1AT | CP2 | CP1CT | CP2AT |

Figure 3.13 Contributions to maximum isometric knee extension - generated by vastus and rectus femoris of the CP-children (CP1 left, red; CP2 right, blue) determined with different modelling approaches, in comparison to ND.

CP1

CP2

Knee Flexion Moment [Nm] of Hamstring

Knee Flexion Moment [Nm] of Hamstring

Knee Flexion Moment [Nm] of Gastrocnemius

Knee Flexion Moment [Nm] of Gastrocnemius

| | Variation of normally developed children | | | Average of normally developed children (ND) |
| CP1 | CP1CT | CP1AT | CP2 | CP1CT | CP2AT |
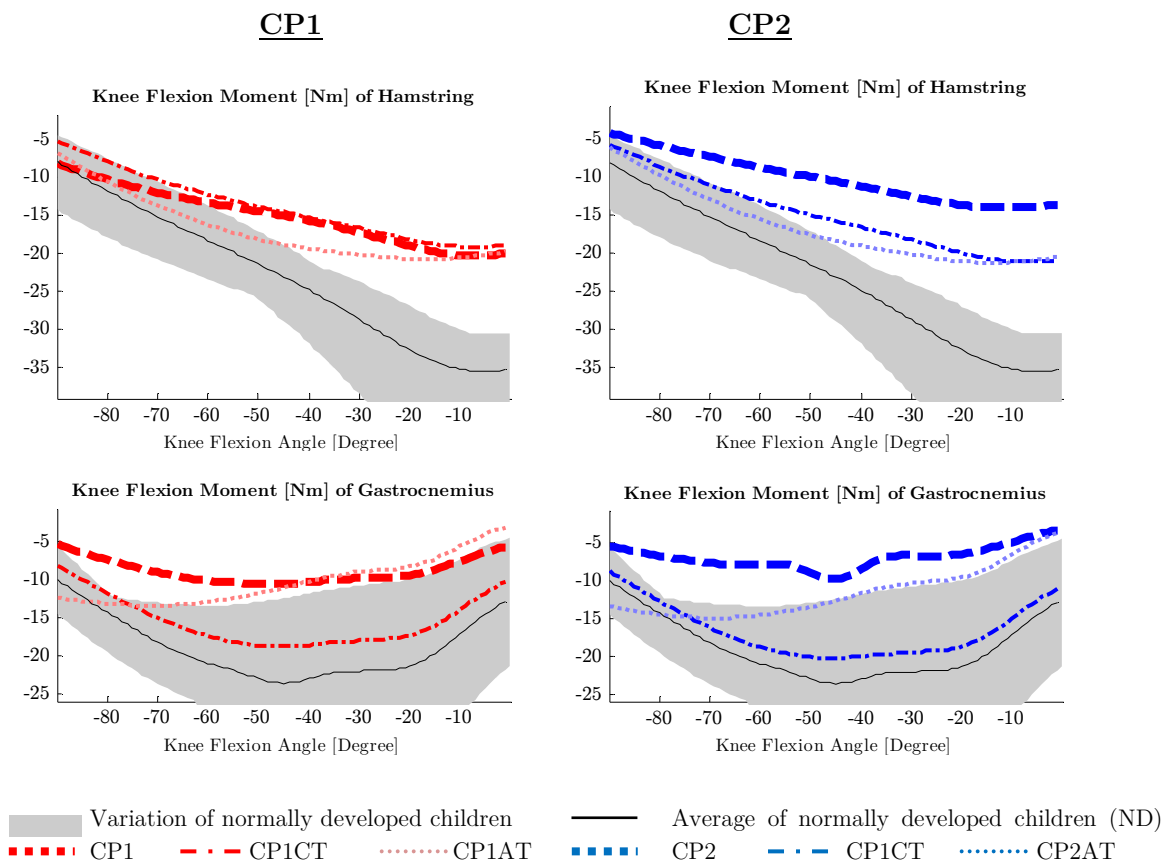
Figure 3.14 Contributions to maximum isometric knee flexion - generated by hamstings and gastrocnemius of the CP-children (CP1 left, red; CP2 right, blue) determined with different modelling approaches, in comparison to ND.

CP1

CP2
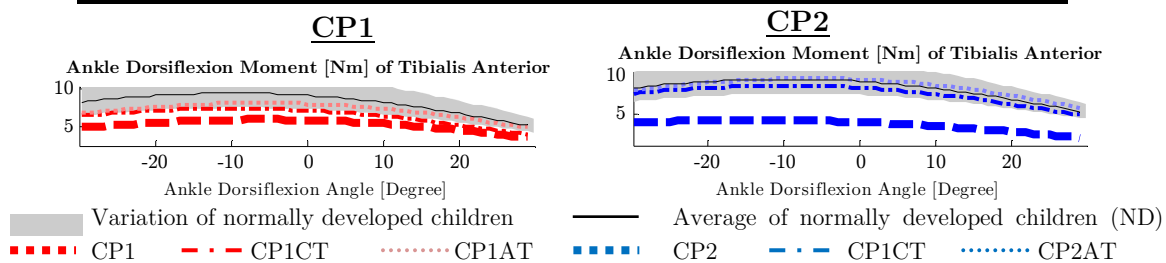
Figure 3.15 Contributions to maximum isometric ankle dorsiflexion - generated by tibialis anterior of the CP-children (CP1 left, red; CP2 right, blue) determined with different modelling approaches, in comparison to ND.

CP1

CP2
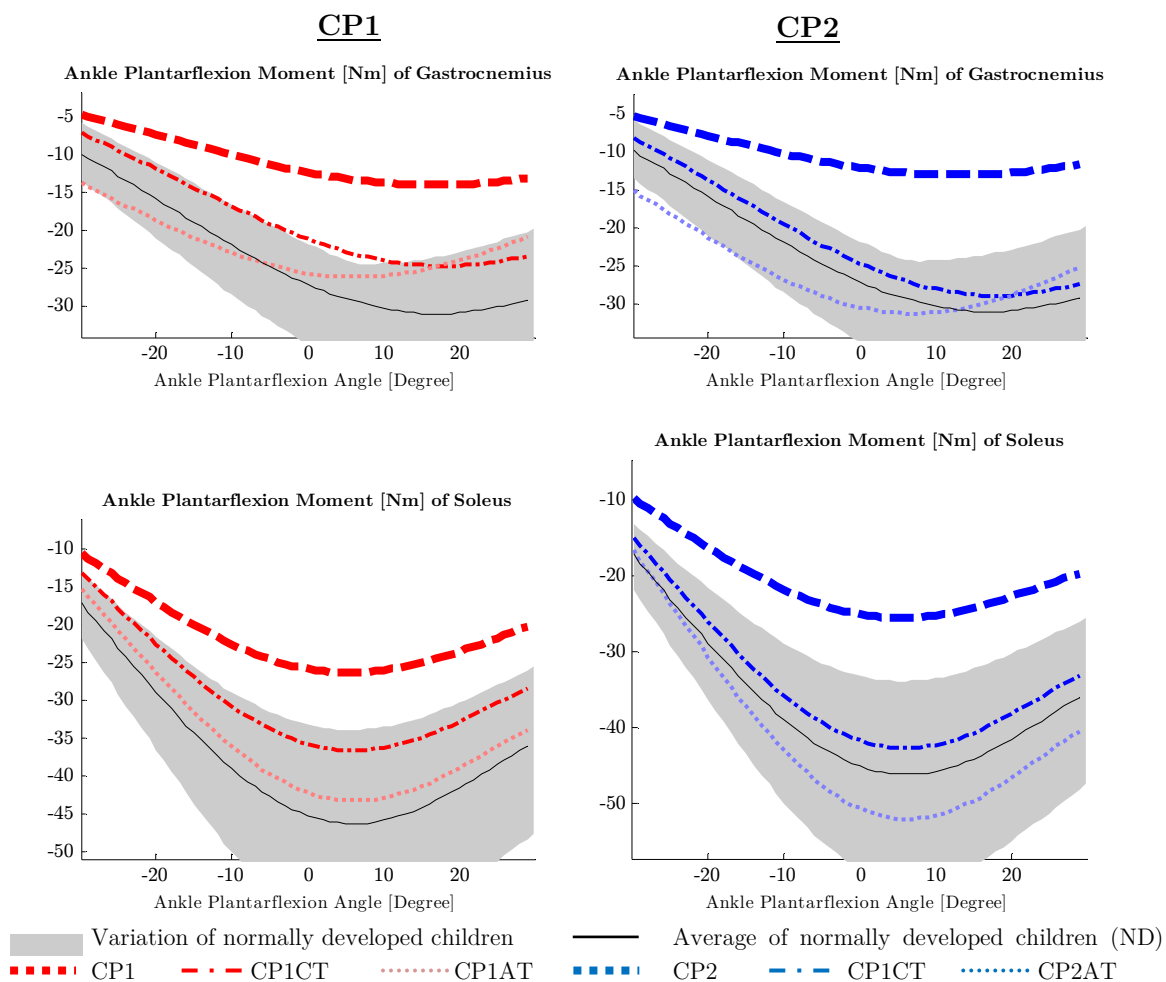
Figure 3.16 Contributions to maximum isometric ankle plantarflexion - generated by gastrocnemius and soleus of the CP-children (CP1 left, red; CP2 right, blue) determined with different modelling approaches, in comparison to ND.

3.2.4 Summary CP modelling

Computational simulations of musculoskeletal models offer a new perspective for medical routine to assess movement disorders and obtain detailed insight into muscle function. A compromise between accuracy and time effort in generating biomechanical models is made, when existing generic models are customized via scaling processes, instead of developing individual models based on MR.

Here was to present model data from two children with cerebral palsy and age matched controls, which were based on magnetic resonance (MR) imaging. Scaled biomechanical models based on a generic adult's model (AT) and an averaged children's model (CT) were assessed by comparing model parameters and maximum joint moment characteristics.

This modelling process via mass-length scaling resulted in a similar body composition of the scaled subject's model and the used template As the anatomical differences between template model and CP-subjects are significant, the consequences using mass-length scaling led to bias in muscle functions compared to the MR-based models. Substantial differences were found in moment arms of the muscles around the hip joint as a scaling process based on gait markers did not reproduce the individual geometry of the pelvis. The higher muscle volume of the template models is preserved in the scaled models and leads to errors in maximum isometric force of up to more than 100%.

These errors propagate to the simulated maximum joint moments. Significant differences due to the selected modelling technique can be seen at:

- Hip flexion moment generated by rectus femoris and iliopsoas
- Hip extension and adduction moment generated by
    adductor magnus in CP2
- Hip abduction moment of the CT-based CP-models
- Knee flexion moment generated by gastrocnemius in AT-based
    compared to CT-based models
- Ankle plantarflexion moment generated by soleus and gastrocnemius

Therefore it can be concluded that MR-based models are preferable when individual muscle function in pathological gait shall be investigated..

4

Results of Gait Simulation

CONTENTS

Results of Gait Simulation

To investigate muscle function in gait of children with cerebral palsy (CP1, CP2) in comparison with the control group, consisting of five, age matched, normally developing children (ND) biomechanical simulations and calculations have been executed using OpenSim, as described in Chapter 2.8 (page 62ff).

A detailed comparison in several gait phases as well as an interpretation of individual muscle forces, lengths, moment arms, joint moments and accelerations in gait is given in the following section. Particular results for all single muscles are shown in Appendix B.2.

Displayed results shall help to understand basic differences in muscle function between normal and crouched gait caused by cerebral palsy. The chicken-and-egg problem, whether a muscles' function is a reaction to the crouched posture or if a specific muscles behaviour or is causing the CP-characteristic crouched gait is approached by investigating the following:

(i)   Chapter 4.2 answers the question which muscles contribute most significantly to the net moments exerted about the hip, knee, and ankle in normal and crouch gait

(ii) In Chapter 4.3 the most significant muscle contributions towards angular accelerations of hip, knee, and ankle in normal and crouch gait are analysed.

(iii) Chapter 4.4 shows, which muscles contribute most significantly to the vertical, lateral and fore-aft accelerations of the centre of mass of the body in normal and crouch gait.

(iv) Chapter 4.5 summarizes results of a muscle length analysis of identified main contributors showing, where on their force-length curves these muscles operate during normal and crouch gait.

(v)   In Chapter 4.6 the contributions of particular muscles towards CoM and joint accelerations are examined. Analyses are given, whether the observed contributions of these muscles might be interpreted as a reaction to the observed crouched posture in CP-gait or if a dysfunction of a certain muscle can be identified as reason for the crouched gait posture

4.1 Kinematic analysis of crouched gait

The gait data presented in Figure 4.1 and Figure 4.2 shows that both CP subjects walked with a typical crouched posture, which is characterized by higher hip and knee flexion in all gait phases. Additionally, CP-children have the pelvis more tilted forward (Figure 4.1b) and a higher pelvic movement in all rotational degrees of freedom than ND. Especially CP1 showed high pelvis list motion in gait in combination with extensive ab-/adduction (Figure 4.1c) and an, in average 20°, inward rotated hip joint.
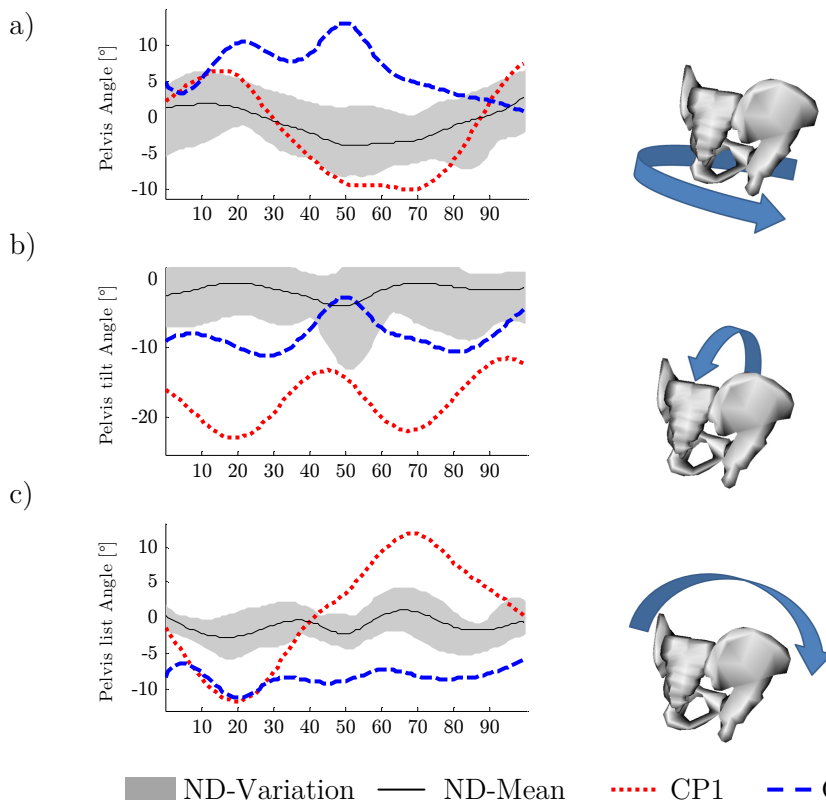
Figure 4.1 Pelvis orientation in gait - a) Pelvis rotation; b)Pelvis tilt; c) Pelvis list of the CP-children (CP1,CP2) and the control group (ND)

CP2 had a mean adduction of 7° during gait (Figure 4.2c) which is caused by enhanced hip adduction in terminal stance to swing phase. Both CP-children showed a hip joint motion range of 40° in the sagittal plane with, in average of a gait cycle, 20° increased hip flexion compared to ND (Figure 4.2a).
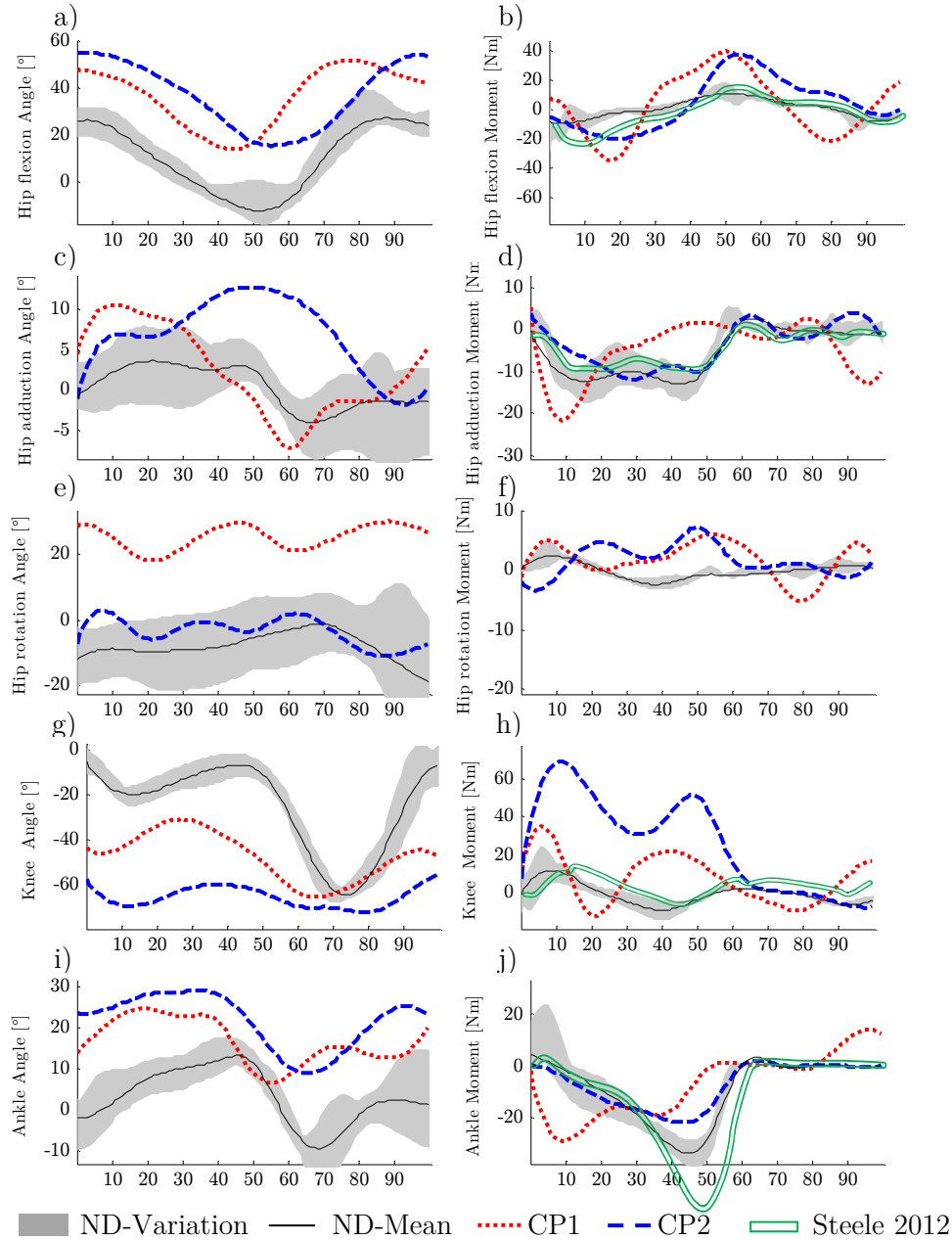
Figure 4.2 Joint angles and joint moments in gait - Comparison of joint angles and joint moments in gait of CP-children (CP1,CP2) and control group (ND) at hip flexion/extension (a,b), abduction/adduction (c,d) and rotation (e,f); and at knee flexion/extension (g,h) and ankle plantar-/dorsiflexion (i,j) in one full gait cycle. Literature data for joint moments from (Steele et al., 2012)

Knee flexion angles for ND in normal gait displayed in Figure 4.2g show a motion range of about 65°. The mean knee flexion in CP1 was +15% compared to ND with a motion range of 35°. The in average +35% increased flexed knee of CP2 compared to ND had a narrow range of utilized knee angle of 20°. CP2 shows an enhanced hip adduction in terminal stance to swing phase. Joint moments for ND are comparable to values given in literature (Steele et al., 2012).
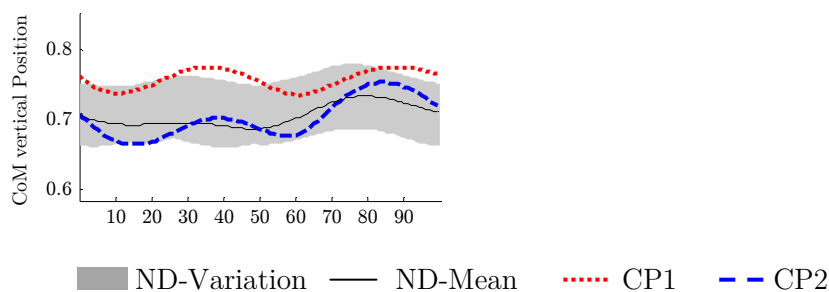
Figure 4.3 CoM vertical position in gait

The course of the vertical CoM position during gait shown in Figure 4.3 illustrates the loss of potential energy in both CP subjects during terminal stance and will be discussed in Chapter 5.4.

4.2 Contributions to joint moments in gait

In the following chapters, characteristics of total joint moment as well as particular muscle contributions to the joint moments of both CP subjects are compared to the average results of the ND control group. 'Common CP' describes behaviour that was seen in both CP subjects, while individual features are noted further. Total joint moments in gait of ND are in accordance to literature data (Steele et al., 2012) as shown in Figure 4.2.

4.2.1 Hip flexion moments (Figure 4.4)

Common CP: Both CP-children show an about threefold higher hip flexion moment in terminal stance and pre-swing phase (Figure 4.4). The contribution of iliopsoas to hip flexion in both CP-children is comparable to the normally developing control group, but significantly more contribution to this motion comes from rectus femoris (see also knee extension in 4.2.3), adductor longus and tensor fasciae latae in second half of stance and during acceleration of swing phase.

CP1: Hip flexion moment in loading response phase of CP1 originates from sartorius.

4.2.2 Hip extension moments (Figure 4.4)

Common CP: A higher hip extension moment can be seen in loading response and mid stance phase of both CP-children, where the hamstrings play an important role.

CP1: Gluteus maximus contributes additionally to hamstrings towards hip extension in terminal stance of CP1. Higher hip extension moment throughout the swing phase may be seen in CP1 that is mainly caused by hamstrings.

CP2: Gluteus medius contributes additionally to hamstrings towards hip extension in CP2.
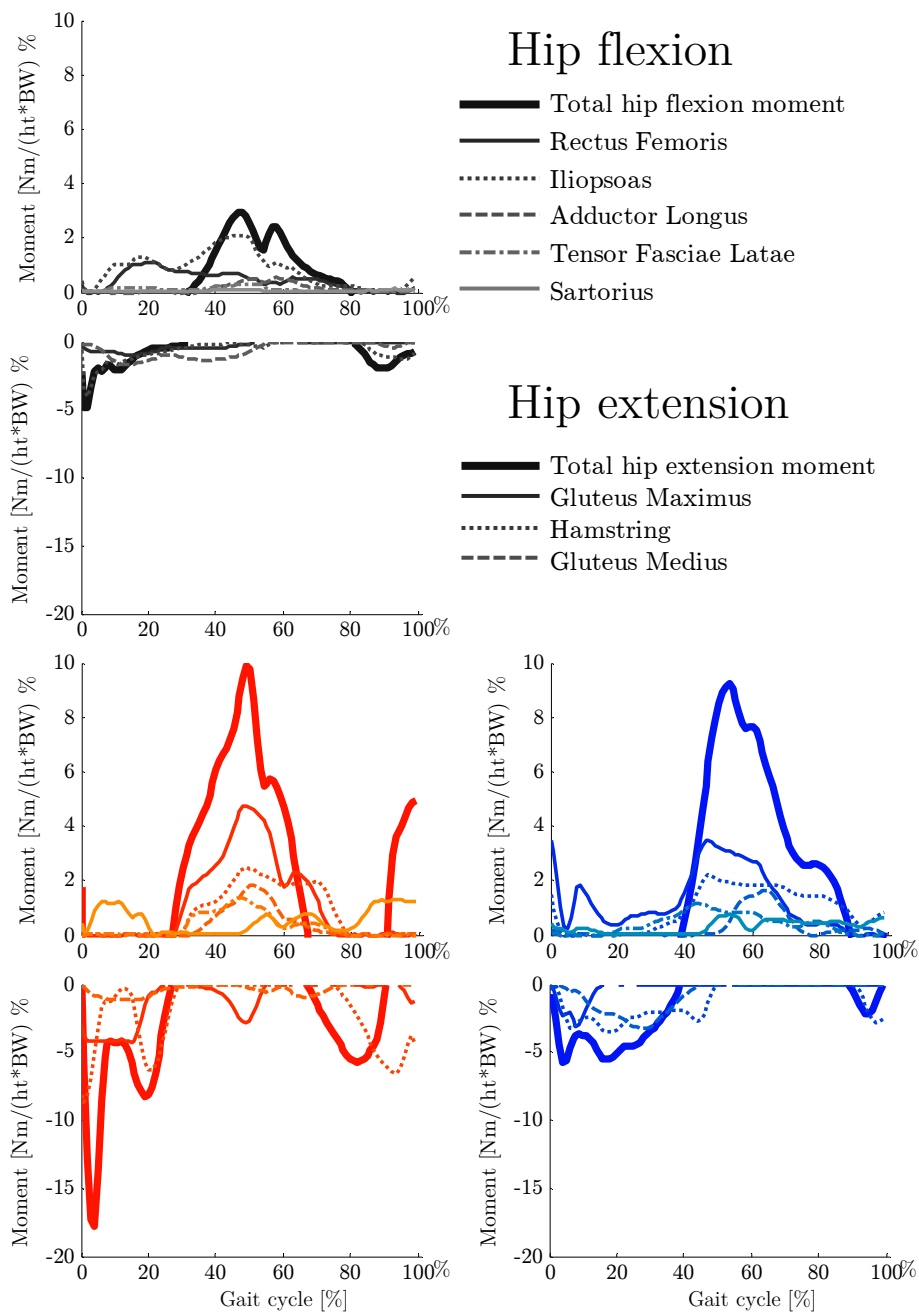
Figure 4.4 Hip flexion/extension moments in gait - Comparison of the hip flexion and extension moments in crouched gait of two subjects with cerebral palsy (CP1: red, CP2: blue) in contrast to normal gait of the control group (ND: black). Thick lines represent the overall joint moments and thin/dashed lines show the individual contributions of the major muscles.
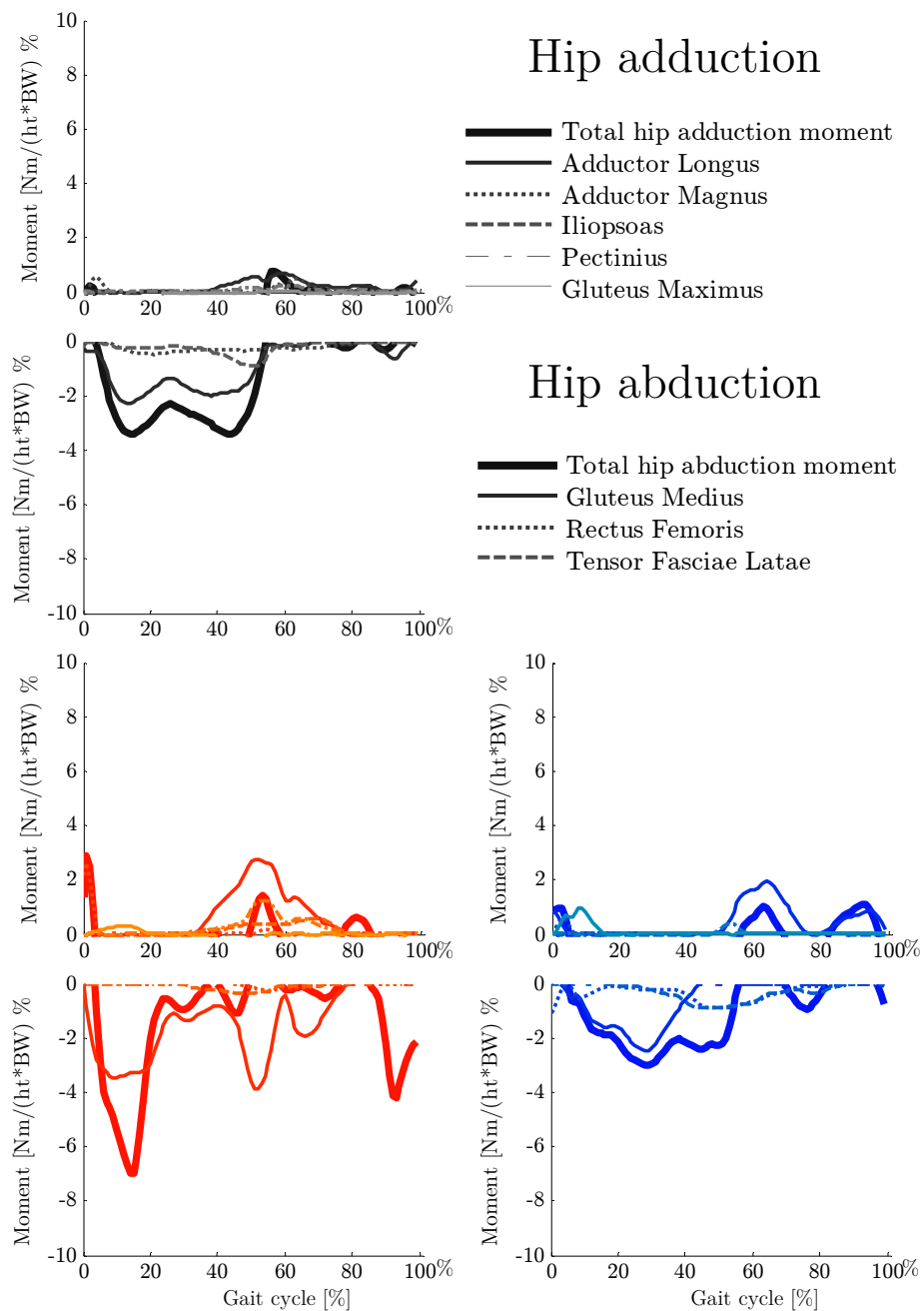
Figure 4.5 Hip add-/abduction moments in gait - Comparison of the hip adduction and abduction moments in crouched gait of two subjects with cerebral palsy (CP1 - red, CP2 - blue) in contrast to normal gait of the control group (ND - black). Thick lines represent the overall joint moments and thin/dashed lines show the individual contributions of major muscles.
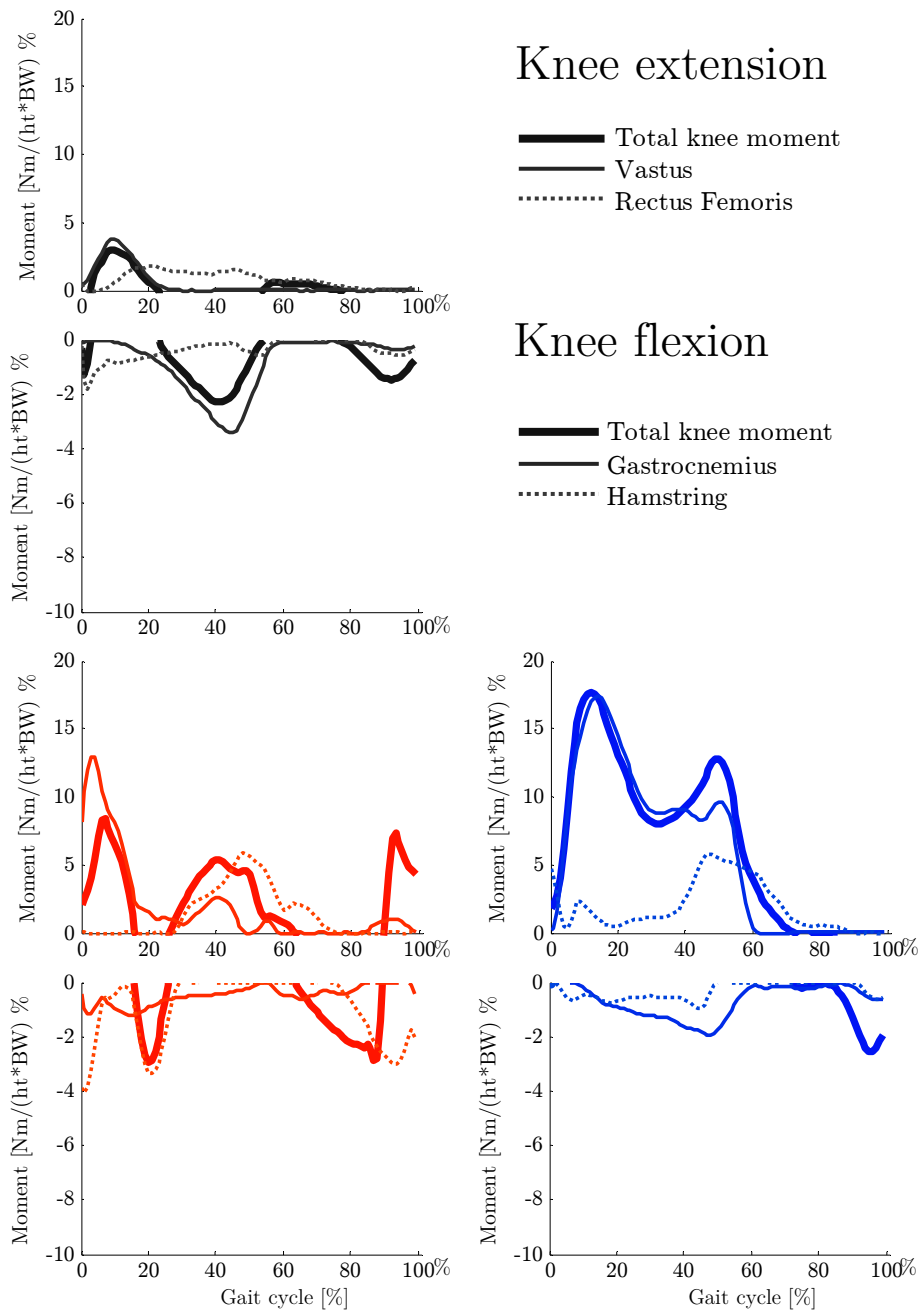
Figure 4.6 Knee extension/flexion moments in gait - Comparison of the knee flexion and extension moments in crouched gait of two subjects with cerebral palsy (CP1: red, CP2: blue) in contrast to normal gait of the control group (ND: black). Thick lines represent the overall joint moments and thin/dashed lines show the individual contributions of the major muscles.
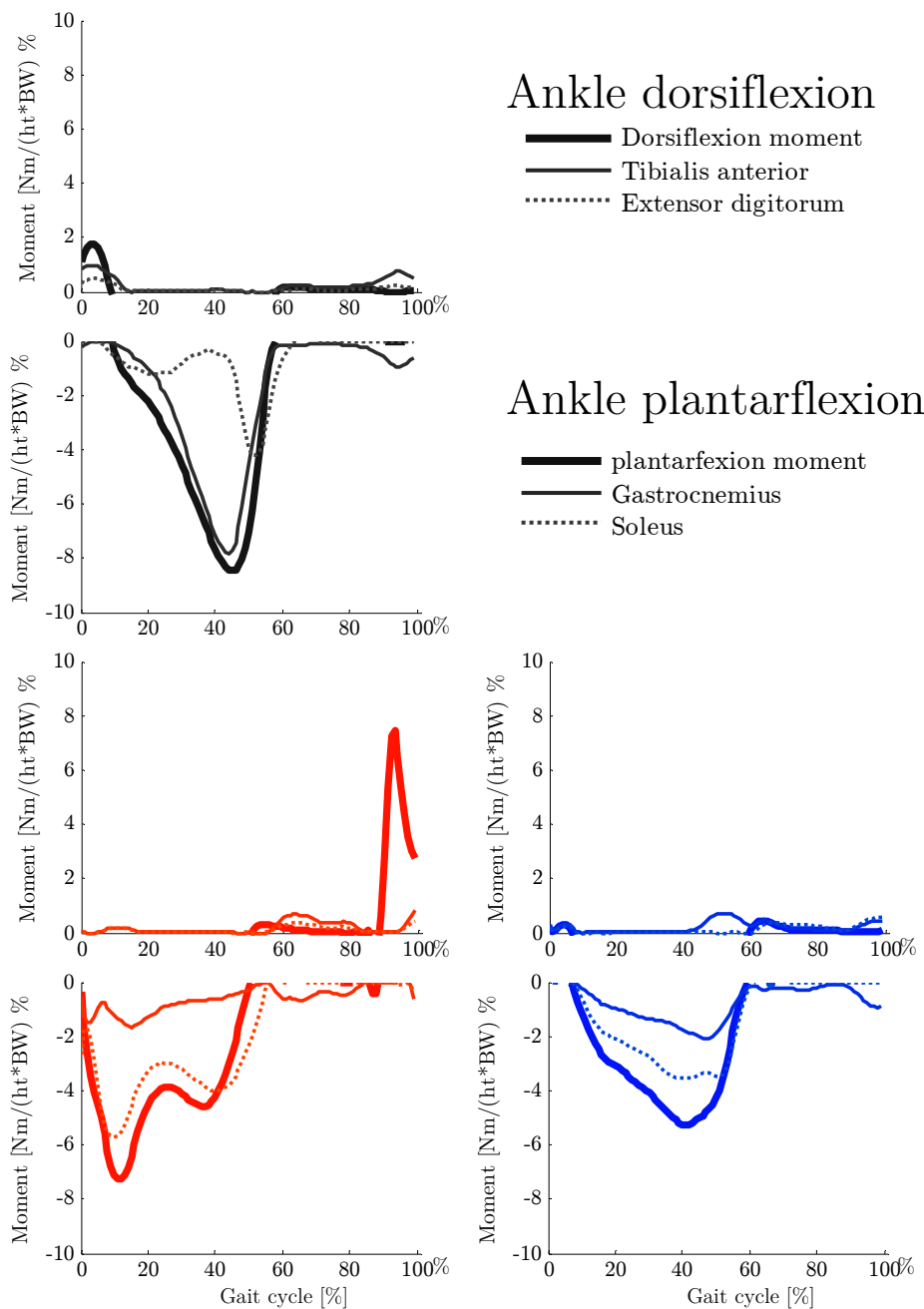
Figure 4.7 Dorsiflexion/plantarflexion moments in gait - Comparison of ankle dorsiflexion and plantarflexion moments in crouched gait of two subjects with cerebral palsy (CP1: red, CP2: blue) in contrast to normal gait of the control group (ND, black). Thick lines represent overall joint moments and thin/dashed lines show individual contributions of major muscles.

4.2.3 Hip ab-/adduction moments (Figure 4.5)

Common CP: The total hip adduction moment is comparable to ND in both CP-children, but adductor longus shows an increased adduction moment in terminal stance and pre-swing, synchronous to its increased hip flexion moment in both cases of CP gait (see Figure 4.4for hip flexion)

CP1: The hip abduction moment is increased in the loading response phase of CP1, mainly driven by gluteus medius. The higher hip adduction moment of to adductor longus is compensated by gluteus medius during pre-swing phase.

CP2: Hip abduction is comparable to ND. No compensation effect for the higher adduction moment of adductor longus is seen in CP2, what may be a reason for the more adducted hip (see Figure 4.2c)

4.2.4 Knee flexion/extension moments (Figure 4.6)

Common CP: Both CP-children show an increased knee extension moment in loading response as well as an additional peak in mid to terminal stance. This knee extension moment peak is generated by rectus femoris in both CP-children and causes rectus femoris to contribute to the hip flexion moment that is seen in mid to terminal stance (see section 4.2.1 or Figure 4.4).

CP1: Knee extension moment in CP1 is decreased and even reverted to a knee flexion moment in mid stance. This knee flexion moment in CP1 is generated by the hamstrings that is active at the same time for extending the hip (see 4.2.2 or Figure 4.4).

4.2.5 Ankle Plantarflexion moments (Figure 4.7)

Common CP: Ankle plantarflexion moment was in both CP-children slightly lower than ND. The role of soleus for generating ankle plantarflexion in both CP is increased compared to ND where this moment is mainly generated by gastrocnemius.

4.3   Contributions to angular accelerations

Muscular contributions of all 52 muscles of the lower limb models were calculated for joint acceleration of hip, knee and ankle during stance phase (55% of gait cycle) by processing the kinematic and kinetic gait data of ND, CP1 and CP2 with the "IncAccPI" plug-in for OpenSim (Dorn et al., 2012a). The joint angles and muscle forces pertaining to the optimization solutions obtained for all subjects were applied to equation (2.20) to determine each muscle's contribution to the joint accelerations during stance and swing. Muscle contributions to the acceleration of the body's centre of mass were found using equations (2.20) and (2.21), noting that the acceleration of the CoM is a function of the accelerations of each of the lower-limb joints.

For better visibility of these results only mayor contributors are shown and further the scale of the ordinate in Figure 4.8 to Figure 4.11 is not uniform across investigated motions. Computed results are shown for the stance phase.

Muscular contributions denoted as 'contralateral' are for muscles on the leg in the opposing gait phase, hence mainly from the leg in the swing phase while the investigated foot is in stance phase. Residual moments describe joint moments that could not be provided by the modelled set of muscles. Such moments are in displayed results mainly acting on the pelvis as MX, MY and MZ and indicate that for better simulation results in CP-gait the connection of HAT and pelvis would require additional actuators. Such additional actuator might be able to transfer acceleration due to balancing actions of the upper body to the lower limbs.

Figure 4.8 Hip flexion/extension accelerations in gait - Angular hip accelerations in crouched gait of two subjects with cerebral palsy (CP1,CP2) in contrast to normal gait of the control group (ND). Thick lines represent the net joint accelerations and thin/dashed lines show the individual contribution of the major muscles.
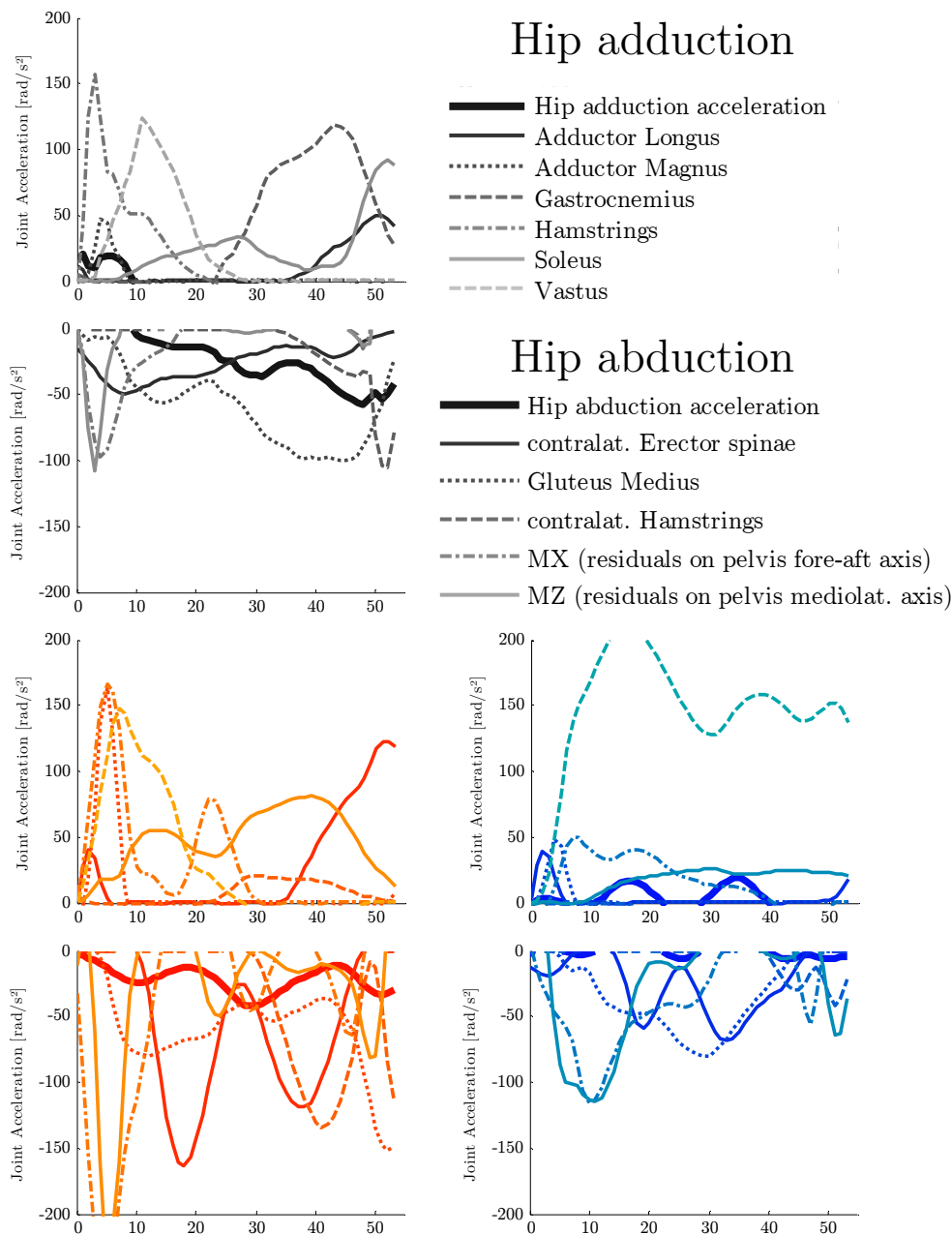
Figure 4.9 Hip add-/abduction accelerations in gait - Angular hip accelerations in crouched gait of two subjects with cerebral palsy (CP1 - red, CP2 - blue) in contrast to normal gait of the control group (ND - black). Thick lines represent the net joint accelerations and thin/dashed lines show the individual contribution of the major muscles.

Figure 4.10 Knee extension/flexion accelerations in gait - Angular knee accelerations in crouched gait of two subjects with cerebral palsy (CP1,CP2) in contrast to normal gait of the control group (ND). Thick lines represent the net joint accelerations and thin/dashed lines show the individual contribution of the major muscles.
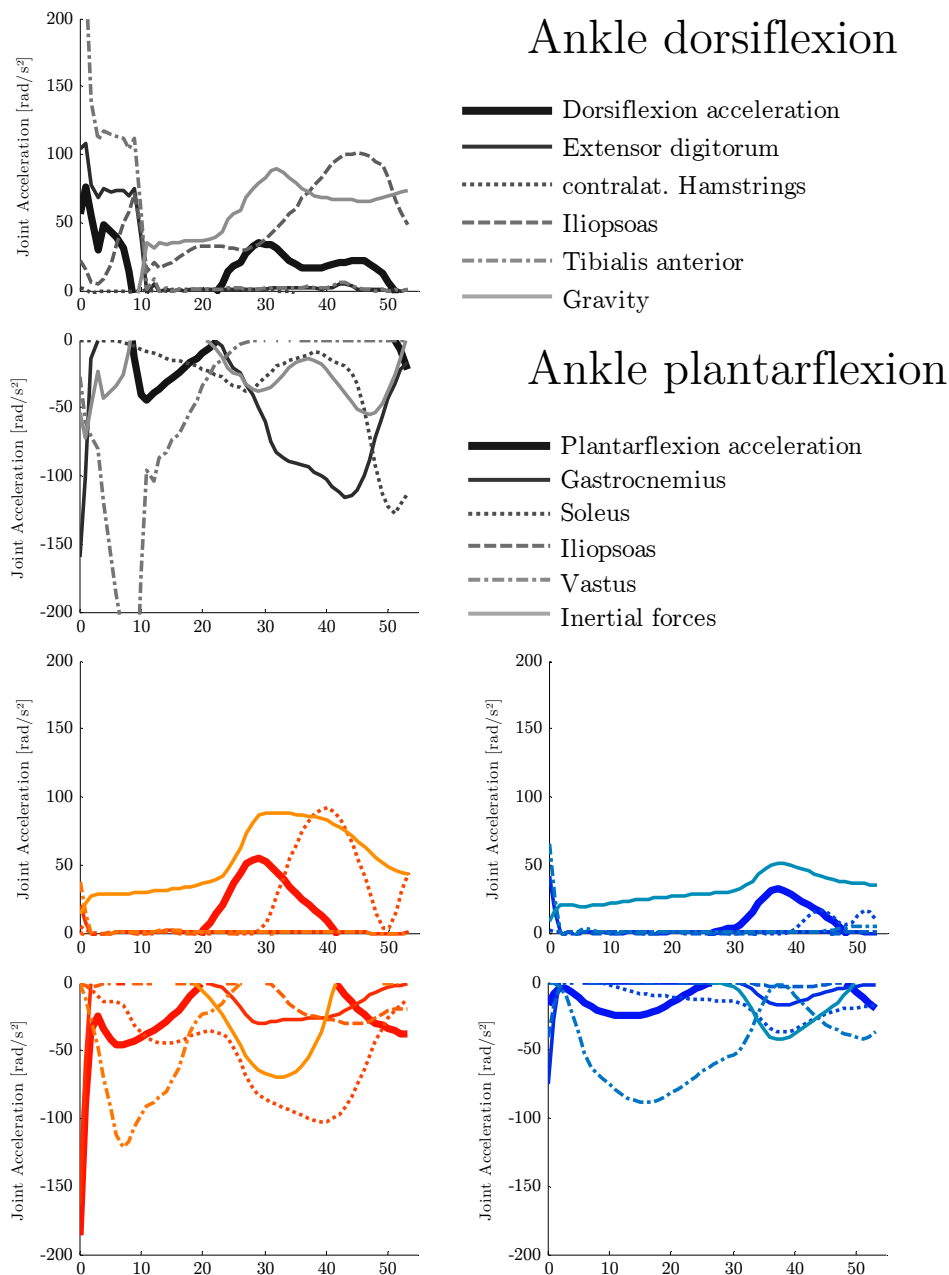
Figure 4.11 Dorsiflexion/plantarflexion accelerations in gait - Angualer ankle accelerations in crouched gait of subjects with cerebral palsy (CP1 - red, CP2 - blue) and normal gait of the control group (ND). Thick lines represent the net joint accelerations and thin/dashed lines the individual contribution of the major muscles.
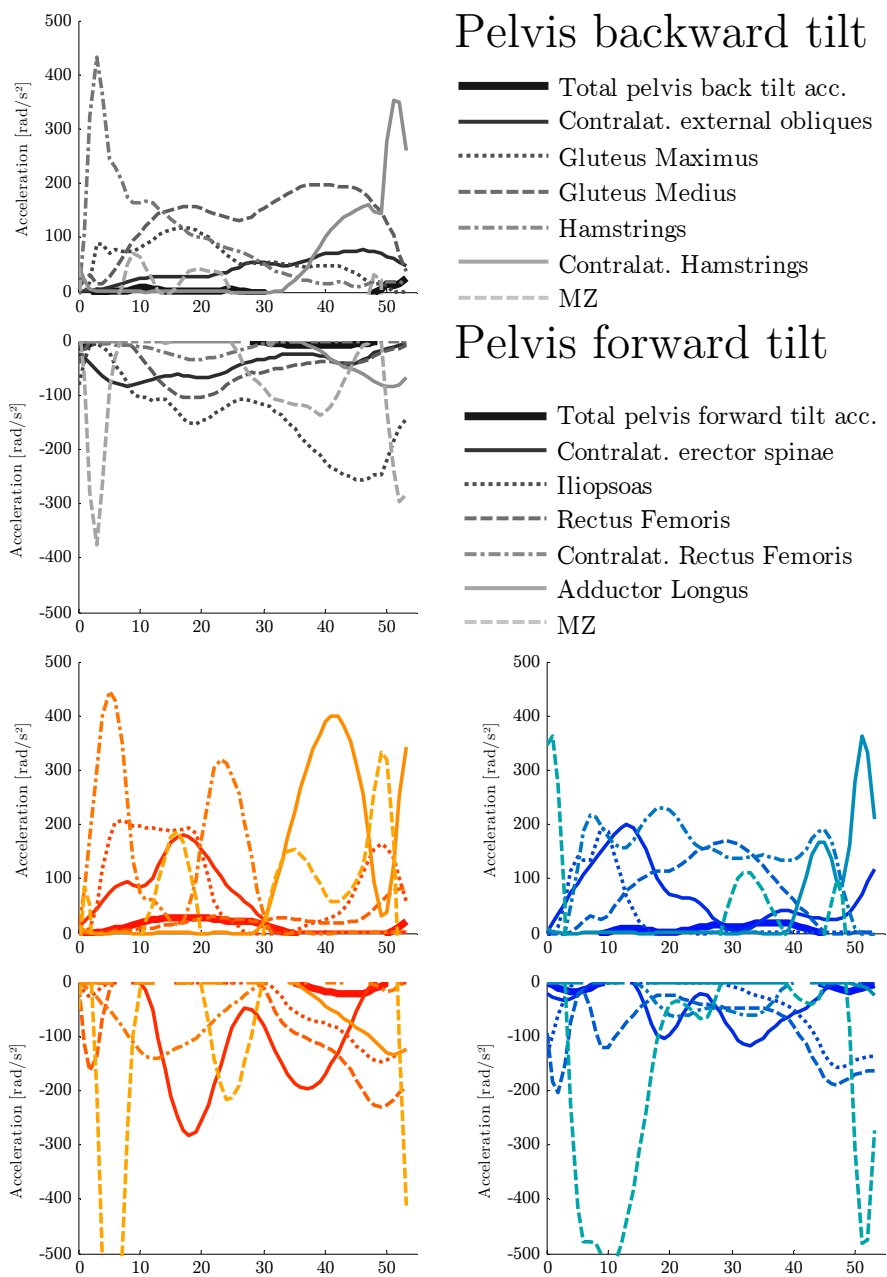
Figure 4.12 Pelvis tilt accelerations in gait - Angular accelerations in crouched gait of subjects with cerebral palsy (CP1 - red, CP2 - blue) and normal gait of the control group (ND). Thick lines represent the net joint accelerations and thin/dashed lines the individual contribution of the major muscles.

111

4.3.1 Acceleration of hip towards flexion

From Figure 4.8:

ND: The iliopsoas is the major accelerator towards hip flexion of ND especially in mid to terminal stance. Rectus femoris acts as hip flexor in mid stance. The contralateral erector spinae muscles are driving the hip towards flexion in loading response and mid stance.

Common CP: The hip flexion in CP is in contrast to ND much more accelerated by residual moments in the medio-lateral axis (MZ) which might be caused by HAT movement and balancing actions. Iliopsoas with less and rectus femoris with more vigor are affecting the hip flexion of both CP-children, but only during in terminal stance and pre-swing phase.

CP1: In CP1 the contralateral erector spinae muscles are mainly driving the hip towards flexion in mid and terminal stance.

> **Interpretation:** *The contralateral erector spinae in CP1 cause a forward tilt (see Figure 4.12) as well as a list of the pelvis together with hip abduction. Forces that change the pelvis orientation might cause the observed hip flexion and abduction acceleration.*

CP2: Hip flexion due to residual or balancing forces is higher in CP2.

4.3.2 Acceleration of hip towards extension

From Figure 4.8

ND: The hip extension in ND is driven by hamstrings and vastus in loading response and then by gluteus maximus in mid stance. Gluteus medius is a major contributor to hip extension throughout the whole stance phase with highest contribution during terminal stance. Contralateral hamstrings are extending the hip in terminal stance and pre-swing.

Common CP: The hip extension is forced in both CP-children by the hamstrings in loading response, followed by the frontal contralateral abdomen muscles (external obliques) together with gluteus maximus in mid

stance. Vastus has less effect on hip extension and its influence is shifted to terminal stance. Contralateral hamstrings extend the hip just before the swing phase.

CP1: In CP1 act hamstrings as hip extensors, first in loading response and later on also in mid stance. Gluteus maximus is accelerating the hip towards extension in loading response and additionally during pre-swing. Contralateral hamstrings in CP1 have a major effect towards hip extension during terminal stance. Gluteus Medius plays a minor role for hip extension in CP1.

CP2: The hamstrings in CP2 generated persistent hip extension acceleration throughout the stance phase. Gluteus Medius in CP2 acts almost similar as in ND as hip extensor, but loses its effect by end of terminal stance.

4.3.3 Acceleration of hip towards adduction

From Figure 4.9:

ND: The hip adduction in the control group is forced by hamstrings after initial contact, followed by vastus in loading response, gastrocnemius in terminal stance and adductor longus together with soleus in pre-swing.

Common CP: No common hip adduction acceleration effects may be identified in the CP-children.

CP1: Adductor magnus and hamstrings act as hip adductors in CP1 after initial contact. Vastus drove hip adduction in loading response, and hamstrings again in mid stance. Soleus had a persistent hip adduction effect throughout stance phase, while gastrocnemius had little effect. Adductor longus showed high effect towards hip adduction in pre-swing.

CP2: The hip adduction in CP2 is mainly accelerated by vastus throughout the stance phase with low support by hamstrings in loading response and soleus in mid-and terminal stance.

4.3.4 Acceleration of hip towards abduction

From Figure 4.9:

ND: The acceleration towards hip abduction in the control group (ND) may be interpreted as balancing effect. From loading response to terminal stance the gluteus medius acts as major hip abductor. Residual moments around anterior-posterior as well as medio-lateral pelvis axis (MX, MZ) are observed after initial contact. Contralateral erector spinae muscles abduct the hip in loading response and mid stance. In pre-swing a hip abduction effect of the contralateral hamstrings is observed.

Common CP: The hip abduction acceleration in the CP-children during loading response is highly dominated by residual moments around anterior-posterior as well as medio-lateral pelvis axis (MX, MZ). This may be caused by balancing effects in connection with the HAT-segment.

CP1: The contralateral erector spinae muscles in CP1 accelerate the hip in mid- and terminal stance towards abduction. The gluteus medius generates persistent hip abduction acceleration throughout the stance phase with extra high abduction acceleration in pre-swing. Contralateral hamstrings generate a high abduction effect in CP1 during mid- and terminal stance.

Interpretation: *The high hip extension (see 4.3.2) and abduction effect of contralateral hamstrings is a coupled motion. This motion is caused in mid- and terminal stance phase. due to motion of the pelvis towards a list in swing phase, as observed in kinematic results (Figure 4.1c). Here, the contralateral leg adducts and extends the hip as a, maybe spastic, reaction of the contralateral hamstrings to their quick passive lengthening in swing (see particular results of CP1 in Figure B.2.91a,b,f, p.B-43).*

Almost no influence to summed hip extension acceleration of the hip-extending contralateral hamstrings is observed, as contralateral erector spinae stabilizes pelvis tilt and as such hip extension (see Figure 4.8). However the enhanced pelvis list motion of CP1 may be caused by the contralateral hamstrings as its adduction effect in the

swing phase of the contralateral leg is not compensated. This in turn requires necessary balance actions such that the swinging leg does not collide with the stance leg, what for example is possible with the observed pelvis list

CP2: The contralateral erector spinae muscles In CP2 are accelerating the hip towards abduction during mid- and terminal stance, but not as much as in CP1. The gluteus medius drives the hip towards abduction from mid to terminal stance, what is almost similar to the function in ND.

4.3.5 Acceleration of knee towards extension

From Figure 4.10:

ND: Knee extension in ND was forced by hamstrings after initial contact, followed by vastus in loading response and gluteus medius in terminal stance. Rectus femoris generated a persistent rising influence towards knee extension starting at mid stance until pre-swing. Soleus and contralateral hamstrings mainly support the knee extension in pre-swing.

Common CP: The vastus in both CP–children is mainly responsible for knee extension acceleration throughout the whole stance phase.

CP1: Soleus accelerates the knee in CP1 towards extension in loading response and mid stance as well as together with contralateral hamstrings in terminal stance.

CP2: Vastus generates in CP2 persistent knee extension acceleration throughout the stance phase.

4.3.6 Acceleration of knee towards flexion

From Figure 4.10:

ND: Knee flexion in the control group is mainly accelerated by iliopsoas, but also by gravity in loading response and mid stance. This knee flexion caused by the iliopsoas is a result of an induced acceleration:
The knee is accelerated towards flexion coupled with the hip flexion effect of iliopsoas (see 4.3.1 and Figure 4.8) as long as the foot is in ground-contact, with highest effects during mid and terminal stance.

Common CP: Active knee flexion only plays a minor in both CP-children, so mainly gravitational forces accelerate the knee towards flexion, in coherence with the knee flexion angle.

CP1: Iliopsoas and soleus accelerate the knee in terminal stance of CP1 slightly towards flexion.

> **Interpretation:** *This may have been a balancing effect in reaction to knee extension of contralateral hamstrings (see 4.3.5).*

CP2: Knee flexion in CP2 is mainly driven by gravity with a slight effect of iliopsoas in pre-swing.

4.3.7 Acceleration of ankle towards dorsiflexion

From Figure 4.11:

ND: Dorsiflexion in ND is forced by extensor digitorum and tibialis anterior at the begin of loading response, followed by gravity in mid- and terminal stance as well as iliopsoas (see also knee flexion, Figure 4.10) in terminal stance.

Common CP: The dorsiflexion in CP is mainly caused by gravity, which affects dorsiflexion depending on the gait posture. No acceleration towards dorsiflexion is observed during loading response.

CP1: The contralateral hamstrings accelerate the ankle towards dorsiflexion in the terminal stance phase of CP1.

4.3.8 Acceleration of ankle towards plantarflexion

From Figure 4.11:

ND: The plantarflexion in loading response of ND is caused by vastus, followed by gastrocnemius in terminal stance and soleus in pre-swing.

Common CP: Gastrocnemius, which had significantly lower maximum isometric force than ND, shows in both CP-children almost no influence towards acceleration of plantarflexion.

CP1: The effect towards plantarflexion of vastus lasts longer in CP1 compared to ND, until mid stance, while soleus drives plantarflexion in mid- and terminal stance and gastrocnemius and iliopsoas slightly in terminal stance.

CP2: Ankle plantarflexion in CP2 is forced by vastus until mid of terminal stance and slightly by soleus in terminal stance, and again by vastus in pre-swing.

4.3.9 Acceleration of pelvis towards tilt

From Figure 4.12:

ND: Hamstrings accelerate the pelvis in loading response of ND towards a backward tilt, what was counteracted by a residual moment on the medio-lateral axis (MZ). Pelvis forward and backward tilt is further affected by gluteus medius and iliopsoas respectively throughout the stance phase. Further acceleration towards backward tilt comes sequentially from gluteus maximus in loading response to mid-stance, contralateral external obliques mainly in terminal stance and contralateral hamstrings with highest effect towards pelvis backward tilt in pre-swing.

Common CP: A high residual balancing moment on the medio-lateral axis (MZ) accelerates the pelvis into a forward tilt in both CP-children in loading response, followed by contralateral erector spinae in mid and terminal stance, rectus femoris and iliopsoas in terminal stance to pre-swing as well as the residual moment MZ again in pre-swing.
The pelvis of the CP-children is accelerated to a backward tilt by gluteus maximus in loading response, hamstrings and contralateral external obliques

in loading response to mid stance and contralateral hamstrings in pre-swing. The high contribution of muscles connecting the trunk with the pelvis on one hand and the high contribution of residual moments on the other hand can be interpreted b the following: Either the maximum isometric forces of these muscles were estimated to low, or the set of muscles connecting the trunk and the pelvis needs to be extended.

CP1: CP1 has a gross backward acceleration of the pelvis in loading response and mid-stance and a forward acceleration in terminal stance. Contralateral erector spine is the main accelerator towards forward tilt of the pelvis in mid to terminal stance supported by contralateral rectus femoris in loading response and mid stance, followed by rectus femoris, iliopsoas and also adductor longus in terminal stance to pre-swing.

Hamstrings have an additional effect in loading response but also mid-stance towards backward tilt of the pelvis in CP1, contralateral external obliques to same motion in loading response and mid stance. Significant high acceleration towards pelvis backward tilt comes from the contralateral hamstrings in terminal stance of CP1.

CP2: CP2 has a high acceleration towards forward tilt of residual balancing moment on the medio-lateral axis (MZ), which is counteracted with a pelvis backward tilt generated by hamstrings, gluteus maximus and contralateral external obliques. Hamstrings and gluteus medius mainly accelerate the pelvis towards backward tilt in mid- and terminal stance.

4.4 Centre of mass accelerations in gait

Muscular contributions of all 52 muscles of the lower limb models were calculated for vertical as well as fore-aft and medio-lateral acceleration of the centre of mass (CoM) for stance phase (55% of gait cycle) by processing the kinematic and kinetic gait data of ND, CP1 and CP2 with the "IncAccPI" plug-in for OpenSim (Dorn et al., 2012a). The CoM is located a few centimetres posterior to the medio-lateral axis of the pelvis in all models. For better visibility of these results only mayor contributors are shown and the ordinate scale in Figure 4.13 and Figure 4.15 is not uniform for all investigated motions. Computed results are shown for the stance phase.

4.4.1 Vertical CoM acceleration

From Figure 4.13:

ND: In the ND models is the CoM accelerated upwards by vastus, gluteus maximus and gluteus medius during loading response and mid stance, while at the same phase iliopsoas generates downward acceleration. Gastrocnemius is the main driver for vertical support of the CoM in terminal stance.

Common CP: Vertical CoM acceleration has highly increased values in both CP-children compared to ND for both orientations, upwards and downwards. In loading response and mid stance is a phase of high upward acceleration of the CoM, while it is extensively lowered in terminal stance, followed by an upward acceleration phase in pre-swing (synchronous to loading response of contralateral leg). Main driver towards upward CoM acceleration in both CP-children is the vastus. The effect of gastrocnemius as vertical accelerator in terminal stance is missing in both CP-children.

> **Interpretation:** *The missing effect of gastrocnemius towards upward acceleration the CoM can explain the negative CoM acceleration in terminal stance of both CP-children.*

CP1: Vastus, gluteus maximus, gluteus medius and hamstrings support the CoM up in loading response of CP1, mainly soleus in terminal stance.

CP2: The upward CoM acceleration in CP2 is mainly driven by vastus

119

4.4.2 Fore-aft CoM acceleration

From Figure 4.15

ND: CoM in ND is decelerated in loading response and mid stance and forward accelerated in terminal stance and pre-swing.
CoM is mainly driven forward by inertia of body and limbs (see Appendix B.3, Figure B.3.1), by hamstrings in loading response and mid stance and by gluteus medius in mid stance, terminal stance and pre-swing
A main decelerator in loading response is vastus. Rectus femoris and soleus have persistent deceleration effect on the CoM throughout the stance phase. Gastrocnemius acts as a CoM decelerator in terminal stance.

Common CP: Vastus acts in both CP-children, similar as in ND, as CoM-decelerator in loading response. No common effects for forward acceleration of the CoM are observed in the CP-cases.

CP1: Hamstrings and gluteus maximus accelerate the CoM forward by end of loading response and in mid stance of CP1. Soleus is together with gastrocnemius accelerating the CoM In terminal stance. Gluteus maximus and gluteus medius drive the CoM forward during pre-swing.
Vastus and rectus femoris decelerate the CoM during terminal stance of CP1 as well as iliopsoas in pre-swing.

CP2: A low but persistent CoM forward acceleration is observed in CP2, caused by the hamstrings throughout the stance phase, as well as by gluteus maximus in loading response and by gluteus medius in mid- and terminal stance. Vastus in CP2 shows highest forward acceleration effects in pre-swing.
Soleus, gastrocnemius and rectus femoris act as persistent CoM decelerators throughout the stance phase as well as iliopsoas in pre-swing.

4.4.3 Medio-lateral CoM acceleration

From Figure 4.15:

ND: Medial acceleration of the CoM in ND is mainly caused by gluteus medius and lateral acceleration by gastrocnemius, both in mid to terminal stance.

Common CP: The gluteus medius accelerates the CoM in both CP-children in medial direction, but with different vigour.

CP1:.Gluteus medius has a significantly high impact on medial CoM acceleration throughout the stance phase of CP1 with highs in mid-stance and pre-swing phase, synchronous to its hip abduction effect. Lateral acceleration in CP1 is driven by soleus in mid-stance and adductor longus in terminal stance to pre-swing, synchronous to its hip adduction effect.

CP2: Vastus is the main driver for CoM medial acceleration in CP2 throughout the stance phase with a maximum effect in terminal stance, which is counteracted by soleus and gastrocnemius
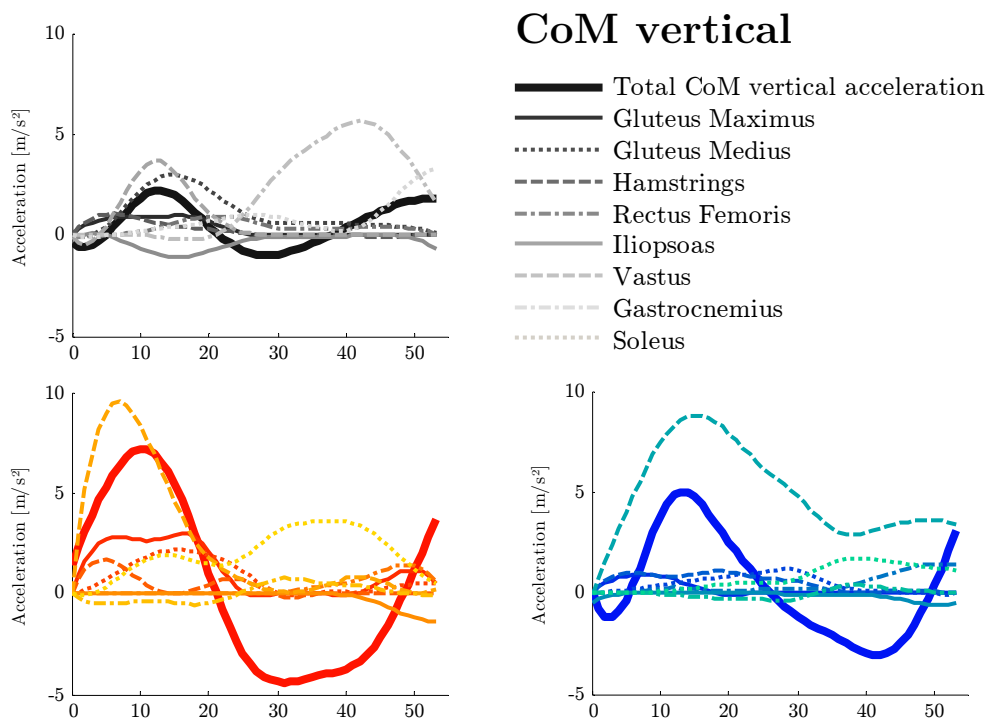
Figure 4.13 CoM vertical accelerations in gait - CoM acclerations in crouched gait of subjects with cerebral palsy (CP1 - red, CP2 - blue) and normal gait of the control group (ND). Thick lines represent the net fore-aft accelerations and thin/dashed lines the individual contribution of the major muscles.
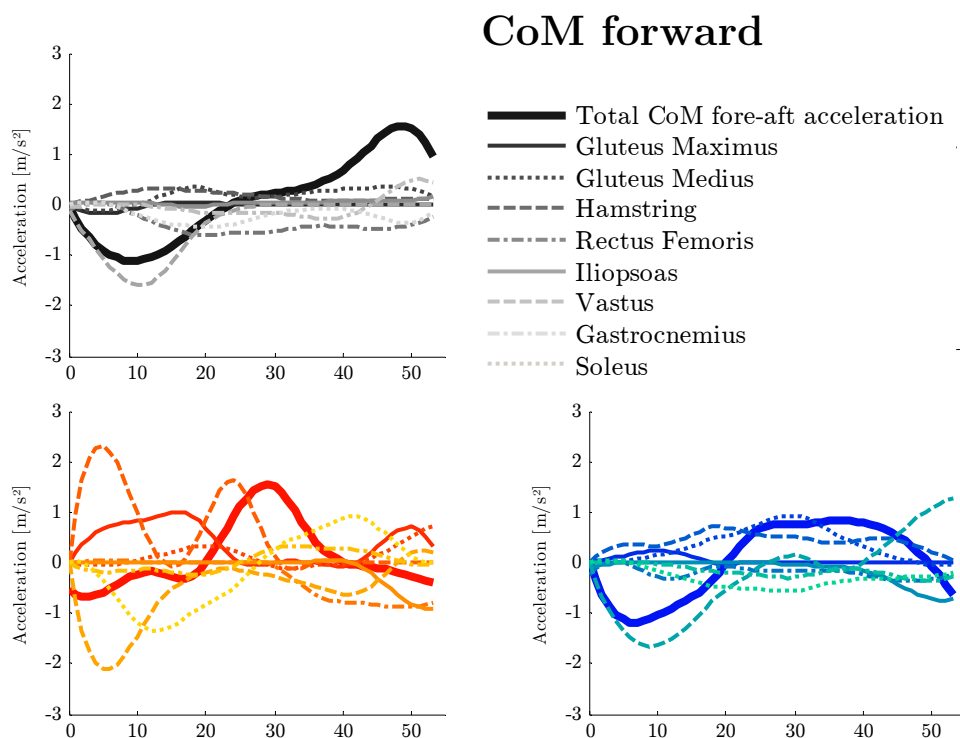
Figure 4.14 CoM fore-aft accelerations in gait - CoM accelerations in crouched gait of subjects with cerebral palsy (CP1 - red, CP2 - blue) and normal gait of the control group (ND). Thick lines represent the net fore-aft accelerations and thin/dashed lines the individual contribution of the major muscles.
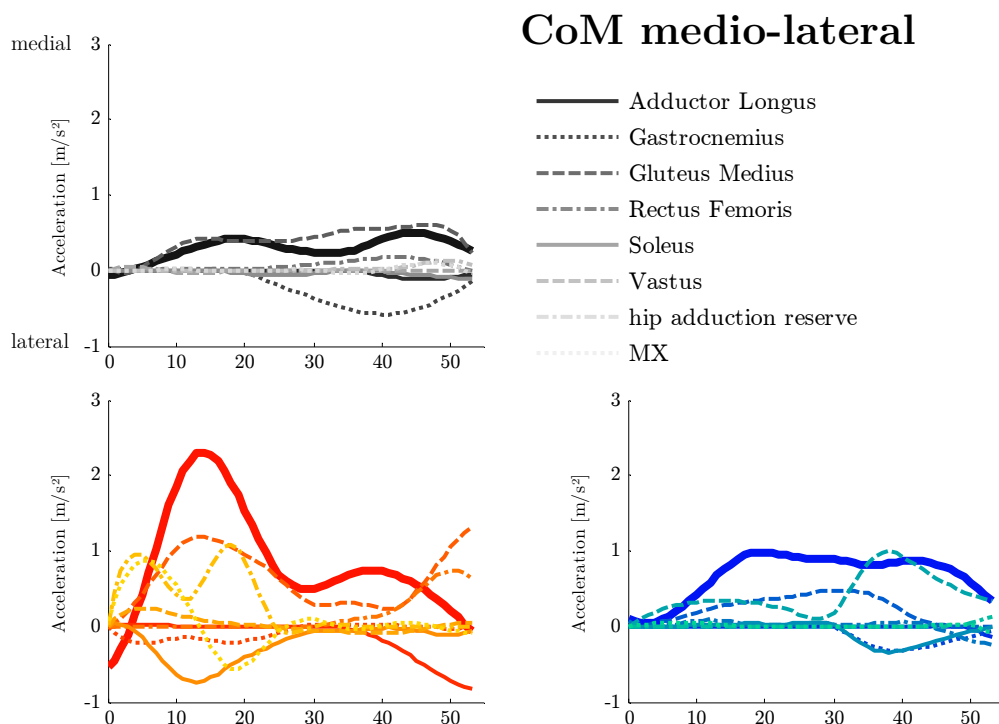
Figure 4.15 CoM medio-lateral accelerations in gait - CoM accelerations in crouched gait of subjects with cerebral palsy (CP1 - red, CP2 - blue) and normal gait of the control group (ND). Thick lines represent the net fore-aft accelerations and thin/dashed lines the individual contribution of the major muscles.

4.5 Normalized Muscle fibre lengths in gait

Muscle lengths in gait were analyzed to get additional information for identifying abnormal muscle function in CP. Figures for normalized muscle fibre lengths in gait are presented in Appendix B, Chapter B.2 (marked (a)) for all muscles.

4.5 Normalized Muscle fibre lengths in gait

A summary of these results condenses the main information concerning the length range during a full gait cycle of the muscles in the models of CP and ND:

Main contributors to gait:

Hamstrings: Figure B.2.9a shows, **similar for both CP-children and ND,** a muscle fibre length between 100%-140% of optimal fibre length.

Iliopsoas: Figure B.2.11a shows for l_m in ND 110%-125% of l_{0m}. Muscle fibre length in **CP-children** was **shorter** with 75%-105% of l_{0m}

Gluteus maximus: l_m is similar in CP and ND with range $\pm 10\%$ of l_{0m}

Gluteus medius: l_m is similar in CP and ND with range $\pm 15\%$ of l_{0m}?

Rectus femoris: Figure B.2.17a, ND 60%-125%, CP1 55%-80%, CP2 75%-125%:$\rightarrow$ **less dynamic range in CP, shorter and less efficient in CP1, similar efficiency as in ND in CP2**

Vastus: Figure B.2.29a, ND 70%-115%, CP1 85-100%, CP2 100%-110%: $\rightarrow$ **less dynamic range in CP, in almost optimal length range of force length curve in both CP-children**

Gastrocnemius: Figure B.2.7a, ND1 50%- 120%, CP 60%-110%: $\rightarrow$ **less dynamic range in both CP-children**

Soleus: Figure B.2.21a, ND 75% to 105%, CP 85%-115%: $\rightarrow$ **similar dynamic range in ND and CP, more efficient in CP**

Muscles with noticeable length characteristics in CP-gait at:

Adductor Longus: Figure B.2.1a, ND: 80%-120%, CP: 60%-80%: $\rightarrow$ **much shorter in both CP-children**

Biceps femoris SH: Figure B.2.1, ND: 75%-140%, CP1: 70%-80% CP2: 95%-105%:$\rightarrow$ **much shorter in CP1, less dynamic range in both CP**

Tibialis anterior: Figure B.2.23a, ND1 60%-80%, CP1 45%-60%, CP2 25%-50%:$\rightarrow$ **much shorter in both CP-children**

Tensor fasciae latae: Figure B.2.27a, ND 120%-145%, CP1 75%-115%, CP2 100%-130%: $\rightarrow$ **shorter but more dynamic range and efficiency in both CP-children**

4.6 Summary of individual muscle analysis

The following individual muscle analysis tries to answer the question, if the observed muscular contributions to joint moments, angular accelerations and CoM accelerations can be interpreted as reaction to the observed posture and gait pattern or if a muscle dysfunction might be the cause for the crouched gait and posture. It is a summary of previous shown results in combination with results for particular muscles results as shown in Appendix B, Chapter B.2.

Adductor Longus:
ND: Adductor longus accelerates hip adduction in pre-swing of ND.
CP: Moment arm for hip flexion in the CP-children is about ~76% of ND; Adductor longus generates hip flexion but also hip adduction moment in terminal stance and pre-swing phase and was much shorter in CP.

CP1: Adductor longus showed high effect towards hip flexion and adduction, pelvis forward tilt as well as CoM deceleration and lateral acceleration in pre-swing. This happened in a gait phase where the muscle is lengthened quickly until reaching a maximum, what however was still quite short compared to ND (Figure 4.16). This can be interpreted a spastic **action** caused by too high lengthening velocity.
CP2: no considerable effect

Figure 4.16 Normalized muscle fibre length of adductor longus

Adductor magnus:
This muscle generates no noticeable joint moments in gait of ND and CP.
ND: Adductor magnus has no considerable effect in normal gait
CP1: F_{max}~75% of ND; Acted as hip adductor after initial contact. (Individual **reaction**)
CP2: Adductor magnus in CP2 has only 50% moment arm for adduction compared to ND. Despite significant higher muscle volume in CP2, this muscle had no considerable effect in gait.

4.6 SUMMARY OF INDIVIDUAL MUSCLE ANALYSIS

Extensor digitorum:

Joint moments generated by extensor digitorum longus not significant

ND: Ext. digitorum forces dorsiflexion in begin of loading response

CP1: no considerable effect (→ **reaction** due to posture)

CP2: no considerable effect (→ **reaction** due to posture)

Gastrocnemius:

ND: During terminal stance acted gastrocnemius towards hip adduction and plantarflexion, horizontal CoM-deceleration and as a main driver for vertical CoM acceleration. Very little contributoin of gastrocnemius towards knee flexion acceleration could be observed in normal gait.

CP: F_{max} for gastrocnemius in CP was decreased to value of ~46% compared to in ND. Almost no plantarflexion moment or acceleration towards plantarflexion was observed in both CP-children. This could be a **reaction** due to short muscle fibre length caused by flexed knees in crouched posture, but this can be almost excluded as muscle fibre length was comparable to ND. On the other hand, the weak performance could have been **actively** caused due to the low maximum isometric force of this muscle.)

CP1: Gastrocnemius was a CoM-forward accelerator in terminal stance.

CP2: no considerable effects

Gluteus Maximus:

ND: Gluteus maximus accelerated hip extension in mid-stance.

CP: F_{max}~66% of ND, Gluteus maximus needed to generate more hip extension moment during loading response as **reaction** to enhanced hip flexion, and accelerated hip extension in mid-stance. During hip extension it also created a pelvis backward tilt.

CP1: Gluteus maximus accelerated CoM vertical and highly forward in loading response of CP1. It acted as hip extensor and CoM-forward acceleration in pre-swing (→all **reactions** to posture)

CP2: Gluteus maximus drove hip extension and that caused CoM-forward acceleration and CoM vertical acceleration in loading response (**reaction** to posture).

Gluteus Medius:

ND: Gluteus medius was a major contributor to accelerate hip extension (coupled with pelvis backward tilt acceleration) throughout the whole stance phase with highest contribution in terminal stance. It was a major hip

abductor from loading response to terminal stance, and accelerated knee extension in terminal stance. The CoM was vertically accelerated by gluteus medius in loading response and mid stance, and this muscle was a main contributor to CoM forward and medio-lateral acceleration in mid stance, terminal stance and pre-swing

CP: Moment arm for hip abduction ~70% of ND; No common behaviour in CP regarding gluteus medius was observed. The effect of gluteus medius in gait seems to be highly dependent on the combination of hip rotation angle and femoral anteversion.

CP1: Gluteus Medius in CP1 generated a persistent hip abduction moment throughout the stance phase with extra high abduction acceleration in pre-swing. (this could be a **reaction** to compensate the or high adductor effects in CP1, caused by adductor longus). Gluteus medius played a minor role for hip extension acceleration in CP1. CoM vertical acceleration in loading response and CoM forward acceleration in pre-swing by gluteus medius in CP1 were much less supported than in ND, however its effect towards medial CoM acceleration was enhanced. The observed function can be interpreted as **reaction** to gait posture that might also be related to the femoral anteversion of 45° (see Table 2.7), which allowed gluteus medius to be more efficient in the observed balancing actions.

It can be seen, that the gait posture of CP1 with the 20° inward rotated hip requires a rotated femur such that gluteus medius can efficiently abduct the hip as required. This hip inward rotation is partly caused by gluteus medius itself. A quick simulation test revealed that a 'normal' or 'corrected' femur would cause gluteus medius in this gait posture to generate high hip flexion moments. However, this does not answer what causes the femoral rotation in CP1, but the effect of the necessary hip outward rotation moment that can cause this deformation was not covered by any of the modelled muscles and was therefore resulting in a residual force on the hip joint.

CP2: Gluteus medius performed more as hip extensor than in CP1, and showed significant CoM forward acceleration in mid-stance.

Hamstrings:

ND: This muscle group could generate high hip extension moments, hip extension acceleration in combination with pelvis backward tilt acceleration during loading response as well as hip adduction and an induced acceleration effects towards knee extension after initial contact. Hamstrings in loading

response and mid stance mainly drove the CoM forward.

CP: F_{max}~65% of ND; The hamstrings in both CP had less dynamic range and their maximal length, just before loading response, was 20% shorter compared to ND. Hamstrings caused a high hip extension moment plus hip extension acceleration together with pelvis backward tilt in loading response and individually in additional gait phases. Although knee flexion moments could be observed, no considerable effect of hamstrings towards knee flexion acceleration could be detected in both CP-children. This effect can be explained as **reaction** to the gait posture:

The hip extension effect of hamstrings dominated in these gait phases and as long as the leg was touching the ground this coupled motion caused indirect a knee extension acceleration that counteracted the direct knee flexion effect of hamstrings. (**reaction** due to posture)

CP1: Hip extension and pelvis backward tilt effect by hamstrings was observed, additionally to loading response, in mid stance. The hip adduction during this phases can be interpreted as coupled effect in connection with the hip extension function (**reaction**). Hamstrings could generate high knee flexion moments during loading response, mid-stance and swing phase in CP1, but this had almost no effect onto knee flexion acceleration. Hamstrings caused vertical acceleration of the CoM and high CoM forward acceleration in loading response as **reaction** to the gait posture. A hip extension moment was observed in swing phase that is reviewed for contralateral hamstrings in next paragraph.

CP2: Hamstrings generated a persistent hip extension moment and acceleration throughout the stance phase, that caused a CoM forward acceleration in mid-stance, coupled with low hip adduction effect in loading response (**reaction** due to posture). Further, the hamstrings caused a pelvis backward tilt in CP2 in mid- and terminal stance. The effect towards knee extension was similar to CP1, as is explained in prior paragraph.

Contralateral hamstrings:

ND: Contralateral hamstrings extended the hip in terminal stance and, additionally to this motion, accelerated hip abduction plus knee extension as well as a pelvis backward tilt in pre-swing of normal gait.

CP: Contralateral hamstrings caused hip extension during terminal stance in both CP-children   .

CP1: Contralateral hamstrings had a major effect towards hip extension and

pelvis backward tilt together with high hip abduction and knee extension during terminal stance. This was caused by acceleration of the pelvis towards list (see motion data in Figure 4.1) and a backward tilt maybe as a possible spastic **action** during the swing of the contralateral leg, when these muscles are extended. Almost no effect of the contralateral hamstrings in overall hip extension could be observed, as contralateral erector spinae reacted to this, however it can be seen in the high range of pelvis list of ±10° in a full gait cycle of CP1 (Figure 4.1c).

CP2: Contralateral hamstrings had moderate hip extension effect at end of terminal stance and in pre-swing, similar to ND.

Iliopsoas: Moments results: nothing noticeable

ND: Iliopsoas was a major contributor in ND towards hip flexion especially in mid to terminal stance and had also indirect effect as main accelerator to knee flexion in loading response and mid stance. Iliopsoas induced dorsiflexion acceleration in terminal stance and downward acceleration of the CoM in loading response and mid stance.

Knee flexion caused by the iliopsoas was a result of a coupled motion: Similar to its hip flexion effect was the knee accelerated towards flexion as long as the foot was in contact with the ground, with highest effects during mid and terminal stance.

CP: Iliopsoas is roughly 20% shorter in CP throughout the whole gait cycle and affected hip flexion coupled with pelvis forward tilt only in late terminal stance and pre-swing, and caused a CoM deceleration in pre–swing of both CP-children. (**reaction** due to crouched gait posture)

CP1: Iliopsoas caused a slight knee flexion and plantarflexion in terminal stance of CP1 (**reaction** due to posture)

CP2: F_{max}~55% of ND; Iliopsoas caused a slight knee flexion towards pre-swing in CP2 (**reaction** due to posture)

Rectus Femoris:,

ND: Rectus femoris in ND generated hip flexion moment and acceleration in mid stance, persistent rising influence towards knee extension starting at mid stance until pre-swing and persistent deceleration on the CoM throughout the stance phase. Length of rectus femoris in ND had a very high dynamic range throughout the gait cycle from 50% to 125% of optimal muscle fibre length.

CP: F_{max}~55% of ND; In contrary to ND, generated rectus femoris in both CP-children enhanced hip flexion moment plus acceleration and pelvis

forward tilt in terminal stance and pre-swing phase with its highest possible vigor. Rectus femoris extension started in terminal stance, what was earlier compared to ND, where the extension started at the swing phase (Figure 4.17 or Appendix B, Figure B.2.17a).

Figure 4.17 Normalized muscle fibre length of rectus femoris

The observed knee extension moment of rectus femoris in terminal stance and pre-swing of the CP-children had no effect on knee extension acceleration. The knee acceleration effect of the rectus femoris in CP might be counteracted by the coupled hip flexion acceleration. This affects, similar as it was observed for the iliopsoas, synchronously to hip flexion, a knee flexion as long as the foot is in contact with the floor. The described hip flexion effect of rectus femoris in CP could be explained by several reasons:

(i)   It could be a **<u>reaction</u>** to cope with the high to hip extension effect of contralateral hamstrings.

(ii) Additionally it might be a **<u>reaction</u>** to compensate for the low contribution to this motion by the shortened and so less effective iliopsoas.

(iii) The hip flexion effect of rectus femoris is observed during a gait phase when the rectus femoris is rapidly extended (Appendix B, Figure B.2.17a) and might therefore be an **<u>active</u>** cause for the flexed hip

CP1: Moment arm of rectus femoris for hip flexion was ~150% of ND, what made it much more efficient for hip flexion; Rectus femoris had a shorter maximum extension length (100% of optimal muscle fibre length compared to 125% in ND) that was reached earlier, just before the swing phase and had a lower dynamic range. Rectus Femoris accelerated the pelvis towards a forward tilt in terminal stance to pre-swing. At begin of the swing phase of what is synchronous to loading response of the other leg, it continued as 'contralateral rectus femoris' its effect towards pelvis forward tilt.

CP2: Rectus femoris had a longer minimum extension length (90% of optimal muscle fibre length compared to 50% in ND) and acted as persistent CoM decelerators throughout the stance phase.

Soleus:

ND: Soleus induced hip adduction and forced plantarflexion in pre-swing, induced as a main supporter the knee extension in pre-swing and affected persistent deceleration effect on the CoM throughout the stance phase.

CP: F_{max}~62% of ND; Soleus of both CP-children **reacted** to the gait posture, by taking over more load for plantarflexion from the too short and as such less effective gastrocnemius. It operated on a similar dynamic length range as ND.

CP1: Soleus in CP1 induced persistent hip adduction effect throughout stance phase, knee extension in loading response and mid stance as coupled effect when extending the ankle and slightly knee flexion in terminal stance. It was main contributor to plantarflexion in mid-and terminal stance and main vertical CoM accelerator in terminal stance. Soleus in CP1 highly decelerated and laterally accelerated the CoM by the end of loading response to mid stance and accelerated the CoM in terminal stance. All observed effects could be described as **reaction** to the gait posture.

CP2: Soleus in CP2 induced hip adduction in mid- and terminal stance, had a slight plantarflexion effect in terminal stance and caused persistent CoM deceleration throughout the stance phase. The observed effects could be described as **reaction** to the gait posture.

Sartorius:

CP1: Sartorius contributed a hip flexion moment in loading response phase of CP1.

Tensor Fasciae Latae: Moment arm for hip flexion ~150% of ND; No noticeable effects were observed.

Tibialis anterior:

ND: Acceleration of ankle dorsiflexion in begin of loading response of ND.

CP: No noticeable effects were observed.

4.6 SUMMARY OF INDIVIDUAL MUSCLE ANALYSIS

Vastus:,

ND: Vastus in ND forced knee extension and induced hip extension, hip adduction and plantarflexion in loading response and mid stance. Together with gluteus medius it supported mainly the CoM in vertical direction during loading response and mid stance, but was also a main CoM decelerator in loading response.

CP: F_{max}~78% of ND; As **reaction** due to the gait posture of both CP-children was vastus responsible for knee extension and positive vertical CoM acceleration throughout the whole stance phase. Also as **reaction** to the posture, vastus induced less hip extension in terminal stance of both CP-children compared to ND. Similar to the control group acted vastus as CoM-decelerator in loading response.

CP1: Vastus was main vertical accelerator for the CoM and synchronously induced hip adduction in loading response. The plantarflexion effect of vastus lasted longer compared to ND, until mid stance. Vastus was one of the CoM decelerators during terminal stance in CP1. All observed effects could be described as **reaction** to the gait posture.

CP2: Vastus in CP2 affected persistent knee extension acceleration and was therefore the main vertical CoM accelerator, what in conjunction induced high hip adduction throughout the whole stance phase. Vastus induced plantarflexion until mid of terminal stance and again in pre-swing. All observed effects could be described as **reaction** to the gait posture.

Erector spinae: No noticeable effects were observed

Contralateral erector spinae:

ND: Contralateral erector spinae induce hip flexion and abduction in loading response and mid stance of the control group.

CP: Contralateral erector spinae cause hip flexion and abduction effects in mid and terminal stance of both CP-children

CP1: Contralateral erector spinae was the main accelerator of hip towards flexion and abduction as well as pelvis forward tilt in mid and terminal stance of CP1. The observed effects could be a coupled **reaction** that might be caused by a HAT balancing motion that tilt the pelvis forward and cause pelvis list and as such flex and abduct the hip.

CP2: Contralateral erector spinae in CP2 induced hip flexion and abduction in mid stance and terminal stance, but less than in CP1.

External obliques: No noticeable effects were observed.

Contralateral external obliques:
ND: Contralateral external obliques caused a pelvis backward tilt in terminal stance of ND.
CP: Contralateral external obliques induced hip extension coupled with pelvis backward tilt in loading response and mid stance of both CP-children. This can be explained as **reaction** when passing on the HAT balancing actions via an effect of backward tilt of the pelvis.

5

Discussion and Conclusions

CONTENTS

5.1   Discussion of modelling method

The developed approach to MR-based biomechanical modelling shows that the generated models could reproduce the maximum isometric joint moment angle characteristics of experimental measurements.As children by the age of 8 years start to develop mature gait patterns, it is assumed that the lower-limb muscles of children and adults have their optimal lengths at the same joint angles. Maximum isometric muscle forces, tendon slack lengths and moment arms for the individual models are based on the data derived from MR images. Resulting maximum isometric joint moments calculated from the MR-based models are similar to the moments obtained from a scaled-generic model, which seems reasonable as usually the gait pattern of the two subject cohorts is similar.

Discussion and Conclusions

Whilst the proposed methodology has not been applied to other modelling platforms (aside from OpenSim) or to models of different anatomical structure, the approach can easily be applied to these scenarios as well. The computational algorithms are implemented in Matlab, and the implementation is based on the structure of OpenSim models, with model parameters changed via Matlab. If an interface to another software platform is available, then the algorithm can easily be applied to read and write model parameters using Matlab.

One limitation of this study concerns how muscle-tendon attachment sites are selected. It is challenging to identify tendon attachment points to the bones, since the attachment site is often not a single point, but an extended area (e.g., for the medial portion of gluteus medius and the medial portion of iliacus) or is located on several positions along a bone (e.g., for the vastus medialis and the medial portion of adductor magnus). The centroid of the muscle belly and tendon can be used to model a muscle's path. However, it remains unclear whether this muscle path is identical with the muscle's line of action. In particular, when the attachment site of the tendon on the bone is extended, it is difficult to determine which parts transfer muscle stress to the skeleton during movement. By selecting the most proximal and distal voxels of a muscle-tendon structure in MR-data as attachment sites and calculating the centroid line as the line of action of the muscle, a rather simple but repeatable method for reproducing the line of action of a muscle was selected.

After a time consuming segmentation process, the customization of a model takes now only about five minutes using the proposed method. The time taken to generate MR-based musculoskeletal models can be reduced even further by automating the steps needed to reproduce the path of each muscle. Nonetheless, most of the time taken to build a MR-based individual musculoskeletal model is related to manual segmentation of the MR images. Atlas-based methods may help in this regard, but if subjects differ from the norm due to individual pathologies, then this approach may not assist in reducing the overall time required for model development.

It can be concluded that the methodology as proposed in Chapter 2.4 is suitable for developing individual models of healthy children based on MR data. The method has the potential to give reasonable results, even if

abnormalities of the musculoskeletal system such as tibial torsion and muscle spasticity will be integrated into the modelling process.

Hence, the generation of the MR-based models of both, the control group and the children with cerebral palsy was done by application of the methods described in Chapter 2.4.

5.2 Discussion and conclusion ND-Models

MR image data of five normally developing children was collected and used to generate musculoskeletal models with individual skeletal geometry, muscle paths and muscle model parameters such as maximum isometric force, muscle fibre length and tendon slack length. These five models were merged to an averaged children's model by averaging bone geometry and muscle architecture and calculating corresponding muscle model parameters. This model replicates almost exactly the mean maximum isometric joint moment - joint angle characteristics of the subject specific models.

Variations in maximum isometric force of the individual children's models compared to a mass-scaled adult model were found in a range from -41% to +45%. These differences have an influence on the investigation of the function of individual muscles in gait, especially on estimations of muscles' contributions to the acceleration of the centre of mass and the body segments.

The individual models of the ND control group generate two to three times larger maximum isometric joint moments for hip extension and ankle plantarflexion compared to the experimental results and literature data. Results show in some cases different characteristics to published simulation data in literature. A reason may be that the method for quick maximum joint moment calculation may be simplified implemented in the used simulation platforms when individual contributions of muscles towards a joint moment are summed. OpenSim for example neither considers passive moments of antagonistic muscles nor the, in Chapter 2.8.1 described, characteristic of some muscles that can act pro and contra an investigated motion. This effect can be seen for hip flexion contribution of hip adductions that is depending on the joint angle.

DISCUSSION AND CONCLUSIONS

The deviation of simulated maximum isometric joint moments for hip extension and ankle plantarflexion to measured data as well as to literature data can be caused either by the unreliability of the applied dynamometry protocol for these two motions, as well as by questionable plausibility of published low values in literature. The following estimation example will support the derived results from the MR-based modelling process:

A stop jump on one leg can generate a ground reaction force up to 3 times the body weight (Wang, 2011). This force, multiplied with a moment arm from ankle joint to the toes of approximately 7% of the body height, results in a normalized plantarflexion moment of 21% [Nm/body weight*body height]. This is the necessary joint moment to generate sufficient GRF when landing. Further, the hip joint needs to be capable of generating a similar moment when the body is vertically decelerated at the stop jump. Maximum isometric joint moments of the simulated maximum plantarflexion and hip extension moments of individual MR-based children's model and the average child model are in this order (Figure 3.4, p.74) in contrary to models from literature.

The dynamometry results for knee flexion and extension (Figure 3.3, p.74) are most likely be influenced by differences in the hip joint angle and the ankle angle during the experiment, in comparison to the assumed angles in simulation. During the measurements the subject was sitting, but the real joint angles were not measured. The hip flexion angle has an effect on rectus femoris and hamstrings length, what influences their characteristics for active contribution as well as their passive resistance for knee moments. Further, as the ankle joint was not locked during measurements of knee flexion moment, the ankle might have plantarflexed when gastrocnemius was activated. The so shortened gastrocnemius might have been less efficient in contributing to the measured maximum isometric knee flexion moments.

For future investigations, the measurement protocol with the dynamometer needs to be refined, especially for hip extension, knee extension and ankle plantarflexion but also for hip ab- and adduction.

Despite the difficulties in experimental verification of the models, it can be concluded that the MR-based models of the control group reproduce the maximum isometric joint moments with reasonable accuracy.

The shown differences in muscle function between adults and children emphasize the need for a generic template model for children for application in studies where no MR image data for individual modelling is available. To the best of my knowledge, this is the first publically available biomechanical model for children that is based on a combination of five or more MR data sets and was validated by means of experimental joint moment measurements. This model can serve as a reference or as template for mass-scaled models in further studies of lower-limb muscle function in children. Researchers can benefit from this quick modelling method together with a reduction of scaling based errors when they apply the average child model that will be accessible on https://simtk.org/home/children.

5.3 Discussion and conclusions CP-Models

To the best of my knowledge, this is the first study that presents individual MR-based models of children with cerebral palsy, which include individual muscle model parameters all major 52 muscles of the lower limb that were set derived from the subject specific anatomy and allow the estimation of muscle forces in gait.

A semi-automated comprehensive process was applied for generation of the individual MR-based models in this study. This process was developed and tested for the ND control group and was basically similar applied for individually modelling of the CP-children. Resulting models incorporate large muscles like gluteus maximus or vastus on only a single line of action and only one source or insertion point, instead of broad attachment sites or multiple lines of action. A similar optimal joint angle (joint angle where the muscle fibres operates their optimal length) in CP-children and normally developing children is assumed for the calculation of muscle-model parameters. This assumption is especially important for estimating the tendon slack length as with that, the same method as for ND could be applied. Any shift of the optimal joint angle is not practical, as most of the major muscles actually operate around their optimal angle in the crouched gait of the investigated CP-children (see gait kinematic results in Chapter 4.1, p.97).

DISCUSSION AND CONCLUSIONS

Individual data of the two children with cerebral palsy are presented without estimation of averaged results of these two subjects. The findings in this study show good coincidence in the summed up total maximum joint moments of both CP-subjects. However, the particular analysis for maximum isometric forces and moment arms as well as the resulting joint moment per muscle at the investigated degrees of freedom show that there are substantial differences between individual contributions of muscles to net joint moment for each subject. An example for this is the different characteristic of adductor magnus towards hip extension, when comparing results of CP1 (left) and CP2 (right) in Figure 3.10 (p.88). Further research with MR-based models will be necessary to emphasize common characteristics in muscle structure of children with cerebral palsy.

An additional aim was the investigation of the model accuracy when models are based on scaled templates of adults and normally developing children. This was done by generating models of CP-children by scaling template models via gait markers and then comparing their maximum joint moment characteristics.

The mass-length scaled CP-models could not reproduce the particular subject specific shape of the pelvis in both CP children. The different shape of the pelvis in the template models compared to the individual pelvis shape of the CP-children leads to significant errors in joint placement, e.g. in hip joint position up to 54%.

The results further indicate that the approach of setting the muscle parameters via mass-length scaling is only with limitations feasible for the generation of subject specific models of children with CP. With the mass-length scaled templates, the generic adult model as well as the average children's model, it is only in a few degrees of freedom possible to obtain a joint moment behaviour that comes close to that of the MR-based CP-models.

Estimated total joint moments of scaled adult template models and MR-based CP-models show good concurrence in some motions. This fact should not lead to the conclusion, that adult template models are well suited for generation of individual CP-models via mass-length scaling. Rather has this to be seen as a coincidence that reveals when the models are analyzed on the individual muscular level (see results in Chapter 3.2.3.1, p.86). Particular analysis for isometric force and moment arm propagation as well as resulting joint moment per muscle in investigated degrees of freedom show that individual contributions of muscles are very different between subjects.

These examples reveal that deviations in moment arms and/or maximum isometric forces of muscles, which contribute to the same motion, can cancel each other out:

> Hip flexion in CP1 (Figure 3.6, p. 84) shows a good match between CP1 and CP1AT for total joint moment but

> Figure 3.8 shows that in CP1AT the rectus femoris contributes significantly less and iliopsoas more towards total joint moment.

> Hip Extension in CP2 (Figure 3.6, p. 84) is similar to CP2AT for total joint moment. However the contribution of gluteus medius is much lower while adductor magnus has a much higher contribution in CP2 compared to CP2AT.

Similar maximum isometric joint moment characteristics can be seen for hip adduction in both CP children as well as for knee flexion in CP1 and knee extension in CP2.

It can be concluded that for analysis of particular muscle functions individual MR-based models are superior compared to template based models. Further it can be concluded that, when generating CP-child models via mass-length-scaling of an average child model the result may even be higher biased as it would be if an adult model is used as template.

5.4 Discussion of gait-simulation results

Individual models of children with cerebral palsy (CP) and a control group (ND) of the same age group were generated based on MRI-data. Static optimization theory was used to calculate the patterns of muscle activations and muscle forces by minimizing the sum of the squares of all muscle activations over one complete cycle of gait. The contributions of muscle forces towards joint moments and accelerations as well as CoM accelerations were calculated in all models to quantify muscle function during the stance phase of normal walking and crouch gait.

Muscle coordination towards the accelerations of the pelvis orientation, hip, knee and ankle joint acceleration as well as to vertical, horizontal and lateral acceleration of the centre of mass (CoM) were analyzed in several phases of single limb stance.

5.4.1 Analysis of muscle function in normal gait

Simulation results for the maximum isometric joint moments, in Chapter 3.1 (p.70ff) of this study, show only small differences between joint moments of average children to that of a mass-length-scaled adult model in most degrees of freedom. However, the muscle specific comparisons of the average maximum isometric muscle forces of children and adults in Table 3.2 (p.71) reveal variations of ±40%. For example have children much smaller muscles on the outer surface of the pelvis (gluteus medius and gluteus min -43%) and less dorsal hip muscles (iliopsoas -30%) but a stronger rectus femoris (+45%) and longer moment arms for some weaker muscles.

Net joint moments in gait were previously shown to be similar in children and adults (Gage, 1991; Lim et al., 2013; Sutherland et al., 1980). However, the differences shown in muscular contributions towards maximum isometric joint moments in adults and children indicate that function of the individual leg muscles may also not be fully corresponding in adults and children during normal gait.

For muscles, which dominated vertical CoM support in normal gait, the results are consistent to analysis of adults from Anderson and Pandy (2003)

or Neptune et al. (2004). Induced acceleration analysis show that vastus, gluteus maximus and gluteus medius generate the majority of vertical support during the first half of stance and ankle plantarflexors provide extensive support in the second half of stance.

Vastus provides the main vertical support in loading response and mid-stance of normally-developing children, but is also the main horizontal decelerator of the CoM in these gait phases. In terminal stance gastrocnemius is the main driver for CoM upward acceleration, so that the vertical CoM position and hence inertia was longer preserved. Rectus femoris and soleus, which provide also vertical support, generate a persistent horizontal deceleration effect on the CoM throughout stance phase

Main drivers towards CoM forward acceleration in ND are the hamstrings and gluteus medius in the first half of stance, while inertia is the main forward accelerator in the second half of stance. However, these results are not completely in accordance to Liu et al. (2006), who used the model by Anderson and Pandy (2003) to quantify muscle contributions and who reported notable contributions of soleus and gastrocnemius in propelling the CoM forward.

Hamstrings, vastus, gluteus maximus, gluteus medius and the contralateral hamstrings sequentially deliver main support towards hip extension in the stance phase of the control group. The ankle plantarflexors show negligible contribution towards hip extension; however, they are accelerating hip abduction in second half of stance. This effect is directly compensated by the hip abduction of gluteus medius while it is simultaneously extending the hip in mid to terminal stance.

Hamstrings, vastus, gluteus medius and soleus are consecutively the main accelerator for the knee towards extension during stance in normal gait of children. Vastus, gastrocnemius and soleus are in succession mainly accelerating the ankle towards plantarflexion.

➔ Summarized, vertical support in ND is dominated by five major muscle groups in the lower limb – vasti, gluteus medius and gluteus maximus during the first half of stance, and gastrocnemius and to some extent soleus during the second half of stance. Forward progression is mainly driven by inertia of the body and limbs.

5.4.2 Analysis of muscle function in crouch gait

A higher **hip extension** moment is seen in loading response and mid stance phase of both CP-children, directly forced by the hamstrings in loading response, followed by gluteus maximus together with the frontal contralateral abdomen muscles (external obliques) that tilts the pelvis backward in mid stance. Hip extension acceleration in second half of stance is very different between subjects: in CP1 to a high extend from the contralateral hamstrings, in CP2 from gluteus medius and vastus.

In contrast to ND, residual moments in the medio-lateral axis (MZ) show increased contribution to accelerate the **hip** towards **flexion** in both CP-children. That may be caused by increased HAT movement and balancing actions that result in pelvis forward tilt in combination with hip flexion. However, both CP-children show an about three times higher hip flexion moment in the terminal stance and pre-swing phases (Figure 4.4). This significantly increased hip flexion moment is mainly caused by rectus femoris, while the contribution of iliopsoas is much lower than in ND. The hip flexion action of rectus femoris is performed with the highest possible vigour of this muscle in both CP-children and can be explained with several reasons:

(i)   A **<u>reaction</u>** to cope with the high hip extension effect of the contralateral hamstrings, that may, especially in CP1, be caused by hamstrings spasticity due to lengthening in this gait phase.

(ii)   Additionally to (i), a **<u>reaction</u>** to compensate for the low hip flexion contribution of the shortened and so less effective iliopsoas.

(iii)   The hip flexion effect of rectus femoris is observed during a gait phase when the rectus femoris is rapidly extended (Appendix B, Figure B.2.17a) and may therefore be an **<u>active</u>** cause for the flexed hip.

No common notable **hip adduction** acceleration effects can be identified in both CP-children. **Hip abduction** acceleration in loading response of both CP-children is highly dominated by residual moments around anterior-posterior as well as medio-lateral pelvis axis (MX, MZ). This can be caused by balancing effects in connection with the HAT-segment, that can't be reproduced by the simulated muscle configuration. Gluteus medius accelerates the CoM medially, but with different vigour in each subject.

Vastus is mainly responsible for **knee extension** acceleration throughout the whole stance phase of both CP-children. The peak in knee extension moment in terminal stance is generated by rectus femoris. This effect is coupled to the observed hip flexion moment and acceleration that is seen in mid to terminal stance of both CP-children, but had no influence towards knee extension acceleration. Active **knee flexion** plays only a minor role in both CP-children, so mainly gravitational forces accelerate the knee towards flexion, in coherence to the knee flexion angle.

Although knee flexion moments can be observed, no considerable effect of hamstrings towards knee flexion acceleration is seen in both CP-children. This can be explained by the fact, that the hip extension by hamstrings induces a knee extension, due to a constrained motion of the shank, as long as the leg touches the ground. This induced knee extension acceleration counteracts the direct knee flexion contribution of hamstrings.

The role of soleus for generating **ankle plantarflexion** is more important in both CP-children compared to ND. In ND the ankle plantarflexion is mainly generated by gastrocnemius, which has a significantly lower maximum isometric force in CP-children. Dorsiflexion in the CP-children is mainly caused by gravity, what is related their crouched gait posture with average ankle of 20° dorsiflexion,.

It was found that vertical CoM acceleration in both CP-children has much higher values in positive as well as in negative direction. Main driver towards **vertical CoM acceleration** in both CP-children is the vastus. The effect of gastrocnemius as vertical accelerator in terminal stance is missing in both CP-children, what explains the negative CoM acceleration in terminal stance of both CP-children.

Vastus acts as **CoM-decelerator** in loading response of both CP-children, similar to its role ND, while for forward acceleration of the CoM in CP no common behaviour could be observed. During different gait phases of each CP-child is the **CoM forward** accelerated with individual contributions of hamstrings and gluteus maximus in first halve of stance, gluteus medius or soleus in mid- to terminal stance and of vastus in pre-swing of CP2.

➔ Summarized, the analyses of muscle function during crouched gait show, that both CP-children have remarkably high hip flexion and knee extension moments generated by rectus femoris in terminal stance and pre-swing. Too high muscle lengthening velocity in rectus femoris may an explanation for this effect. Increased muscle lengthening velocity of hamstrings can be a reason for the induced hip extension acceleration during swing phase, which further induces hip extension acceleration on the contralateral stance leg, as is observable especially in terminal stance of CP1. Further both CP-children use their abdominal and back musculature to move the pelvis with much higher dynamics than ND. A better replication of the muscles connecting the trunk with the pelvis may help to understand the way how children use inertia of the upper body to induce acceleration on their hip joints for flexion, extension and abduction. Vastus is the main accelerator towards knee extension in CP due to the crouched posture in gait. Very low active knee flexion is determined for both CP-children. Gastrocnemius contributes in crouch gait lower than in ND to both, plantarflexion and CoM upward acceleration in terminal stance. Forward CoM acceleration in CP-gait is individually composed either by hip extensor muscles in first half and soleus in second half of stance (CP1) or by hamstrings throughout stance phase supported by hip extensor in loading response and abductor muscles in mid to terminal stance (CP2).

5.4.2.1 Contribution of hamstrings to hip extension in CP

Regarding the contribution of hamstrings to hip extension of in CP gait, the first hypothesis of this study state that:

Excessive passive forces are generated in hamstrings during crouch gait, because these muscles are abnormally short. Thus, lower-than-normal forces are generated in gluteus maximus to compensate for the excessive force in hamstrings.

It was found that:

> ➢ **Hamstrings can generate passive forces in swing phase of crouch gait, but not due their shortage but because of exceeding a critical lengthening velocity, as shown in on cases. However, this action of hamstrings in swing phase has no influence on the contributions of gluteus maximus to hip flexion.**

Muscle fibres of hamstrings in CP-gait are on average around 10% shorter than in ND throughout the gait cycle.

A higher hip extension moment and acceleration is seen in loading response and mid stance phase of both CP-children, where hamstrings play an important role for hip extension, together with gluteus maximus in CP1 and gluteus medius in CP2.

Hamstrings cause a high hip extension moment in swing phase of CP1, by absorbing energy when they produce hip flexion moment while they are lengthened. This characteristic has direct influence on the hip extension of the stance leg in terminal stance as can be seen when analyzing the contribution of the contralateral hamstrings towards hip flexion acceleration. This unusual behaviour can directly be linked to a spastic action of hamstrings due to too high lengthening velocity.

5.4.2.2 Contribution of hamstrings to knee flexion in CP

Regarding the role for knee flexion of hamstrings in CP-gait, the second hypothesis in this study states that:

Hamstrings act to accelerate the knee toward flexion with more vigor during the stance phase of crouch gait than during the stance phase of normal gait.

It was found that:

> ✘ **Active knee flexion plays only a minor role in both CP-children, so mainly gravitational forces (in in relation to the knee flexion angle) accelerate the knee towards flexion.**

The knee flexion moment of hamstrings was increased on one subject (CP1) during stance phase. However, the hip extension generated by hamstrings counteracts the contribution of hamstrings towards knee flexion

as the hip extension induces synchronously ann acceleration of the knee towards extension, as long as the knee flexion is constrained with the foot having ground contact.

5.4.2.3 Contribution of vastus towards knee extension and CoM accelerations

Regarding the role for knee extension and CoM accelerations of the vasti, the third hypothesis of this study states that:

Vasti is the major contributor to accelerating the knee toward extension throughout stance, and therefore, this muscle dominates vertical support and forward progression in crouch gait. As with normal gait, vasti slows forward progression during the first half of stance and speeds forward progression during the second half of stance.

It was found that:

✓ **In both CP–children mainly the vastus is responsible for knee extension acceleration throughout the whole stance phase:**

In CP1 additionally soleus accelerates the knee towards extension in loading response and mid stance and the contralateral hamstrings in terminal stance.

In CP2 the vastus generates persistent high knee extension acceleration throughout the stance phase, what is mainly necessary due to the crouched gait posture.

✓ **Vastus was the main driver towards positive vertical CoM acceleration in both CP-children:**

It is found that vertical CoM acceleration in both CP-children has much higher values in positive as well as in negative direction. In loading response and mid stance, a phase of high upward acceleration of the CoM is observed, while in terminal stance the pelvis is significantly lowered, followed by an upward acceleration phase in pre-swing (which is synchronous to the loading response of contralateral leg).

Further was found that:

! In contrast to ND the vertical CoM acceleration generated by gastrocnemius is missing in both CP-children. This may explain the negative CoM acceleration in terminal stance, as gravitational forces cannot compensated significantly. Consequently, kinetic energy is lost and cannot be used for CoM accelerations. Vertical and forward accelerations are timed differently in crouch gait compared to ND and are mainly driven by musculature.

> In CP1 vastus, gluteus maximus, gluteus medius and hamstrings act as vertical accelerator for the CoM in loading response and mainly soleus in terminal stance.

> In CP2 the CoM is mainly vertically accelerated by the vastus and hamstrings during the stance phase.

! In both CP-children vastus acts as CoM-decelerator in loading response, similar as in ND. In CP1 has vastus almost no forward acceleration effect, while in CP2 the highest forward acceleration due to vastus is observed in pre-swing.

5.5 General discussion and conclusions

The results of this study are significant on a number of levels:

First, a process for comprehensible generation of individual musculoskeletal models based on data obtained from in vivo MR imaging was developed, which may facilitate the use of custom biomechanical models in future clinical practice. The developed methods were applied to generate individual models of normally developing children and of children with CP who have bony deformities like femoral anteversion and tibial rotation. These custom models incorporate individual musculoskeletal geometry and physiological properties of the 52 major lower-limb muscles.

Second, most currently used models of children with cerebral palsy are based on data obtained from a healthy adult male. This adult model shows distinct differences in muscle function compared to children. Virtually no data was available up to now that quantifies the geometric and architectural

properties of leg muscles either in healthy children or in children with CP. Hence, geometric and architectural properties of the five normally developing children were merged to generate an averaged children's model, which almost exactly replicates the mean maximum isometric joint moment – joint angle trajectories of the subject specific models. This model can serve as a reference or as template for quick generation of mass-length scaled models of lower-limb muscle function in children, in studies where less time or no MR-data is available. The average child model is accessible on: https://simtk.org/home/children.

Third, the different characteristics of geometric and architectural properties in the two investigated subjects with CP clearly show that individual modelling is necessary for further assessment of muscle function in motion for diagnostic purposes. Models of children with CP, which were generated by mass-length scaling of either a template model of an adult or the new average children's model, show significant deviations in functional muscle characteristics compared to the MR-based models.

Fourth, based on the finding that the net joint moments in gait are similar in children and adults, it was assumed up to now, that the individual leg muscles also work in the same way. The calculations using the MR-based models in this study reveal the time histories of leg muscle forces generated in normal gait of children. However, the results show, in comparison to data shown in literature, that leg-muscle function is not completely the same in both cohorts, healthy children and adults. These results can serve as an important guideline for a large number of clinical gait laboratories around the world that use gait data obtained from healthy children as a baseline comparison in clinical gait studies of children with CP.

Fifth, information on the time histories of leg-muscle forces and their contribution towards joint moments as well as joint and CoM acceleration during gait are useful to surgeons and physical therapists in pre-operative and therapy planning. These results may play an important role in the selection of which muscle or tendon may be lengthened or transferred. The results can further help to optimize appropriate methods in physical rehabilitation, such as prescribing muscle-strengthening exercises to alleviate the effects of lower-limb muscle weakness, or the prescription of the correct ortheses to treat a specific abnormality.

5.5 General discussion and conclusions

Data on kinematics, like limb motion described by joint angle trajectories and kinetics given by net muscle moments, are being used at present for the selection of therapy in medical routine. However, these data do not provide sufficient quantitative information about the function of the individual muscles during gait. Calculations of muscle lengths and of critical lengthening velocity have identified in the literature as possible cause of spasticity during gait. These calculations were done by using computer models of musculoskeletal geometry, but this approach does neither provide information about the amount of force a muscle may be producing during a given period of the gait cycle nor about its role in supporting forward and vertical CoM acceleration.

The approach presented in this study allows to obtain time histories of individual leg-muscle lengths, shortening velocity, muscle forces and contributions to direct as well as to induced joint angle accelerations for the gait pattern of a child with CP. This knowledge allows to gain further insight into the roles of specific muscles during gait and also helps to identify reasons for the abnormal gait pattern in pathological gait.

Bibliography

Ackland, D.C., Lin, Y.-C., Pandy, M.G., 2012. Sensitivity of model predictions of muscle function to changes in moment arms and muscle–tendon properties: A Monte-Carlo analysis. J. Biomech. 45, 1–9.

Anderson, D.E., Madigan, M.L., Nussbaum, M.A., 2007. Maximum voluntary joint torque as a function of joint angle and angular velocity: model development and application to the lower limb. J. Biomech. 40, 3105–13.

Anderson, F.C, 1999. A dynamic optimization solution for a complete cycle of normal gait. University of Texas, 1999, Austin.

Anderson, F.C., Pandy, M.G., 1999. A Dynamic Optimization Solution for Vertical Jumping in Three Dimensions. Comput. Methods Biomech. Biomed. Engin. 2, 201–231.

Anderson, F.C., Pandy, M.G., 2001a. Dynamic optimization of human walking. J. Biomech. Eng. 123, 381–390.

Anderson, F.C., Pandy, M.G., 2001b. Static and dynamic optimization solutions for gait are practically equivalent. J. Biomech. 34, 153–61.

Anderson, F.C., Pandy, M.G., 2003. Individual muscle contributions to support in normal walking. Gait Posture 17, 159–169.

Anderson, F.C., Pandy, M.G., Fc, A., A, P.M.G., 1999. A Dynamic Optimization Solution for Vertical Jumping in Three Dimensions. Comp. Meth. Biomech Biomed. Eng, Vol. 2, 201–231.

Arnold, A.S., Blemker, S.S., Delp, S.L., 2001. Evaluation of a Deformable Musculoskeletal Model for Estimating Muscle–Tendon Lengths During Crouch Gait. Ann. Biomed. Eng. 29, 263–274.

Arnold, A.S., Liu, M.Q., Schwartz, M.H., OUnpuu, S., Dias, L.S., Delp, S.L., 2005. Do the hamstrings operate at increased muscle–tendon lengths and velocities after surgical lengthening? ˜. J. Biomech.

Arnold, A.S., Salinas, S., Asakawa, D.J., Delp, S.L., 2000. Accuracy of Muscle Moment Arms Estimated from MRI-Based Musculoskeletal Models of the Lower Extremity. Comput. Aided Surg. 5, 108 –119.

Arnold, E.M., Ward, S.R., Lieber, R.L., Delp, S.L., 2010. A model of the lower limb for analysis of human movement. Ann. Biomed. Eng. 38, 269–79.

Bibliography

Beynnon, B.D., Fleming, B.C., Churchill, D.L., Brown, D., 2003. The effect of anterior cruciate ligament deficiency and functional bracing on translation of the tibia relative to the femur during nonweightbearing and weightbearing. Am. J. Sports Med. 31, 99–105.

Bleck, E.E., 1990. Management of the lower extremities in children who have cerebral palsy. J. Bone Joint Surg. Am. 72, 140–4.

Blemker, S.S., Asakawa, D.S., Gold, G.E., Delp, S.L., 2007. Image-Based Musculoskeletal Modeling: Applications, Advances, and Future Opportunities. J. Magn. Reson. Imaging 451, 441– 451.

Bobbert, M.F., Harlaar, J., 1993. Evaluation of moment-angle curves in isokinetic knee extension. Med. Sci. Sports Exerc. 25, 251–9.

Brand, R., Pedersen DR, Friederich JA, 1986. The Sensitivity of Muscle Froce Predictions to Changes in Physiologic Cross-Sectional Area. J. Biomech. 19, 589–596.

Brand, R.A., Pedersen, D.R., Friederich, J.A., 1986. The sensitivity of muscle force predictions to changes in physiologic cross-sectional area. J. Biomech. 19, 589–96.

Brunner, R., Dreher, T., Romkes, J., Frigo, C., 2008. Effects of plantarflexion on pelvis and lower limb kinematics. Gait Posture 28, 150–6.

Butler, D.L., Grood, E.S., Noyes, F.R., Zernicke, R.F., 1978. Biomechanics of ligaments and tendons. Exerc. Sport Sci. Rev. 6, 125–81.

Cahalan, T.D., Johnson, M.E., Liu, S., Chao, E.Y., 1989. Quantitative measurements of hip strength in different age groups. Clin. Orthop. Relat. Res. 136–45.

CDC, 2013. No Title [WWW Document]. URL http://www.cdc.gov/ncbddd/cp/data.html

Correa, A.T., 2011. Patienet-Specific Computational Tools For Assessing Muscle Function in Children with Cerebral Palsy. Ann. Neurol. The University of Melbourne.

Correa, T. a, Baker, R., Graham, H.K., Pandy, M.G., 2011. Accuracy of generic musculoskeletal models in predicting the functional roles of muscles in human gait. J. Biomech. 44, 2096–105.

Correa, T. a, Pandy, M.G., 2011. A mass-length scaling law for modeling muscle strength in the lower limb. J. Biomech. 44, 2782–9.

Correa, T. a, Schache, A.G., Graham, H.K., Baker, R., Thomason, P., Pandy, M.G., 2012. Potential of lower-limb muscles to accelerate the body during cerebral palsy gait. Gait Posture 36, 194–200.

Correa, T., Pandy, M., 2012. On the potential of lower limb muscles to accelerate the body's centre of mass during walking. Comput. Methods Biomech. Biomed. Engin.

Crowninshield, R.D., 1983. A physiologically based criterion for muscle force predictions on locomotion. Bull. Hosp. Jt. Dis. Orthop. Inst. 43, 164–70.

Damiano, D., Laws, E., Carmines, D., 2006. Relationship of spasticity to knee angular velocity and motion during gait in cerebral palsy. Gait Posture 23, 1–8.

Davis, R.B., Tyburski, D., Gage, J.R., 1991. Gait analysis data collection and reduction technique. Hum. Mov. Sci. 10, 575–587.

Delp, S., Arnold, A., 1996. Hamstrings and psoas lengths during normal and crouch gait: Implications for muscle-tendon surgery. J. Orthop. ….

Delp, S.L., 1990. Surgery simulation: A computer graphics system to analyze and design muskulioskeletal reconstructions of the lower limb.

Delp, S.L., Anderson, F.C., Arnold, A.S., Loan, P., Habib, A., John, C.T., Guendelman, E., Thelen, D.G., 2007. OpenSim: Open-Source Software to Create and Analyze Dynamic Simulations of Movement. IEEE Trans. Biomed. Eng. 54, 1940–1950.

Delp, S.L., Arnold, A.S., Speers, R.A., Moore, C.A., 1996. Hamstrings and psoas lengths during normal and crouch gait: implications for muscle-tendon surgery. J. Orthop. Res. 14, 144–51.

Delp, S.L., Loan, J.P., 1995. A graphics-based software system to develop and analyze models of musculoskeletal structures. Comput. Biol. Med. 25, 21–34.

Delp, S.L., Loan, J.P., 2000. A Computational Framework for Simulating and Analyzing Human and Animal Movement. Comput. Med.

Delp, S.L., Loan, J.P., Hoy, M.G., Zajac, F.E., Topp, E.L., Rosen, J.M., W, S.L.D.E., 1990. An interactive graphics-based model of the lower extremity to study orthopaedic surgical. Proced. IEEE Trans. Biomed. Eng. 37, 757–767.

BIBLIOGRAPHY

DeLuca, P.A., Davis, R.B., Ounpuu, S., Rose, S., Sirkin, R., 1997. Alterations in surgical decision making in patients with cerebral palsy based on three-dimensional gait analysis. J. Pediatr. Orthop. 17, 608–14.

Dhawlikar, S.H., Root, L., Mann, R.L., 1992. Distal lengthening of the hamstrings in patients who have cerebral palsy. Long-term retrospective analysis. J. Bone Joint Surg. Am. 74, 1385–91.

Dietz, V., Berger, W., 1995. Cerebral palsy and muscle transformation. Dev. Med. Child Neurol. 37, 180–4.

Dorn, T., Tjio, W., 2006. Computer Simulation of Human Walking and Running using Inverse Dynamics and Static Optimisation.

Dorn, T.W., 2008. Gait Extraction Toolbox.

Dorn, T.W., Lin, Y.-C., Pandy, M.G., 2012a. Estimates of muscle function in human gait depend on how foot-ground contact is modelled. Comput. Methods Biomech. Biomed. Engin. 15, 657–68.

Dorn, T.W., Schache, A.G., Pandy, M.G., 2012b. Muscular strategy shift in human running: dependence of running speed on hip and ankle muscle performance. J. Exp. Biol. 215, 1944–56.

Eames, N.W.A., Baker, R.J., Cosgrove, A.P., 1997. Defining gastrocnemius length in ambulant children. Gait Posture 6, 9–17.

Eek, M.N., Kroksmark, A.-K., Beckung, E., 2006. Isometric muscle torque in children 5 to 15 years of age: normative data. Arch. Phys. Med. Rehabil. 87, 1091–9.

Erdemir, A., McLean, S., Herzog, W., van Den Bogert, A.J., 2007. Model-based estimation of muscle forces exerted during movements. Clin. Biomech. (Bristol, Avon) 22, 131–54.

Friederich, J.A., Brand, R.A., 1990. Muscle Fiber Architecture in the Human Lower Limb. J. Biomech. 23, 91–95.

Gage, J.R., 1990. Surgical treatment of knee dysfunction in cerebral palsy. Clin. Orthop. Relat. Res. 45–54.

Gage, J.R., 1991. Gait Analysis in Cerebral Palsy (Clinics in Developmental Medicine (Mac Keith Press)). Cambridge University Press.

Gage, J.R., 2004. Treatment of Gait Problems in Cerebral Palsy.

Gage, J.R., Fabian, D., Hicks, R., Tashman, S., 1984. Pre- and postoperative gait analysis in patients with spastic diplegia: a preliminary report. J. Pediatr. Orthop. 4, 715–25.

Gage, J.R., Schwartz, M.S., 2002. Dynamic deformities and lever-arm dysfunction. In: Paley, D. (Ed.), Principles of Deformity Correction. Springer-Verlag.

Garner, B.A., Pandy, M.G., 2000. The Obstacle-Set Method for Representing Muscle Paths in Musculoskeletal Models. Comput. Methods Biomech. Biomed. Engin. 3, 1–30.

Gföhler, M., 2004. Dynamic simulation of FES-cycling: influence of individual parameters. In: IEEE Transactions on Neural Systems and Rehabilitation Engineering. TNSRE, pp. 398 – 405.

Gföhler, M., Lugner, P., 2000. Cycling by means of functional electrical stimulation. IEEE Trans. Rehabil. Eng. 8, 233–43.

Granata, K.P., Abel, M.F., Damiano, D.L., 2000. Joint angular velocity in spastic gait and the influence of muscle-tendon lengthening. J. Bone Joint Surg. Am. 82, 174–86.

Hainisch, R., Karim, Z.M., Kranzl, A., Gföhler, M., Pandy, M.G., 2010. Scaling Of Biomechanical Models: A Comparison Of Motion-Tracking Markers And Anatomical Landmarks From Mri. In: 9th International Symposium on Computer Methods in Biomechanics and Biomedical Engineering, CMBBE2010. Arup, Solihull, UK, Valencia, Spain, p. 6 pages.

Herzog, W., 1992. Sensitivity of muscle force estimations to changes in muscle input parameters using nonlinear optimization approaches. J. Biomech. Eng. 114, 267–8.

Hill, A. V, 1938. The heat of shortening and the dynamic constants of muscle. Proc. R. Soc. London. Ser. B, 136–195.

Himmelmann, K., Hagberg, G., Uvebrant, P., 2010. The changing panorama of cerebral palsy in Sweden. X. Prevalence and origin in the birth-year period 1999-2002. Acta Paediatr. 99, 1337–43.

Inman, V.T., Ralston, H.J., Todd, F., 1981. Human walking. Baltimore.

Kaufman, K.R., An, K.W., Litchy, W.J., Chao, E.Y., 1991. Physiological prediction of muscle forces--I. Theoretical formulation. Neuroscience 40, 781–92.

Bibliography

Kerrigan, D.C., Burke, D.T., Nieto, T.J., Riley, P.O., 2001. Can toe-walking contribute to stiff-legged gait? Am. J. Phys. Med. Rehabil. 80, 33–7.

Klein Horsman, M.D., Koopman, H.F.J.M., van Der Helm, F.C.T., Prosé, L.P., Veeger, H.E.J., Horsman, M.D.K., Helm, F.C.T. Van Der, Prose, L.P., 2007. Morphological muscle and joint parameters for musculoskeletal modelling of the lower extremity. Clin. Biomech. (Bristol, Avon) 22, 239–47.

Krägeloh-Mann, I., Hagberg, G., Meisner, C., Haas, G., Eeg-Olofsson, K.E., Selbmann, H.K., Hagberg, B., Michaelis, R., 1995. Bilateral spastic cerebral palsy--a collaborative study between southwest Germany and western Sweden. III: Aetiology. Dev. Med. Child Neurol. 37, 191–203.

Krogt, M. van der, 2009. Gait Deviations in Children with Cerebral Palsy: a Modeling Approach.

Krogt, M.M. Van Der, Doorenbosch, C.A.M., Harlaar, J., van der Krogt, M.M., 2009. The effect of walking speed on hamstrings length and lengthening velocity in children with spastic cerebral palsy. Gait Posture 29, 640–4.

Kuo, A.D., 1998. A least-squares estimation approach to improving the precision of inverse dynamics computations. J. Biomech. Eng. 120, 148–59.

Kuo, A.D., Zajac, F.E., 1993. A biomechanical analysis of muscle strength as a limiting factor in standing posture. J. Biomech. 26 Suppl 1, 137–50.

Laplaza, F.J., Root, L., Tassanawipas, A., Glasser, D.B., 1993. Femoral torsion and neck-shaft angles in cerebral palsy. J. Pediatr. Orthop. 13, 192–9.

Lebiedowska, M.K., Polisiakiewicz, A., 1997. Changes in the lower leg moment of inertia due to child's growth. J. Biomech. 30, 723–8.

Lenzi, D., Cappello, A., Chiari, L., 2003. Influence of body segment parameters and modeling assumptions on the estimate of center of mass trajectory. J. Biomech. 36, 1335–1341.

Lim, Y.P., Lin, Y.-C., Pandy, M.G., 2013. Muscle function during gait is invariant to age when walking speed is controlled. Gait Posture 38, 253–9.

Lin, C.J., Guo, L.Y., Su, F.C., Chou, Y.L., Cherng, R.J., 2000. Common abnormal kinetic patterns of the knee in gait in spastic diplegia of cerebral palsy. Gait Posture 11, 224–232.

Lin, Y., Kim, H.J., Pandy, M.G., 2011. A computationally efficient method for assessing muscle function during human locomotion 436–449.

Lin, Y.-C., Dorn, T.W., Schache, a. G., Pandy, M.G., 2011. Comparison of different methods for estimating muscle forces in human movement. Proc. Inst. Mech. Eng. Part H J. Eng. Med. 226, 103–112.

Liu, M.Q., Anderson, F.C., Pandy, M.G., Delp, S.L., 2006. Muscles that support the body also modulate forward progression during walking. J. Biomech. 39, 2623–2630.

Liu, M.Q., Anderson, F.C., Schwartz, M.H., Delp, S.L., 2008. Muscle contributions to support and progression over a range of walking speeds. J. Biomech. 41, 3243–52.

Lu, T.W., O'connor, J.J., O'Connor, J.J., 1999. Bone position estimation from skin marker co-ordinates using global optimisation with joint constraints. J. Biomech. 32, 129–34.

McManus, V., Guillem, P., Surman, G., Cans, C., 2006. SCPE work, standardization and definition--an overview of the activities of SCPE: a collaboration of European CP registers. Zhongguo Dang Dai Er Ke Za Zhi 8, 261–5.

Mokhtarzadeh, H., Perraton, L., Fok, L., Muñoz, M.A., Clark, R., Pivonka, P., Bryant, A.L., 2014. A comparison of optimisation methods and knee joint degrees of freedom on muscle force predictions during single-leg hop landings. J. Biomech.

Murray, M.P., Gardner, G.M., Mollinger, L.A., Sepic, S.B., 1980. Strength of isometric and isokinetic contractions: knee muscles of men aged 20 to 86. Phys. Ther. 60, 412–9.

Murray, W.M., Arnold, A.S., Salinas, S., Durbhakula, M.M., Buchanan, T.S., Delp, S.L., 1998. Building biomechanical models based on medical image data: An assessment of model accuracy, Medical Image Computing and Computer-Assisted Intervention — MICCAI'98, Lecture Notes in Computer Science. Springer-Verlag, Berlin/Heidelberg.

Neptune, R.R., Hull, M.L., 1998. Evaluation of performance criteria for simulation of submaximal steady-state cycling using a forward dynamic model. J. Biomech. Eng. 120, 334–41.

Neptune, R.R., Kautz, S.A., Zajac, F.E., 2001. Contributions of the individual ankle plantar flexors to support , forward progression and swing initiation during walking. J. Biomech. 34, 1387–1398.

BIBLIOGRAPHY

Neptune, R.R., Zajac, F.E., Kautz, S. a, 2004. Muscle force redistributes segmental power for body progression during walking. Gait Posture 19, 194–205.

O'Brien, T.D., Reeves, N.D., Baltzopoulos, V., Jones, D. a, Maganaris, C.N., 2010a. Muscle-tendon structure and dimensions in adults and children. J. Anat. 216, 631–42.

O'Brien, T.D., Reeves, N.D., Baltzopoulos, V., Jones, D. a, Maganaris, C.N., Brien, T.D.O., 2010b. In vivo measurements of muscle specific tension in adults and children. Exp. Physiol. 95, 202–10.

Olson, V.L., Smidt, G.L., Johnston, R.C., 1972. The maximum torque generated by the eccentric, isometric, and concentric contractions of the hip abductor muscles. Phys. Ther. 52, 149–58.

Pakula, A.T., Van Naarden Braun, K., Yeargin-Allsopp, M., 2009. Cerebral palsy: classification and epidemiology. Phys. Med. Rehabil. Clin. N. Am. 20, 425–52.

Palisano, R., Rosenbaum, P., Walter, S., Russell, D., Wood, E., Galuppi, B., 1997. Development and reliability of a system to classify gross motor function in children with cerebral palsy. Dev. Med. Child Neurol. 39, 214–23.

Pandy, M.G., 2001. COMPUTER MODELING AND SIMULATION OF HUMAN MOVEMENT. Annu. Rev. Biomed. Eng. 3, 245–73.

Pandy, M.G., Andriacchi, T.P., 2010. Muscle and joint function in human locomotion. Annu. Rev. Biomed. Eng. 12, 401–33.

Pandy, M.G., Garner, B.A., Anderson, F.C., 1995. Optimal control of non-ballistic muscular movements: a constraint-based performance criterion for rising from a chair. J. Biomech. Eng. 117, 15–26.

Pandy, M.G., Zajac, F.E., 1991. Optimal muscular coordination strategies for jumping. J. Biomech. 24, 1–10.

Pandy, M.G., Zajac, F.E., Sim, E., Levine, W.S., 1990. An optimal control model for maximum-height human jumping. J. Biomech. 23, 1185–98.

Park, M.S., Chung, C.Y., Lee, S.H., Choi, I.H., Cho, T.-J., Yoo, W.J., Park, B.S.M.Y., Lee, K.M., 2009. Effects of distal hamstring lengthening on sagittal motion in patients with diplegia: hamstring length and its clinical use. Gait Posture 30, 487–91.

Pataky, T.C., Zatsiorsky, V.M., Challis, J.H., 2003. A simple method to determine body segment masses in vivo: reliability, accuracy and sensitivity analysis. Clin. Biomech. 18, 364–368.

Paulev, P.-E., Zubieta-Calleja, G., 2004. New Human Physiology. Kopenhagen, Denmark.

Raasch, C.C., Zajac, F.E., Ma, B., Levine, W.S., 1997. Muscle coordination of maximum-speed pedaling. J. Biomech. 30, 595–602.

Rab, G., 1992. Diplegic gait: Is there more than spasticity. In: Sussman MD (Ed.), The Diplegic Child. American Academy of Orthopaedic Surgeons, Rosemont, Illinois.

Raikova, R.T., Prilutsky, B.I., 2001. Sensitivity of predicted muscle forces to parameters of the optimization-based human leg model revealed by analytical and numerical analyses. J. Biomech. 34, 1243–1255.

Redl, C., Gfoehler, M., Pandy, M.G., 2007. Sensitivity of muscle force estimates to variations in muscle-tendon properties. Hum. Mov. Sci. 26, 306–19.

Reinbolt, J. a., Seth, A., Delp, S.L., 2011. Simulation of human movement: applications using OpenSim. Procedia IUTAM 2, 186–198.

Rodda, J.M., Graham, H.K., Carson, L., Galea, M.P., Wolfe, R., 2004. Sagittal gait patterns in spastic diplegia. J. Bone Joint Surg. Br. 86, 251–8.

Rosenbaum, P., Paneth, N., Leviton, A., Goldstein, M., Bax, M., Damiano, D., Dan, B., Jacobsson, B., 2007. A report: the definition and classification of cerebral palsy April 2006. Dev. Med. Child Neurol. Suppl. 109, 8–14.

Scheys, L., Jonkers, I., Loeckx, D., Maes, F., Spaepen, A., Suetens, P., 2006. Image Based Muskuloskeltal Modeling Allows Personalized Biomechanical Analysis of Gait. Image (Rochester, N.Y.) 58–66.

Scheys, L., Loeckx, D., Spaepen, A., Suetens, P., Jonkers, I., 2009. Atlas-based non-rigid image registration to automatically define line-of-action muscle models: a validation study. J. Biomech. 42, 565–72.

Scheys, L., Spaepen, A., Suetens, P., Jonkers, I., Van Campenhout, A., 2008. Calculated moment-arm and muscle-tendon lengths during gait differ substantially using MR based versus rescaled generic lower-limb musculoskeletal models. Gait Posture 28, 640–8.

Bibliography

Schutte, L.M., Hayden, S.W., Gage, J.R., 1997. Lengths of hamstrings and psoas muscles during crouch gait: effects of femoral anteversion. J. Orthop. Res. 15, 615–21.

Scovil, C.Y., Ronsky, J.L., 2006. Sensitivity of a Hill-based muscle model to perturbations in model parameters. J. Biomech. 39, 2055–63.

Seth, A., Pandy, M.G.A., 2007. A neuromusculoskeletal tracking method for estimating individual muscle forces in human movement. J. Biomech. 40, 356–66.

Seth, A., Sherman, M., Reinbolt, J., Delp, S., 2011. OpenSim: a musculoskeletal modeling and simulation framework for in silico investigations and exchange. Procedia IUTAM 2, 212–232.

Spoor, C.W., van Leeuwen, J.L., 1992. Knee muscle moment arms from MRI and from tendon travel. J. Biomech. 25, 201–6.

Steele, K.M., Seth, A., Hicks, J.L., Schwartz, M.H., Delp, S.L., 2013. Muscle contributions to vertical and fore-aft accelerations are altered in subjects with crouch gait. Gait Posture 38, 86–91.

Steele, K.M., Seth, A., Hicks, J.L., Schwartz, M.S., Delp, S.L., 2010. Muscle contributions to support and progression during single-limb stance in crouch gait. J. Biomech. 43, 2099–105.

Steele, K.M., van der Krogt, M.M., Schwartz, M.H., Delp, S.L., 2012. How much muscle strength is required to walk in a crouch gait? J. Biomech. 45, 2564–9.

Stingeder, C., 2009. Three dimensional modelling of the lower limb of children with cerebral palsy and healthy children based on MRI - data. Vienna University of Technology.

Sutherland, D.H., Cooper, L., 1978. The pathomechanics of progressive crouch gait in spastic diplegia. Orthop. Clin. North Am. 9, 143–54.

Sutherland, D.H., Davids, J.R., 1993. Common gait abnormalities of the knee in cerebral palsy. Clin. Orthop. Relat. Res. 139–47.

Sutherland, D.H., Olshen, R., Cooper, L., Woo, S.L., 1980. The development of mature gait. J. Bone Joint Surg. Am. 62, 336–53.

Thelen, D.G., Anderson, F.C., Delp, S.L., 2003. Generating dynamic simulations of movement using computed muscle control. J. Biomech. 36, 321–328.

Thometz, J., Simon, S., Rosenthal, R., 1989. The effect on gait of lengthening of the medial hamstrings in cerebral palsy. J. Bone Joint Surg. Am. 71, 345–53.

Van der Krogt, M.M., Delp, S.L., Schwartz, M.H., 2012. How robust is human gait to muscle weakness? Gait Posture 36, 113–9.

Van der Krogt, M.M., Doorenbosch, C. a M., Harlaar, J., 2008. Validation of hamstrings musculoskeletal modeling by calculating peak hamstrings length at different hip angles. J. Biomech. 41, 1022–8.

Van der Krogt, M.M., Doorenbosch, C.A.M., Becher, J.G., Harlaar, J., 2010. Dynamic spasticity of plantar flexor muscles in cerebral palsy gait. J. Rehabil. Med. 42, 656–63.

Van Eijden, T.M., Weijs, W.A., Kouwenhoven, E., Verburg, J., 1987. Forces acting on the patella during maximal voluntary contraction of the quadriceps femoris muscle at different knee flexion/extension angles. Acta Anat. (Basel). 129, 310–4.

Van Soest, A.J., Schwab, A.L., Bobbert, M.F., van Ingen Schenau, G.J., 1993. The influence of the biarticularity of the gastrocnemius muscle on vertical-jumping achievement. J. Biomech. 26, 1–8.

Wang, L., 2011. The lower extremity biomechanics of single- and double-leg stop-jump tasks 151–156.

Ward, S., Smallwood, L., Lieber, R., 2005. Scaling of human lower extremity muscle architecture to skeletal dimensions. ISB XXth Congr. … 925.

Ward, S.R., Eng, C.M., Smallwood, L.H., Lieber, R.L., Pt, S.R.W., Bs, C.M.E., Bs, L.H.S., 2009. Are current measurements of lower extremity muscle architecture accurate? Clin. Orthop. Relat. Res. 467, 1074–82.

Waters, R.L., Perry, J., McDaniels, J.M., House, K., 1974. The relative strength of the hamstrings during hip extension. J. Bone Joint Surg. Am. 56, 1592–7.

Weijs, W., Hillen, B., 1985. Cross-sectional areas and estimated intrinsic strength of the human jaw muscles. Acta Morphol Neerl Scand. 23(3), 267–74.

Westwell, M., Ounpuu, S., DeLuca, P., 2009. Effects of orthopedic intervention in adolescents and young adults with cerebral palsy. Gait Posture 30, 201–6.

Wickiewicz, T.L.T., Roy, R.R., Powell, P., VR, Edgerton, V.R., 1983. Muscle architecture of the human lower limb. Clin. Orthop. Relat. Res. 275–283.

163

Bibliography

Winby, C.R., Lloyd, D.G., Kirk, T.B., 2008. Evaluation of different analytical methods for subject-specific scaling of musculotendon parameters. J. Biomech. 41, 1682–8.

Winter, D.A., 2009. Biomechanics and Motor Control of Human Movement. John Wiley & Sons.

Zajac, F.E., 1989. Muscle and tendon: properties, models, scaling, and application to biomechanics and motor control. Crit. Rev. Biomed. Eng. 17, 359–411.

Zajac, F.E., 1993. Muscle coordination of movement: a perspective. J. Biomech. 26 Suppl 1, 109–24.

Zajac, F.E., Gordon, M.E., 1989. Determining muscle's force and action in multi-articular movement. Exerc. Sport Sci. Rev. 17, 187–230.

Zajac, F.E., Neptune, R.R., Kautz, S.A., 2003. Biomechanics and muscle coordination of human walking Part II: Lessons from dynamical simulations and clinical implications. Gait Posture 17, 1–17.

Zwick, E.B., Saraph, V., Zwick, G., Steinwender, C., Linhart, W.E., Steinwender, G., 2002. Medial hamstring lengthening in the presence of hip flexor tightness in spastic diplegia. Gait Posture 16, 288–96.

Appendices

A

Model Descriptions

The following pages show individual muscle model parameters as well as all geometric parameters of the developed models. The muscle model parameters: are denoted in original values that have been derived based on radiology data, the geometric values such as joint centre locations or coordinates of the muscle attachment sites and muscle path points are denoted in the coordinate system of the parent limb segment.

The model parameters for the average children's model are given in section A.2 (p. A-23ff)

A.1 Individual Model Parameters

A.1.1 Model of Subject ND1

Muscle	Max. Force [N]	l_{0m}[cm]	TSL[cm]	pennation [degree]
Adductor longus	238	9,00	10,22	6,6
Adductor magnus	891	12,45	11,64	15,6
Hamstrings	737	11,97	23,94	8,0
Biceps femoris short head	183	9,31	8,46	12,3
Iliopsoas	525	8,93	8,09	12,5
Gluteus maximus	884	14,30	12,43	21,9
Gluteus medius	599	6,34	2,61	20,5
Gluteus minimus	156	5,11	0,81	10,0
Gracilis	93	19,29	12,51	8,2
Pectinius	273	10,84	6,37	0,0
Piriformis	364	2,03	6,53	10,0
Sartorius	65	34,17	8,16	0,0
Tensor fasciae latae	90	8,16	32,17	3,0
Rectus femoris	701	6,61	29,39	13,9
Vastus	2766	8,60	25,22	17,5
Peroneus	455	4,02	34,77	13,0
Gastrocnemius	1474	4,43	33,54	10,9
Soleus	2055	3,46	26,38	28,3
Tibialis anterior	339	5,39	28,29	9,6
Tibialis posterior	666	2,92	29,75	13,7
Extensor digitorum	258	5,70	38,15	7,0
Flexor digitorum longus	170	3,54	35,76	13,6
Flexor hallucis longus	273	4,21	35,95	16,9

Table A.1.1 Muscle Model Parameters for model of ND1 Individual Hill-type muscle model parameters

Segment	Joint Center location [cm]			Reference Segment
	X ant.-post.	Y sup.-inf.	Z med.-lat.	
Pelvis center	0,00	79,20	0,00	Ground
Right hip	-3,83	-0,05	6,67	Pelvis
Left hip	-3,85	-0,06	-6,27	Pelvis
Right knee *	0,00	-0,34	0,00	Right Femur
Left knee *	0,00	-0,34	0,00	Left Femur
Right ankle	0,91	-0,32	1,11	Right Tibia
Left ankle	-0,12	-0,31	-1,11	Left Tibia
Right Toes	14,39	0,00	0,00	Right Calcaneus
Left Toes	14,39	0,00	0,00	Left Calcaneus

Table A.1.2 Joint Centres for Model of model of ND1 *Coordinates for knee joint centre at 0° knee angle

Muscle	Coordinates [mm]			Point Type	Ref. Body
	X	Y	Z		
Adductor longus	-5,2	-95,9	17,2	Source	Pelvis
	3,6	-209,4	3,8	Insertion	Femur
Adductor magnus	-48,4	-128,3	27,9	Source	Pelvis
	8,0	-269,2	-11,8	Insertion	Femur
Hamstrings	-75,7	-117,9	54,9	Source	Pelvis
	-23,7	-30,8	-21,5	Fixed Path	Tibia
	-8,0	-45,3	-21,1	Insertion	Tibia
Biceps femoris short head	-7,2	-150,8	11,3	Source	Femur
	-8,7	-29,9	36,1	Fixed Path	Tibia
	-8,9	-43,5	32,3	Insertion	Tibia
Iliopsoas	-38,6	23,0	37,3	Source	Pelvis
	-15,1	-54,7	58,5	Fixed Path	Pelvis
	-13,3	-71,3	63,0	Via Point	Pelvis
	7,1	-44,1	3,1	Fixed Path	Femur
	-6,6	-51,3	1,0	Insertion	Femur
Gluteus maximus	-87,9	9,6	57,0	Source	Pelvis
	-84,8	-64,3	75,7	Fixed Path	Pelvis
	-37,8	-41,9	-15,8	Fixed Path	Femur
	-6,9	-138,2	10,5	Insertion	Femur
Gluteus medius	-61,0	12,6	64,3	Source	Pelvis
	-24,4	-0,3	26,9	Insertion	Femur
Gluteus minimus	-51,4	-11,7	66,5	Source	Pelvis
	-14,1	-1,5	33,6	Insertion	Femur
Gracilis	-39,4	-128,4	24,2	Fixed Path	Pelvis
	-23,1	-4,8	-31,6	Via Point	Tibia
	-14,1	-21,5	-30,9	Fixed Path	Tibia
	-0,4	-47,1	-21,3	Insertion	Tibia
Pectinius	-16,9	-78,8	37,2	Source	Pelvis
	4,9	-122,6	0,8	Insertion	Femur
Piriformis	-87,5	-23,4	22,2	Source	Pelvis
	-82,2	-43,1	45,2	Fixed Path	Pelvis
	-16,9	-2,8	13,6	Insertion	Femur
Sartorius	8,3	-28,8	80,1	Source	Pelvis
	-9,6	-302,5	-35,7	Fixed Path	Femur
	-13,1	-33,4	-36,0	Fixed Path	Tibia
	-10,9	-45,1	-33,3	Fixed Path	Tibia
	2,2	-63,8	-23,5	Insertion	Tibia
Tensor fasciae latae	-0,2	-18,5	85,1	Source	Pelvis
	23,7	-90,4	41,8	Fixed Path	Femur
	18,5	-333,0	28,8	Fixed Path	Femur
	15,9	-40,3	26,5	Insertion	Tibia
Rectus femoris	-13,5	-32,3	73,8	Source	Pelvis
	29,0	-349,9	0,3	Via Point	Femur
	55,0	15,9	0,0	Moving Point	Tibia

Table A.1.3 Muscle Point Coordinates for ND1 (a) Attachment sites and muscle path defining points in reference frame of related limb segment

Muscle	Coordinates [mm]			Point Type	Ref. Body
	X	Y	Z		
	3,9	-26,3	26,8	Source	Femur
Vastus	13,1	-180,5	17,7	Fixed Path	Femur
	28,0	-347,5	1,6	Via Point	Femur
	50,2	19,8	0,0	Moving Point	Tibia
	-6,6	-59,0	30,9	Source	Tibia
	-17,2	-344,9	23,5	Fixed Path	Tibia
	-13,5	-359,3	22,8	Fixed Path	Tibia
Peroneus	36,3	18,7	18,0	Fixed Path	Calcaneus
	55,4	8,6	23,1	Fixed Path	Calcaneus
	69,3	5,6	9,6	Fixed Path	Calcaneus
	97,8	6,9	-15,0	Insertion	Calcaneus
	-6,0	-309,4	-9,0	Source	Femur
Gastrocnemius	-18,4	-320,7	-8,5	Via Point	Femur
	0,0	25,2	-4,3	Insertion	Calcaneus
Soleus	1,2	-66,2	7,5	Source	Tibia
	0,0	25,2	-4,3	Insertion	Calcaneus
	18,1	-86,7	11,3	Source	Tibia
Tibialis anterior	10,2	-159,4	15,9	Fixed Path	Tibia
	20,9	-305,7	-6,0	Fixed Path	Tibia
	94,8	14,5	-24,8	Insertion	Calcaneus
	1,9	-91,8	4,8	Source	Tibia
Tibialis posterior	-13,0	-306,7	-11,5	Fixed Path	Tibia
	33,9	27,2	-23,3	Fixed Path	Calcaneus
	62,8	12,9	-22,8	Insertion	Calcaneus
	4,8	-76,1	23,7	Source	Tibia
	25,9	-334,6	-0,5	Fixed Path	Tibia
Extensor digitorum	77,1	33,2	-8,4	Fixed Path	Calcaneus
	132,4	6,2	-2,5	Fixed Path	Calcaneus
	5,2	4,4	-0,9	Fixed Path	Toes
	40,1	-0,3	4,3	Insertion	Toes
	-6,8	-120,7	-0,5	Source	Tibia
	-7,0	-293,9	-13,7	Fixed Path	Tibia
Flexor digitorum longus	35,4	25,6	-22,8	Fixed Path	Calcaneus
	57,6	14,3	-21,4	Fixed Path	Calcaneus
	134,8	-6,6	9,4	Fixed Path	Calcaneus
	-1,5	-6,3	12,0	Fixed Path	Toes
	23,2	-5,8	17,5	Fixed Path	Toes
	35,9	-4,9	19,7	Insertion	Toes
	-12,7	-101,4	22,6	Source	Tibia
	-16,8	-311,4	9,5	Fixed Path	Tibia
Flexor hallucis longus	30,4	22,4	-19,6	Fixed Path	Calcaneus
	84,4	5,5	-20,8	Fixed Path	Calcaneus
	140,3	-4,3	-21,9	Fixed Path	Calcaneus
	12,6	-5,2	-21,5	Fixed Path	Toes
	45,7	-6,7	-14,7	Insertion	Toes

Table A.1.4 Muscle Point Coordinates for ND1 (b) Muscle geometry points in reference frame of related limb segment

A.1.2 Model of Subject ND2

Muscle	Max. Force [N]	l_{0m}[cm]	TSL[cm]	pennation [degree]
Adductor longus	170	7,45	8,10	6,6
Adductor magnus	471	10,07	10,76	15,6
Hamstrings	479	10,03	19,51	8,0
Biceps femoris short head	77	8,08	5,54	12,3
Iliopsoas	165	8,49	3,26	12,5
Gluteus maximus	582	13,43	7,51	21,9
Gluteus medius	437	6,35	3,14	20,5
Gluteus minimus	100	4,96	1,26	10,0
Gracilis	53	16,23	11,95	8,2
Pectinius	59	8,97	0,87	0,0
Piriformis	163	1,85	9,14	10,0
Sartorius	49	30,08	7,06	0,0
Tensor fasciae latae	75	7,24	28,49	3,0
Rectus femoris	405	5,72	25,03	13,9
Vastus	1983	7,28	21,17	17,5
Peroneus	243	3,68	33,15	13,0
Gastrocnemius	714	4,07	29,66	10,9
Soleus	1127	3,19	22,34	28,3
Tibialis anterior	234	4,95	27,02	9,6
Tibialis posterior	385	2,68	27,54	13,7
Extensor digitorum	185	5,21	27,41	7,0
Flexor digitorum longus	86	3,22	33,17	13,6
Flexor hallucis longus	152	3,83	35,39	16,9

Table A.1.2.1 Muscle Model Parameters for model of ND2 Individual Hill-type muscle model parameters

Segment	Joint Center location [cm]			Reference Segment
	X ant.-post.	Y sup.-inf.	Z med.-lat.	
Pelvis center	0,00	71,10	0,00	Ground
Right hip	-2,48	-0,06	5,86	Pelvis
Left hip	-2,00	-0,06	-5,58	Pelvis
Right knee *	0,00	-0,29	0,00	Right Femur
Left knee *	0,00	-0,29	0,00	Left Femur
Right ankle	3,95	-0,28	-0,62	Right Tibia
Left ankle	3,23	-0,29	1,49	Left Tibia
Right Toes	12,46	0,00	0,00	Right Calcaneus
Left Toes	12,46	0,00	0,00	Left Calcaneus

Table A.1.2.2 Joint Centres for Model of model of ND2 *Coordinates for knee joint centre at 0° knee angle

Muscle	Coordinates [mm]			Point Type	Ref. Body
	X	Y	Z		
Adductor longus	13,0	-86,0	11,5	Source	Pelvis
	-1,8	-174,5	10,5	Insertion	Femur
Adductor magnus	-19,2	-106,2	23,1	Source	Pelvis
	4,2	-225,0	-0,3	Insertion	Femur
Hamstrings	-50,8	-102,7	54,7	Source	Pelvis
	-20,4	-19,5	-17,3	Fixed Path	Tibia
	-7,7	-36,3	-17,6	Insertion	Tibia
Biceps femoris short head	-0,9	-170,9	20,7	Source	Femur
	-24,0	-29,9	36,0	Fixed Path	Tibia
	-18,1	-46,8	32,5	Insertion	Tibia
Iliopsoas	-25,6	1,9	39,7	Source	Pelvis
	1,4	-39,3	54,7	Fixed Path	Pelvis
	3,3	-57,2	59,4	Via Point	Pelvis
	1,8	-39,1	9,9	Fixed Path	Femur
	-10,9	-48,3	9,9	Insertion	Femur
Gluteus maximus	-72,2	9,3	38,6	Source	Pelvis
	-64,1	-48,6	62,8	Fixed Path	Pelvis
	-42,5	-34,2	12,9	Fixed Path	Femur
	-8,8	-105,2	21,2	Insertion	Femur
Gluteus medius	-36,4	7,8	53,9	Source	Pelvis
	-19,3	-2,6	39,5	Insertion	Femur
Gluteus minimus	-27,2	-10,5	66,5	Source	Pelvis
	-13,0	0,8	41,3	Insertion	Femur
Gracilis	-6,5	-101,4	17,3	Fixed Path	Pelvis
	-25,0	-4,5	-27,5	Via Point	Tibia
	-15,2	-29,0	-26,3	Fixed Path	Tibia
	3,3	-54,6	-16,1	Insertion	Tibia
Pectinius	-1,2	-69,1	32,5	Source	Pelvis
	0,4	-76,7	8,6	Insertion	Femur
Piriformis	-66,9	4,1	19,2	Source	Pelvis
	-53,3	-39,2	43,6	Fixed Path	Pelvis
	-10,9	-2,6	32,1	Insertion	Femur
Sartorius	1,4	-19,5	73,6	Source	Pelvis
	-15,0	-263,6	-24,9	Fixed Path	Femur
	-12,0	-33,2	-28,1	Fixed Path	Tibia
	-6,5	-44,5	-24,8	Fixed Path	Tibia
	5,3	-56,7	-14,8	Insertion	Tibia
Tensor fasciae latae	-1,8	-3,3	83,4	Source	Pelvis
	23,3	-72,8	46,1	Fixed Path	Femur
	16,1	-296,5	27,4	Fixed Path	Femur
	15,9	-37,3	24,5	Insertion	Tibia
Rectus femoris	-1,0	-38,2	69,4	Source	Pelvis
	24,8	-301,7	0,7	Via Point	Femur
	49,1	13,4	0,0	Moving Point	Tibia

Table A.1.2.3 Muscle Point Coordinates for ND2 (a) Attachment sites and muscle path defining points in reference frame of related limb segment

Muscle	Coordinates [mm]			Point Type	Ref. Body
	X	Y	Z		
	5,7	-16,5	27,7	Source	Femur
Vastus	6,5	-156,2	27,9	Fixed Path	Femur
	23,7	-299,4	2,8	Via Point	Femur
	45,0	17,1	0,0	Moving Point	Tibia
	-15,8	-34,9	38,8	Source	Tibia
	-19,3	-304,8	9,1	Fixed Path	Tibia
	-14,5	-314,3	9,5	Fixed Path	Tibia
Peroneus	32,0	16,5	15,9	Fixed Path	Calcaneus
	48,9	7,6	20,4	Fixed Path	Calcaneus
	61,1	5,0	8,5	Fixed Path	Calcaneus
	86,3	6,1	-13,2	Insertion	Calcaneus
	-7,5	-279,8	4,8	Source	Femur
Gastrocnemius	-10,5	-282,4	4,8	Via Point	Femur
	0,0	22,2	-3,8	Insertion	Calcaneus
Soleus	2,3	-69,5	16,1	Source	Tibia
	0,0	22,2	-3,8	Insertion	Calcaneus
	6,1	-27,4	32,1	Source	Tibia
Tibialis anterior	4,3	-139,0	18,2	Fixed Path	Tibia
	20,8	-267,0	1,7	Fixed Path	Tibia
	83,7	12,8	-21,9	Insertion	Calcaneus
	-4,2	-46,6	23,2	Source	Tibia
Tibialis posterior	-9,2	-262,4	-11,1	Fixed Path	Tibia
	29,9	24,0	-20,5	Fixed Path	Calcaneus
	55,4	11,4	-20,2	Insertion	Calcaneus
	-4,1	-97,8	26,7	Source	Tibia
	17,3	-292,1	12,8	Fixed Path	Tibia
Extensor digitorum	68,0	29,3	-7,4	Fixed Path	Calcaneus
	116,9	5,5	-2,2	Fixed Path	Calcaneus
	4,6	3,9	-0,8	Fixed Path	Toes
	35,4	-0,3	3,8	Insertion	Toes
	3,7	-88,8	3,9	Source	Tibia
	-2,5	-290,2	-22,6	Fixed Path	Tibia
	31,3	22,6	-20,1	Fixed Path	Calcaneus
Flexor digitorum longus	50,8	12,6	-18,9	Fixed Path	Calcaneus
	119,0	-5,8	8,3	Fixed Path	Calcaneus
	-1,4	-5,6	10,5	Fixed Path	Toes
	20,5	-5,1	15,4	Fixed Path	Toes
	31,6	-4,3	17,4	Insertion	Toes
	-13,2	-79,3	26,1	Source	Tibia
	-15,9	-292,1	-15,0	Fixed Path	Tibia
Flexor hallucis longus	26,8	19,8	-17,3	Fixed Path	Calcaneus
	74,5	4,9	-18,4	Fixed Path	Calcaneus
	123,9	-3,8	-19,3	Fixed Path	Calcaneus
	11,1	-4,6	-19,0	Fixed Path	Toes
	40,3	-5,9	-13,0	Insertion	Toes

Table A.1.2.4 Muscle Point Coordinates for ND2 (b) Muscle geometry points in reference frame of related limb segment

A.1.3 Model of Subject ND3

Muscle	Max. Force [N]	l_{0m}[cm]	TSL[cm]	pennation [degree]
Adductor longus	236	8,59	8,78	6,6
Adductor magnus	625	11,78	10,29	15,6
Hamstrings	673	11,54	24,03	8,0
Biceps femoris short head	159	9,14	8,29	12,3
Iliopsoas	538	8,86	10,28	12,5
Gluteus maximus	880	14,55	9,52	21,9
Gluteus medius	716	6,57	4,11	20,5
Gluteus minimus	155	5,19	3,42	10,0
Gracilis	92	18,69	11,65	8,2
Pectinius	197	10,24	3,25	0,0
Piriformis	219	2,00	8,77	10,0
Sartorius	75	33,61	7,86	0,0
Tensor fasciae latae	160	8,04	31,74	3,0
Rectus femoris	765	6,42	28,47	13,9
Vastus	2974	8,27	23,33	17,5
Peroneus	375	4,12	35,49	13,0
Gastrocnemius	1047	4,56	34,26	10,9
Soleus	1598	3,58	25,12	28,3
Tibialis anterior	328	5,55	29,60	9,6
Tibialis posterior	509	3,01	31,07	13,7
Extensor digitorum	242	5,84	37,49	7,0
Flexor digitorum longus	147	3,61	38,24	13,6
Flexor hallucis longus	135	4,29	34,99	16,9

Table A.1.3.1 Muscle Model Parameters for model of ND3 Individual Hill-type muscle model parameters

Segment	X ant.-post.	Y sup.-inf.	Z med.-lat.	Reference Segment
Pelvis center	0,00	81,00	0,00	Ground
Right hip	-2,35	-0,06	6,52	Pelvis
Left hip	-2,10	-0,06	-6,33	Pelvis
Right knee *	0,00	-0,33	0,00	Right Femur
Left knee *	0,00	-0,33	0,00	Left Femur
Right ankle	3,53	-0,32	-0,61	Right Tibia
Left ankle	4,31	-0,33	-0,27	Left Tibia
Right Toes	14,20	0,00	0,00	Right Calcaneus
Left Toes	14,20	0,00	0,00	Left Calcaneus

Joint Center location [cm]

Table A.1.3.2 Joint Centres for Model of model of ND3 *Coordinates for knee joint centre at 0° knee angle

Muscle	Coordinates [mm]			Point Type	Ref. Body
	X	Y	Z		
Adductor longus	20,9	-90,6	16,0	Source	Pelvis
	-0,1	-199,0	6,1	Insertion	Femur
Adductor magnus	-22,1	-117,4	27,4	Source	Pelvis
	-2,6	-243,3	-2,5	Insertion	Femur
Hamstrings	-52,1	-102,1	58,9	Source	Pelvis
	-28,6	-26,1	-19,0	Fixed Path	Tibia
	-6,5	-49,1	-20,2	Insertion	Tibia
Biceps femoris short head	-5,4	-166,0	18,8	Source	Femur
	-19,2	-28,1	46,7	Fixed Path	Tibia
	-14,8	-45,4	39,6	Insertion	Tibia
Iliopsoas	-57,7	64,1	33,1	Source	Pelvis
	4,5	-38,3	63,8	Fixed Path	Pelvis
	7,2	-55,6	67,9	Via Point	Pelvis
	4,3	-44,6	11,3	Fixed Path	Femur
	-7,4	-52,3	10,6	Insertion	Femur
Gluteus maximus	-89,0	17,2	52,1	Source	Pelvis
	-68,9	-54,6	75,0	Fixed Path	Pelvis
	-44,3	-36,9	16,3	Fixed Path	Femur
	-7,8	-127,1	22,8	Insertion	Femur
Gluteus medius	-44,7	11,4	67,7	Source	Pelvis
	-19,7	-11,6	47,3	Insertion	Femur
Gluteus minimus	-38,9	6,8	76,9	Source	Pelvis
	-8,0	-8,7	46,7	Insertion	Femur
Gracilis	-7,0	-109,0	20,1	Fixed Path	Pelvis
	-20,1	-3,4	-28,9	Via Point	Tibia
	-9,9	-25,0	-27,8	Fixed Path	Tibia
	6,2	-50,9	-16,7	Insertion	Tibia
Pectinius	6,4	-72,4	45,9	Source	Pelvis
	-2,2	-116,4	10,8	Insertion	Femur
Piriformis	-59,6	-7,0	30,2	Source	Pelvis
	-63,4	-36,4	38,9	Fixed Path	Pelvis
	-12,3	-3,0	36,4	Insertion	Femur
Sartorius	-0,7	-27,6	87,3	Source	Pelvis
	-9,2	-300,3	-30,5	Fixed Path	Femur
	-8,2	-35,8	-32,4	Fixed Path	Tibia
	-0,3	-49,1	-28,9	Fixed Path	Tibia
	17,8	-68,3	-16,4	Insertion	Tibia
Tensor fasciae latae	-9,5	-8,6	102,7	Source	Pelvis
	28,9	-81,8	60,0	Fixed Path	Femur
	18,0	-342,6	40,7	Fixed Path	Femur
	12,1	-44,1	36,3	Insertion	Tibia
Rectus femoris	3,4	-36,1	80,9	Source	Pelvis
	27,9	-342,7	0,9	Via Point	Femur
	55,7	14,8	0,0	Moving Point	Tibia

Table A.1.3.3 Muscle Point Coordinates for ND2 (a) Attachment sites and muscle path defining points in reference frame of related limb segment

Muscle	Coordinates [mm]			Point Type	Ref. Body
	X	Y	Z		
Vastus	10,7	-25,5	35,0	Source	Femur
	11,2	-176,4	32,7	Fixed Path	Femur
	27,1	-340,5	3,1	Via Point	Femur
	51,3	19,1	0,0	Moving Point	Tibia
Peroneus	-11,7	-50,8	39,6	Source	Tibia
	-19,5	-341,2	17,5	Fixed Path	Tibia
	-17,1	-350,1	17,1	Fixed Path	Tibia
	36,0	18,5	17,8	Fixed Path	Calcaneus
	54,9	8,5	22,9	Fixed Path	Calcaneus
	68,7	5,6	9,5	Fixed Path	Calcaneus
	96,9	6,8	-14,8	Insertion	Calcaneus
Gastrocnemius	-7,9	-309,2	-3,4	Source	Femur
	-16,0	-316,4	-3,2	Via Point	Femur
	0,0	25,0	-4,3	Insertion	Calcaneus
Soleus	2,8	-77,0	16,5	Source	Tibia
	0,0	25,0	-4,3	Insertion	Calcaneus
Tibialis anterior	13,3	-38,0	34,7	Source	Tibia
	6,2	-155,3	26,6	Fixed Path	Tibia
	25,1	-301,5	3,6	Fixed Path	Tibia
	94,0	14,3	-24,6	Insertion	Calcaneus
Tibialis posterior	-6,1	-49,8	26,5	Source	Tibia
	-7,3	-289,7	-7,2	Fixed Path	Tibia
	33,6	26,9	-23,0	Fixed Path	Calcaneus
	62,2	12,8	-22,6	Insertion	Calcaneus
Extensor digitorum	-5,5	-41,6	41,0	Source	Tibia
	20,4	-326,0	19,1	Fixed Path	Tibia
	76,4	32,9	-8,3	Fixed Path	Calcaneus
	131,2	6,2	-2,5	Fixed Path	Calcaneus
	5,1	4,4	-0,9	Fixed Path	Toes
	39,7	-0,3	4,3	Insertion	Toes
Flexor digitorum longus	-7,8	-87,8	5,8	Source	Tibia
	-3,0	-320,8	-22,7	Fixed Path	Tibia
	35,1	25,4	-22,6	Fixed Path	Calcaneus
	57,1	14,2	-21,2	Fixed Path	Calcaneus
	133,6	-6,5	9,3	Fixed Path	Calcaneus
	-1,5	-6,3	11,8	Fixed Path	Toes
	23,0	-5,7	17,3	Fixed Path	Toes
	35,5	-4,8	19,5	Insertion	Toes
Flexor hallucis longus	-13,6	-136,7	27,8	Source	Tibia
	-19,0	-320,3	-8,9	Fixed Path	Tibia
	30,1	22,2	-19,4	Fixed Path	Calcaneus
	83,6	5,5	-20,6	Fixed Path	Calcaneus
	139,1	-4,3	-21,7	Fixed Path	Calcaneus
	12,5	-5,2	-21,4	Fixed Path	Toes
	45,3	-6,6	-14,6	Insertion	Toes

Table A.1.3.4 Muscle Point Coordinates for ND2 (b) Muscle geometry points in reference frame of related limb segment

A.1.4 Model of Subject ND4

Muscle	Max. Force [N]	l_{0m}[cm]	TSL[cm]	pennation [degree]
Adductor longus	170	8,07	7,01	6,6
Adductor magnus	580	10,99	11,85	15,6
Hamstrings	606	10,76	22,90	8,0
Biceps femoris short head	153	8,54	10,12	12,3
Iliopsoas	343	8,87	5,99	12,5
Gluteus maximus	667	13,83	8,62	21,9
Gluteus medius	600	6,44	3,89	20,5
Gluteus minimus	125	5,10	1,73	10,0
Gracilis	60	17,35	9,95	8,2
Pectinius	160	9,78	4,77	0,0
Piriformis	206	1,95	6,19	10,0
Sartorius	62	31,75	8,41	0,0
Tensor fasciae latae	88	7,63	30,54	3,0
Rectus femoris	494	6,10	27,84	13,9
Vastus	2063	7,83	21,87	17,5
Peroneus	385	3,74	31,15	13,0
Gastrocnemius	920	4,14	32,50	10,9
Soleus	1308	3,24	23,10	28,3
Tibialis anterior	252	5,03	22,37	9,6
Tibialis posterior	462	2,72	25,43	13,7
Extensor digitorum	224	5,30	29,48	7,0
Flexor digitorum longus	164	3,28	35,03	13,6
Flexor hallucis longus	299	3,90	37,06	16,9

Table A.1.4.1 Muscle Model Parameters for model of ND4 Individual Hill-type muscle model parameters

Segment	Joint Center location [cm]			Reference Segment
	X ant.-post.	Y sup.-inf.	Z med.-lat.	
Pelvis center	0,00	69,06	0,00	Ground
Right hip	-3,35	-0,06	5,70	Pelvis
Left hip	-3,53	-0,06	-6,31	Pelvis
Right knee *	0,00	-0,31	0,00	Right Femur
Left knee *	0,00	-0,31	0,00	Left Femur
Right ankle	3,47	-0,29	0,23	Right Tibia
Left ankle	1,65	-0,29	-1,81	Left Tibia
Right Toes	13,12	0,00	0,00	Right Calcaneus
Left Toes	13,12	0,00	0,00	Left Calcaneus

Table A.1.4.2 Joint Centres for Model of model of ND4 *Coordinates for knee joint centre at 0° knee angle

Muscle	Coordinates [mm]			Point Type	Ref. Body
	X	Y	Z		
Adductor longus	-6,8	-76,9	13,8	Source	Pelvis
	2,0	-165,9	1,2	Insertion	Femur
Adductor magnus	-41,3	-102,8	20,3	Source	Pelvis
	4,6	-238,5	-1,4	Insertion	Femur
Hamstrings	-70,1	-90,1	54,2	Source	Pelvis
	-21,3	-21,0	-21,8	Fixed Path	Tibia
	-4,8	-38,2	-19,3	Insertion	Tibia
Biceps femoris short head	-3,7	-136,1	16,3	Source	Femur
	-16,9	-30,1	37,2	Fixed Path	Tibia
	-10,5	-44,6	31,5	Insertion	Tibia
Iliopsoas	-43,4	35,0	35,9	Source	Pelvis
	-7,6	-42,5	59,7	Fixed Path	Pelvis
	-5,4	-55,2	61,3	Via Point	Pelvis
	5,8	-42,6	5,2	Fixed Path	Femur
	-6,5	-46,2	4,3	Insertion	Femur
Gluteus maximus	-82,5	11,6	49,9	Source	Pelvis
	-83,1	-52,5	67,7	Fixed Path	Pelvis
	-45,7	-36,6	11,4	Fixed Path	Femur
	-7,2	-119,2	17,2	Insertion	Femur
Gluteus medius	-59,8	31,7	64,8	Source	Pelvis
	-24,2	3,5	26,9	Insertion	Femur
Gluteus minimus	-46,4	0,3	66,7	Source	Pelvis
	-10,7	0,1	31,3	Insertion	Femur
Gracilis	-30,5	-101,4	13,2	Fixed Path	Pelvis
	-20,3	-4,3	-29,9	Via Point	Tibia
	-11,3	-20,8	-28,9	Fixed Path	Tibia
	-1,2	-32,2	-28,2	Insertion	Tibia
Pectinius	-8,7	-60,1	31,3	Source	Pelvis
	1,3	-117,9	3,8	Insertion	Femur
Piriformis	-65,4	-15,0	22,2	Source	Pelvis
	-74,1	-32,5	36,3	Fixed Path	Pelvis
	-16,7	0,7	15,8	Insertion	Femur
Sartorius	-10,1	-6,9	78,6	Source	Pelvis
	-8,5	-279,7	-32,8	Fixed Path	Femur
	-7,3	-32,1	-33,7	Fixed Path	Tibia
	-4,1	-43,2	-30,6	Fixed Path	Tibia
	9,7	-55,8	-23,5	Insertion	Tibia
Tensor fasciae latae	-19,5	0,3	83,2	Source	Pelvis
	29,2	-73,4	43,0	Fixed Path	Femur
	22,4	-278,5	30,5	Fixed Path	Femur
	13,1	-37,5	33,2	Insertion	Tibia
Rectus femoris	-12,2	-27,5	72,7	Source	Pelvis
	25,4	-323,6	0,6	Via Point	Femur
	49,5	13,6	0,0	Moving Point	Tibia

Table A.1.4.3 Muscle Point Coordinates for ND4 (a) Attachment sites and muscle path defining points in reference frame of related limb segment

Muscle	Coordinates [mm]			Point Type	Ref. Body
	X	Y	Z		
Vastus	10,5	-23,1	23,3	Source	Femur
	13,9	-165,7	21,2	Fixed Path	Femur
	25,1	-322,2	1,9	Via Point	Femur
	45,4	17,4	0,0	Moving Point	Tibia
Peroneus	-11,8	-60,7	35,6	Source	Tibia
	-21,6	-307,4	14,1	Fixed Path	Tibia
	-21,2	-316,7	16,1	Fixed Path	Tibia
	32,8	16,9	16,2	Fixed Path	Calcaneus
	50,1	7,8	20,9	Fixed Path	Calcaneus
	62,6	5,1	8,7	Fixed Path	Calcaneus
	88,4	6,2	-13,5	Insertion	Calcaneus
Gastrocnemius	-5,3	-280,3	0,8	Source	Femur
	-20,1	-294,0	0,9	Via Point	Femur
	0,0	22,8	-3,9	Insertion	Calcaneus
Soleus	1,5	-65,9	13,3	Source	Tibia
	0,0	22,8	-3,9	Insertion	Calcaneus
Tibialis anterior	4,4	-79,0	24,0	Source	Tibia
	8,6	-141,2	20,2	Fixed Path	Tibia
	23,4	-271,6	3,3	Fixed Path	Tibia
	85,7	13,1	-22,4	Insertion	Calcaneus
Tibialis posterior	4,6	-73,3	15,2	Source	Tibia
	-5,1	-268,5	-17,0	Fixed Path	Tibia
	30,7	24,6	-21,0	Fixed Path	Calcaneus
	56,7	11,7	-20,7	Insertion	Calcaneus
Extensor digitorum	-1,0	-81,4	30,0	Source	Tibia
	17,7	-293,9	8,2	Fixed Path	Tibia
	69,7	30,0	-7,6	Fixed Path	Calcaneus
	119,7	5,6	-2,2	Fixed Path	Calcaneus
	4,7	4,0	-0,9	Fixed Path	Toes
	36,2	-0,3	3,9	Insertion	Toes
Flexor digitorum longus	2,6	-76,7	-1,1	Source	Tibia
	-0,9	-293,5	-23,5	Fixed Path	Tibia
	32,0	23,2	-20,6	Fixed Path	Calcaneus
	52,0	12,9	-19,3	Fixed Path	Calcaneus
	121,9	-6,0	8,5	Fixed Path	Calcaneus
	-1,4	-5,7	10,8	Fixed Path	Toes
	20,9	-5,2	15,8	Fixed Path	Toes
	32,4	-4,4	17,8	Insertion	Toes
Flexor hallucis longus	-10,9	-68,4	24,1	Source	Tibia
	-17,9	-283,4	-8,2	Fixed Path	Tibia
	27,5	20,3	-17,7	Fixed Path	Calcaneus
	76,3	5,0	-18,8	Fixed Path	Calcaneus
	126,9	-3,9	-19,8	Fixed Path	Calcaneus
	11,4	-4,7	-19,5	Fixed Path	Toes
	41,3	-6,0	-13,3	Insertion	Toes

Table A.1.4.4 Muscle Point Coordinates for ND4 (b) Muscle geometry points in reference frame of related limb segment

A.1.5 Model of Subject ND5

Muscle	Max. Force [N]	l_{0m}[cm]	TSL[cm]	pennation [degree]
Adductor longus	176	7,78	9,07	6,6
Adductor magnus	612	10,45	10,95	15,6
Hamstrings	692	10,30	21,92	8,0
Biceps femoris short head	145	8,25	10,28	12,3
Iliopsoas	357	8,65	6,64	12,5
Gluteus maximus	810	13,36	9,38	21,9
Gluteus medius	551	6,27	3,80	20,5
Gluteus minimus	174	4,93	2,31	10,0
Gracilis	73	16,68	12,03	8,2
Pectinius	192	9,49	4,87	0,0
Piriformis	304	1,93	7,56	10,0
Sartorius	57	30,64	7,71	0,0
Tensor fasciae latae	83	7,34	29,66	3,0
Rectus femoris	580	5,82	26,11	13,9
Vastus	2556	7,45	21,54	17,5
Peroneus	410	3,74	28,06	13,0
Gastrocnemius	1113	4,13	31,39	10,9
Soleus	1685	3,24	23,21	28,3
Tibialis anterior	309	5,03	21,96	9,6
Tibialis posterior	624	2,73	24,72	13,7
Extensor digitorum	226	5,30	28,20	7,0
Flexor digitorum longus	151	3,28	34,27	13,6
Flexor hallucis longus	336	3,90	35,09	16,9

Table A.1.5.1 Muscle Model Parameters for model of ND5 Individual Hill-type muscle model parameters

Segment	Joint Center location [cm] X ant.-post.	Y sup.-inf.	Z med.-lat.	Reference Segment
Pelvis center	0,00	74,40	0,00	Ground
Right hip	-3,51	-0,06	6,20	Pelvis
Left hip	-3,55	-0,06	-5,99	Pelvis
Right knee *	0,00	-0,30	0,00	Right Femur
Left knee *	0,00	-0,30	0,00	Left Femur
Right ankle	4,23	-0,29	3,12	Right Tibia
Left ankle	4,84	-0,29	-2,14	Left Tibia
Right Toes	12,76	0,00	0,00	Right Calcaneus
Left Toes	12,76	0,00	0,00	Left Calcaneus

Table A.1.5.2 Joint Centres for Model of model of ND5 *Coordinates for knee joint centre at 0° knee angle

Muscle	Coordinates [mm]			Point Type	Ref. Body
	X	**Y**	**Z**		
Adductor longus	-1,4	-72,2	12,7	Source	Pelvis
	2,5	-179,5	3,1	Insertion	Femur
Adductor magnus	-40,8	-98,5	26,0	Source	Pelvis
	9,8	-223,4	-5,3	Insertion	Femur
Hamstrings	-72,1	-86,0	44,4	Source	Pelvis
	-18,1	-25,2	-19,4	Fixed Path	Tibia
	-6,6	-38,8	-19,3	Insertion	Tibia
Biceps femoris short head	-8,4	-120,5	12,1	Source	Femur
	-16,9	-24,6	39,4	Fixed Path	Tibia
	-15,6	-42,5	34,4	Insertion	Tibia
Iliopsoas	-52,0	38,9	43,4	Source	Pelvis
	-8,5	-39,7	61,5	Fixed Path	Pelvis
	-6,2	-54,3	63,1	Via Point	Pelvis
	6,3	-41,1	5,3	Fixed Path	Femur
	-6,1	-47,5	5,0	Insertion	Femur
Gluteus maximus	-93,0	23,3	53,7	Source	Pelvis
	-83,9	-53,9	65,6	Fixed Path	Pelvis
	-47,4	-35,3	-1,8	Fixed Path	Femur
	-7,6	-112,0	13,9	Insertion	Femur
Gluteus medius	-39,7	20,4	70,2	Source	Pelvis
	-14,1	-4,5	37,8	Insertion	Femur
Gluteus minimus	-51,4	-2,1	70,4	Source	Pelvis
	-24,9	-7,1	35,4	Insertion	Femur
Gracilis	-32,1	-97,7	16,7	Fixed Path	Pelvis
	-25,0	-5,7	-29,9	Via Point	Tibia
	-14,7	-27,7	-28,8	Fixed Path	Tibia
	2,6	-54,5	-20,3	Insertion	Tibia
Pectinius	-10,4	-51,2	34,4	Source	Pelvis
	-1,5	-108,9	4,6	Insertion	Femur
Piriformis	-69,7	-5,6	10,4	Source	Pelvis
	-74,4	-31,2	35,7	Fixed Path	Pelvis
	-21,0	-2,7	16,6	Insertion	Femur
Sartorius	-0,4	-9,8	76,0	Source	Pelvis
	-4,4	-268,0	-35,9	Fixed Path	Femur
	-4,8	-33,6	-33,5	Fixed Path	Tibia
	-3,0	-44,7	-30,4	Fixed Path	Tibia
	6,4	-55,2	-21,7	Insertion	Tibia
Tensor fasciae latae	-9,1	3,9	80,6	Source	Pelvis
	25,6	-73,3	51,8	Fixed Path	Femur
	14,6	-299,8	36,7	Fixed Path	Femur
	11,8	-35,2	31,3	Insertion	Tibia
Rectus femoris	-9,4	-28,4	73,5	Source	Pelvis
	25,4	-309,1	0,7	Via Point	Femur
	40,1	16,4	0,0	Moving Point	Tibia

Table A.1.5.3 Muscle Point Coordinates for ND5 (a) Attachment sites and muscle path defining points in reference frame of related limb segment

Muscle	Coordinates [mm]			Point Type	Ref. Body
	X	Y	Z		
Vastus	3,0	-12,6	29,0	Source	Femur
	12,9	-159,6	24,5	Fixed Path	Femur
	24,8	-307,3	2,3	Via Point	Femur
	35,2	19,0	0,0	Moving Point	Tibia
Peroneus	-13,7	-91,3	28,9	Source	Tibia
	-21,3	-310,1	14,9	Fixed Path	Tibia
	-19,7	-317,2	15,5	Fixed Path	Tibia
	32,8	16,9	16,2	Fixed Path	Calcaneus
	50,0	7,8	20,9	Fixed Path	Calcaneus
	62,6	5,1	8,7	Fixed Path	Calcaneus
	88,4	6,2	-13,5	Insertion	Calcaneus
Gastrocnemius	-6,5	-275,6	0,3	Source	Femur
	-15,7	-283,9	0,3	Via Point	Femur
	0,0	22,8	-3,9	Insertion	Calcaneus
Soleus	-0,8	-64,5	10,4	Source	Tibia
	0,0	22,8	-3,9	Insertion	Calcaneus
Tibialis anterior	9,2	-82,3	16,3	Source	Tibia
	9,9	-140,1	21,0	Fixed Path	Tibia
	24,9	-271,0	0,8	Fixed Path	Tibia
	85,7	13,1	-22,4	Insertion	Calcaneus
Tibialis posterior	1,1	-81,1	18,5	Source	Tibia
	-4,9	-250,0	-9,2	Fixed Path	Tibia
	30,6	24,5	-21,0	Fixed Path	Calcaneus
	56,7	11,7	-20,6	Insertion	Calcaneus
Extensor digitorum	-3,6	-94,0	26,2	Source	Tibia
	22,3	-297,0	12,3	Fixed Path	Tibia
	69,7	30,0	-7,6	Fixed Path	Calcaneus
	119,6	5,6	-2,2	Fixed Path	Calcaneus
	4,7	4,0	-0,9	Fixed Path	Toes
	36,2	-0,3	3,9	Insertion	Toes
Flexor digitorum longus	0,6	-85,9	-2,0	Source	Tibia
	-3,6	-296,0	-26,5	Fixed Path	Tibia
	32,0	23,1	-20,6	Fixed Path	Calcaneus
	52,0	12,9	-19,3	Fixed Path	Calcaneus
	121,8	-6,0	8,5	Fixed Path	Calcaneus
	-1,4	-5,7	10,8	Fixed Path	Toes
	20,9	-5,2	15,8	Fixed Path	Toes
	32,4	-4,4	17,8	Insertion	Toes
Flexor hallucis longus	-21,1	-91,1	24,8	Source	Tibia
	-12,1	-296,8	-19,6	Fixed Path	Tibia
	27,5	20,3	-17,7	Fixed Path	Calcaneus
	76,3	5,0	-18,8	Fixed Path	Calcaneus
	126,8	-3,9	-19,8	Fixed Path	Calcaneus
	11,4	-4,7	-19,5	Fixed Path	Toes
	41,3	-6,0	-13,3	Insertion	Toes

Table A.1.5.4 Muscle Point Coordinates for ND5 (b) Muscle geometry points in reference frame of related limb segment

A.1.6 Model of Subject CP1

Muscle	Max. Force [N]	l_{0m}[cm]	TSL[cm]	pennation [degree]
Adductor longus	180	8,65	10,42	6,6
Adductor magnus	502	11,45	13,33	15,6
Hamstrings	486	11,47	24,13	8,0
Biceps femoris short head	125	9,34	9,70	12,3
Iliopsoas	329	10,72	4,30	12,5
Gluteus maximus	599	16,00	10,32	21,9
Gluteus medius	529	7,81	3,13	20,5
Gluteus minimus	93	6,08	1,77	10,0
Gracilis	75	18,54	11,43	8,2
Pectinius	184	10,68	4,17	0,0
Piriformis	162	2,31	6,71	10,0
Sartorius	69	35,22	7,49	0,0
Tensor fasciae latae	100	8,51	31,84	3,0
Rectus femoris	399	6,67	30,59	13,9
Vastus	1988	8,43	23,45	17,5
Peroneus	254	4,21	35,28	13,0
Gastrocnemius	586	4,68	35,91	10,9
Soleus	1125	3,67	26,98	28,3
Tibialis anterior	242	5,69	25,61	9,6
Tibialis posterior	451	3,08	27,84	13,7
Extensor digitorum	173	5,96	34,30	7,0
Flexor digitorum longus	67	3,68	35,96	13,6
Flexor hallucis longus	181	4,37	39,44	16,9

Table A.1.6.1 Muscle Model Parameters for model of CP1 Individual Hill-type muscle model parameters

Segment	Joint Center location [cm]			Reference Segment
	X ant.-post.	Y sup.-inf.	Z med.-lat.	
Pelvis center	0,00	76,79	0,00	Ground
Right hip	-4,79	-0,08	6,80	Pelvis
Left hip	-4,39	-0,07	-6,86	Pelvis
Right knee *	0,00	-0,34	0,00	Right Femur
Left knee *	0,00	-0,34	0,00	Left Femur
Right ankle	-0,92	-0,33	-1,04	Right Tibia
Left ankle	-3,16	-0,35	-0,59	Left Tibia
Right Toes	14,37	0,00	0,00	Right Calcaneus
Left Toes	14,37	0,00	0,00	Left Calcaneus

Table A.1.6.2 Joint Centres for Model of model of CP1 *Coordinates for knee joint centre at 0° knee angle

Muscle	Coordinates [mm]			Point Type	Ref. Body
	X	**Y**	**Z**		
Adductor longus	-5,2	-95,9	17,2	Source	Pelvis
	3,6	-209,4	3,8	Insertion	Femur
Adductor magnus	-48,4	-128,3	27,9	Source	Pelvis
	8,0	-269,2	-11,8	Insertion	Femur
Hamstrings	-75,7	-117,9	54,9	Source	Pelvis
	-23,7	-30,8	-21,5	Fixed Path	Tibia
	-8,0	-45,3	-21,1	Insertion	Tibia
Biceps femoris short head	-7,2	-150,8	11,3	Source	Femur
	-8,7	-29,9	36,1	Fixed Path	Tibia
	-8,9	-43,5	32,3	Insertion	Tibia
Iliopsoas	-38,6	23,0	37,3	Source	Pelvis
	-15,1	-54,7	58,5	Fixed Path	Pelvis
	-13,3	-71,3	63,0	Via Point	Pelvis
	7,1	-44,1	3,1	Fixed Path	Femur
	-6,6	-51,3	1,0	Insertion	Femur
Gluteus maximus	-87,9	9,6	57,0	Source	Pelvis
	-84,8	-64,3	75,7	Fixed Path	Pelvis
	-37,8	-41,9	-15,8	Fixed Path	Femur
	-6,9	-138,2	10,5	Insertion	Femur
Gluteus medius	-61,0	12,6	64,3	Source	Pelvis
	-24,4	-0,3	26,9	Insertion	Femur
Gluteus minimus	-51,4	-11,7	66,5	Source	Pelvis
	-14,1	-1,5	33,6	Insertion	Femur
Gracilis	-39,4	-128,4	24,2	Fixed Path	Pelvis
	-23,1	-4,8	-31,6	Via Point	Tibia
	-14,1	-21,5	-30,9	Fixed Path	Tibia
	-0,4	-47,1	-21,3	Insertion	Tibia
Pectinius	-16,9	-78,8	37,2	Source	Pelvis
	4,9	-122,6	0,8	Insertion	Femur
Piriformis	-87,5	-23,4	22,2	Source	Pelvis
	-82,2	-43,1	45,2	Fixed Path	Pelvis
	-16,9	-2,8	13,6	Insertion	Femur
Sartorius	8,3	-28,8	80,1	Source	Pelvis
	-9,6	-302,5	-35,7	Fixed Path	Femur
	-13,1	-33,4	-36,0	Fixed Path	Tibia
	-10,9	-45,1	-33,3	Fixed Path	Tibia
	2,2	-63,8	-23,5	Insertion	Tibia
Tensor fasciae latae	-0,2	-18,5	85,1	Source	Pelvis
	23,7	-90,4	41,8	Fixed Path	Femur
	18,5	-333,0	28,8	Fixed Path	Femur
	15,9	-40,3	26,5	Insertion	Tibia
Rectus femoris	-13,5	-32,3	73,8	Source	Pelvis
	29,0	-349,9	0,3	Via Point	Femur
	55,0	15,9	0,0	Moving Point	Tibia

Table A.1.6.3 Muscle Point Coordinates for CP1 (a) Attachment sites and muscle path defining points in reference frame of related limb segment

Muscle	Coordinates [mm]			Point Type	Ref. Body
	X	Y	Z		
Vastus	3,9	-26,3	26,8	Source	Femur
	13,1	-180,5	17,7	Fixed Path	Femur
	28,0	-347,5	1,6	Via Point	Femur
	50,2	19,8	0,0	Moving Point	Tibia
Peroneus	-6,6	-59,0	30,9	Source	Tibia
	-17,2	-344,9	23,5	Fixed Path	Tibia
	-13,5	-359,3	22,8	Fixed Path	Tibia
	36,3	18,7	18,0	Fixed Path	Calcaneus
	55,4	8,6	23,1	Fixed Path	Calcaneus
	69,3	5,6	9,6	Fixed Path	Calcaneus
	97,8	6,9	-15,0	Insertion	Calcaneus
Gastrocnemius	-6,0	-309,4	-9,0	Source	Femur
	-18,4	-320,7	-8,5	Via Point	Femur
	0,0	25,2	-4,3	Insertion	Calcaneus
Soleus	1,2	-66,2	7,5	Source	Tibia
	0,0	25,2	-4,3	Insertion	Calcaneus
Tibialis anterior	18,1	-86,7	11,3	Source	Tibia
	10,2	-159,4	15,9	Fixed Path	Tibia
	20,9	-305,7	-6,0	Fixed Path	Tibia
	94,8	14,5	-24,8	Insertion	Calcaneus
Tibialis posterior	1,9	-91,8	4,8	Source	Tibia
	-13,0	-306,7	-11,5	Fixed Path	Tibia
	33,9	27,2	-23,3	Fixed Path	Calcaneus
	62,8	12,9	-22,8	Insertion	Calcaneus
Extensor digitorum	4,8	-76,1	23,7	Source	Tibia
	25,9	-334,6	-0,5	Fixed Path	Tibia
	77,1	33,2	-8,4	Fixed Path	Calcaneus
	132,4	6,2	-2,5	Fixed Path	Calcaneus
	5,2	4,4	-0,9	Fixed Path	Toes
	40,1	-0,3	4,3	Insertion	Toes
Flexor digitorum longus	-6,8	-120,7	-0,5	Source	Tibia
	-7,0	-293,9	-13,7	Fixed Path	Tibia
	35,4	25,6	-22,8	Fixed Path	Calcaneus
	57,6	14,3	-21,4	Fixed Path	Calcaneus
	134,8	-6,6	9,4	Fixed Path	Calcaneus
	-1,5	-6,3	12,0	Fixed Path	Toes
	23,2	-5,8	17,5	Fixed Path	Toes
	35,9	-4,9	19,7	Insertion	Toes
Flexor hallucis longus	-12,7	-101,4	22,6	Source	Tibia
	-16,8	-311,4	9,5	Fixed Path	Tibia
	30,4	22,4	-19,6	Fixed Path	Calcaneus
	84,4	5,5	-20,8	Fixed Path	Calcaneus
	140,3	-4,3	-21,9	Fixed Path	Calcaneus
	12,6	-5,2	-21,5	Fixed Path	Toes
	45,7	-6,7	-14,7	Insertion	Toes

Table A.1.6.4 Muscle Point Coordinates for CP1 (b) Muscle geometry points in reference frame of related limb segment

A.1.7 Model of Subject CP2

Muscle	Max. Force [N]	l_{0m}[cm]	TSL[cm]	pennation [degree]
Adductor longus	200	10,10	10,16	6,6
Adductor magnus	763	13,93	13,81	15,6
Hamstrings	467	13,30	23,20	8,0
Biceps femoris short head	146	10,28	7,35	12,3
Iliopsoas	266	9,72	4,09	12,5
Gluteus maximus	576	15,95	7,85	21,9
Gluteus medius	688	7,02	1,84	20,5
Gluteus minimus	126	5,62	0,18	10,0
Gracilis	50	21,37	13,09	8,2
Pectinius	67	12,09	0,48	0,0
Piriformis	245	2,26	8,70	10,0
Sartorius	77	37,80	9,75	0,0
Tensor fasciae latae	105	9,05	35,40	3,0
Rectus femoris	369	7,37	32,86	13,9
Vastus	2605	9,62	26,31	17,5
Peroneus	206	4,28	31,52	13,0
Gastrocnemius	530	4,75	35,69	10,9
Soleus	1102	3,71	26,39	28,3
Tibialis anterior	168	5,75	26,94	9,6
Tibialis posterior	524	3,12	30,94	13,7
Extensor digitorum	199	6,06	34,29	7,0
Flexor digitorum longus	121	3,76	38,36	13,6
Flexor hallucis longus	146	4,46	36,68	16,9

Table A.1.7.1 Muscle Model Parameters for model of CP2 Individual Hill-type muscle model parameters

Segment	Joint Center location [cm]			Reference Segment
	X ant.-post.	Y sup.-inf.	Z med.-lat.	
Pelvis center	0,00	84,15	0,00	Ground
Right hip	-3,41	-0,06	7,29	Pelvis
Left hip	-3,52	-0,06	-7,72	Pelvis
Right knee *	0,00	-0,38	0,00	Right Femur
Left knee *	0,00	-0,39	0,00	Left Femur
Right ankle	0,00	-0,34	0,00	Right Tibia
Left ankle	0,00	-0,34	0,00	Left Tibia
Right Toes	15,58	0,00	0,00	Right Calcaneus
Left Toes	15,58	0,00	0,00	Left Calcaneus

Table A.1.7.2 Joint Centres for Model of model of CP2 *Coordinates for knee joint centre at 0° knee angle

Muscle	Coordinates [mm]			Point Type	Ref. Body
	X	Y	Z		
Adductor longus	12,7	-86,4	19,0	Source	Pelvis
	3,8	-221,5	9,1	Insertion	Femur
Adductor magnus	-35,8	-133,3	44,6	Source	Pelvis
	11,3	-309,8	-6,0	Insertion	Femur
Hamstrings	-54,7	-126,9	63,3	Source	Pelvis
	-19,2	-26,7	-24,7	Fixed Path	Tibia
	-10,4	-38,9	-22,5	Insertion	Tibia
Biceps femoris short head	6,4	-214,4	21,6	Source	Femur
	-25,3	-29,2	35,5	Fixed Path	Tibia
	-17,6	-47,6	31,4	Insertion	Tibia
Iliopsoas	-44,3	8,8	71,6	Source	Pelvis
	-5,3	-43,4	75,4	Fixed Path	Pelvis
	-3,4	-58,7	76,5	Via Point	Pelvis
	-0,8	-52,6	4,5	Fixed Path	Femur
	-9,4	-60,9	6,0	Insertion	Femur
Gluteus maximus	-108,6	5,8	60,4	Source	Pelvis
	-82,6	-52,7	72,9	Fixed Path	Pelvis
	-55,5	-46,3	-7,6	Fixed Path	Femur
	-11,5	-121,0	17,3	Insertion	Femur
Gluteus medius	-65,9	4,9	75,0	Source	Pelvis
	-27,3	0,3	30,2	Insertion	Femur
Gluteus minimus	-50,5	-24,4	75,5	Source	Pelvis
	-16,7	-0,5	37,5	Insertion	Femur
Gracilis	-15,1	-124,8	23,5	Fixed Path	Pelvis
	-30,1	-5,4	-30,2	Via Point	Tibia
	-19,5	-28,7	-28,7	Fixed Path	Tibia
	5,3	-51,4	-17,7	Insertion	Tibia
Pectinius	-10,8	-76,4	49,8	Source	Pelvis
	-1,5	-104,7	-0,3	Insertion	Femur
Piriformis	-94,4	-14,9	18,5	Source	Pelvis
	-75,7	-56,2	48,9	Fixed Path	Pelvis
	-19,0	-3,5	18,1	Insertion	Femur
Sartorius	-5,3	-14,4	93,7	Source	Pelvis
	-20,8	-342,1	-31,5	Fixed Path	Femur
	-9,4	-37,3	-26,6	Fixed Path	Tibia
	-0,8	-52,6	-23,7	Fixed Path	Tibia
	16,0	-66,1	-17,4	Insertion	Tibia
Tensor fasciae latae	-7,5	-7,2	97,6	Source	Pelvis
	24,8	-97,6	50,4	Fixed Path	Femur
	25,4	-368,4	29,6	Fixed Path	Femur
	18,7	-40,7	28,5	Insertion	Tibia
Rectus femoris	-12,8	-32,3	83,5	Source	Pelvis
	29,1	-395,8	0,4	Via Point	Femur
	43,0	19,3	0,0	Moving Point	Tibia

Table A.1.7.3 Muscle Point Coordinates for CP2 (a) Attachment sites and muscle path defining points in reference frame of related limb segment

Muscle	Coordinates [mm]			Point Type	Ref. Body
	X	Y	Z		
Vastus	5,7	-30,1	28,6	Source	Femur
	7,6	-202,8	23,8	Fixed Path	Femur
	28,3	-393,6	2,1	Via Point	Femur
	37,2	22,0	0,0	Moving Point	Tibia
Peroneus	-14,1	-107,0	26,8	Source	Tibia
	-16,9	-354,3	12,8	Fixed Path	Tibia
	-11,6	-365,2	14,9	Fixed Path	Tibia
	37,6	19,3	18,6	Fixed Path	Calcaneus
	57,3	8,9	23,9	Fixed Path	Calcaneus
	71,7	5,8	9,9	Fixed Path	Calcaneus
	101,2	7,2	-15,5	Insertion	Calcaneus
Gastrocnemius	-5,3	-358,8	-6,6	Source	Femur
	-16,0	-368,3	-6,2	Via Point	Femur
	0,0	26,1	-4,5	Insertion	Calcaneus
Soleus	0,6	-75,3	5,6	Source	Tibia
	0,0	26,1	-4,5	Insertion	Calcaneus
Tibialis anterior	13,6	-77,8	16,4	Source	Tibia
	11,5	-162,6	22,0	Fixed Path	Tibia
	25,8	-308,4	11,8	Fixed Path	Tibia
	98,1	15,0	-25,7	Insertion	Calcaneus
Tibialis posterior	-2,2	-65,1	26,1	Source	Tibia
	1,3	-291,1	-7,7	Fixed Path	Tibia
	35,1	28,1	-24,1	Fixed Path	Calcaneus
	64,9	13,4	-23,6	Insertion	Calcaneus
Extensor digitorum	-0,8	-89,3	24,8	Source	Tibia
	21,5	-332,5	21,6	Fixed Path	Tibia
	79,8	34,3	-8,7	Fixed Path	Calcaneus
	137,0	6,5	-2,6	Fixed Path	Calcaneus
	5,3	4,6	-1,0	Fixed Path	Toes
	41,5	-0,3	4,4	Insertion	Toes
Flexor digitorum longus	-2,0	-104,8	0,6	Source	Tibia
	-0,6	-335,8	-21,8	Fixed Path	Tibia
	36,7	26,5	-23,6	Fixed Path	Calcaneus
	59,6	14,8	-22,1	Fixed Path	Calcaneus
	139,5	-6,8	9,8	Fixed Path	Calcaneus
	-1,6	-6,6	12,4	Fixed Path	Toes
	24,0	-6,0	18,1	Fixed Path	Toes
	37,1	-5,0	20,4	Insertion	Toes
Flexor hallucis longus	-14,2	-136,7	19,1	Source	Tibia
	-7,8	-342,0	-17,9	Fixed Path	Tibia
	31,5	23,2	-20,3	Fixed Path	Calcaneus
	87,3	5,7	-21,5	Fixed Path	Calcaneus
	145,2	-4,5	-22,6	Fixed Path	Calcaneus
	13,0	-5,4	-22,3	Fixed Path	Toes
	47,3	-6,9	-15,2	Insertion	Toes

Table A.1.7.4 Muscle Point Coordinates for CP2 (b) Muscle geometry points in reference frame of related limb segment

A.2 Parameters of Average Children's Model

Muscle	Max. Force [N]	l_{0m}[cm]	TSL[cm]	pennation [degree]
Adductor longus	198	8,17	8,64	6,6
Adductor magnus	637	11,15	11,08	15,6
Hamstrings	637	10,92	22,42	8,0
Biceps femoris short head	143	8,66	8,49	12,3
Iliopsoas	377	8,75	6,99	12,5
Gluteus maximus	764	13,86	9,35	21,9
Gluteus medius	579	6,39	3,42	20,5
Gluteus minimus	142	5,05	1,83	10,0
Gracilis	74	17,65	11,60	8,2
Pectinius	175	9,86	3,97	0,0
Piriformis	251	1,95	7,55	10,0
Sartorius	61	32,05	7,74	0,0
Tensor fasciae latae	98	7,68	30,42	3,0
Rectus femoris	585	6,13	27,34	13,9
Vastus	2461	7,89	22,59	17,5
Peroneus	372	3,86	32,45	13,0
Gastrocnemius	1048	4,26	32,27	10,9
Soleus	1547	3,34	23,99	28,3
Tibialis anterior	292	5,19	25,76	9,6
Tibialis posterior	527	2,81	27,63	13,7
Extensor digitorum	227	5,47	31,92	7,0
Flexor digitorum longus	143	3,39	35,28	13,6
Flexor hallucis longus	239	4,02	35,70	16,9

Table A.2.1 Muscle Model Parameters for Average Children's Model Individual Hill-type muscle model parameters

Segment	Joint Center location [cm]			Reference Segment
	X ant.-post.	Y sup.-inf.	Z med.-lat.	
Pelvis center	0,00	73,70	0,00	Ground
Right hip	3,06	-0,06	6,14	Pelvis
Left hip	3,06	-0,06	-6,14	Pelvis
Right knee *	0,00	-0,32	0,00	Right Femur
Left knee *	0,00	-0,32	0,00	Left Femur
Right ankle	0,00	-0,33	0,00	Right Tibia
Left ankle	0,00	-0,33	0,00	Left Tibia
Right Toes	13,89	0,00	0,00	Right Calcaneus
Left Toes	13,89	0,00	0,00	Left Calcaneus

Table A.2.2 Joint Centres for Model of Average Child Model *Coordinates for knee joint centre at 0° knee angle

Muscle	Coordinates [mm]			Point Type	Ref. Body
	X	Y	Z		
Adductor longus	7,4	-80,1	14,8	Source	Pelvis
	1,9	-186,3	3,2	Insertion	Femur
Adductor magnus	-33,3	-106,7	24,4	Source	Pelvis
	4,7	-237,5	-3,7	Insertion	Femur
Hamstrings	-65,8	-96,4	51,5	Source	Pelvis
	-22,5	-23,1	-19,5	Fixed Path	Tibia
	-6,4	-41,3	-18,9	Insertion	Tibia
Biceps femoris short head	-5,1	-152,7	17,8	Source	Femur
	-18,5	-27,7	41,0	Fixed Path	Tibia
	-14,9	-44,9	36,3	Insertion	Tibia
Iliopsoas	-45,5	38,8	38,6	Source	Pelvis
	-2,2	-40,3	60,4	Fixed Path	Pelvis
	-0,4	-55,8	63,3	Via Point	Pelvis
	5,2	-42,3	7,6	Fixed Path	Femur
	-8,5	-49,2	6,8	Insertion	Femur
Gluteus maximus	-88,5	19,6	50,0	Source	Pelvis
	-79,7	-51,2	68,5	Fixed Path	Pelvis
	-45,4	-36,4	12,3	Fixed Path	Femur
	-7,7	-120,7	18,3	Insertion	Femur
Gluteus medius	-47,7	17,0	65,4	Source	Pelvis
	-17,9	-2,4	38,7	Insertion	Femur
Gluteus minimus	-42,7	-2,4	70,6	Source	Pelvis
	-13,7	-1,9	38,6	Insertion	Femur
Gracilis	-20,9	-104,1	16,8	Fixed Path	Pelvis
	-23,1	-4,7	-29,0	Via Point	Tibia
	-12,6	-27,3	-27,8	Fixed Path	Tibia
	3,5	-50,4	-20,5	Insertion	Tibia
Pectinius	-2,5	-62,8	34,8	Source	Pelvis
	0,4	-112,5	6,0	Insertion	Femur
Piriformis	-69,7	-5,3	21,0	Source	Pelvis
	-69,6	-32,9	40,4	Fixed Path	Pelvis
	-15,8	-1,2	23,6	Insertion	Femur
Sartorius	-3,2	-16,0	79,2	Source	Pelvis
	-10,7	-283,9	-31,3	Fixed Path	Femur
	-6,9	-33,6	-30,9	Fixed Path	Tibia
	-2,9	-44,2	-27,9	Fixed Path	Tibia
	9,7	-60,1	-19,2	Insertion	Tibia
Tensor fasciae latae	-10,8	-2,3	88,2	Source	Pelvis
	30,0	-76,6	48,8	Fixed Path	Femur
	17,3	-313,6	34,3	Fixed Path	Femur
	12,9	-37,9	31,3	Insertion	Tibia
Rectus femoris	-4,6	-33,3	74,6	Source	Pelvis
	26,3	-326,6	0,7	Via Point	Femur
	50,3	14,2	0,0	Moving Point	Tibia

Table A.2.3 Muscle Point Coordinates for Average Child Model (a)
Attachment sites and muscle path defining points in reference frame of related limb segment

Muscle	Coordinates [mm]			Point Type	Ref. Body
	X	Y	Z		
Vastus	9,5	-18,4	27,5	Source	Femur
	12,8	-167,6	26,3	Fixed Path	Femur
	25,7	-324,7	2,4	Via Point	Femur
	46,0	18,0	0,0	Moving Point	Tibia
Peroneus	-12,8	-57,4	37,2	Source	Tibia
	-20,4	-318,9	14,5	Fixed Path	Tibia
	-18,1	-327,8	15,3	Fixed Path	Tibia
	33,9	17,4	16,8	Fixed Path	Calcaneus
	51,7	8,0	21,5	Fixed Path	Calcaneus
	64,6	5,2	9,0	Fixed Path	Calcaneus
	91,3	6,4	-14,0	Insertion	Calcaneus
Gastrocnemius	-8,4	-292,4	1,6	Source	Femur
	-16,7	-299,9	1,6	Via Point	Femur
	0,0	23,5	-4,0	Insertion	Calcaneus
Soleus	-2,2	-65,9	15,1	Source	Tibia
	0,0	23,5	-4,0	Insertion	Calcaneus
Tibialis anterior	8,9	-53,9	27,3	Source	Tibia
	7,8	-145,4	21,9	Fixed Path	Tibia
	24,2	-280,6	3,0	Fixed Path	Tibia
	88,5	13,5	-23,1	Insertion	Calcaneus
Tibialis posterior	-1,9	-61,1	21,4	Source	Tibia
	-6,1	-271,4	-11,8	Fixed Path	Tibia
	31,6	25,3	-21,7	Fixed Path	Calcaneus
	58,6	12,1	-21,3	Insertion	Calcaneus
Extensor digitorum	-2,5	-69,2	32,2	Source	Tibia
	20,4	-306,3	13,6	Fixed Path	Tibia
	71,9	31,0	-7,8	Fixed Path	Calcaneus
	123,5	5,8	-2,3	Fixed Path	Calcaneus
	4,8	4,2	-0,9	Fixed Path	Toes
	37,4	-0,3	4,0	Insertion	Toes
Flexor digitorum longus	-0,8	-88,0	1,1	Source	Tibia
	-2,7	-303,0	-23,5	Fixed Path	Tibia
	33,1	23,9	-21,2	Fixed Path	Calcaneus
	53,7	13,4	-20,0	Fixed Path	Calcaneus
	125,8	-6,1	8,8	Fixed Path	Calcaneus
	-1,4	-5,9	11,2	Fixed Path	Toes
	21,6	-5,4	16,3	Fixed Path	Toes
	33,5	-4,6	18,4	Insertion	Toes
Flexor hallucis longus	-15,2	-97,1	25,6	Source	Tibia
	-14,7	-302,3	-13,5	Fixed Path	Tibia
	28,4	20,9	-18,3	Fixed Path	Calcaneus
	78,7	5,2	-19,4	Fixed Path	Calcaneus
	130,9	-4,0	-20,4	Fixed Path	Calcaneus
	11,8	-4,9	-20,1	Fixed Path	Toes
	42,6	-6,2	-13,7	Insertion	Toes

Table A.2.4 Muscle Point Coordinates for Average Child Model (b) Muscle geometry points in reference frame of related limb segment

B

Muscle Function in Models

Contents

APPENDICES

B.1 Moment arms and max. isometric joint moments per muscle

The following pages show moment arms and maximum isomeric joint moments for the models of two children with CP compared to average values and variation of ND over the entire motion range of the corresponding joints. Moment arms have been scaled with the relation of individual to average body height of the control group. Joint moments have been normalized as proposed by (Eek et al., 2006) with regard to average body properties.

<u>**Noticeable differences**</u>

Adductor Longus: with higher moment arm in hip flexion and adduction

Adductor Magnus: in CP2 with much higher moment arm for hip extension but less for adduction and similar hip extension moment as ND

Gastrocnemius: only 50% of maximum joint moment for knee extension and plantarflexion in CP compared to ND

Gluteus maximus: shorter moment arm in CP1 and overall only 50% of maximum hip extension moment in both CP-children compared to ND.

Glutus Medius: shorer moment arm for hip abduction and longer moment arm for hip extension in both CP-children compared to ND. Therefore was in both CP-children a similar max. hip extension moment as in ND possible.

Hamstrings: Only 50% of maximum hip extension and knee flexion moment of ND was possible in both CP-children.

Iliopsoas: nothing noticeable

Rectus Femoris: longer Moment arm for hip flexion in CP1, but only around 50% of maximum hip flexion moment of ND possible in both CP

Soleus: around 50% of maximum plantarflexion moment of ND possible in both CP

Vastus: around 75% and 85% of maximum knee extension moment of ND possible in CP1 and CP2 respectively

B.1.1 Adductor longus

a)

b)

c)

d)
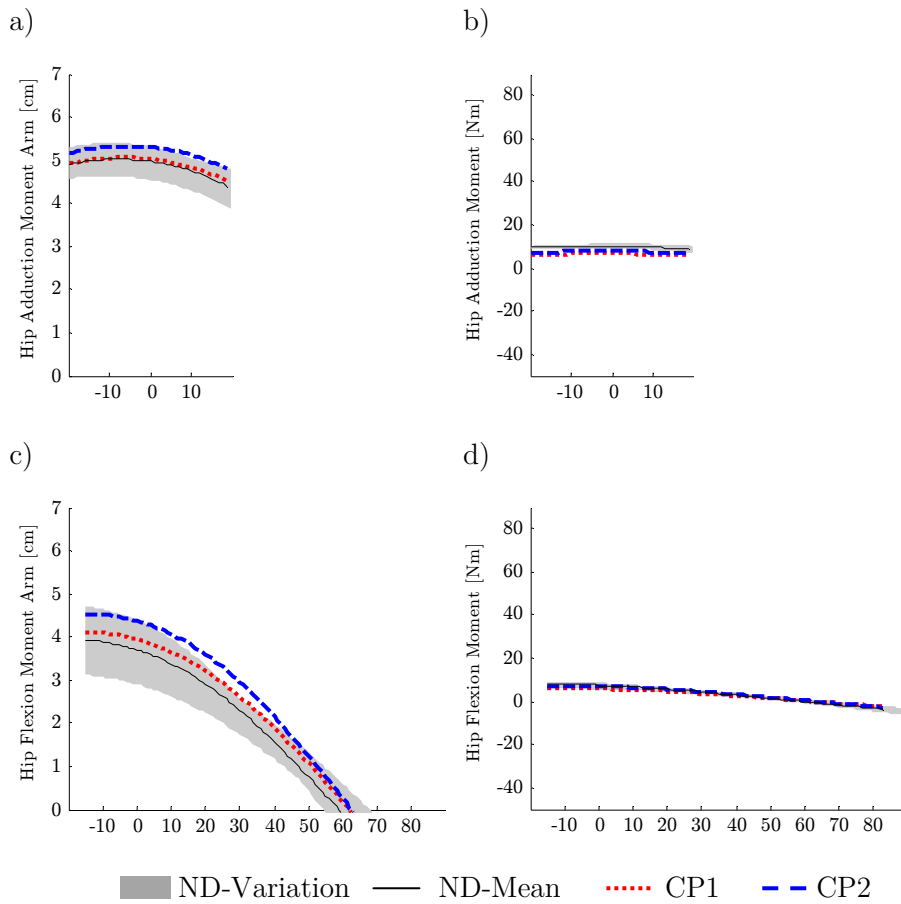
Figure B.1.1 MA and max. isometric joint moment for adductor longus - Moment arm and maximum isometric joint moment of the CP-children (CP1, CP2) and the control group (ND) for hip adduction from -20° to 20° (a,b) and hip flexion from -10° to 90° (c,d)

B.1.2 Adductor Magnus

a)

b)

c)
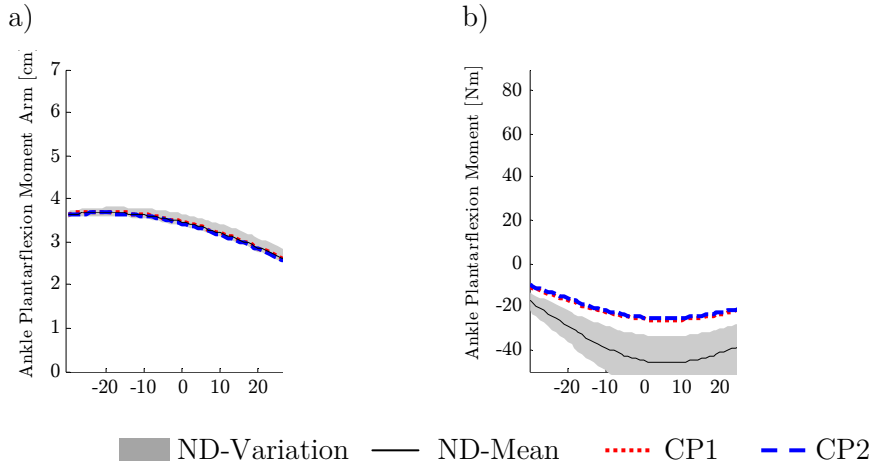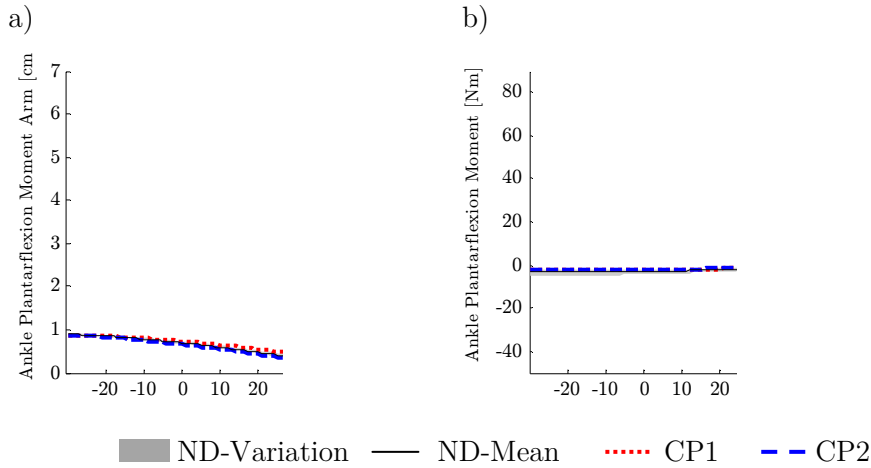
d)
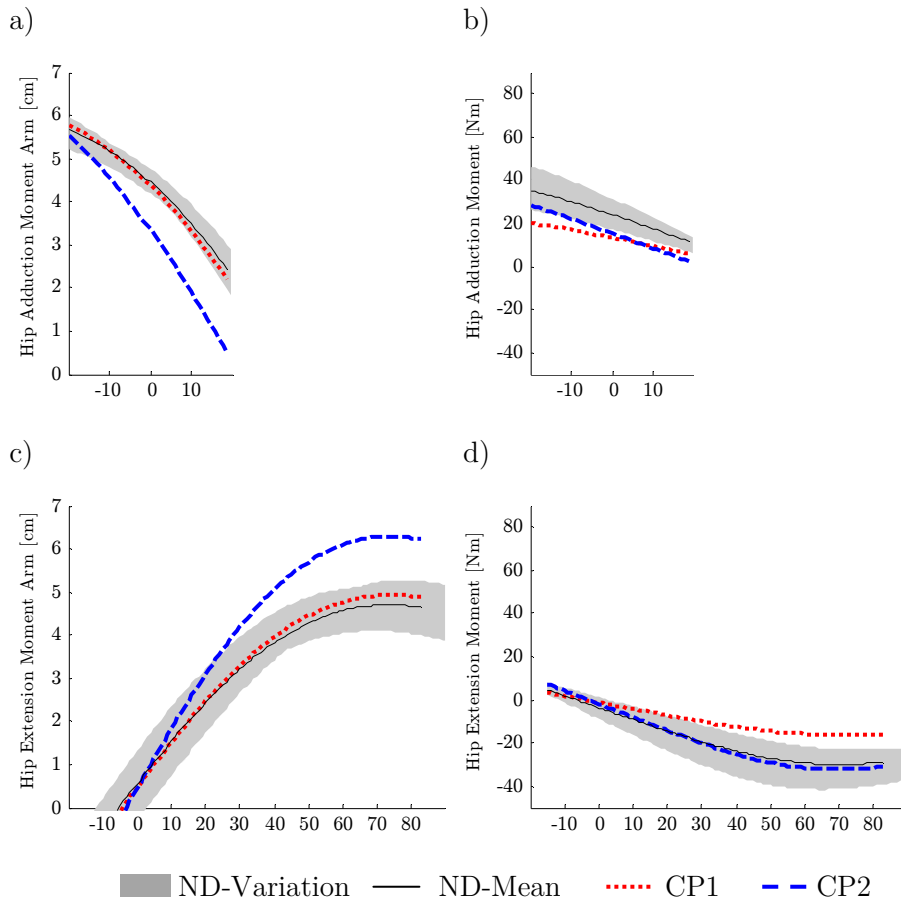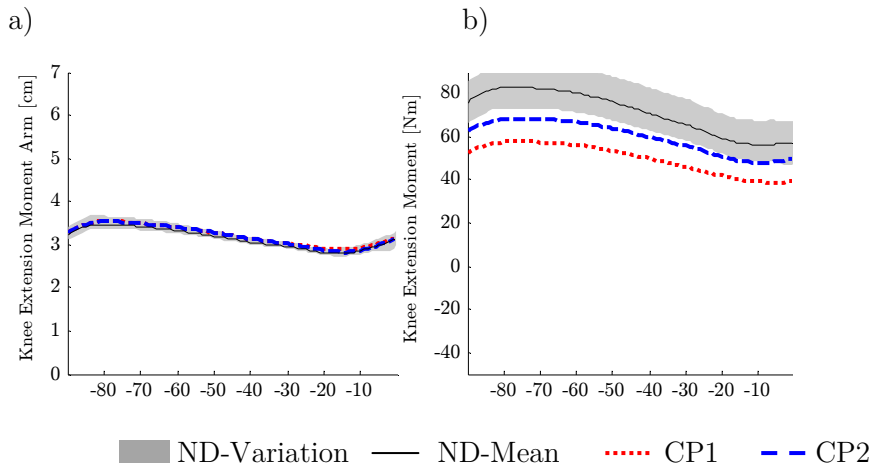

Figure B.1.2 MA and max. isometric joint moment for adductor magnus - Moment arm and maximum isometric joint moment of the CP-children (CP1,CP2) and the control group (ND) at hip extension from -20° to 20° (a,b) and hip flexion from -10° to 90° (c,d)

B.1.3 Biceps femoris

a)

b)
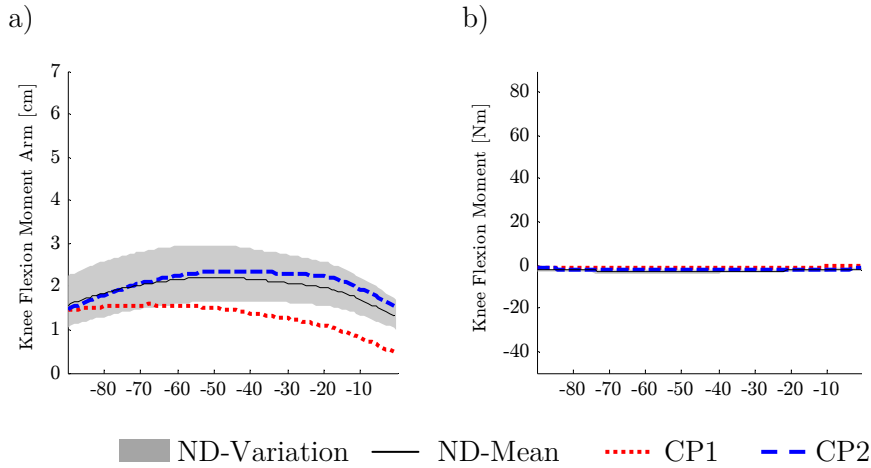
Figure B.1.3 MA and max. isometric joint moment for biceps femoris - Trajectories of moment arm and maximum isometric joint moment of the CP-children (CP1,CP2) and the control group (ND) at knee flexion from -80° to 0° (a,b)
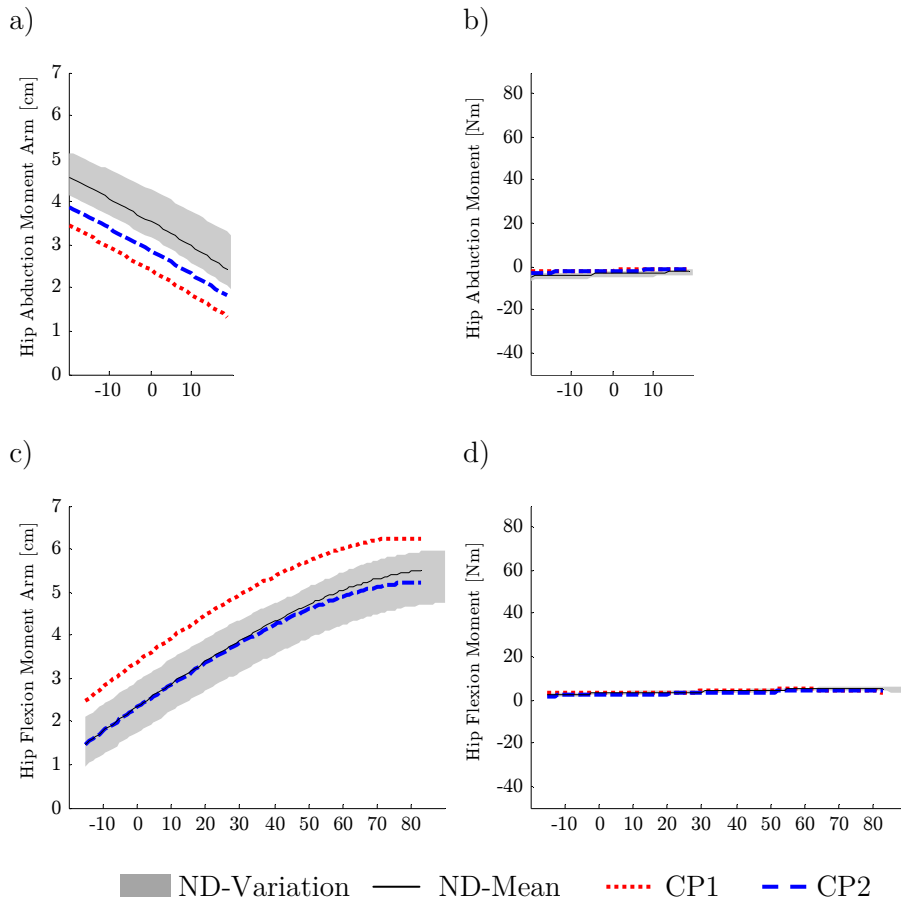
B.1.4 Extensor digitorum

a)

b)
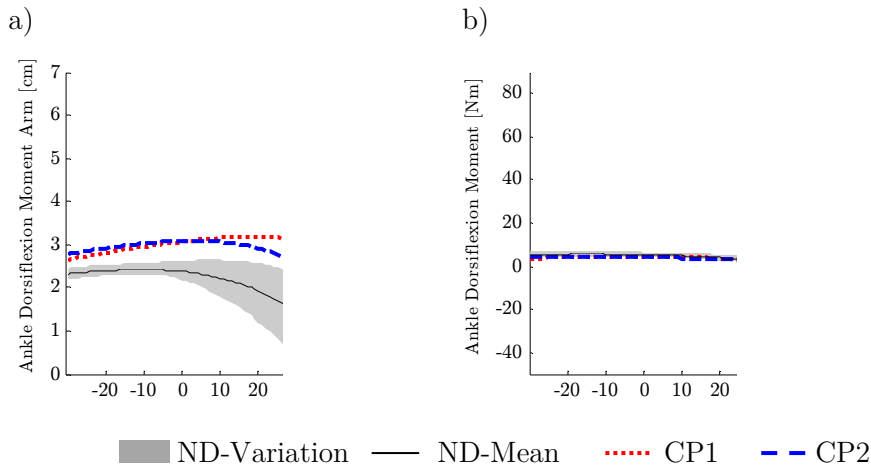
Figure B.1.4 MA and max. isometric joint moment for extensor digitorum - Trajectories of moment arm and maximum isometric joint moment of the CP-children (CP1,CP2) and the control group (ND) at ankle dorsiflexion from -80° to 0° (a,b)

B.1.5 Flexor digitorum longus

a)

b)
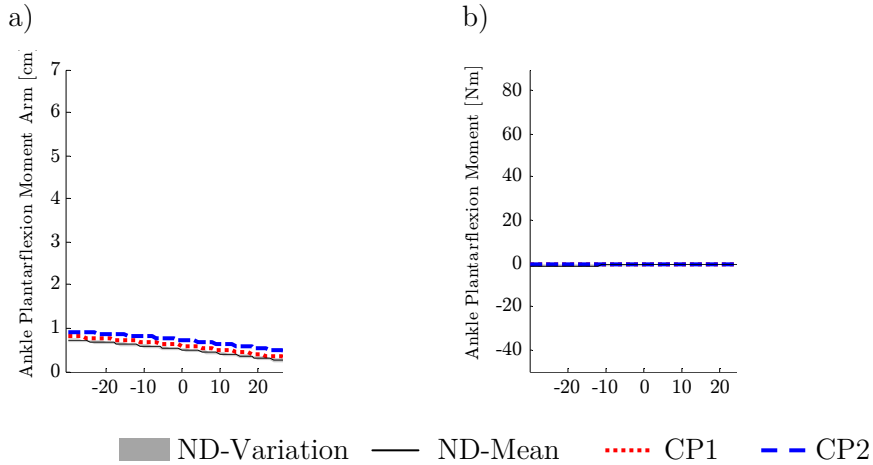
Figure B.1.5 MA and max. isometric joint moment for flexor digitorum - Trajectories of moment arm and maximum isometric joint moment of the CP-children (CP1,CP2) and the control group for ankle plantarflexion from -30° to 30° (a,b)

## B.1.6 Flexor hallucis longus

a)

b)
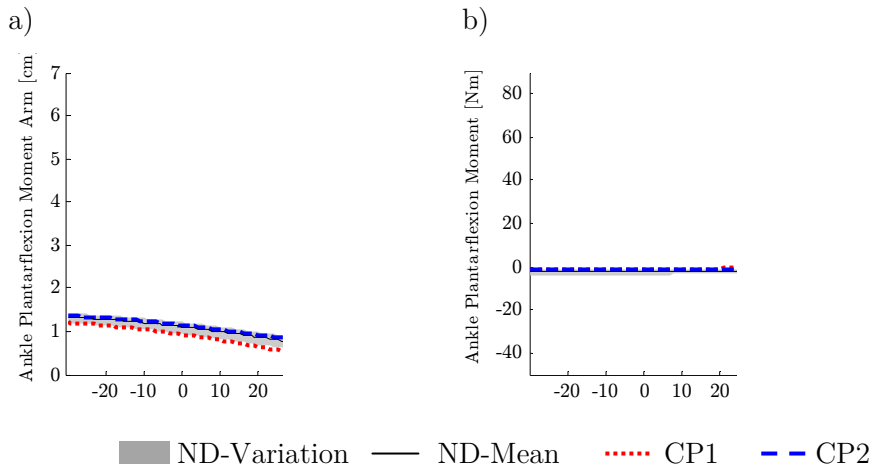
Figure B.1.6 MA and max. isometric joint moment for flexor hal. longus - Trajectories of moment arm and maximum isometric joint moment of the CP-children (CP1,CP2) and the control group (ND) for ankle plantarflexion from -30° to 30° (a,b)

B.1.7 Gastrocnemius

a)

b)

c)

d)

ND-Variation ——— ND-Mean ····· CP1 – – CP2
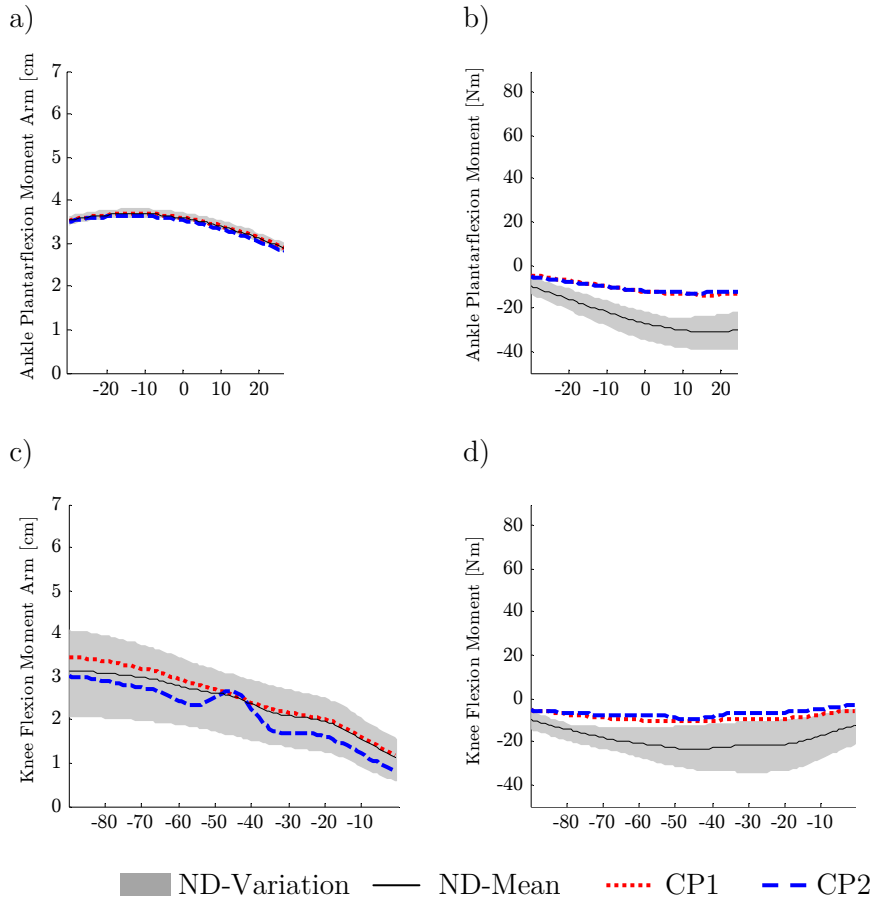
Figure B.1.7 MA and max. isometric joint moment for gastrocnemius - Trajectories of moment arm and maximum isometric joint moment of the CP-children (CP1,CP2) and the control group (ND) for ankle plantarflexion from -30° to 30° (a,b) and knee flexion from -90° to 0° (c,d)

B.1.8 Gluteus maximus

a)

b)

c)

d)
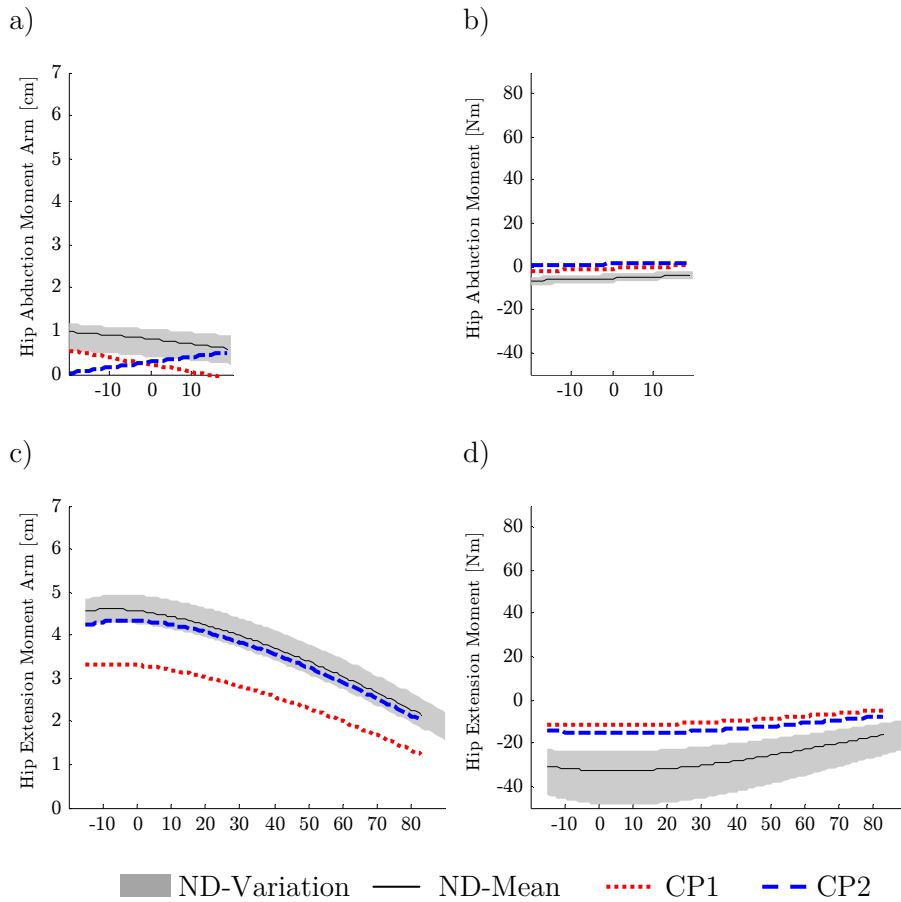
Figure B.1.8 MA and max. isometric joint moment for gluteus maximus - Trajectories of moment arm and maximum isometric joint moment of the CP-children (CP1,CP2) and the control group (ND) for hip abduction from -20° to 20° (a,b) and hip extension from -15° to 90° (c,d)

B.1.9 Gluteus medius

a)

b)

c)

d)
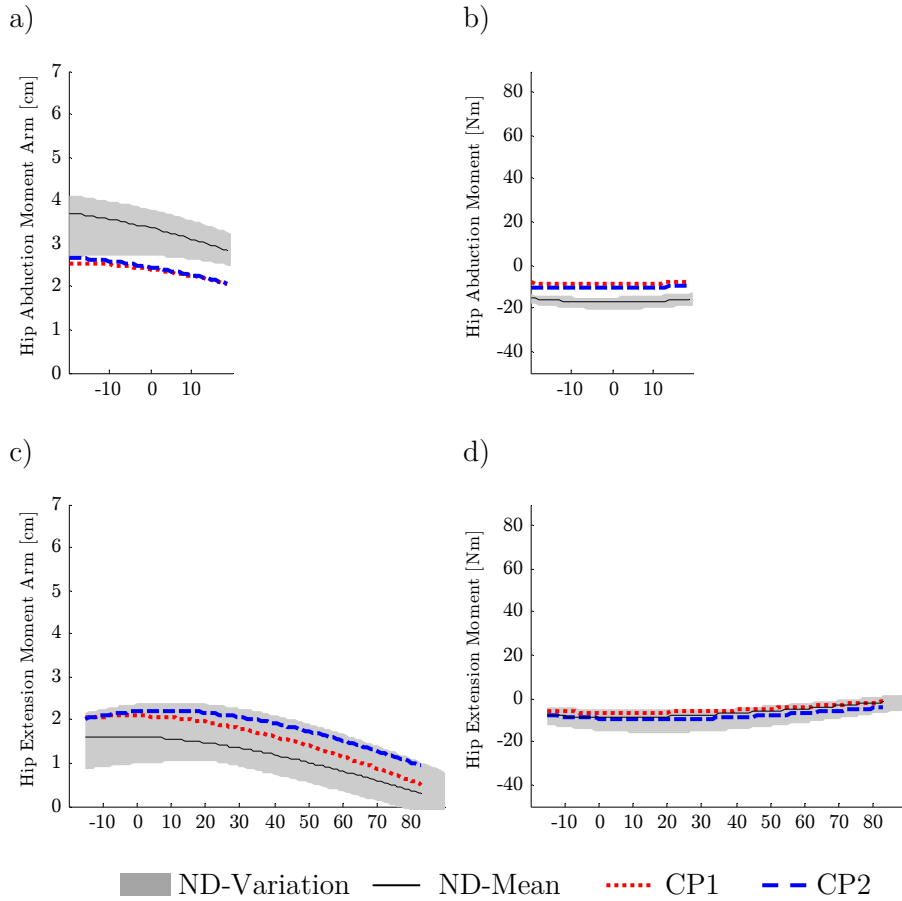
Figure B.1.9 MA and max. isometric joint moment for gluteus medius - Trajectories of moment arm and maximum isometric joint moment of the CP-children (CP1,CP2) and the control group (ND) for hip abduction from -20° to 20° (a,b) and hip extension from -15° to 90° (c,d)

B.1.10 Gluteus minimus
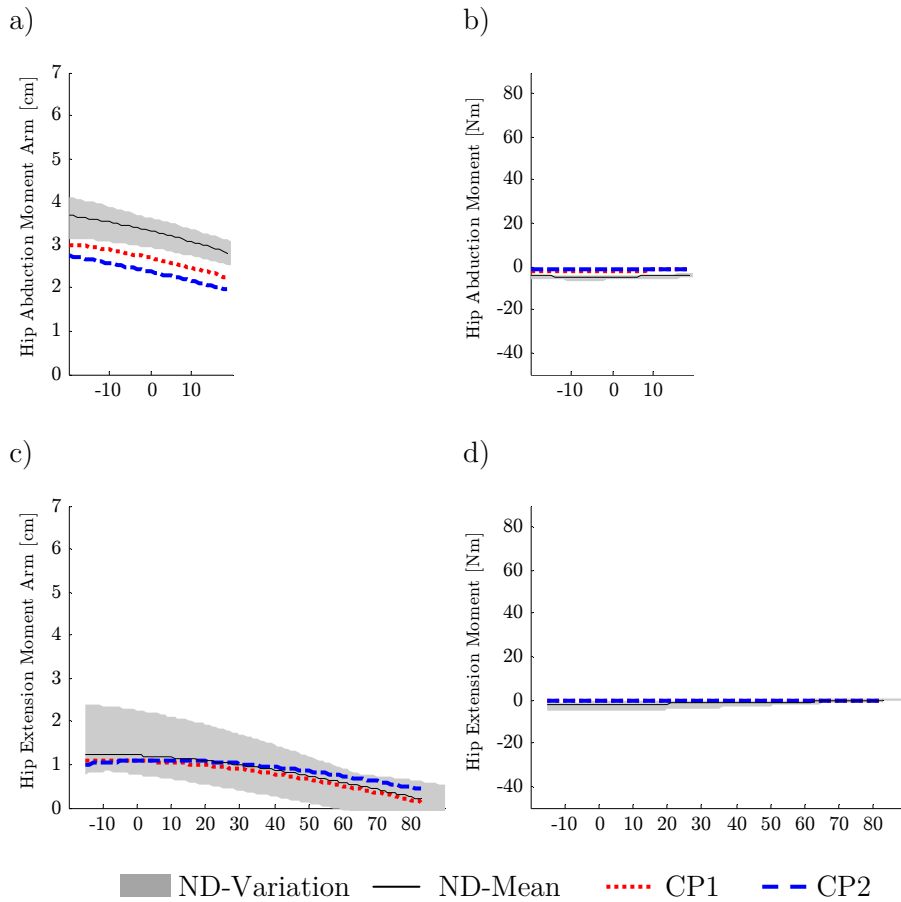
Figure B.1.10 MA and max. isometric joint moment for gluteus medius - Trajectories of moment arm and maximum isometric joint moment of the CP-children (CP1,CP2) and the control group (ND) for hip abduction from -20° to 20° (a,b) and hip extension from -15° to 90° (c,d)
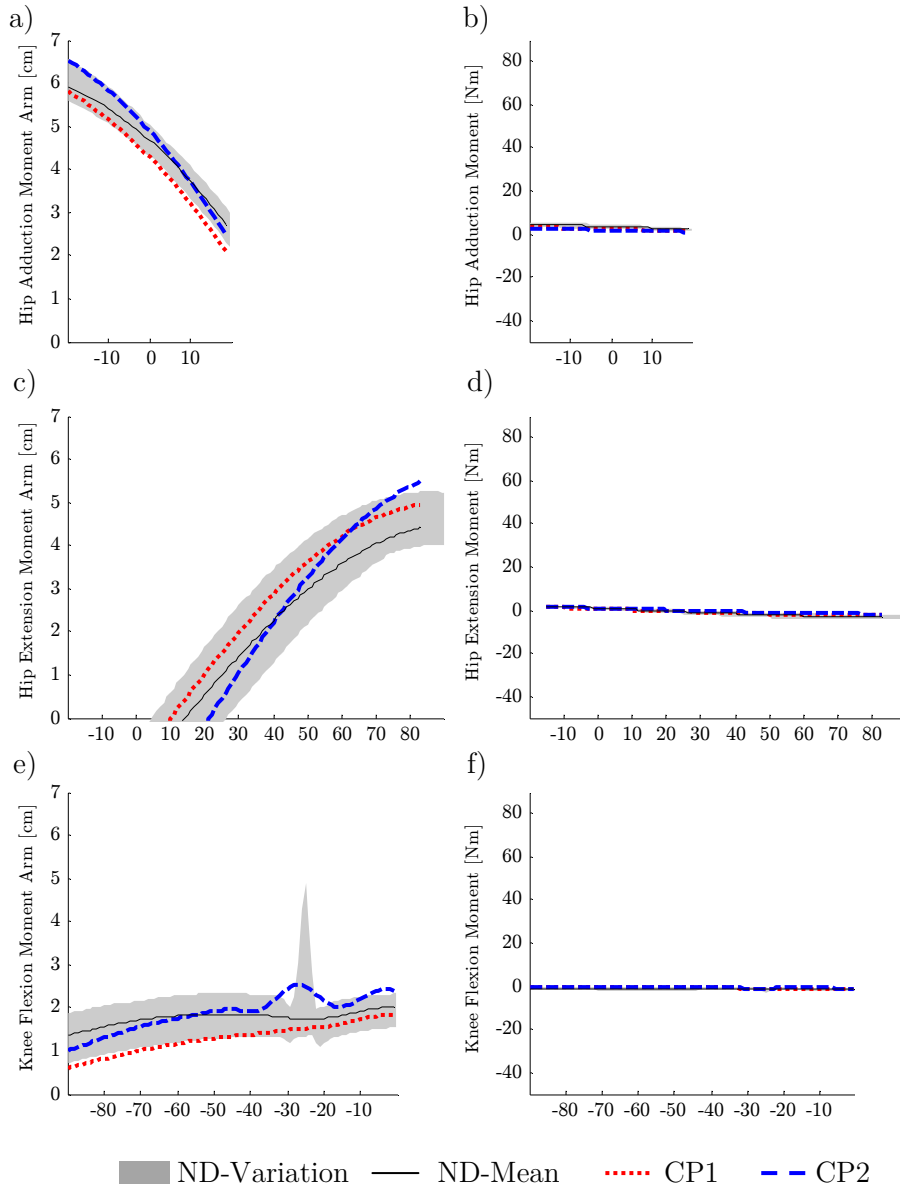
B.1.11   Gracilis

Figure B.1.11 MA and max. isometric joint moment for gracilis - Trajectories of moment arm and maximum isometric joint moment of the CP-children (CP1,CP2) and the control group (ND) for hip adduction from -20° to 20° (a,b), hip extension from -15° to 90° (c,d) and knee flexion from -90° to 0° (e,f)
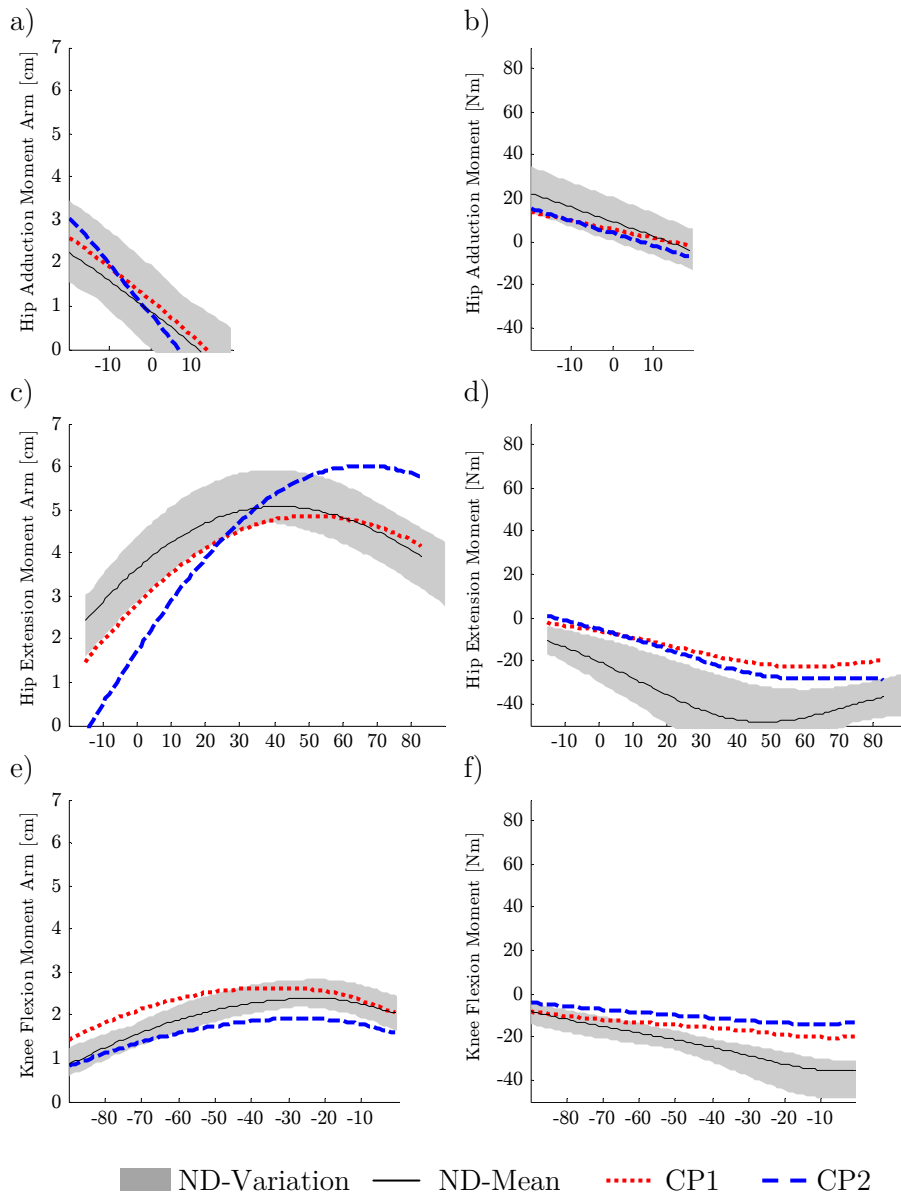
B.1.12 Hamstrings

Figure B.1.12 MA and max. isometric joint moment for hamstings -
Trajectories of moment arm and maximum isometric joint moment of the
CP-children (CP1,CP2) and the control group (ND) for hip adduction from -
20° to 20° (a,b), hip extension from -15° to 90° (c,d) and knee flexion from -
90° to 0° (e,f)

B.1.13 Iliopsoas

a)

b)
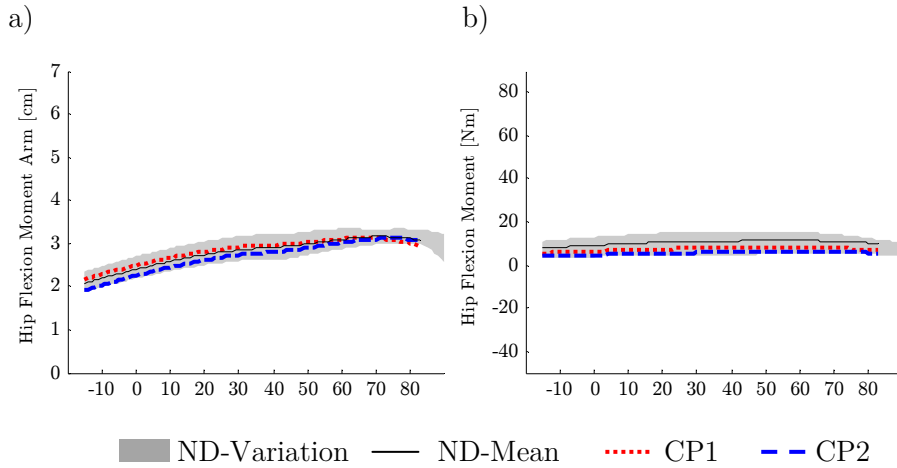
Figure B.1.13 MA and max. isometric joint moment for iliopsoas - Trajectories of moment arm and maximum isometric joint moment of the CP-children (CP1,CP2) and the control group (ND) for hip flexion from -15° to 90° (a,b)

B.1.14 Peroneus

a)

b)
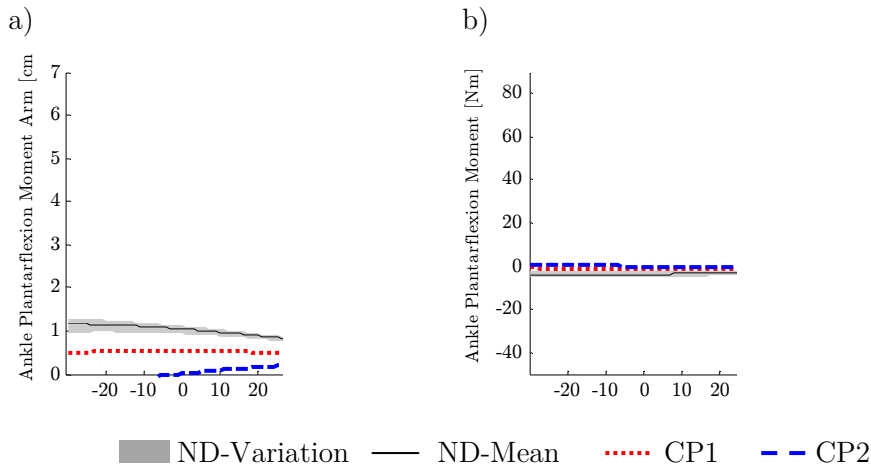
Figure B.1.14 MA and max. isometric joint moment for peroneus - Trajectories of moment arm and maximum isometric joint moment of the CP-children (CP1,CP2) and the control group (ND) for ankle plantarfelxion from -30° to 30° (a,b)

B.1.15   Pectinius

a)

b)

c)

d)
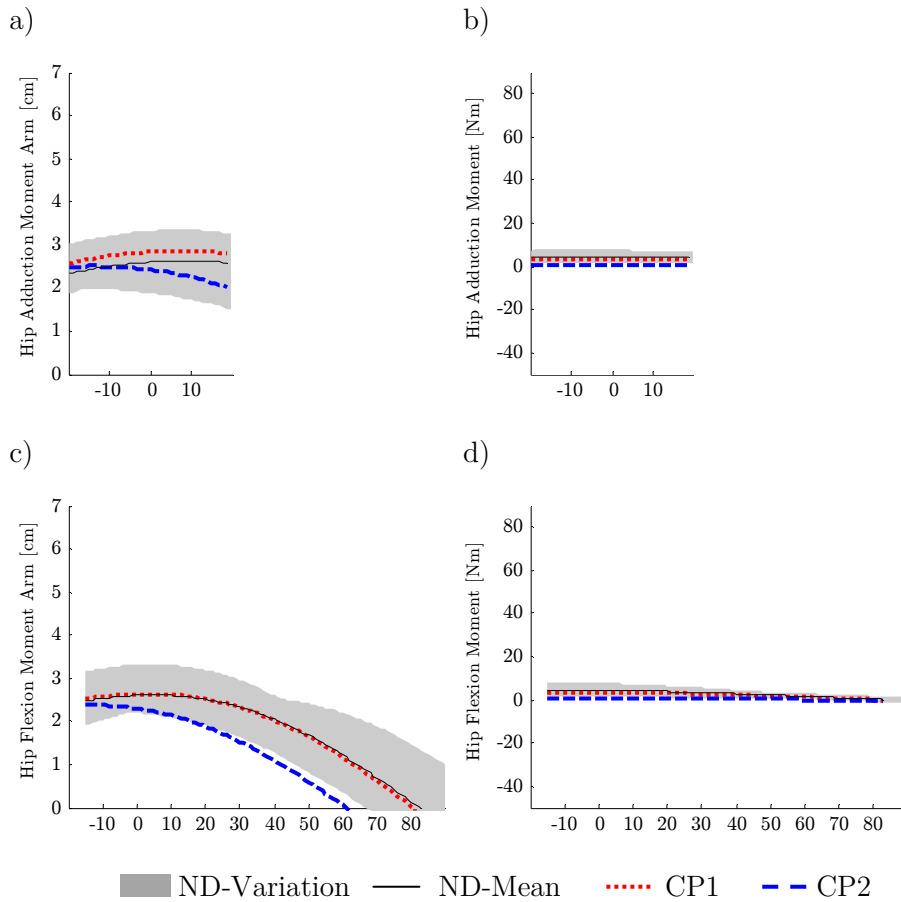
Figure B.1.15 MA and max. isometric joint moment for pectinius - Trajectories of moment arm and maximum isometric joint moment of the CP-children (CP1,CP2) and the control group (ND) for hip adduction from -20° to 20° (a,b) and hip flexion from -15° to 90° (c,d)

B.1.16 Piriformis

a)

b)

c)

d)
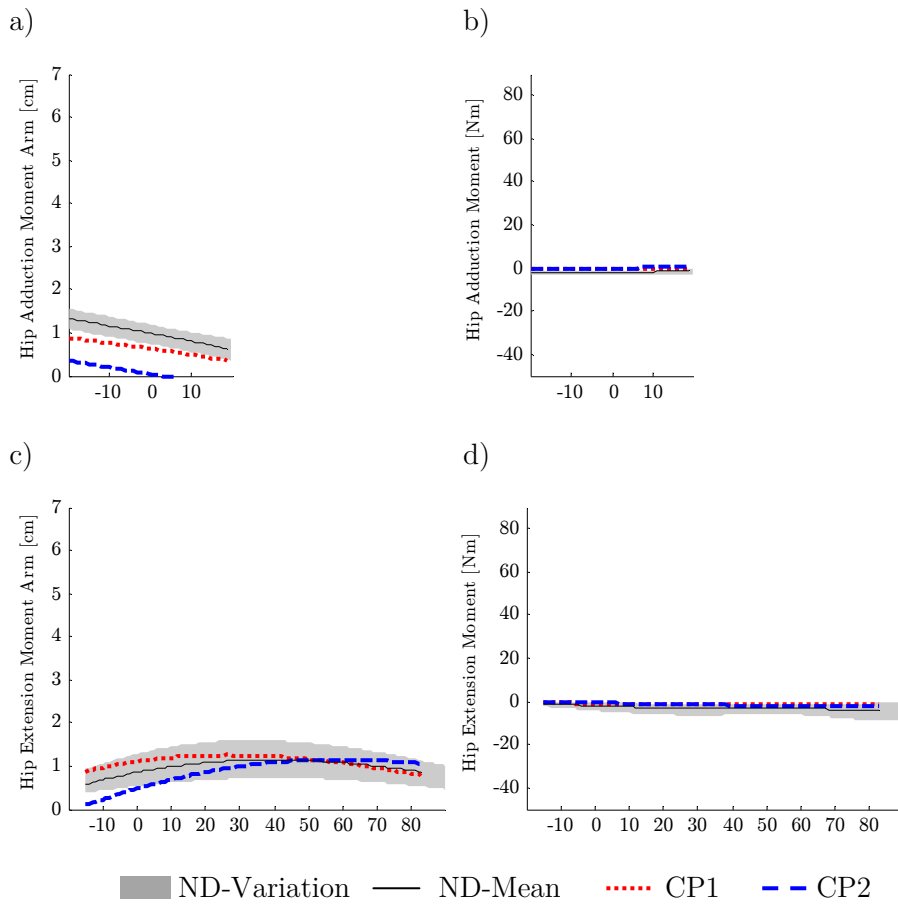
Figure B.1.16 MA and max. isometric joint moment for piriformis - Trajectories of moment arm and maximum isometric joint moment of the CP-children (CP1,CP2) and the control group (ND) for hip adduction from -20° to 20° (a,b) and hip extension from -15° to 90° (c,d)

B.1.17 Rectus femoris
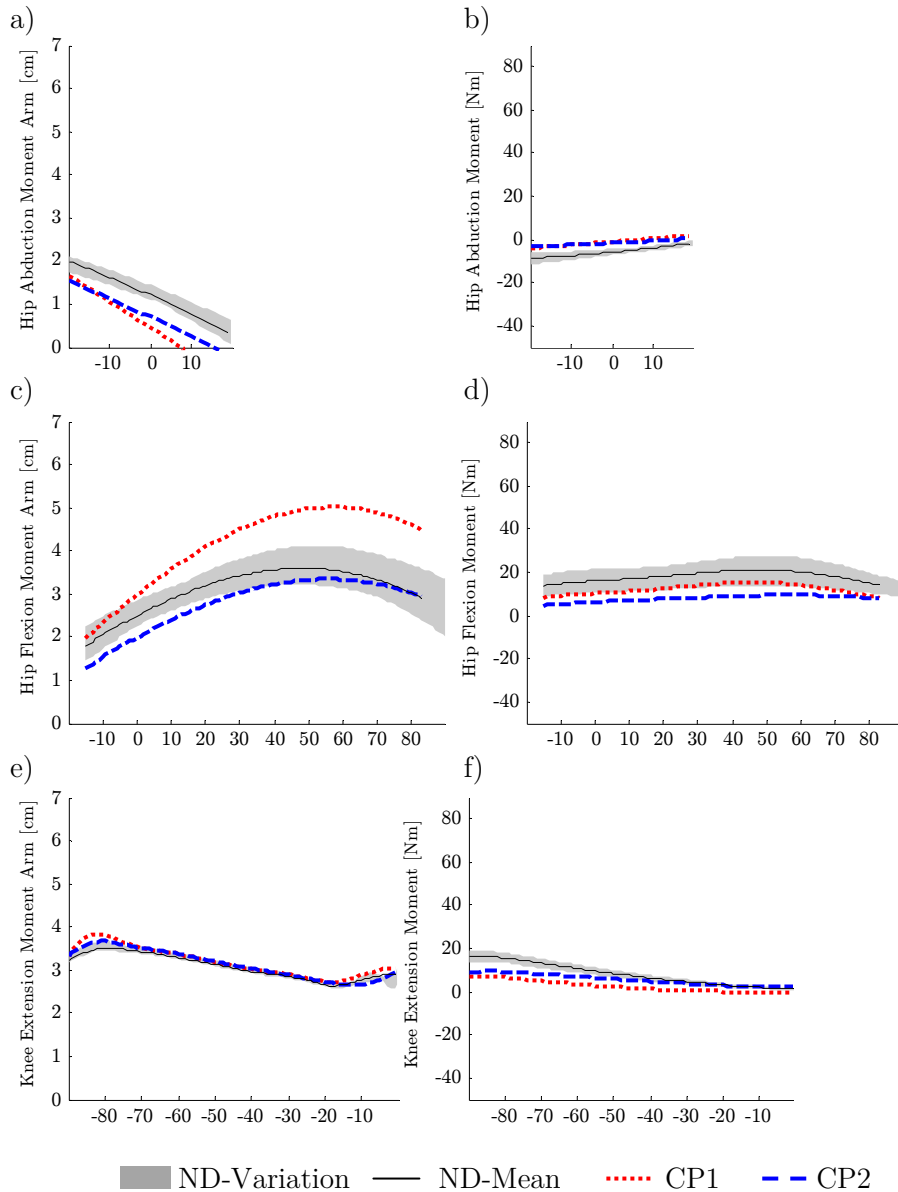
Figure B.1.17 MA and max. isometric joint moment for rectus femoris -
Trajectories of moment arm and maximum isometric joint moment of the
CP-children (CP1,CP2) and the control group (ND) for hip abduction from -
20° to 20° (a,b), hip flexion from -15° to 90° (c,d) and knee extension from -
90° to 0° (e,f)

B.1.18 Sartorius
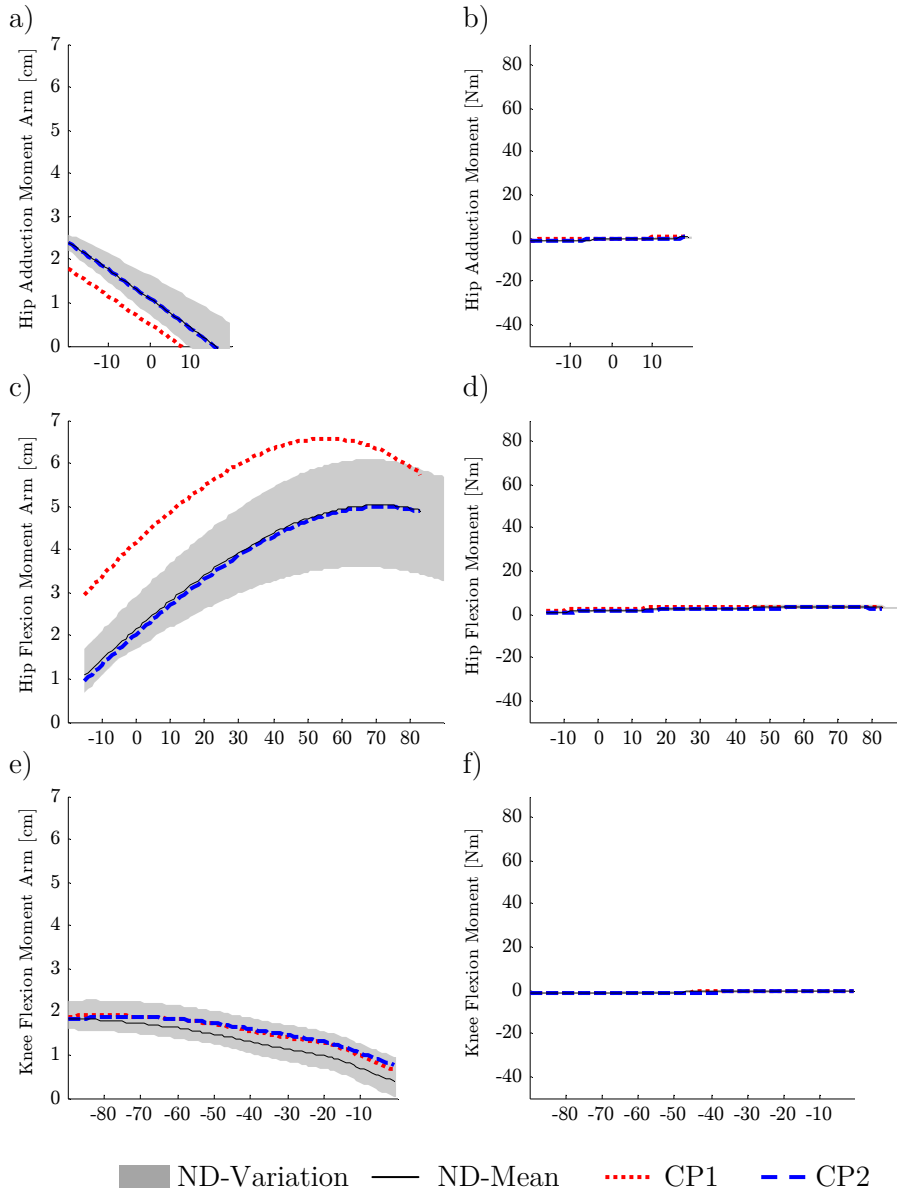
Figure B.1.18 MA and max. isometric joint moment for sartorius - Trajectories of moment arm and maximum isometric joint moment of the CP-children (CP1,CP2) and the control group (ND) for hip adduction from -20° to 20° (a,b), hip flexion from -15° to 90° (c,d) and knee flexion from -90° to 0° (e,f)

B.1.19   Soleus

a)

b)

ND-Variation ——— ND-Mean ······ CP1 – – CP2

Figure B.1.19 MA and max. isometric joint moment for sartorius - Trajectories of moment arm and maximum isometric joint moment of the CP-children (CP1,CP2) and the control group (ND) for ankle plantarflexion from -30° to 30° (a,b)

B.1.20   Tibialis anterior

a)

b)

ND-Variation ——— ND-Mean ······ CP1 – – CP2
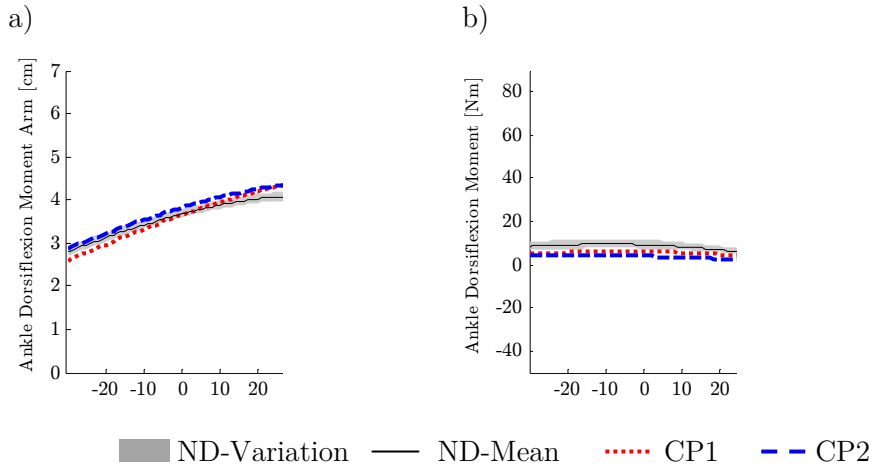
Figure B.1.20 MA and max. isometric joint moment for tibialis anterior - Trajectories of moment arm and maximum isometric joint moment of the CP-children (CP1,CP2) and the control group (ND) for ankle dorsiflexion from -30° to 30° (a,b)

B.1.21   Tibialis posterior

a)   b)

Figure B.1.21 MA and max. isometric joint moment for tibialis posterior - Trajectories of moment arm and maximum isometric joint moment of the CP-children (CP1,CP2) and the control group (ND) for ankle plantarflexion from -30° to 30° (a,b)

B.1.22   Vastus

a)   b)

Figure B.1.22 MA and max. isometric joint moment for vastus - Trajectories of moment arm and maximum isometric joint moment of the CP-children (CP1,CP2) and the control group (ND) for knee extension from -90° to 0° (a,b)

B.1.23 Tensor fasciae latae

a)

b)

c)

d)

ND-Variation —— ND-Mean ······ CP1 – – CP2

Figure B.1.23 MA and max. isometric joint moment for tensor fas. latae -
Trajectories of moment arm and maximum isometric joint moment of the
CP-children (CP1,CP2) and the control group (ND) for hip abduction from -
20° to 20° (a,b) and hip flexion from -15° to 90° (c,d)

B.2 Muscle Function in Gait

The following pages show muscle function and individual contributions to joint and centre of mass (CoM) accelerations during gait. Results for two children with cerebral palsy are compared to average values and variation of the control group. Muscle fibre lengths are shown in percent of optimal muscle fibre length. Muscle forces are denoted in relation to body weight in [N/kg] and moment arms were scaled with relation of individual to average body height of the control group. Joint moments were normalized according to (Eek et al., 2006).
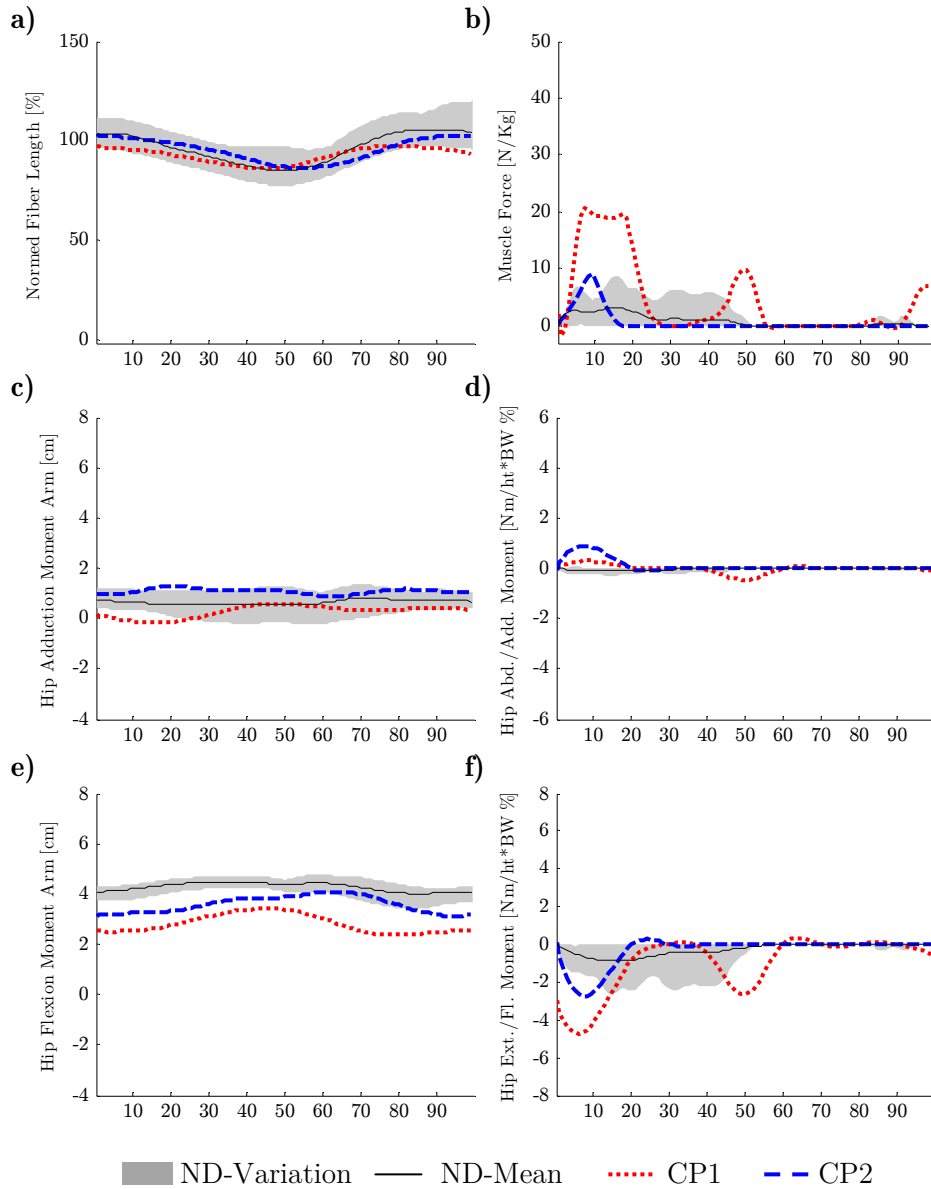
B.2.1 Adductor Longus in Gait
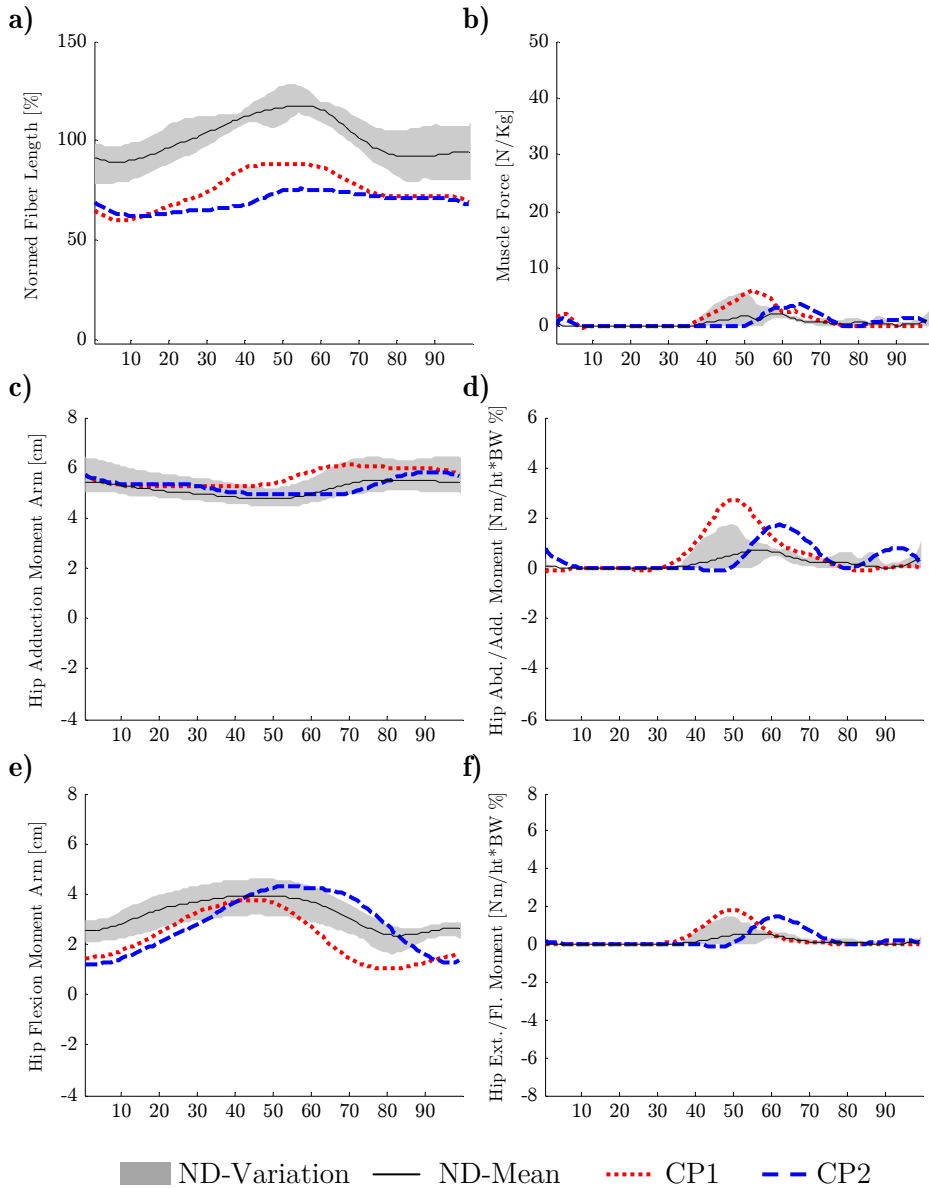
Figure B.2.1 Adductor longus: Function in gait - Normalized muscle fibre length (a), muscle force per kg body weight (b) as well as moment arm and normalized joint moment for hip adduction (c,d) and hip flexion (e,f) of the CP-children (CP1,CP2) and the control group (ND) in a full gait cycle.
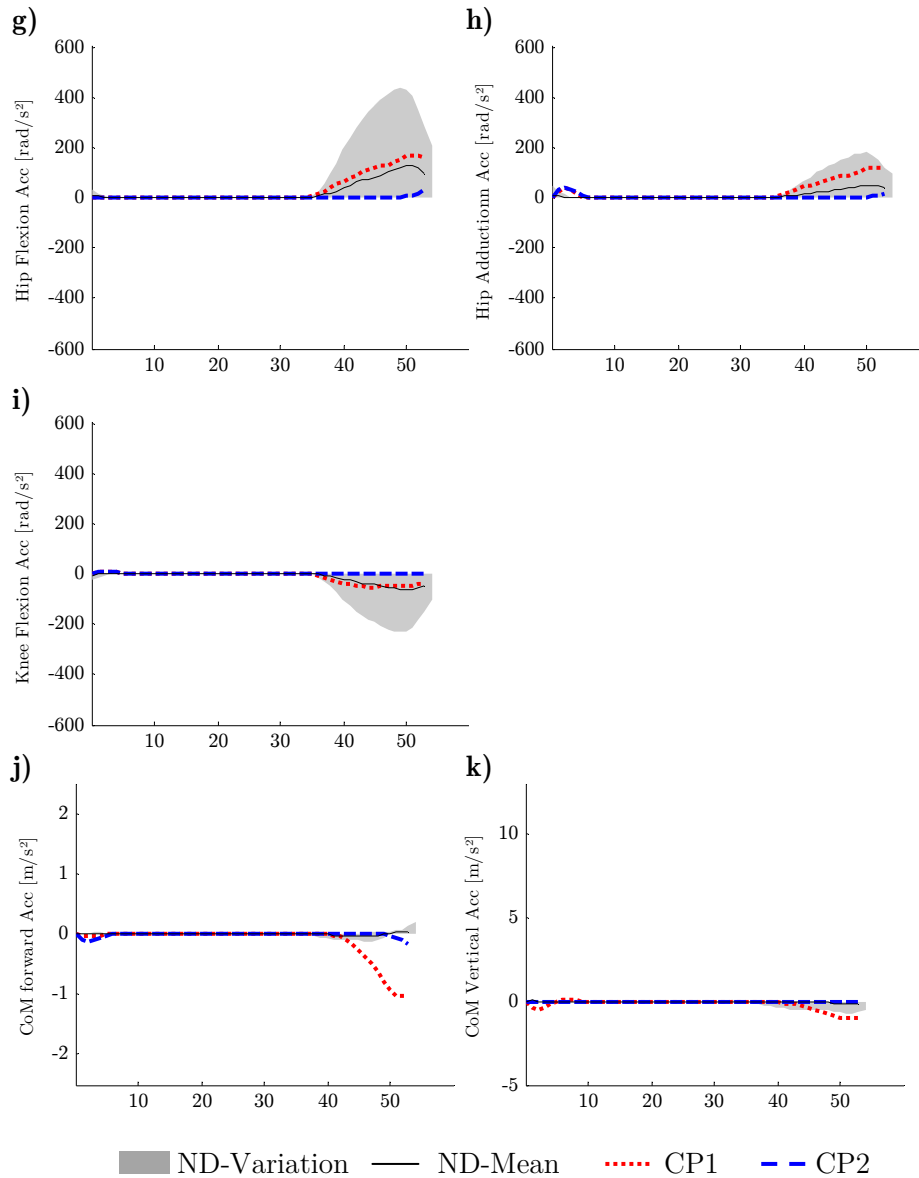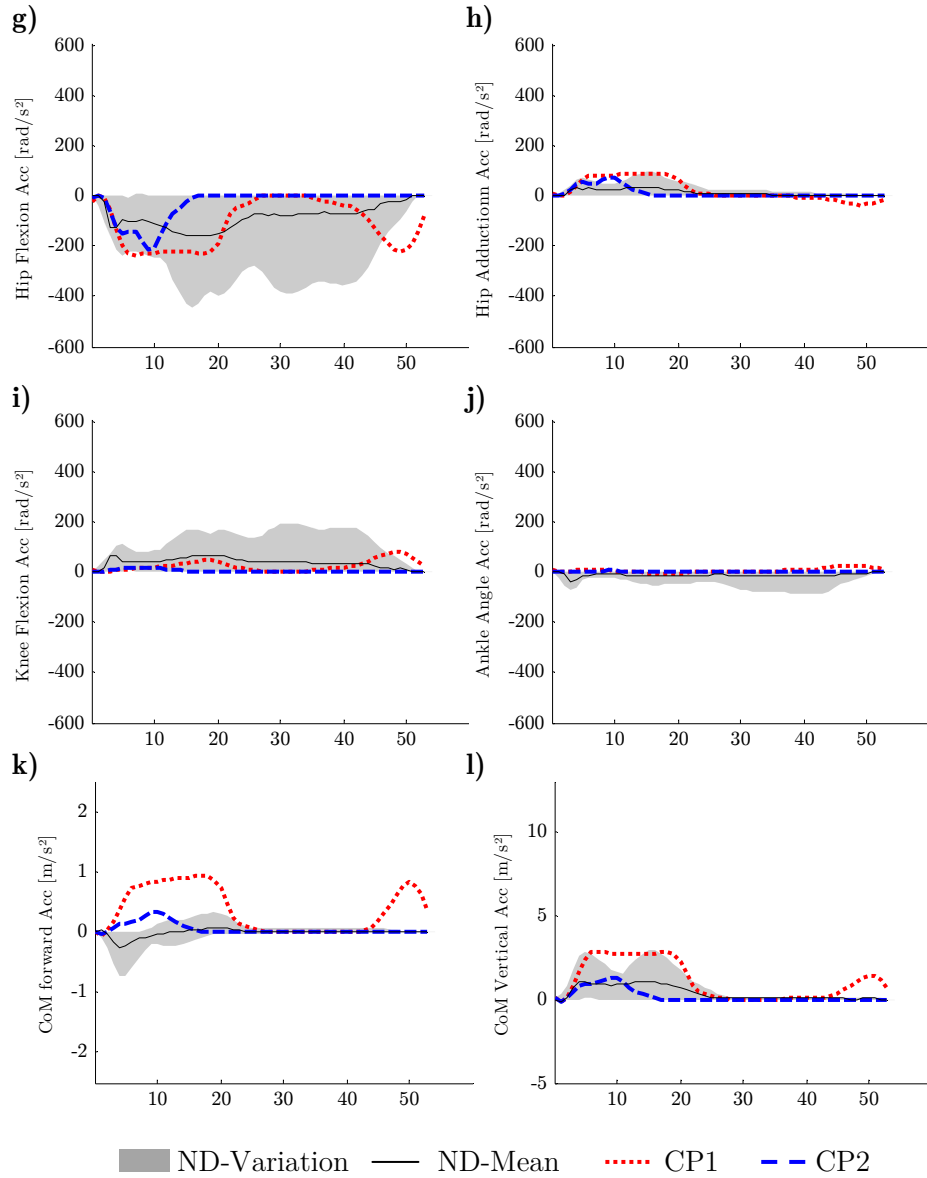
Figure B.2.1 Adductor longus: Accelerations in gait - Contribution to hip (g,h), knee (i) and ankle joint (h) angular acceleration as well as fore-aft (j) and vertical (k) acceleration of the centre of mass (CoM) in the CP-children (CP1,CP2) and the control group (ND) in stance phase.

B.2.2 Adductor Magnus in Gait
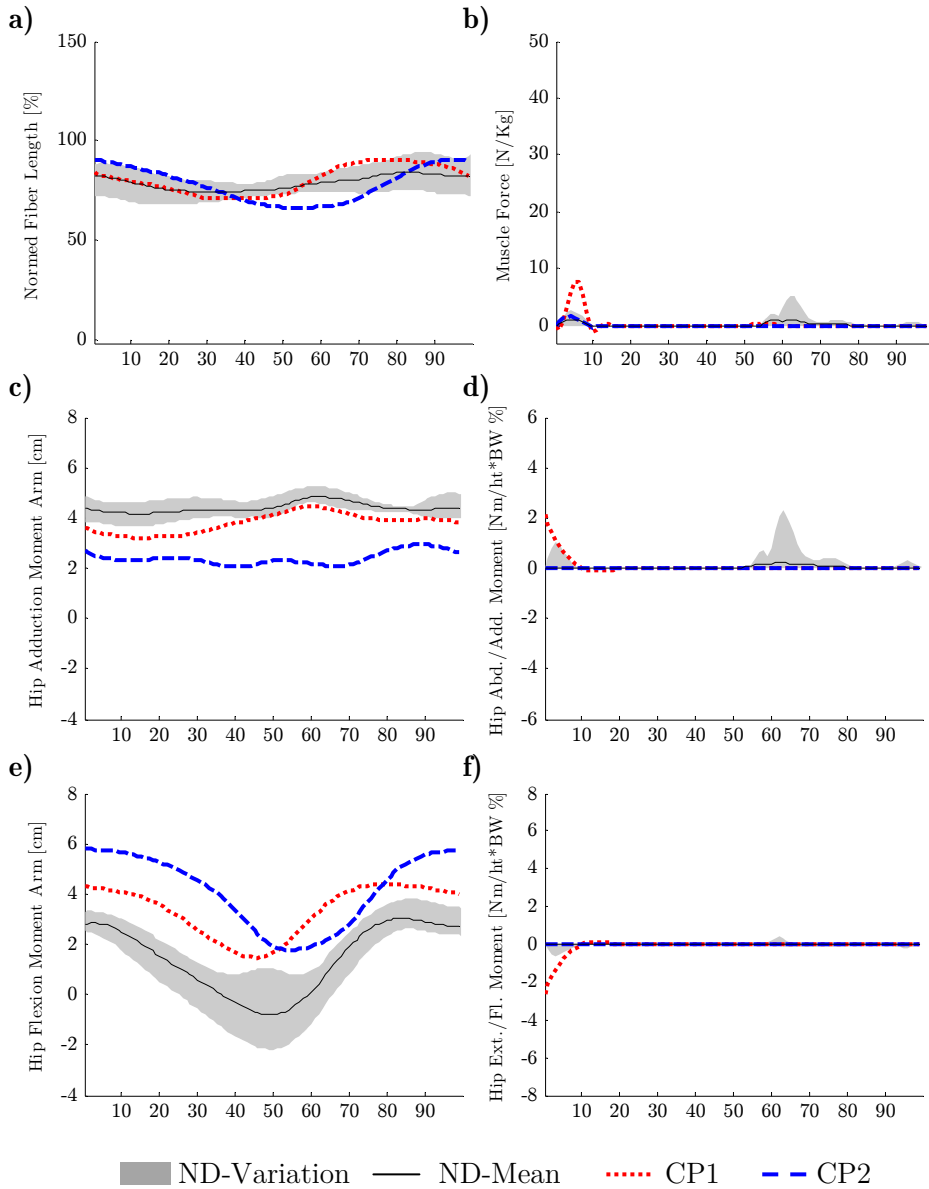
Figure B.2.1 Adductor magnus: Function in gait - Normalized muscle fibre length (a), muscle force per kg body weight (b) as well as moment arm and normalized joint moment for hip adduction (c,d) and hip flexion (e,f) of the CP-children (CP1,CP2) and the control group (ND) in a full gait cycle.

g)

h)

i)

j)

k)

ND-Variation —— ND-Mean ⋯⋯ CP1 – – CP2
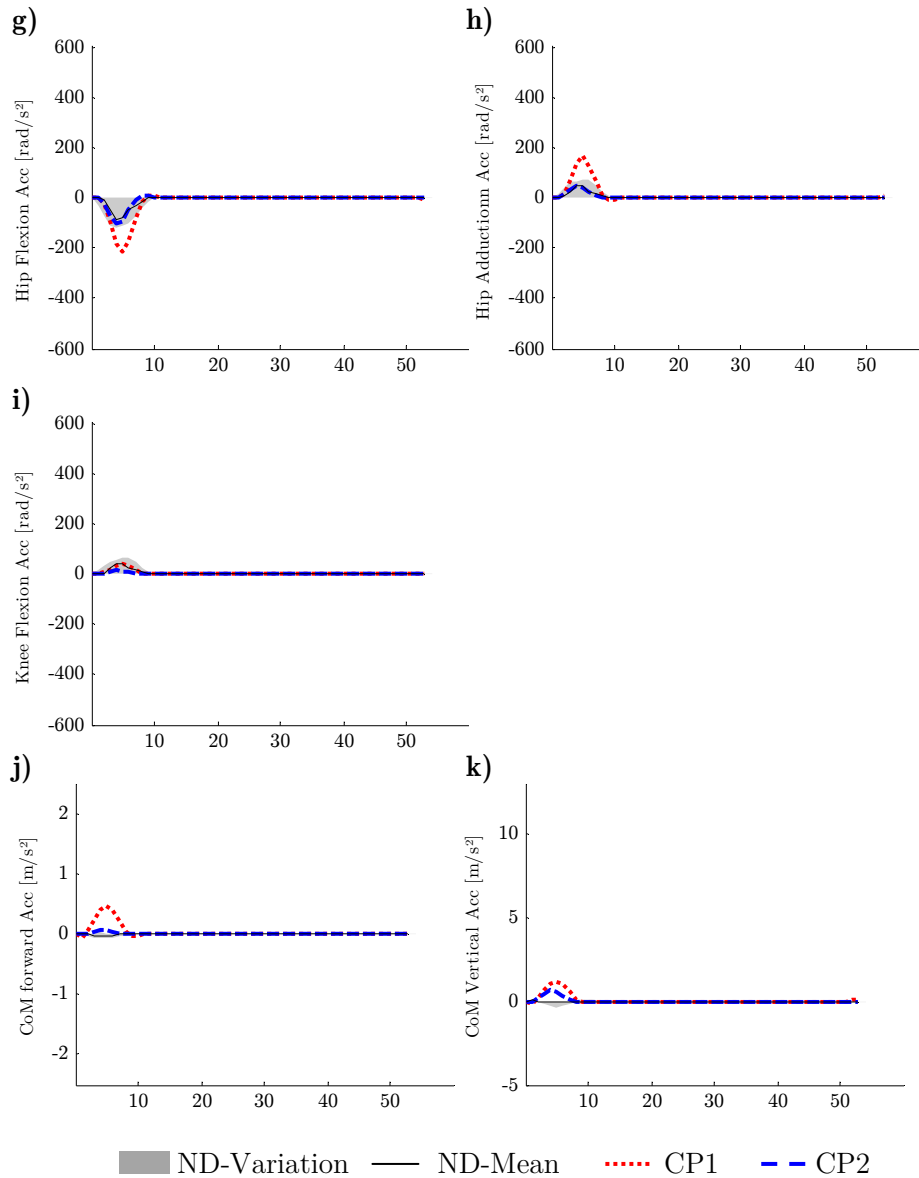
Figure B.2.2 Adductor longus: Accelerations in gait - Contribution to hip (g,h) and knee (i) angular acceleration as well as fore-aft (j) and vertical (k) acceleration of the centre of mass (CoM) in the CP-children (CP1,CP2) and the control group (ND) in stance phase.
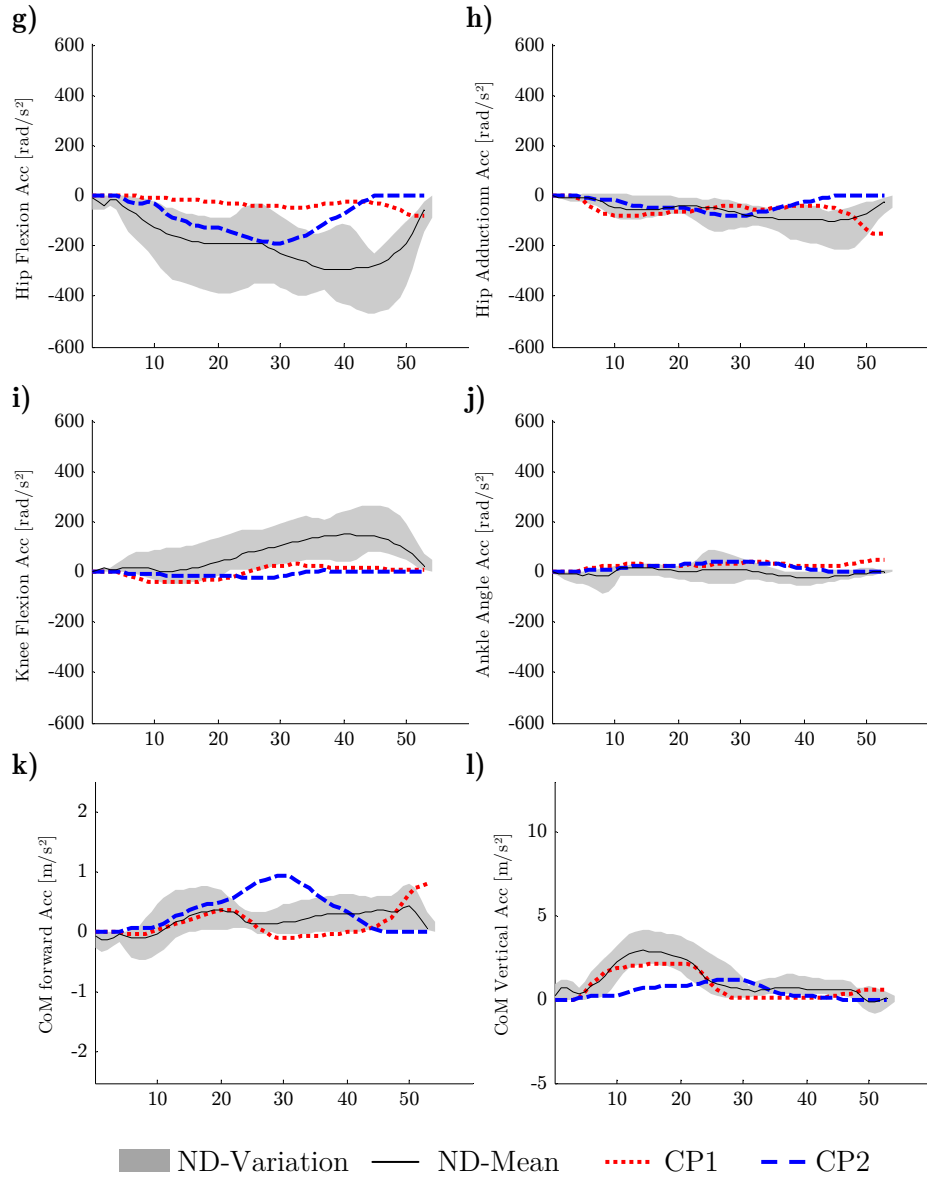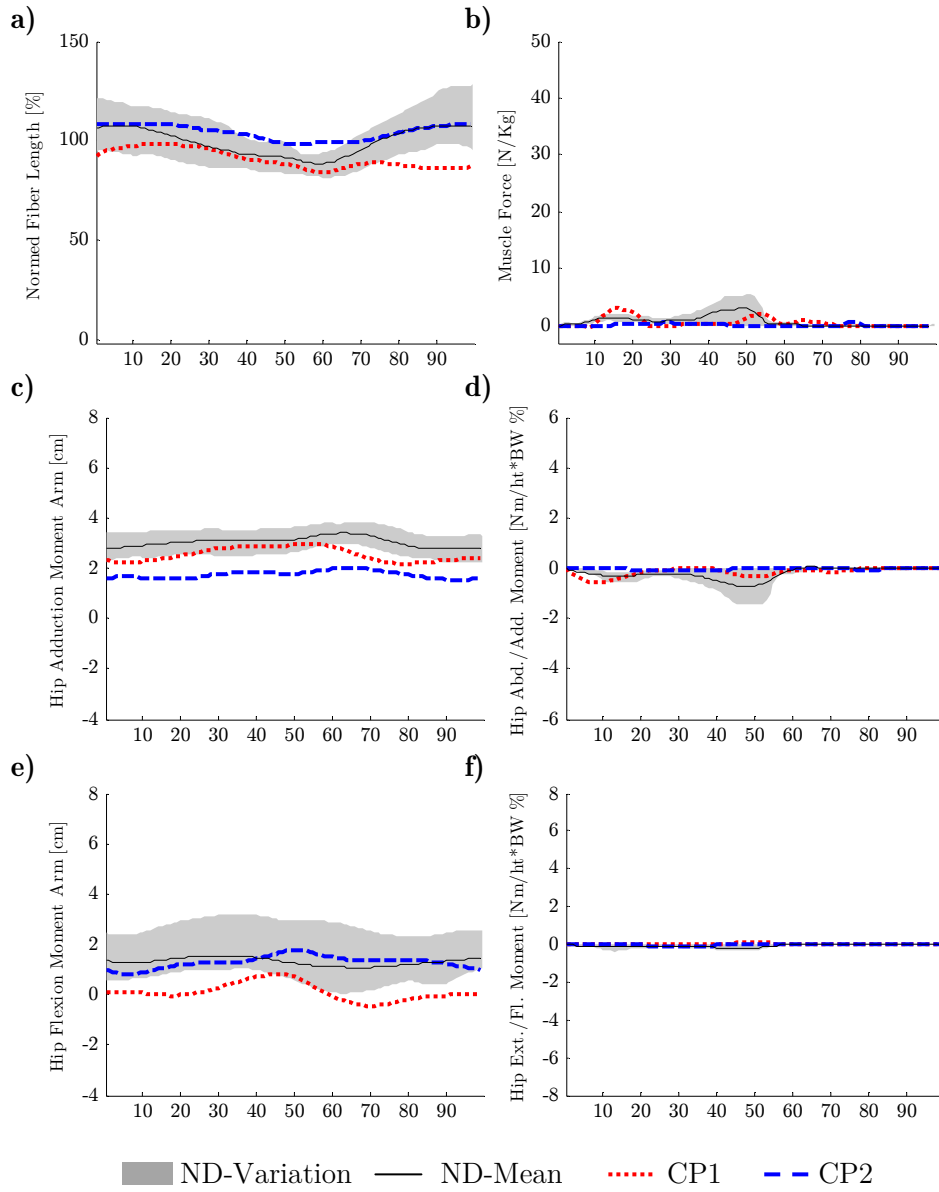
B.2.3 Biceps Femoris Shorthead in Gait
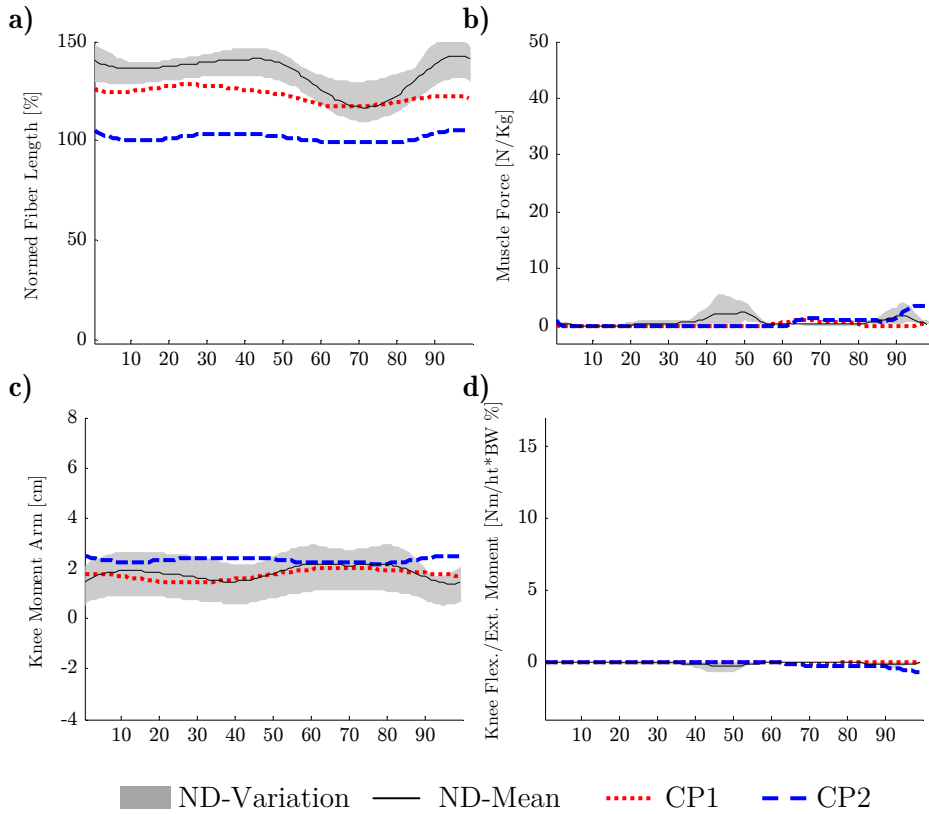
Figure B.2.1 Biceps Femoris Shorthead: Function in gait - Normalized muscle fibre length (a), muscle force per kg body weight (b) as well as moment arm and normalized joint moment for knee flexion (c,d) of the CP-children (CP1,CP2) and the control group (ND) in a full gait cycle.

e)

f)

g)

h)

ND-Variation ——— ND-Mean ······ CP1 − − CP2
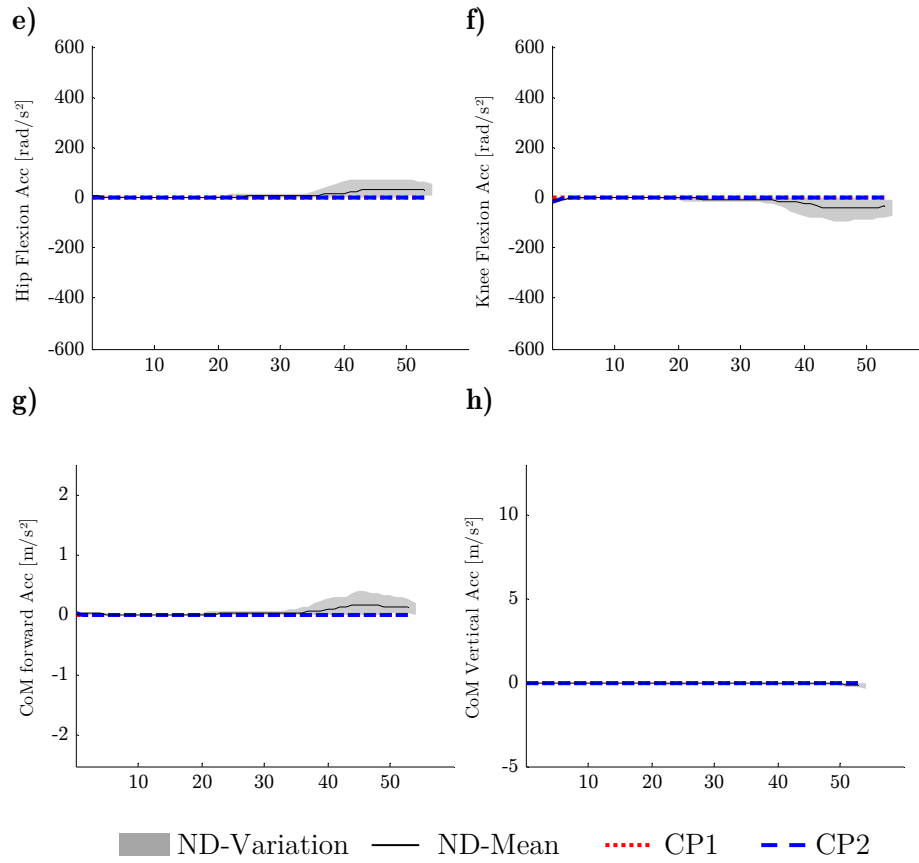
**Figure B.2.2 Bicepts Femoris Shorthead: Accelerations in gait** - Contribution to hip (e,f), knee (g) and ankle joint (h) angular acceleration as well as fore-aft (i) and vertical (j) acceleration of the centre of mass (CoM) in the CP-children (CP1,CP2) and the control group (ND) in stance phase.
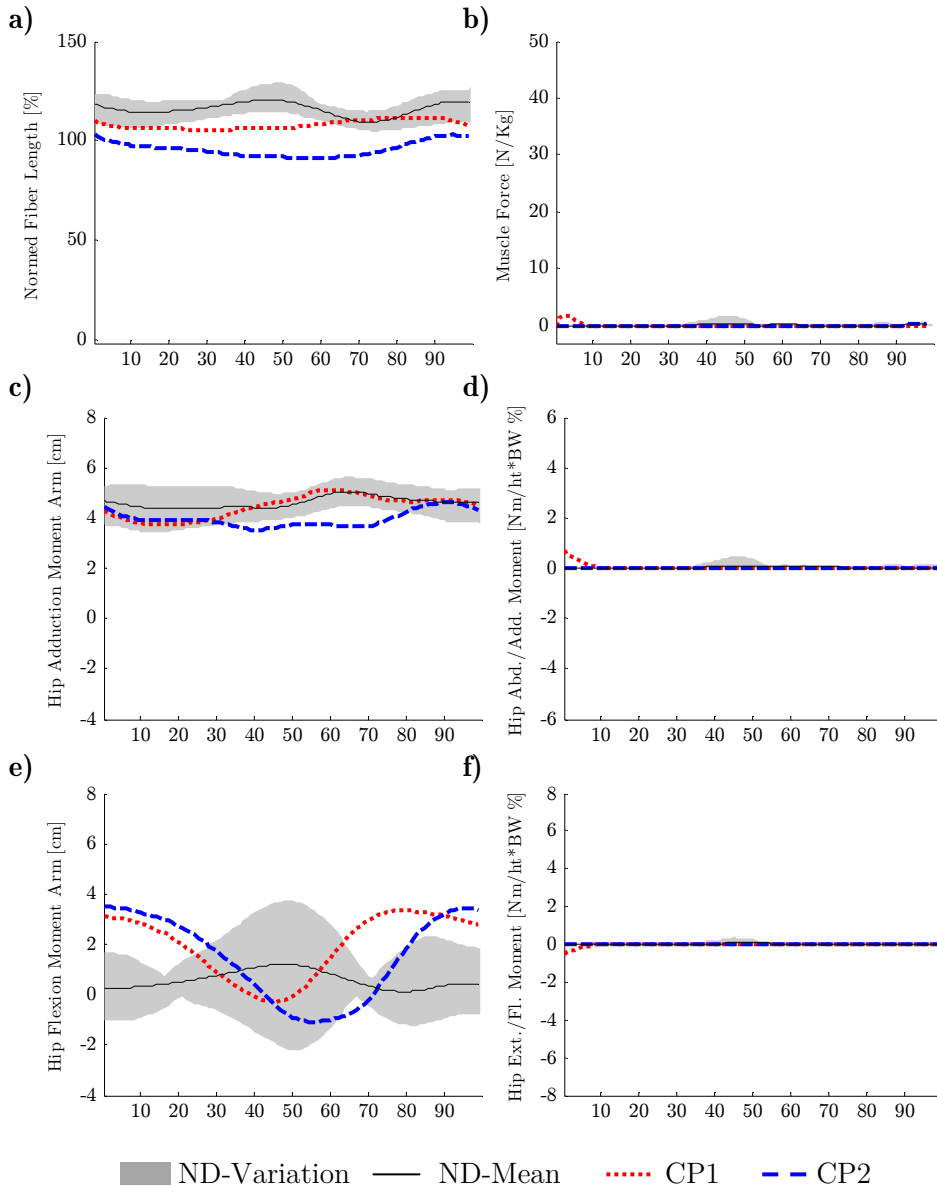
B.2.4 Extensor digitorum in Gait
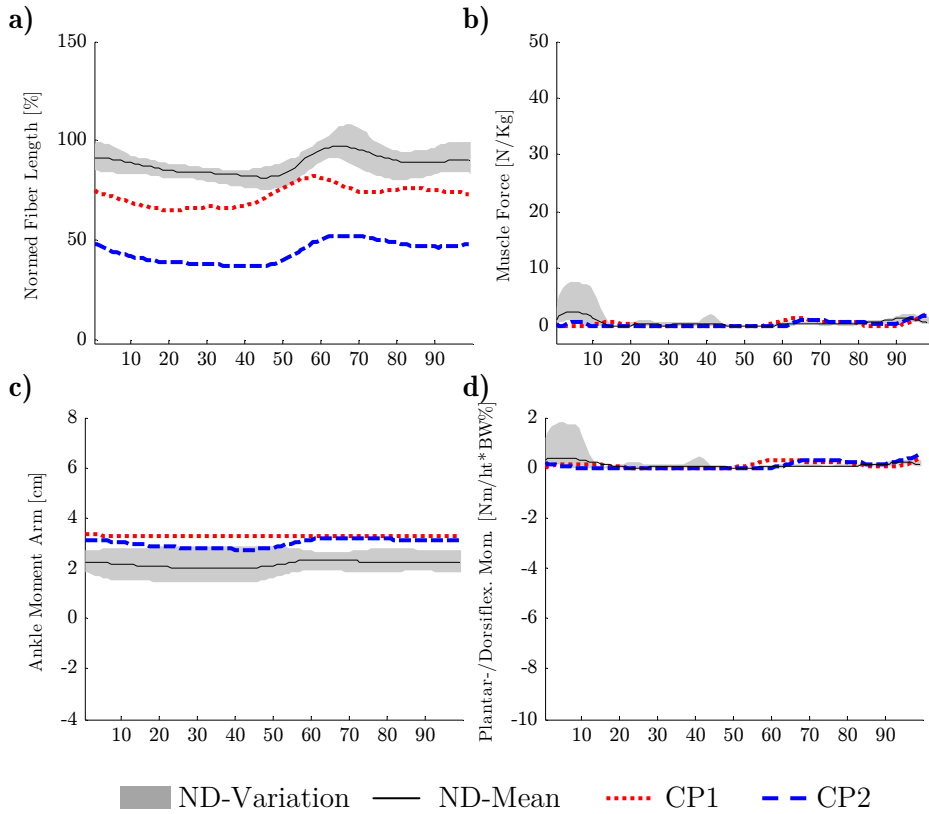
Figure B.2.3 Extensor digitorum: Function in gait - Normalized muscle fibre length (a), muscle force per kg body weight (b) as well as moment arm and normalized joint moment for ankle joint (c,d) of the CP-children (CP1,CP2) and the control group (ND) in a full gait cycle.
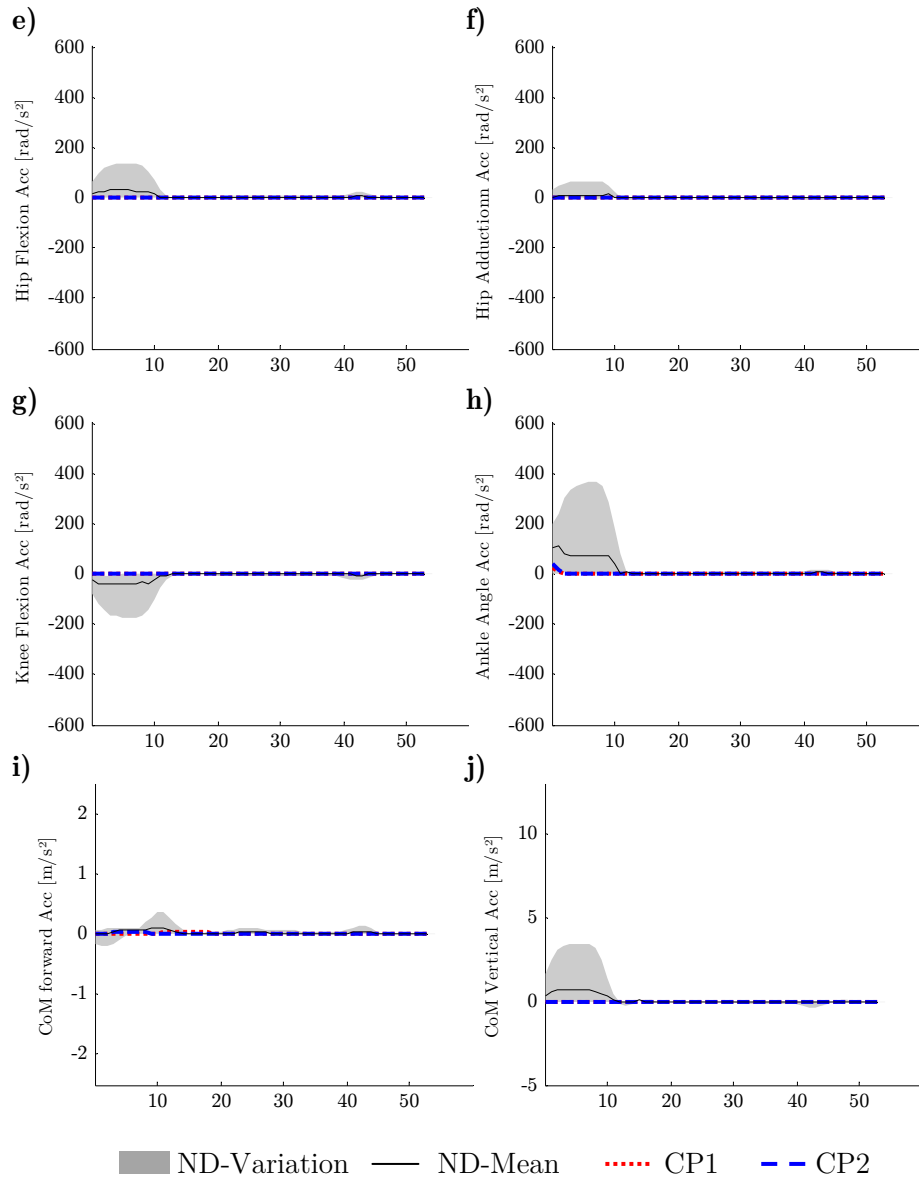
Figure B.2.4 Extensor digitorum: Accelerations in gait - Contribution to hip (e,f), knee (g) and ankle joint (h) angular acceleration as well as fore-aft (i) and vertical (j) acceleration of the centre of mass (CoM) in the CP-children (CP1,CP2) and the control group (ND) in stance phase.

B.2.5 Flexor digitorum longus in Gait
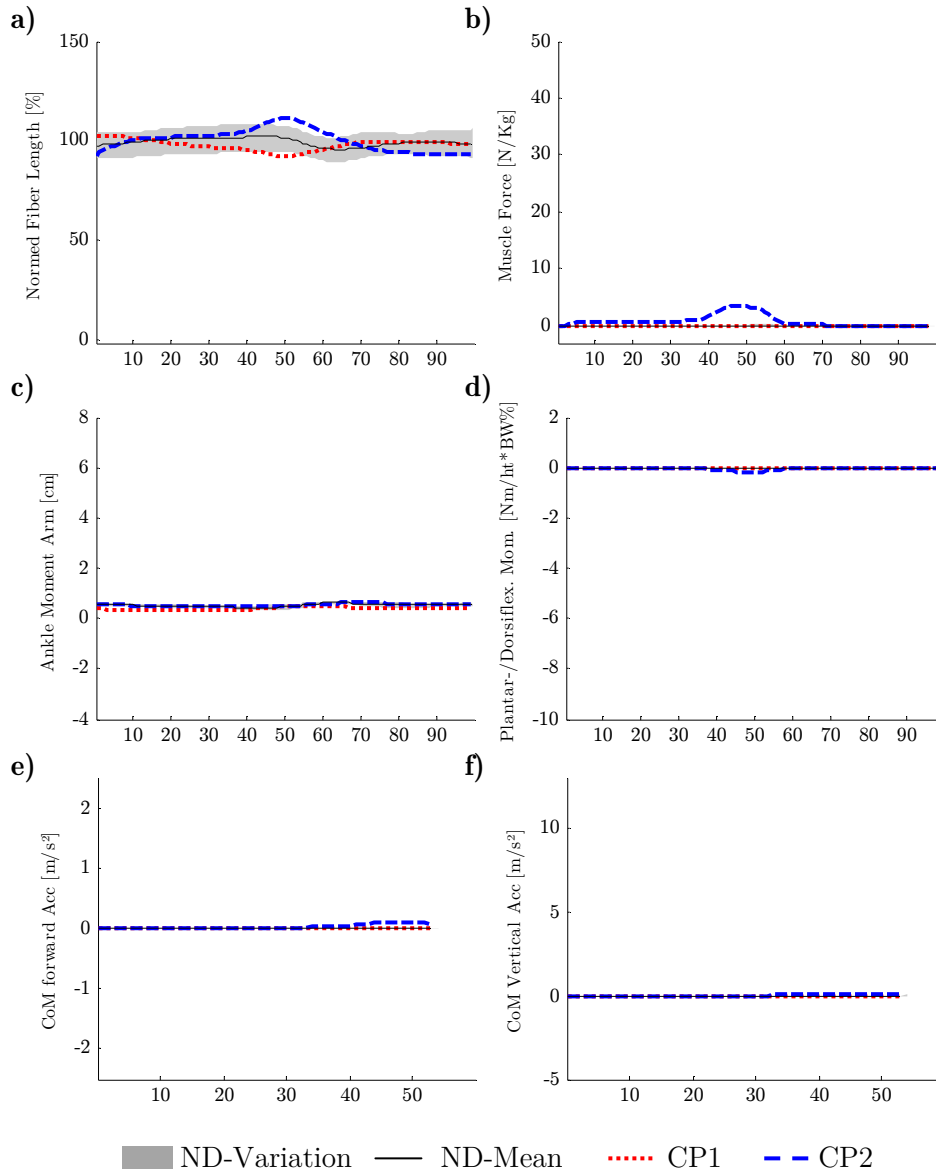
Figure B.2.5 Flexor digitorum longus in gait - Normalized muscle fibre length (a), muscle force per kg body weight (b), moment arm and normalized joint moment for ankle joint (c,d) in a full gait cycle as well as contribution to fore-aft (e) and vertical (f) acceleration of the centre of mass of the CP-children (CP1,CP2) and the control group (ND) in stance phase.
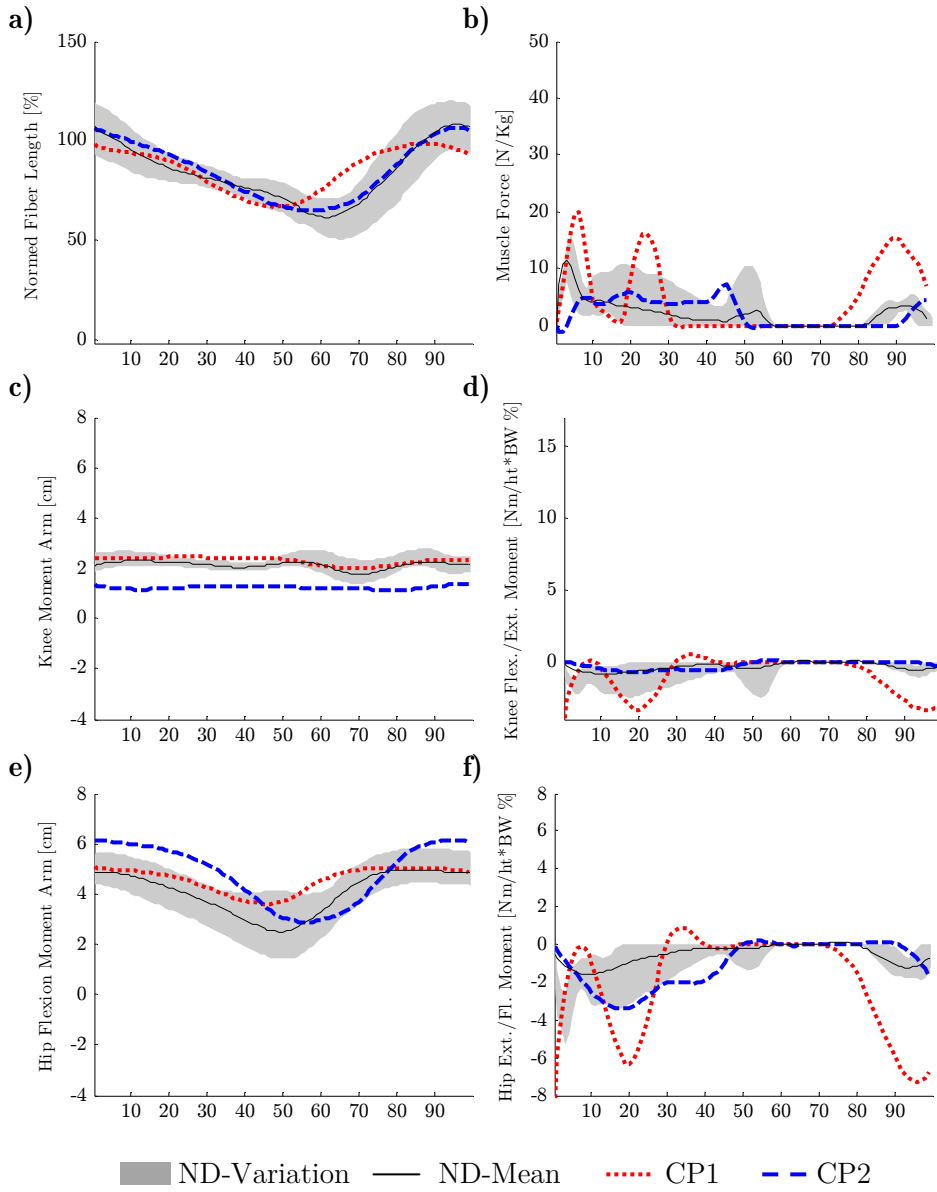
B.2.6 Flexor hallucis longus in Gait
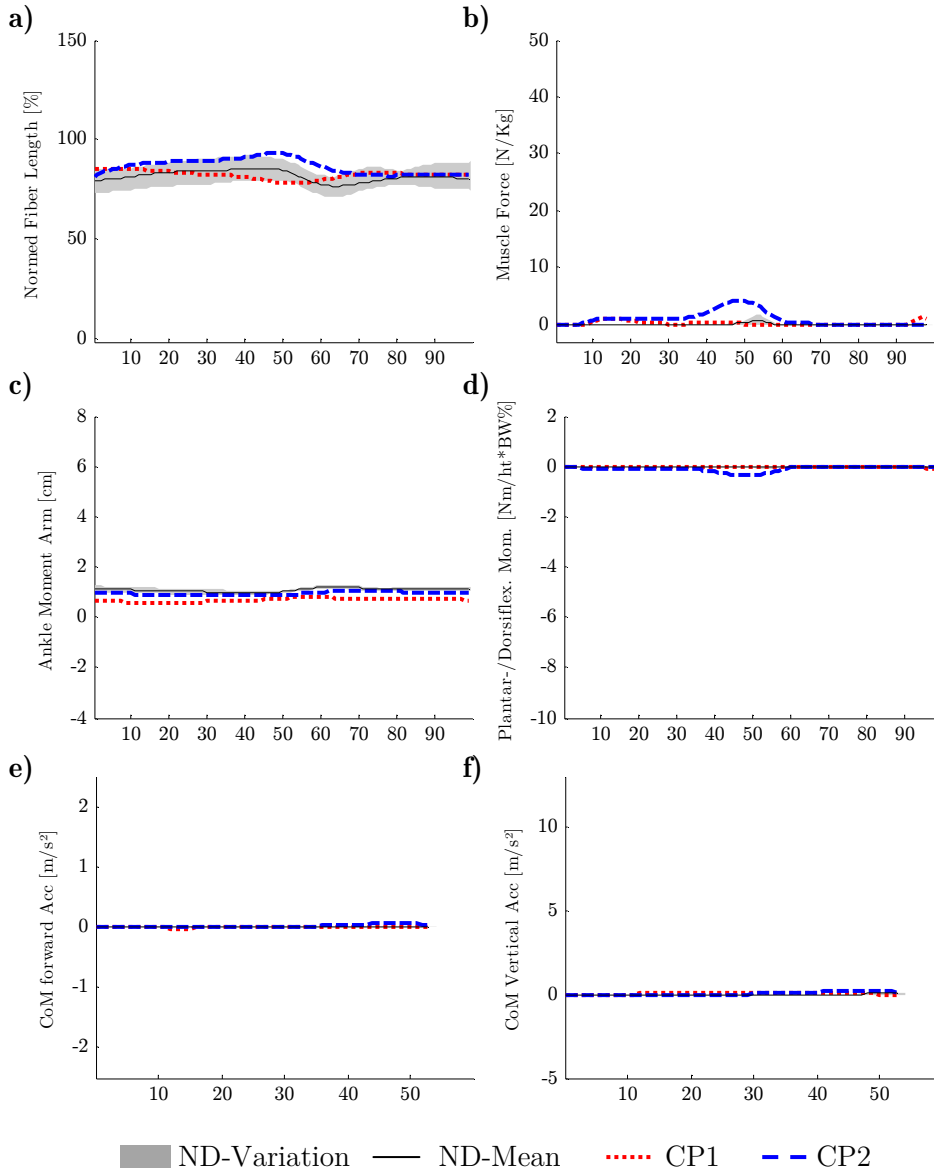
Figure B.2.6 Flexor hallucis longus in gait - Normalized muscle fibre length (a), muscle force per kg body weight (b), moment arm and normalized joint moment for ankle joint (c,d) in a full gait cycle as well as contribution to fore-aft (j) and vertical (k) acceleration of the centre of mass (CoM) of the CP-children (CP1,CP2) and the control group (ND) stance phase.

B.2.7 Gastrocnemius in Gait
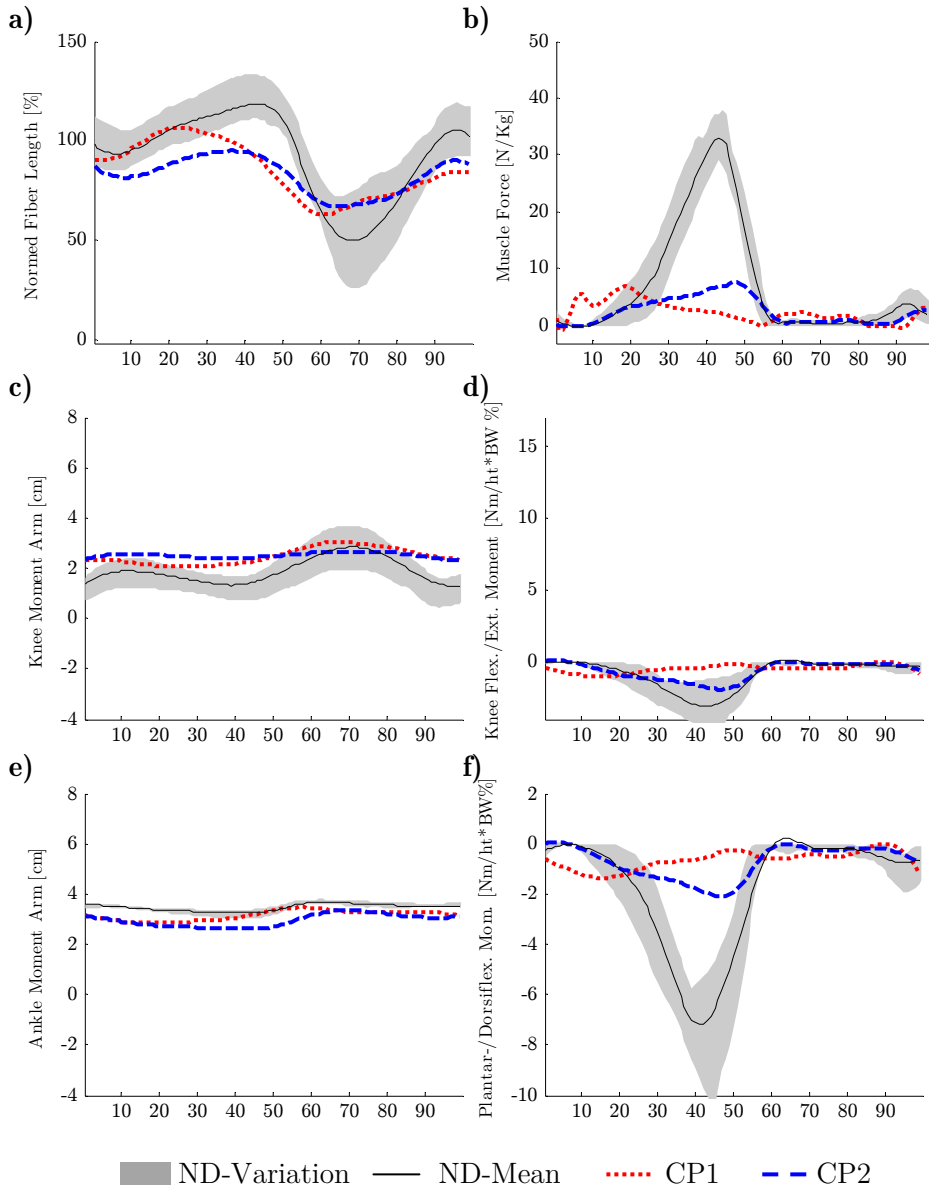
Figure B.2.7 Gastrocnemius: Function in gait - Normalized muscle fibre length (a), muscle force per kg body weight (b) as well as moment arm and normalized joint moment for knee (c,d) and ankle joint (e,f) of the CP-children (CP1,CP2) and the control group (ND) in a full gait cycle.
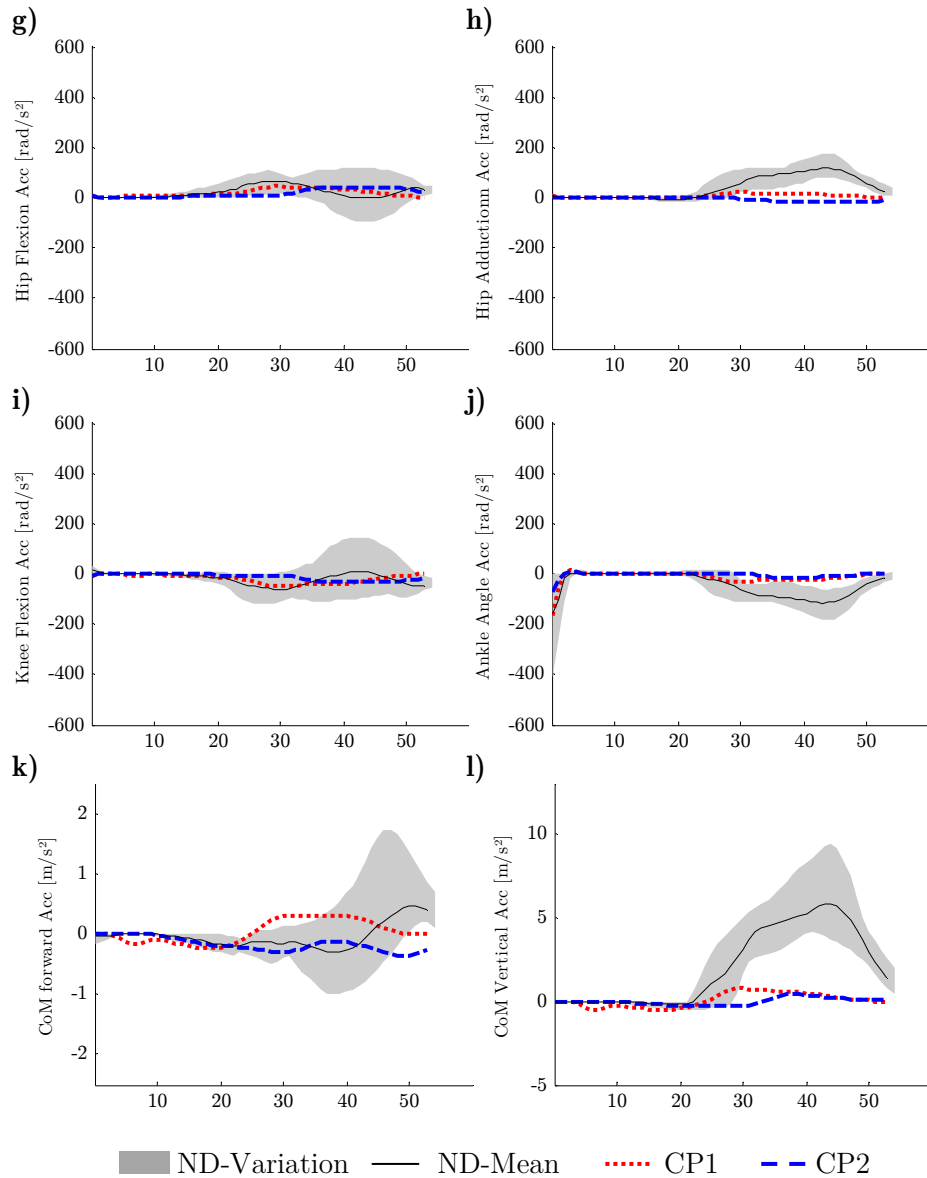
Figure B.2.8 Gastrocnemius: Accelerations in gait - Contribution to hip (g,h), knee (i) and ankle joint (j) angular acceleration as well as fore-aft (k) and vertical (l) acceleration of the centre of mass (CoM) in the CP-children (CP1,CP2) and the control group (ND) in stance phase.

B.2.8 Gluteus Maximus in Gait

Figure B.2.1 Gluteus maximus: Function in gait - Normalized muscle fibre length (a), muscle force per kg body weight (b) as well as moment arm and normalized joint moment for hip adduction (c,d) and hip flexion (e,f) of the CP-children (CP1,CP2) and the control group (ND) in a full gait cycle.
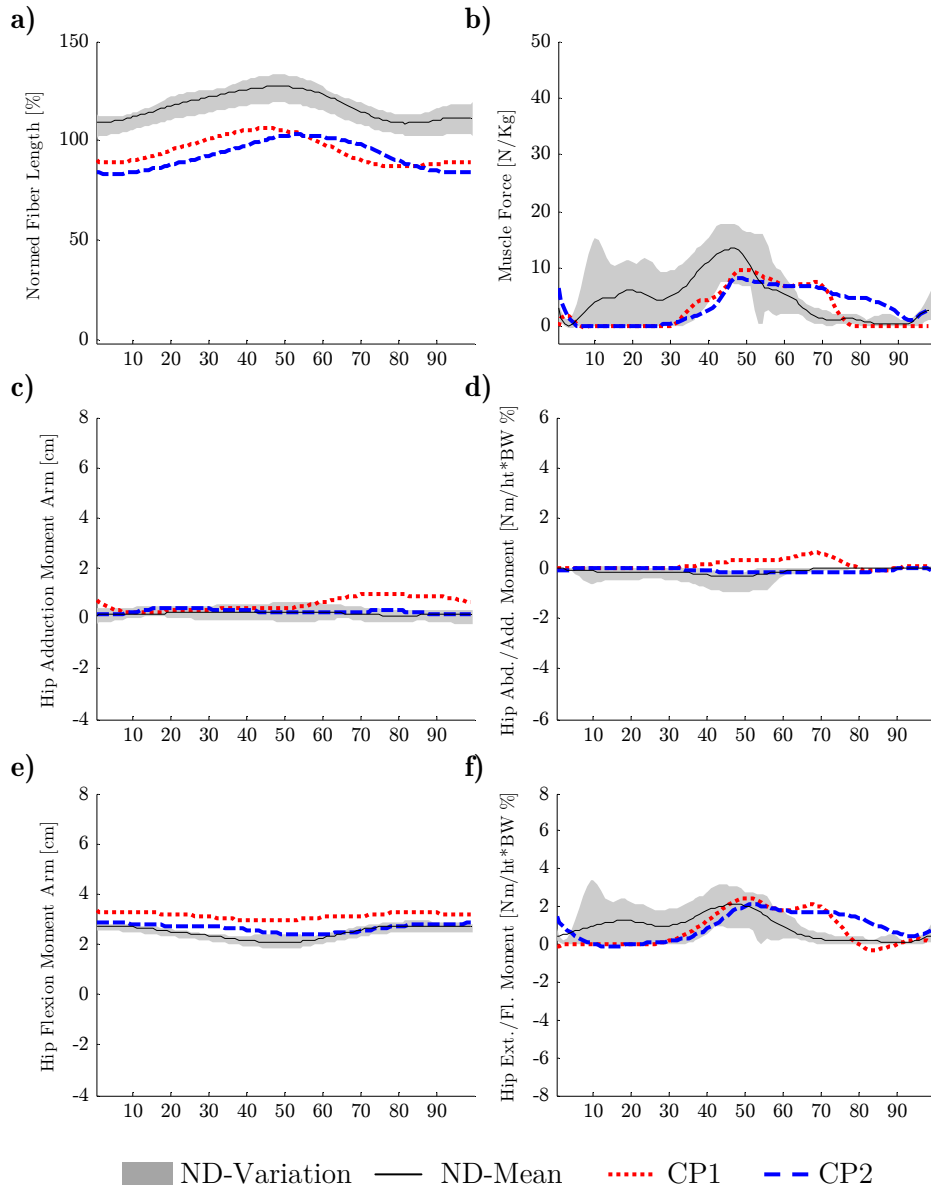
Figure B.2.2 Gluteus maximus: Accelerations in gait - Contribution to hip (g,h), knee (i) and ankle joint (j) angular acceleration as well as fore-aft (k) and vertical (l) acceleration of the centre of mass (CoM) in the CP-children (CP1,CP2) and the control group (ND) in stance phase.
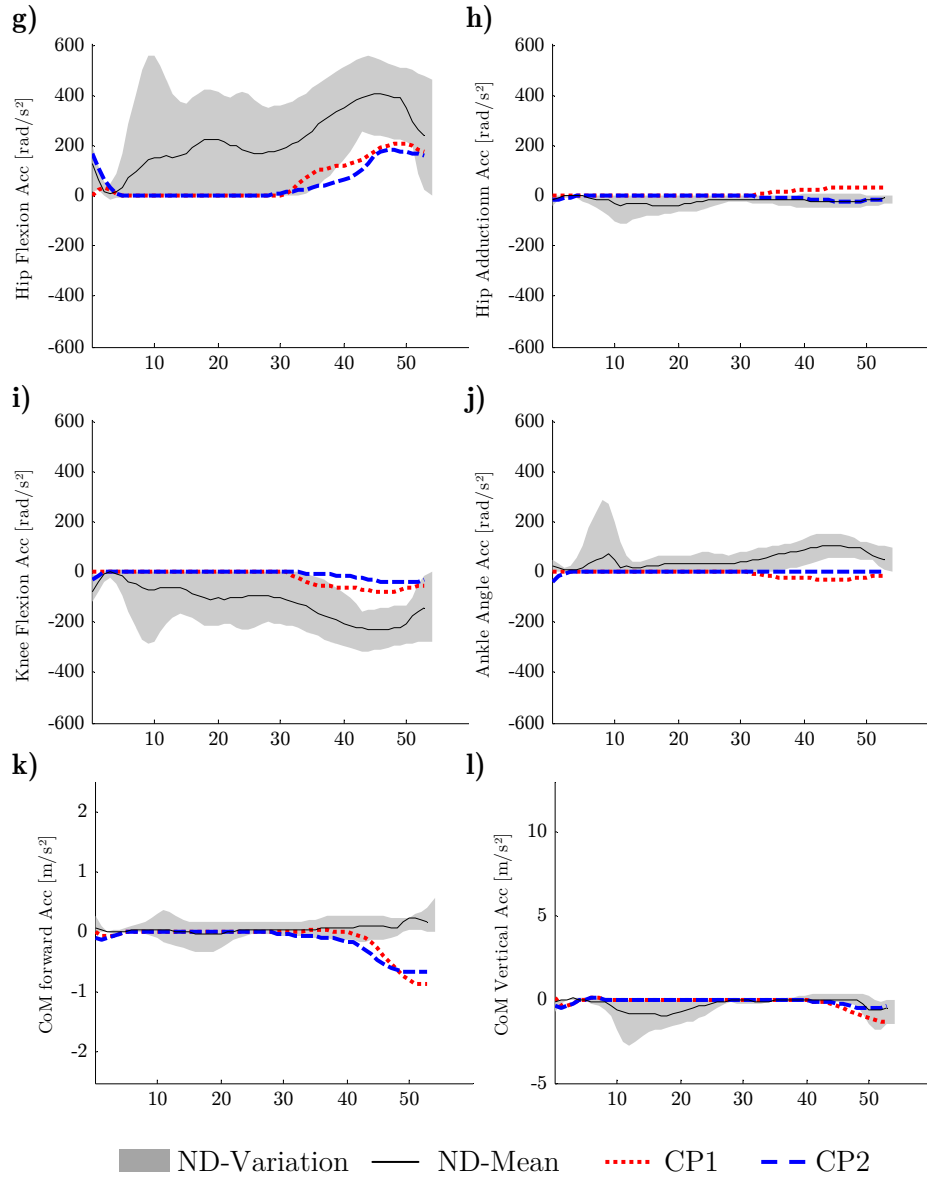
B.2.9 Gluteus Medius in Gait
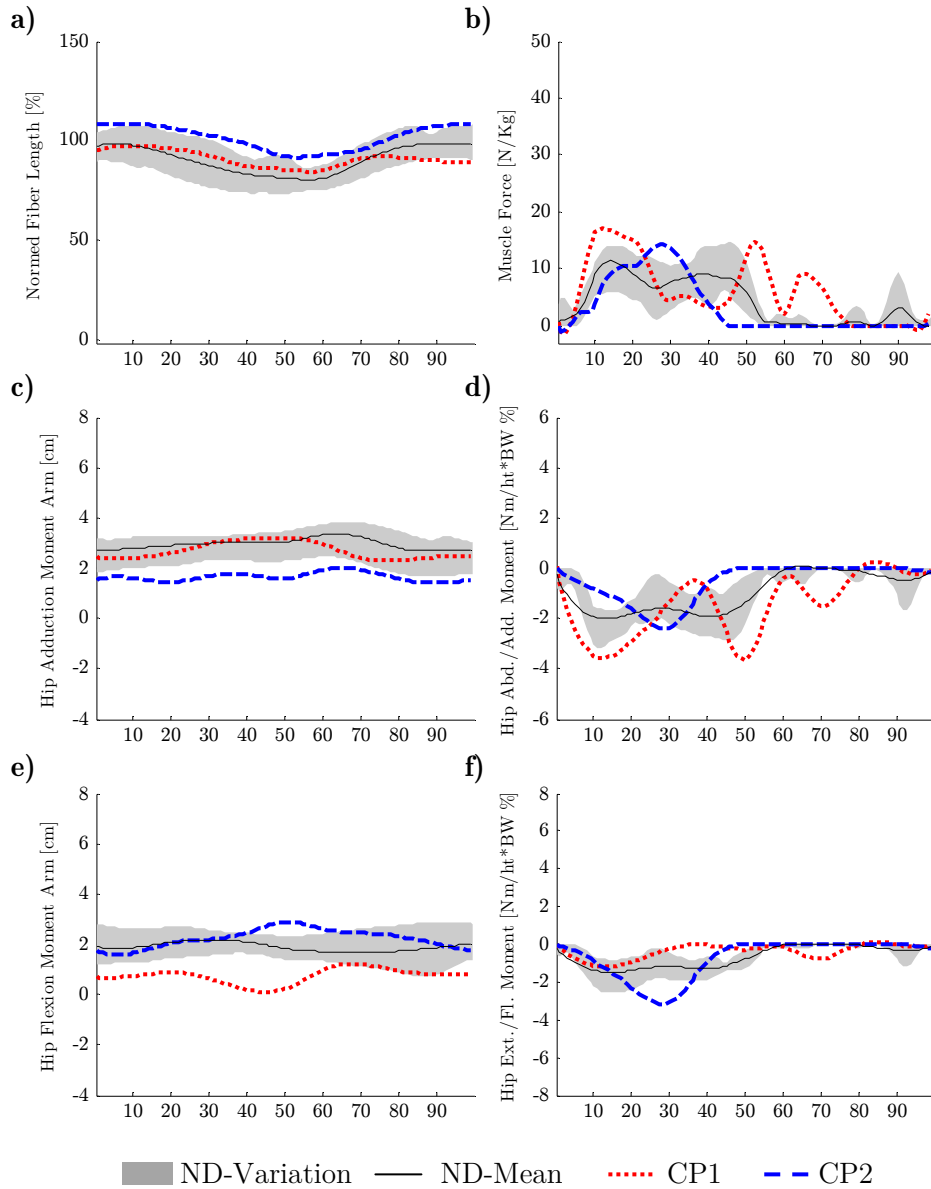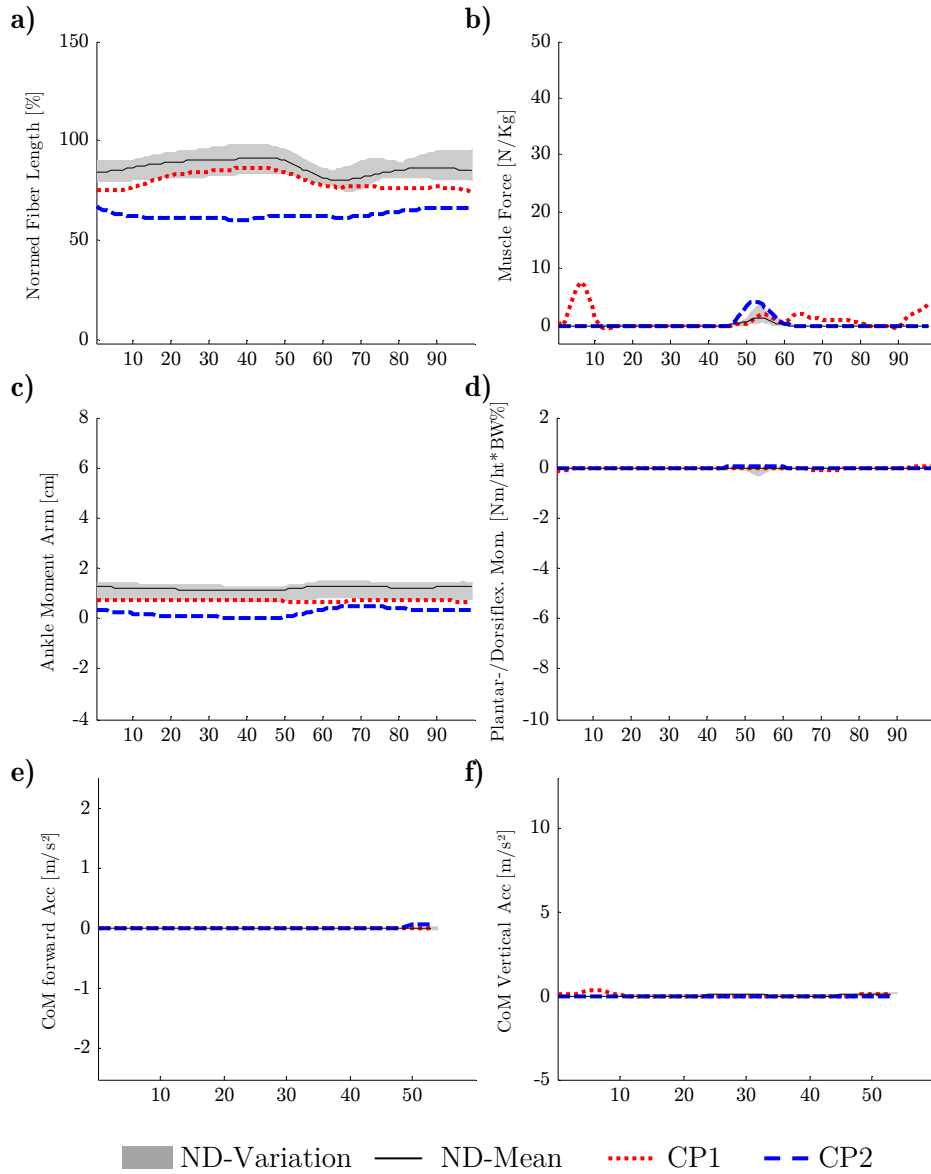

Figure B.2.3 Gluteus medius: Function in gait - Normalized muscle fibre length (a), muscle force per kg body weight (b) as well as moment arm and normalized joint moment for hip adduction (c,d) and hip flexion (e,f) of the CP-children (CP1,CP2) and the control group (ND) in a full gait cycle.

Figure B.2.4 Gluteus medius: Accelerations in gait - Contribution to hip (g,h), knee (i) and ankle joint (j) angular acceleration as well as fore-aft (k) and vertical (l) acceleration of the centre of mass (CoM) in the CP-children (CP1,CP2) and the control group (ND) in a stance phase.

B.2.10 Gluteus Minimus in Gait

Figure B.2.5 Gluteus minimus: Function in gait - Normalized muscle fibre length (a), muscle force per kg body weight (b) as well as moment arm and normalized joint moment for hip adduction (c,d) and hip flexion (e,f) of the CP-children (CP1,CP2) and the control group (ND) in a full gait cycle.

g)

h)

i)

j)

k)

ND-Variation   ND-Mean   CP1   CP2
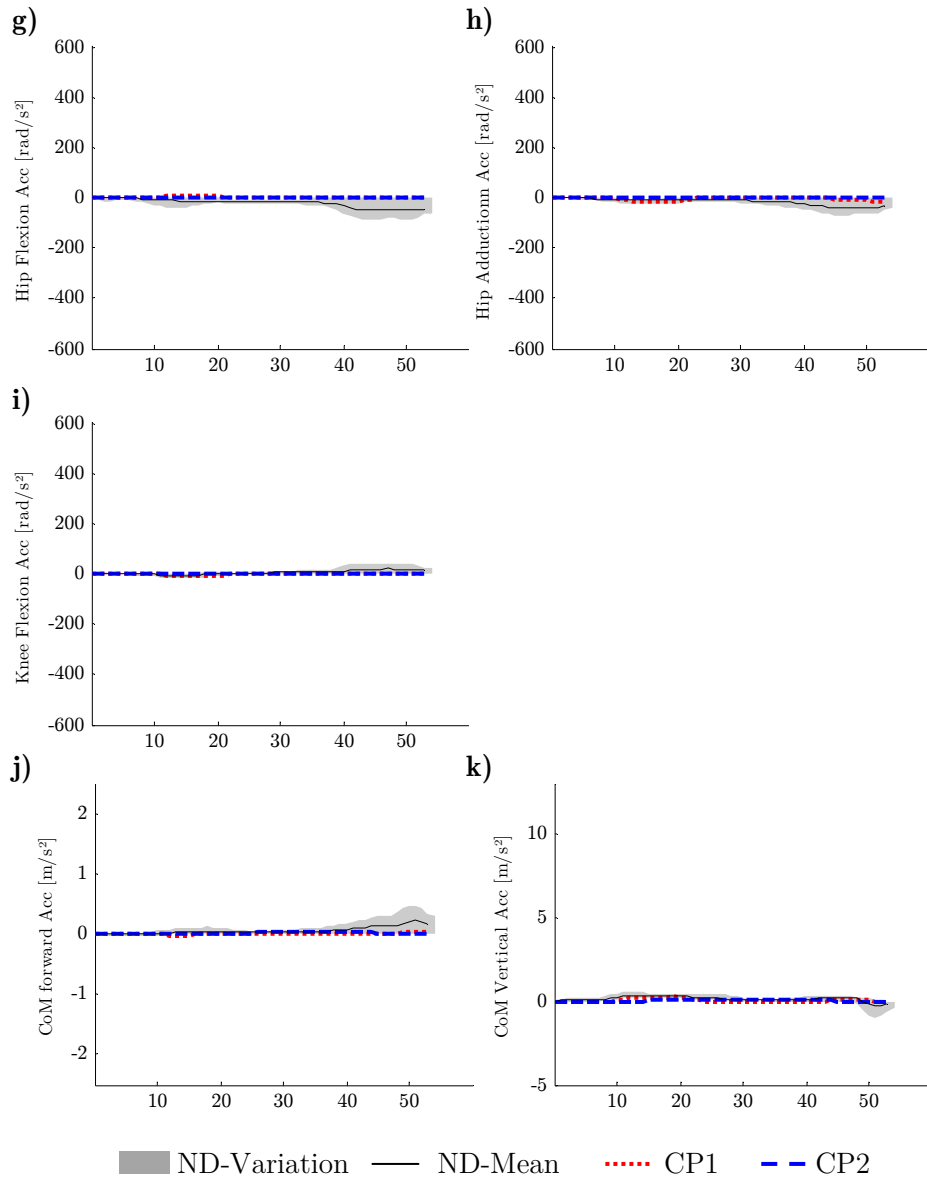
Figure B.2.6 Gluteus minimus: Accelerations in gait - Contribution to hip (g,h) and knee (i) angular acceleration as well as fore-aft (j) and vertical (k) acceleration of the centre of mass (CoM) in the CP-children (CP1,CP2) and the control group (ND) in stance phase.
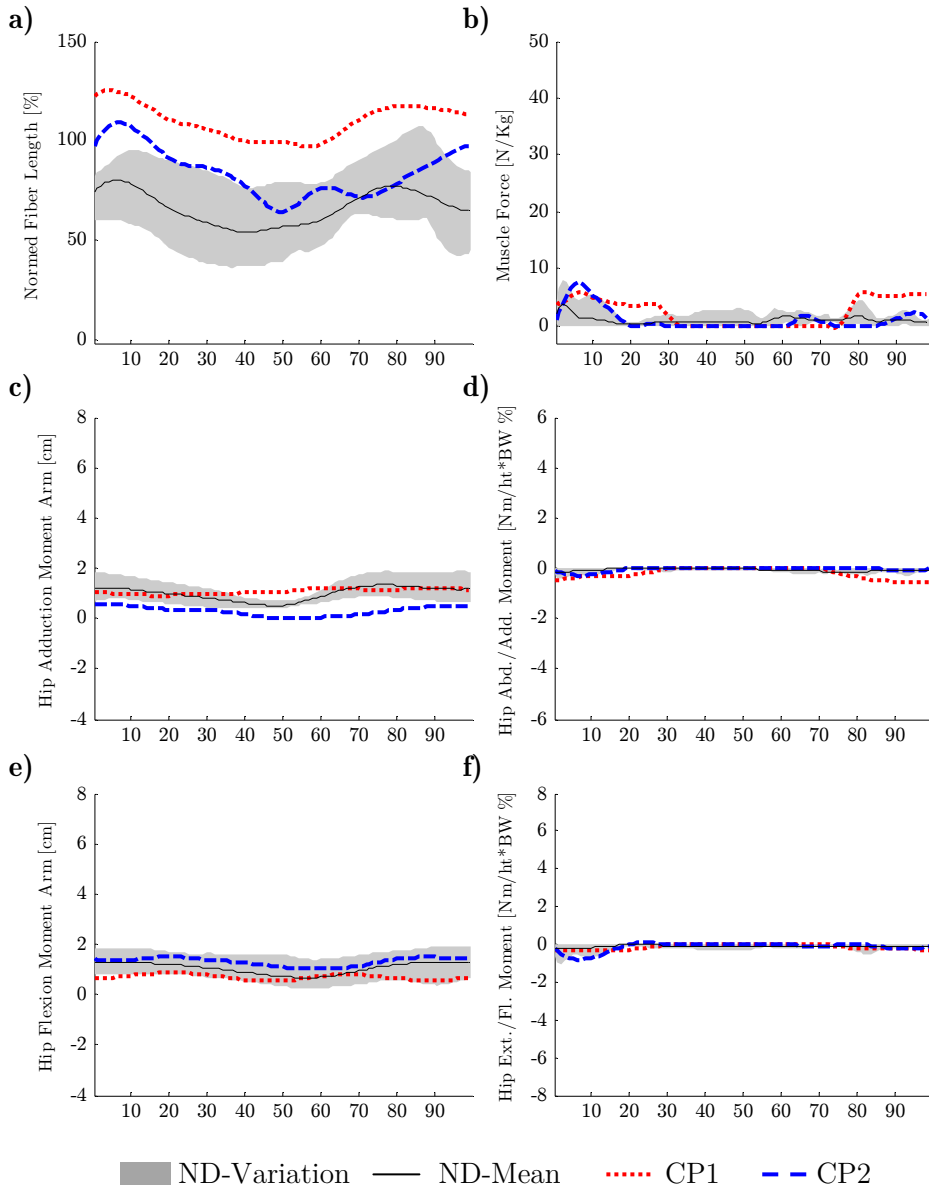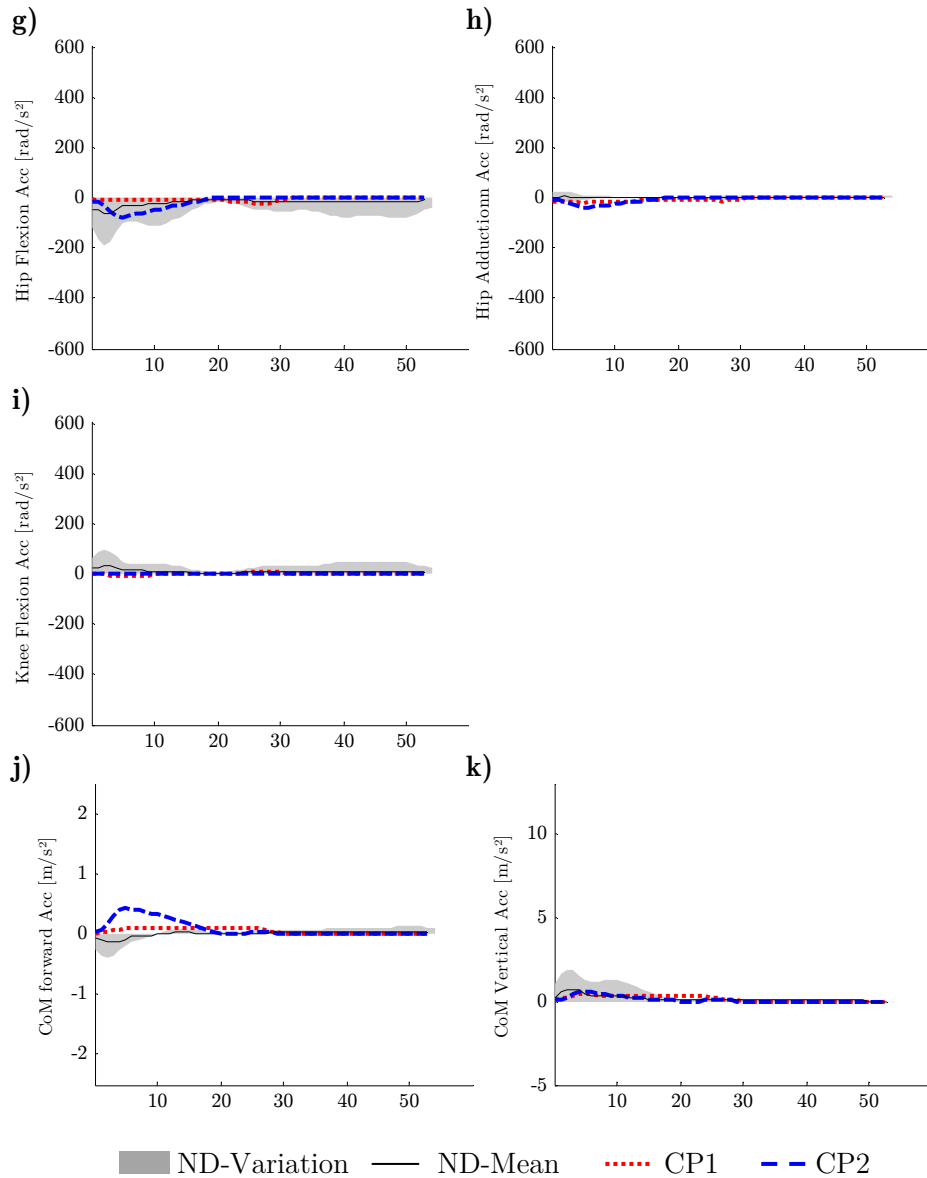
B.2.11   Gracilis in Gait

Figure B.2.7 Gracilis: Function in gait - Normalized muscle fibre length (a), muscle force per kg body weight (b) as well as moment arm and normalized joint moment for hip adduction (c,d) and hip flexion (e,f) of the CP-children (CP1,CP2) and the control group (ND) in a full gait cycle.
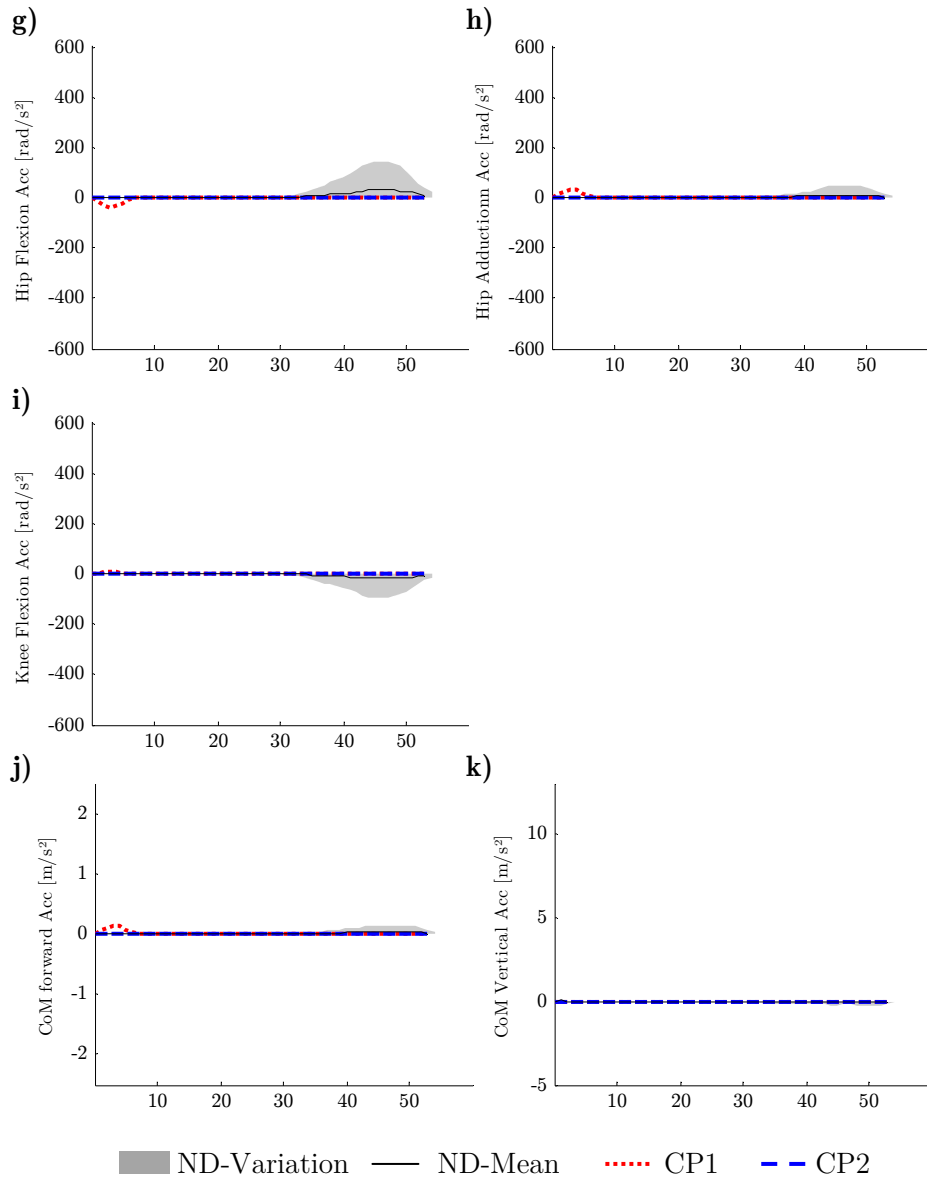
Figure B.2.8 Gracilis: Accelerations in gait - Contribution to hip (g,h) and knee (i) angular acceleration as well as fore-aft (j) and vertical (k) acceleration of the centre of mass (CoM) in the CP-children (CP1,CP2) and the control group (ND) in stance phase.
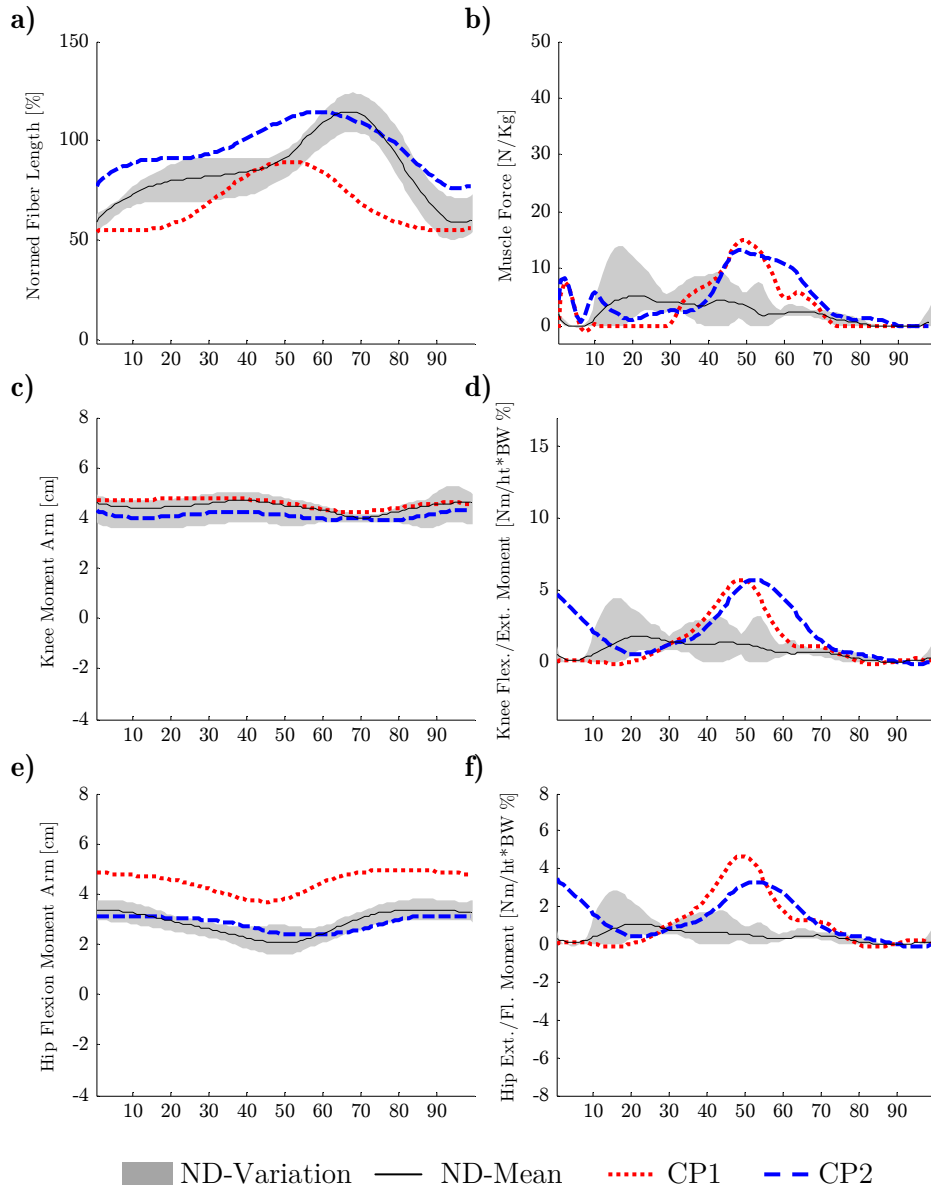
B.2.12   Hamstrings in Gait

Figure B.2.9 Hamstrings: Function in gait - Normalized muscle fibre length (a), muscle force per kg body weight (b) as well as moment arm and normalized joint moment for knee flexion/extension (c,d) and hip flexion/extension (e,f) of the CP-children (CP1,CP2) and the control group (ND) in a full gait cycle.
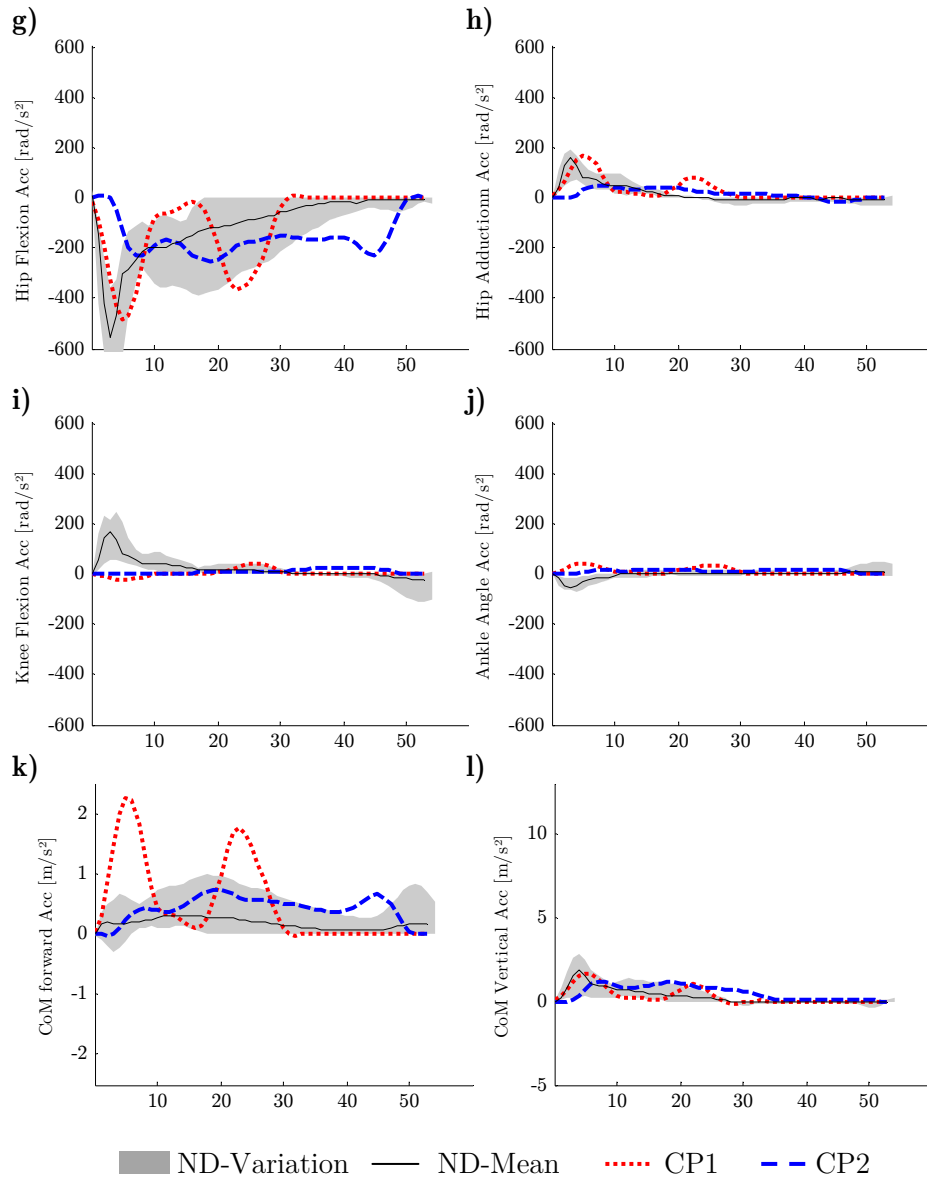
Figure B.2.10 Hamstrings: Accelerations in gait - Contribution to hip (g,h), knee (i) and ankle joint (j) angular acceleration as well as fore-aft (k) and vertical (l) acceleration of the centre of mass (CoM) in the CP-children (CP1,CP2) and the control group (ND) in stance phase.

B.2.13 Iliopsoas in Gait

Figure B.2.11 Iliopsoas: Function in gait - Normalized muscle fibre length (a), muscle force per kg body weight (b) as well as moment arm and normalized joint moment for hip adduction (c,d) and hip flexion (e,f) of the CP-children (CP1,CP2) and the control group (ND) in a full gait cycle.
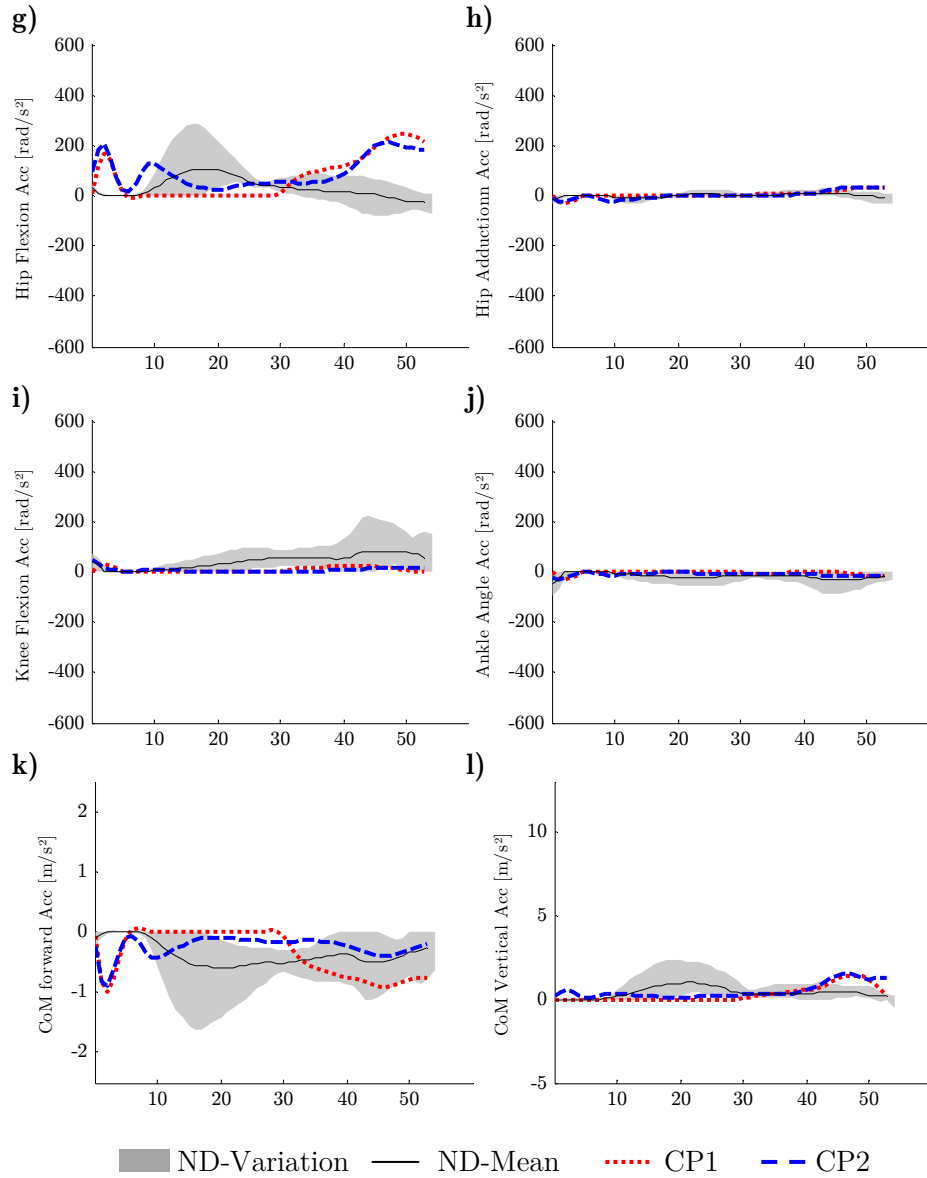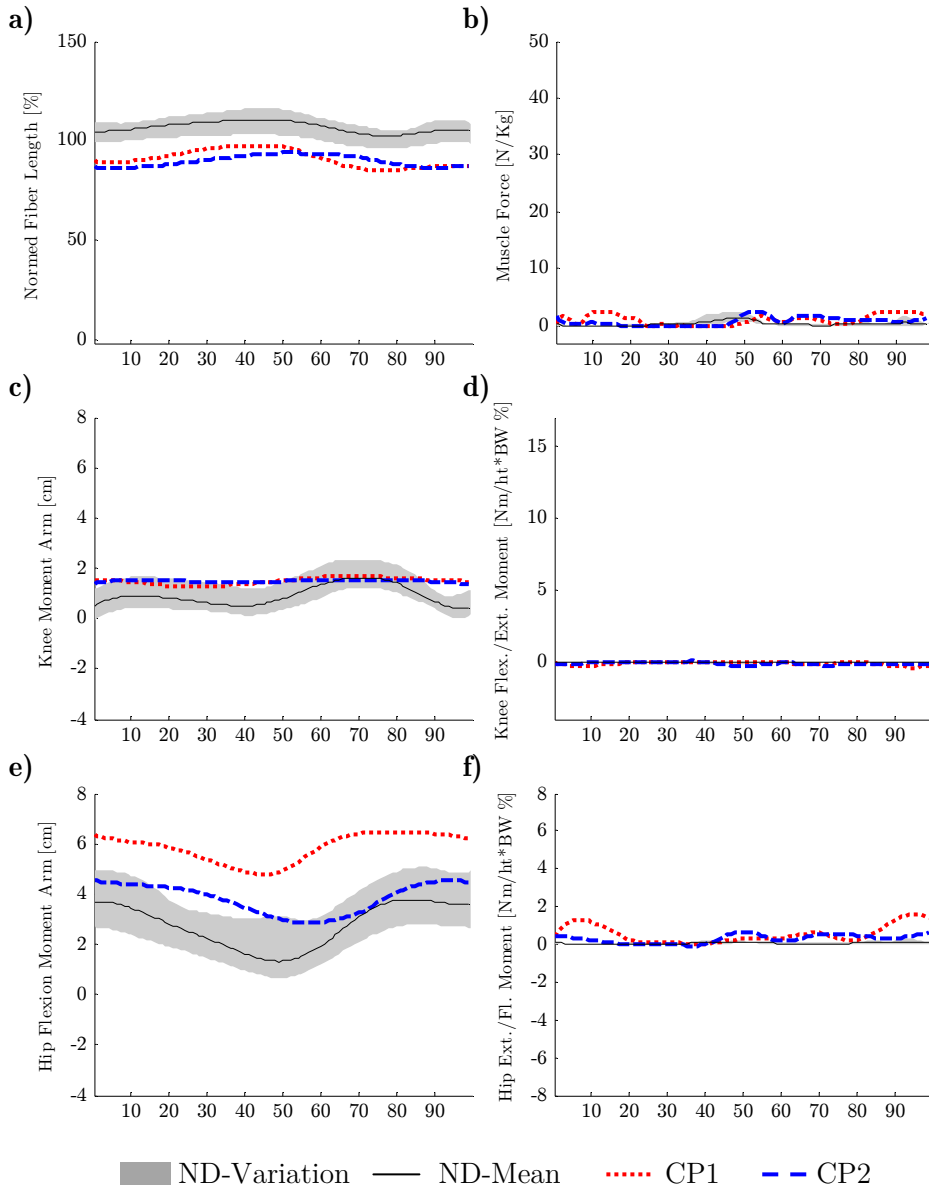
Figure B.2.12 Iliopsoas: Accelerations in gait - Contribution to hip (g,h), knee (i) and ankle joint (j) angular acceleration as well as fore-aft (k) and vertical (l) acceleration of the centre of mass (CoM) in the CP-children (CP1,CP2) and the control group (ND) in stance phase.

B.2.14   Peroneus in Gait

Figure B.2.13 Peroneus in gait - Normalized muscle fibre length (a), muscle force per kg body weight (b), moment arm and normalized joint moment for ankle joint (c,d) in a full gait cycle as well as contribution to fore-aft (e) and vertical (f) acceleration of the centre of mass of the CP-children (CP1,CP2) and the control group (ND) in stance phase.

B.2.15   Pectinius in Gait

a)

b)

c)

d)

e)

f)

ND-Variation ——— ND-Mean ········· CP1 – – CP2
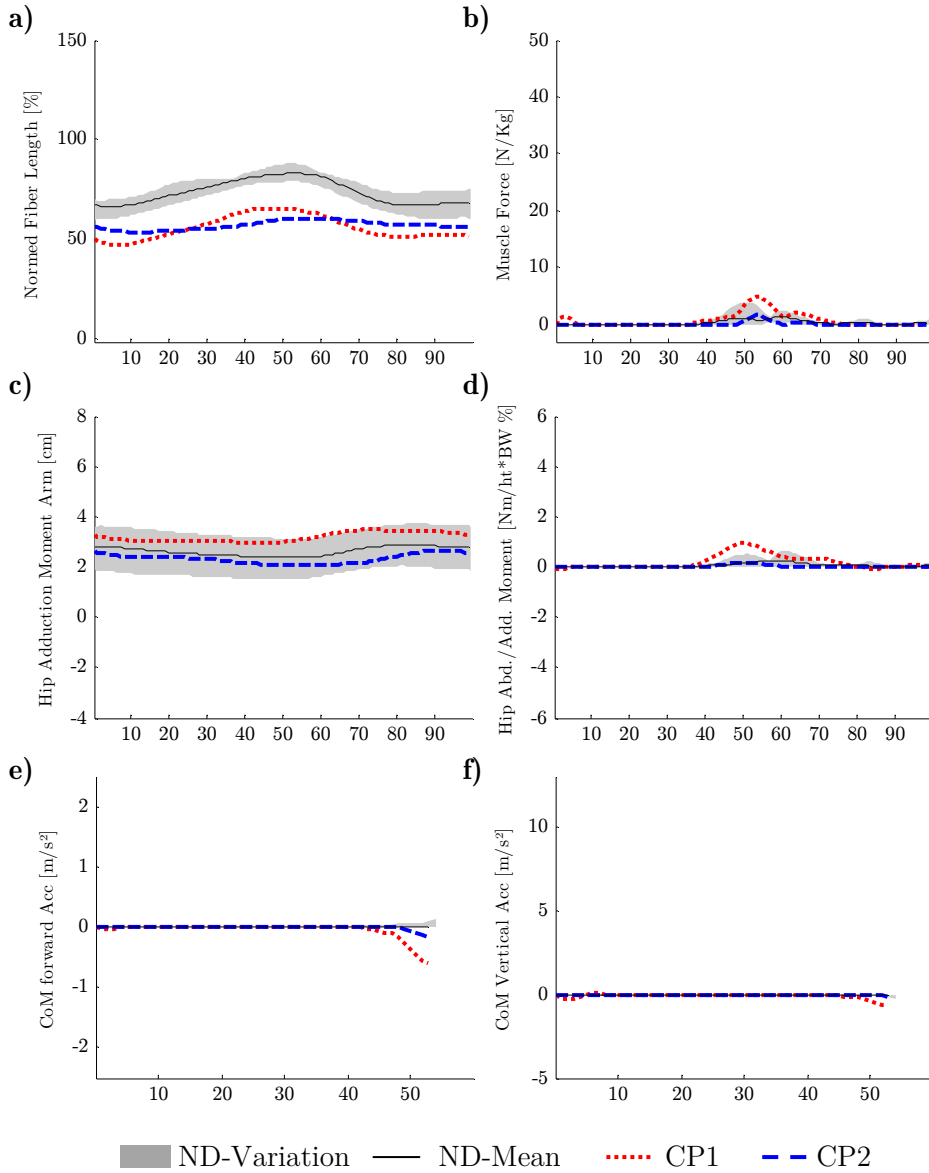
Figure B.2.14 Pectinius in gait - Normalized muscle fibre length (a), muscle force per kg body weight (b), moment arm and normalized joint moment for ankle joint (c,d) in a full gait cycle as well as contribution to fore-aft (e) and vertical (f) acceleration of the centre of mass of the CP-children (CP1,CP2) and the control group (ND) in stance phase.
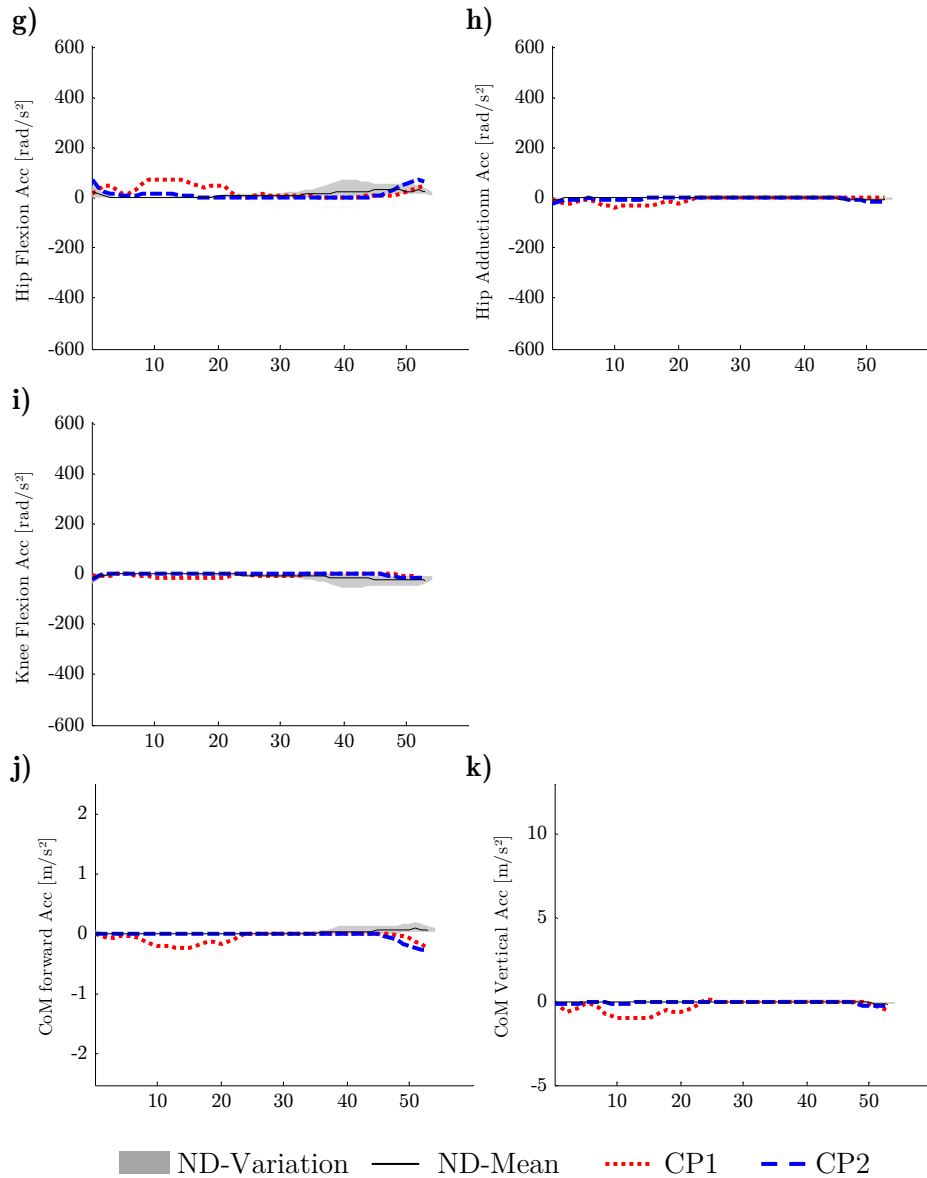
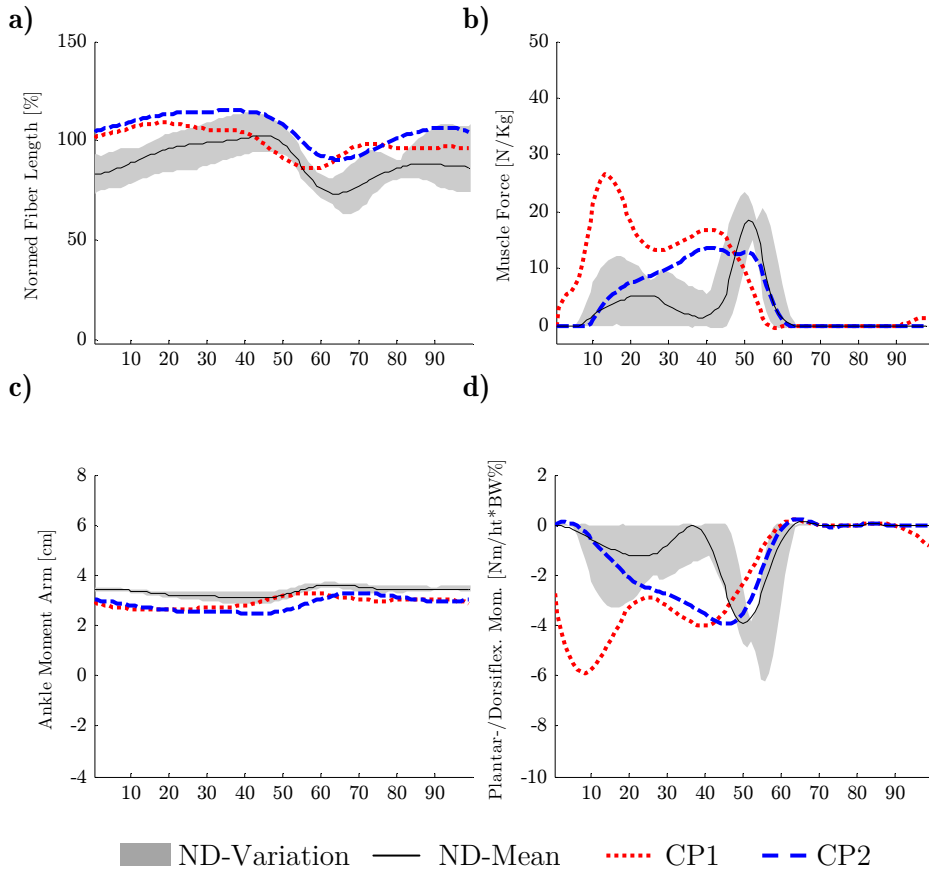## B.2.16   Piriformis in Gait

Figure B.2.15 Piriformis: Function in gait - Normalized muscle fibre length (a), muscle force per kg body weight (b) as well as moment arm and normalized joint moment for hip adduction (c,d) and hip flexion (e,f) of the CP-children (CP1,CP2) and the control group (ND) in a full gait cycle.
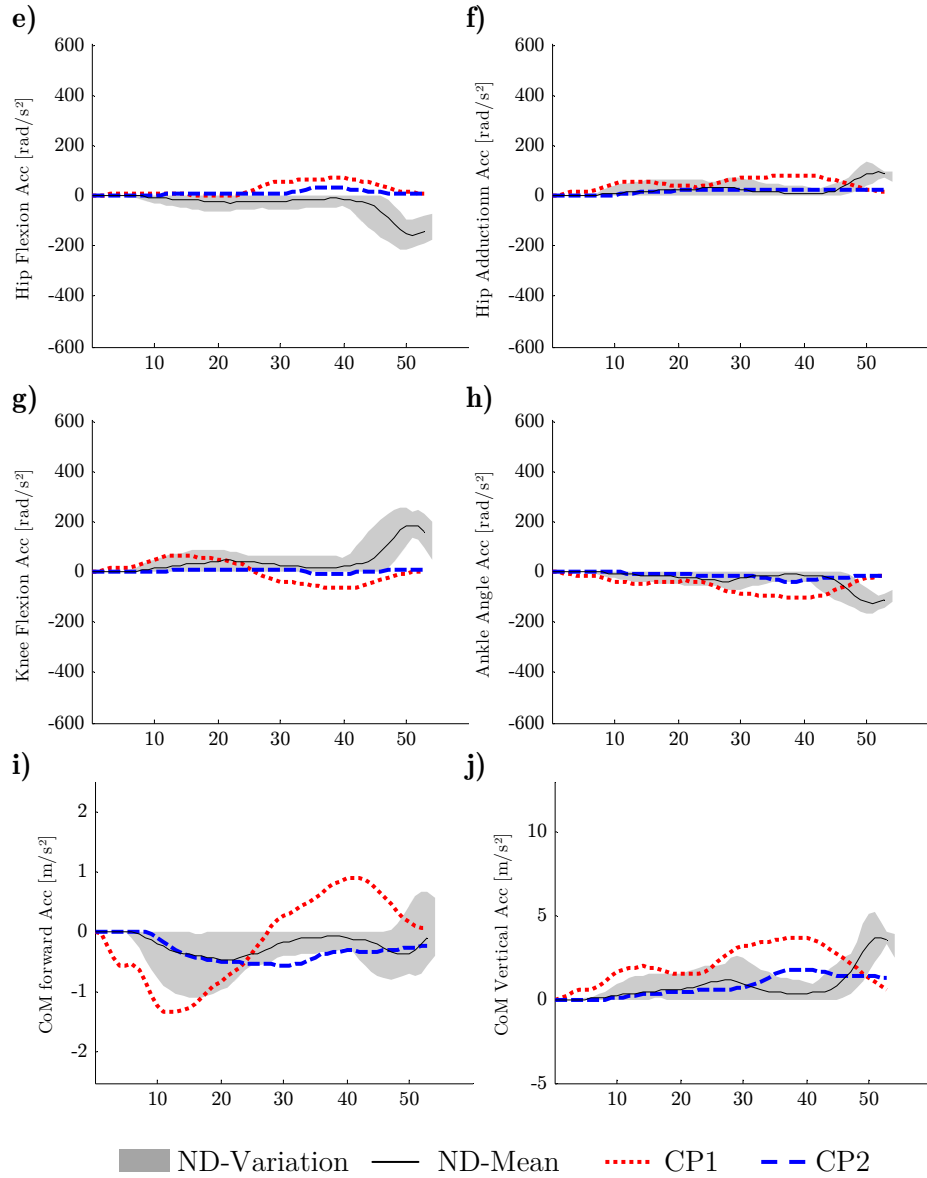
Figure B.2.16 Piriformis: Accelerations in gait - Contribution to hip (g,h) and knee (i) angular acceleration as well as fore-aft (j) and vertical (k) acceleration of the centre of mass (CoM) in the CP-children (CP1,CP2) and the control group (ND) in stance phase.

B.2.17 Rectus Femoris in Gait
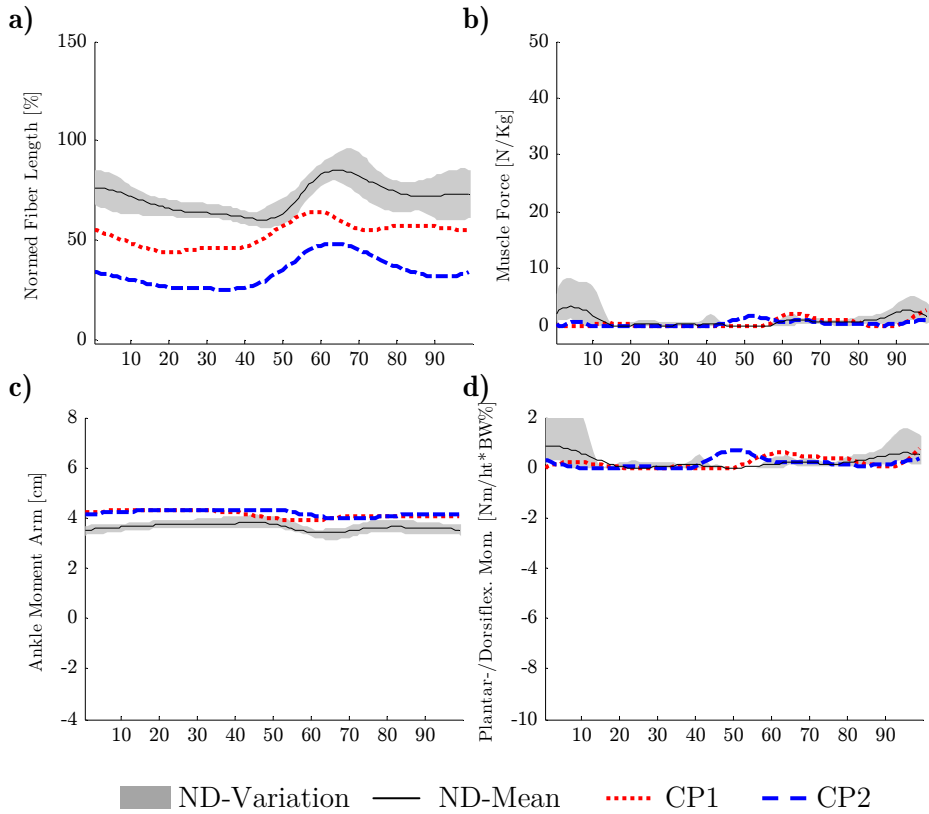

Figure B.2.17 Rectus femoris: Function in gait - Normalized muscle fibre length (a), muscle force per kg body weight (b) as well as moment arm and normalized joint moment for knee flexion/extension (c,d) and hip flexion/extension (e,f) of the CP-children (CP1,CP2) and the control group (ND) in a full gait cycle.
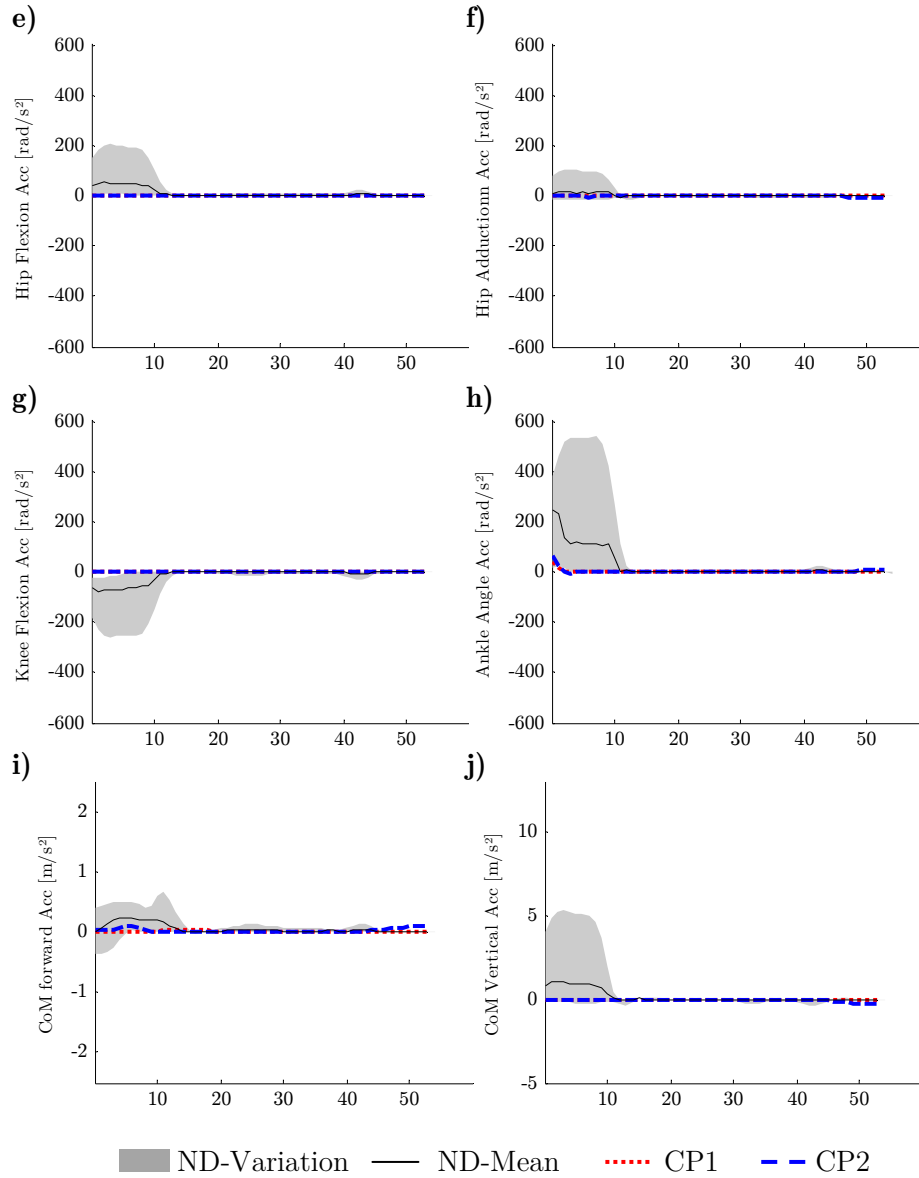
Figure B.2.18 Rectus femoris: Accelerations in gait - Contribution to hip (g,h), knee (i) and ankle joint (j) angular acceleration as well as fore-aft (k) and vertical (l) acceleration of the centre of mass (CoM) in the CP-children (CP1,CP2) and the control group (ND) in stance phase.

B.2.18 Sartorius in Gait

Figure B.2.19 Sartorius: Function in gait - Normalized muscle fibre length (a), muscle force per kg body weight (b) as well as moment arm and normalized joint moment for knee flexion/extension (c,d) and hip flexion/extension (e,f) of the CP-children (CP1,CP2) and the control group (ND) in a full gait cycle.

Figure B.2.20 Sartorius: Accelerations in gait - Contribution to hip (g,h) and knee (i) angular acceleration as well as fore-aft (j) and vertical (k) acceleration of the centre of mass (CoM) in the CP-children (CP1,CP2) and the control group (ND) in stance phase.
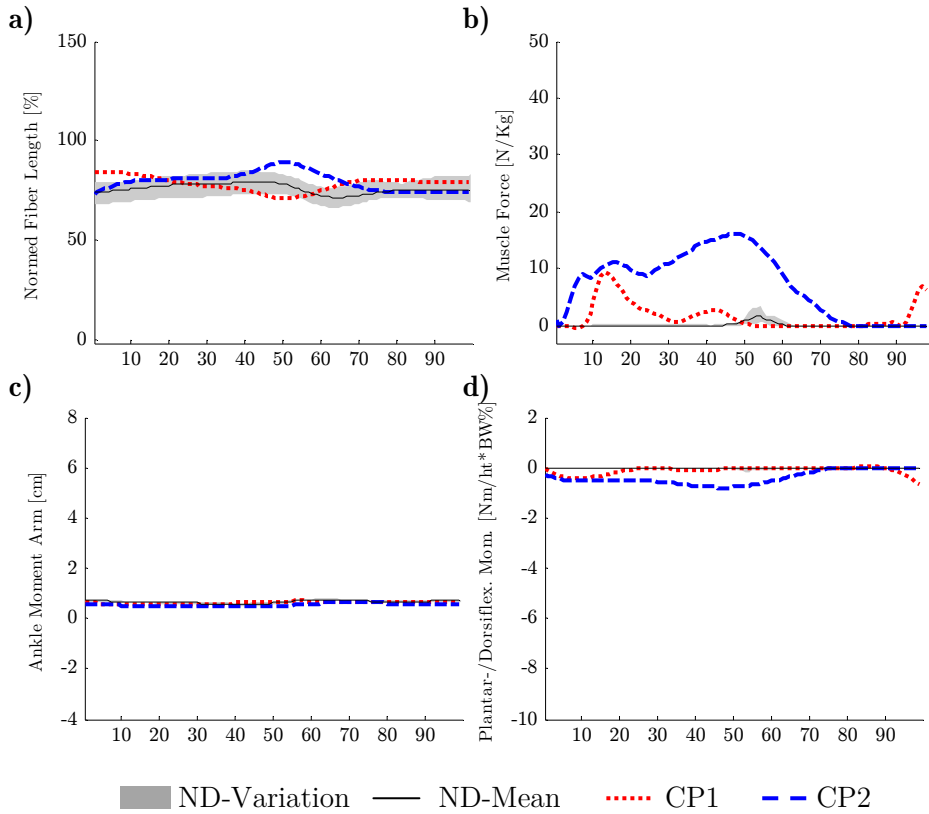
B.2.19   Soleus in Gait

Figure B.2.21 Soleus: Function in gait - Normalized muscle fibre length (a), muscle force per kg body weight (b) as well as moment arm and normalized joint moment for ankle joint (c,d) of the CP-children (CP1,CP2) and the control group (ND) in a full gait cycle.
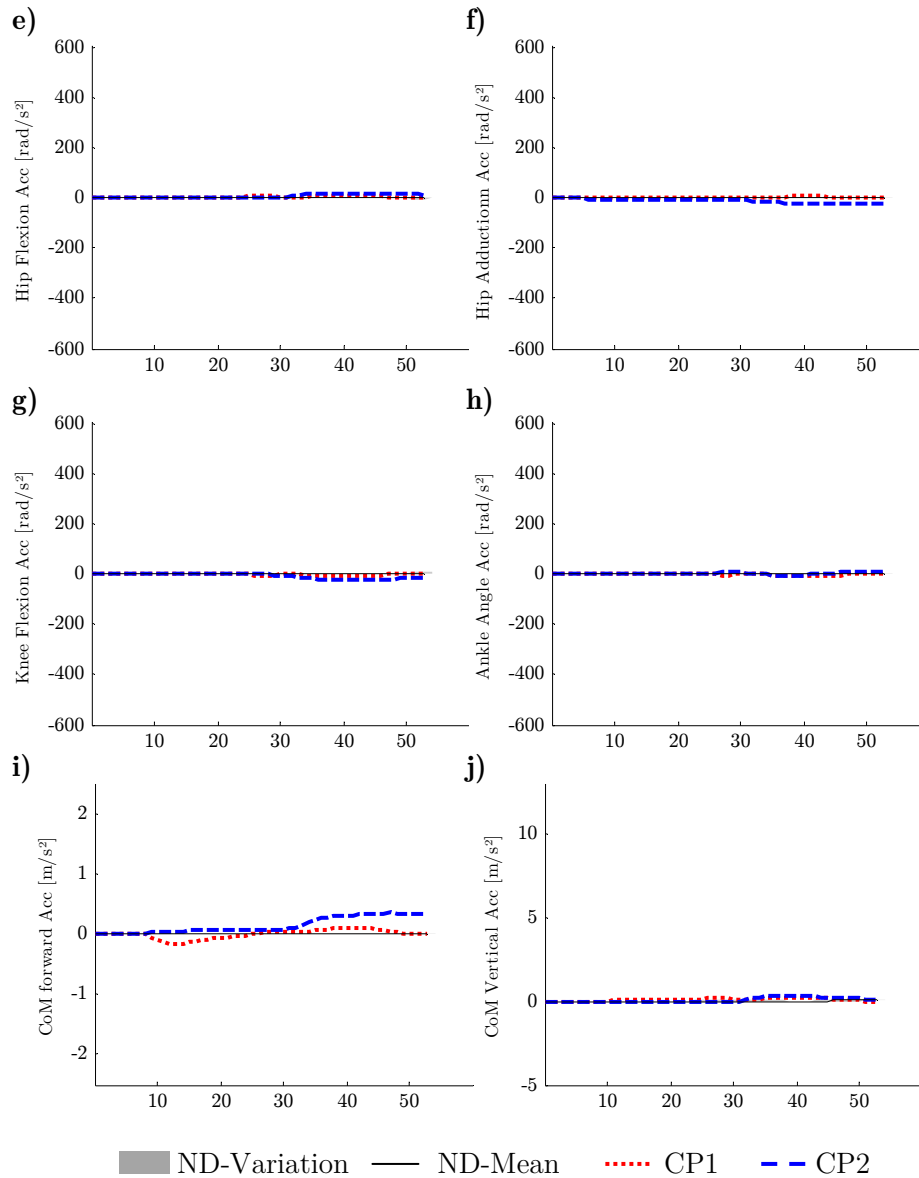
Figure B.2.22 Soleus: Accelerations in gait - Contribution to hip (e,f), knee (g) and ankle joint (h) angular acceleration as well as fore-aft (i) and vertical (j) acceleration of the centre of mass (CoM) in the CP-children (CP1,CP2) and the control group (ND) in stance phase

B.2.20 Tibialis anterior in Gait

Figure B.2.23 Tibialis anterior: Function in gait - Normalized muscle fibre length (a), muscle force per kg body weight (b) as well as moment arm and normalized joint moment for ankle joint (c,d) of the CP-children (CP1,CP2) and the control group (ND) in a full gait cycle.
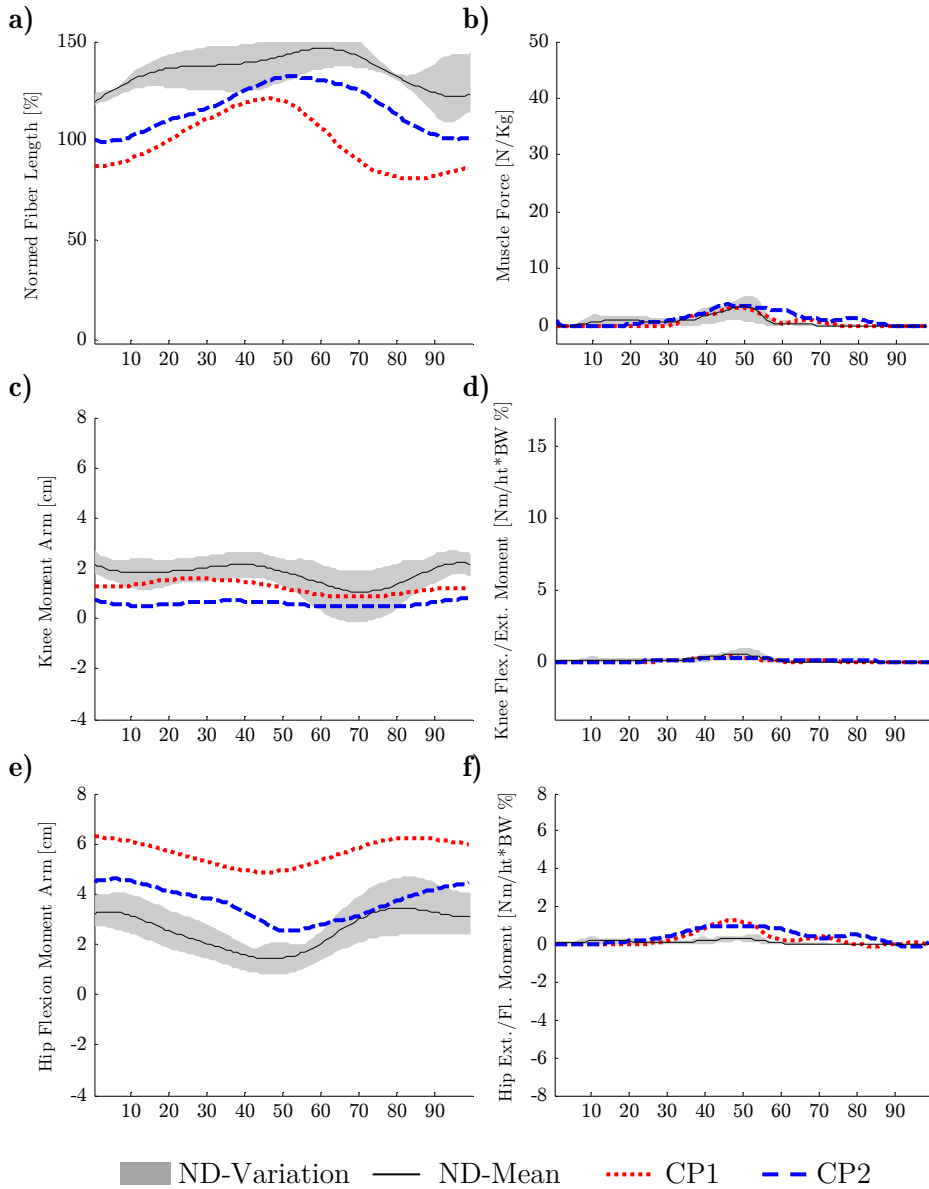
Figure B.2.24 Tibialis anterior: Accelerations in gait - Contribution to hip (e,f), knee (g) and ankle joint (h) angular acceleration as well as fore-aft (i) and vertical (j) acceleration of the centre of mass (CoM) in the CP-children (CP1,CP2) and the control group (ND) in stance phase.

B.2.21 Tibialis posterior in Gait

Figure B.2.25 Tibialis posterior: Function in gait - Normalized muscle fibre length (a), muscle force per kg body weight (b) as well as moment arm and normalized joint moment for ankle joint (c,d) of the CP-children (CP1,CP2) and the control group (ND) in a full gait cycle.

Figure B.2.26 Tibialis anterior: Accelerations in gait - Contribution to hip (e,f), knee (g) and ankle joint (h) angular acceleration as well as fore-aft (i) and vertical (j) acceleration of the centre of mass (CoM) in the CP-children (CP1,CP2) and the control group (ND) in stance phase.
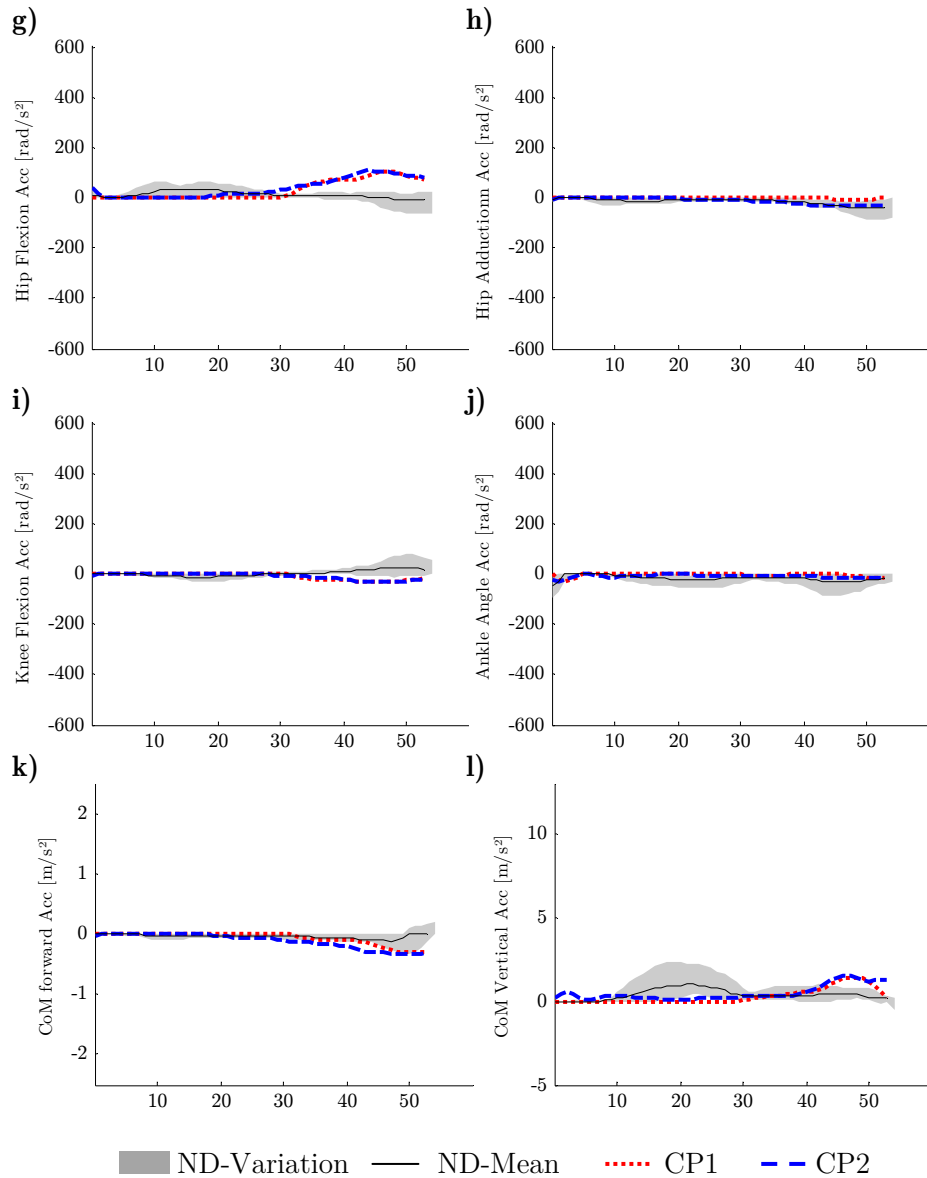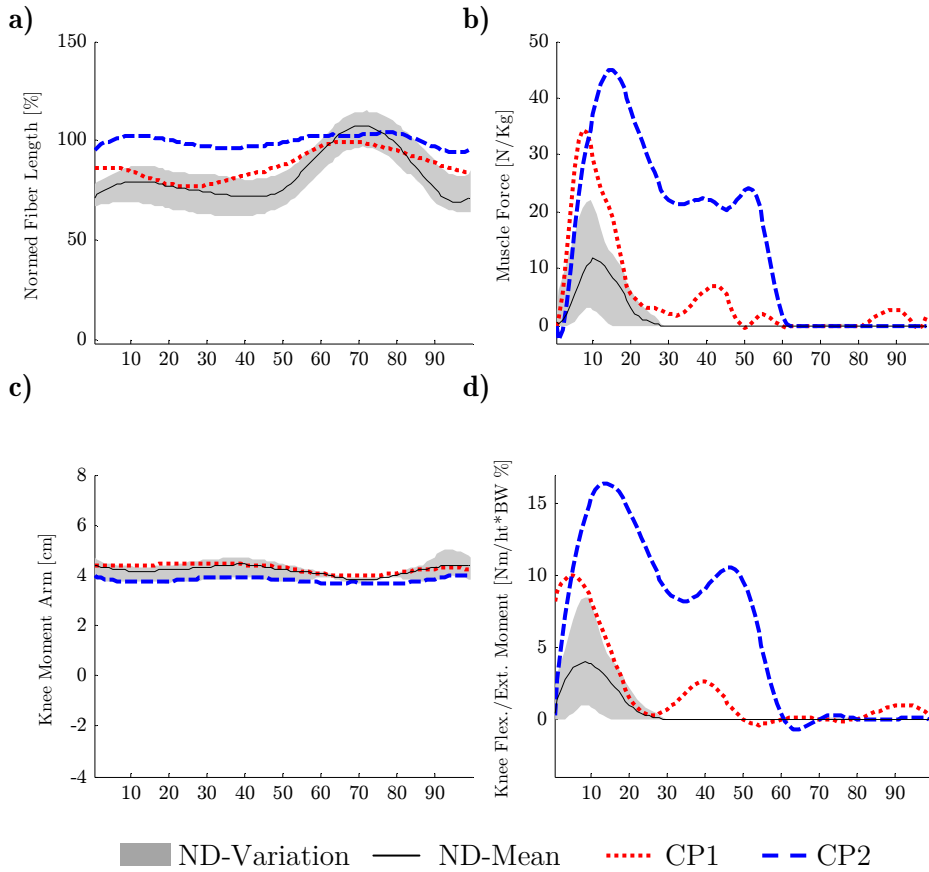
B.2.22 Tensor fasciae latae in Gait

Figure B.2.27 Tensor fasciae latae: Function in gait - Normalized muscle fibre length (a), muscle force per kg body weight (b) as well as moment arm and normalized joint moment for knee flexion/extension (c,d) and hip flexion/extension (e,f) of the CP-children (CP1,CP2) and the control group (ND) in a full gait cycle.
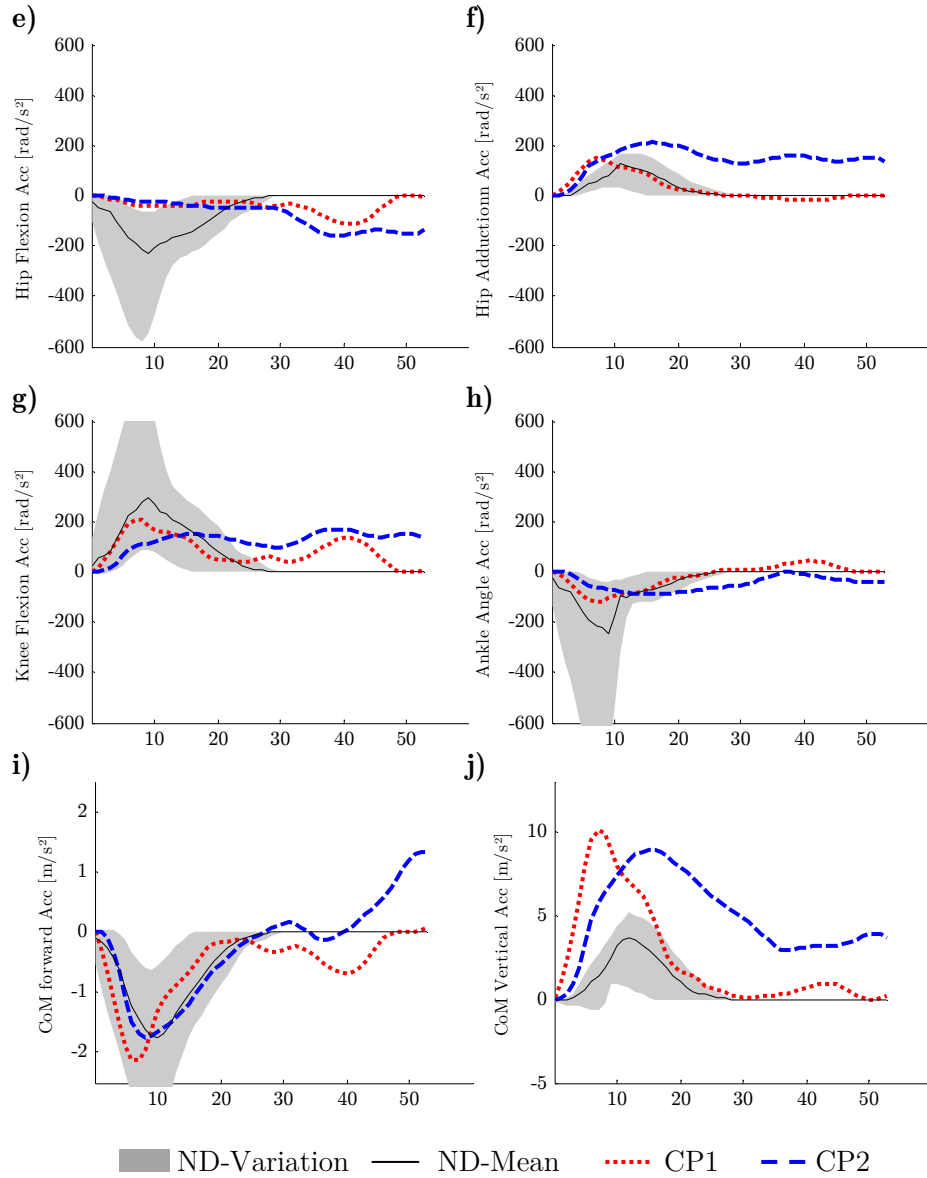
Figure B.2.28 Tensor fasciae latae: Accelerations in gait - Contribution to hip (g,h), knee (i) and ankle joint (j) angular acceleration as well as fore-aft (k) and vertical (l) acceleration of the centre of mass (CoM) in the CP-children (CP1,CP2) and the control group (ND) in stance phase.

B.2.23   Vastus in Gait

a)

b)

c)

d)

Figure B.2.29 Vastus: Function in gait - Normalized muscle fibre length (a), muscle force per kg body weight (b) as well as moment arm and normalized joint moment for knee joint (c,d) of the CP-children (CP1,CP2) and the control group (ND) in a full gait cycle.
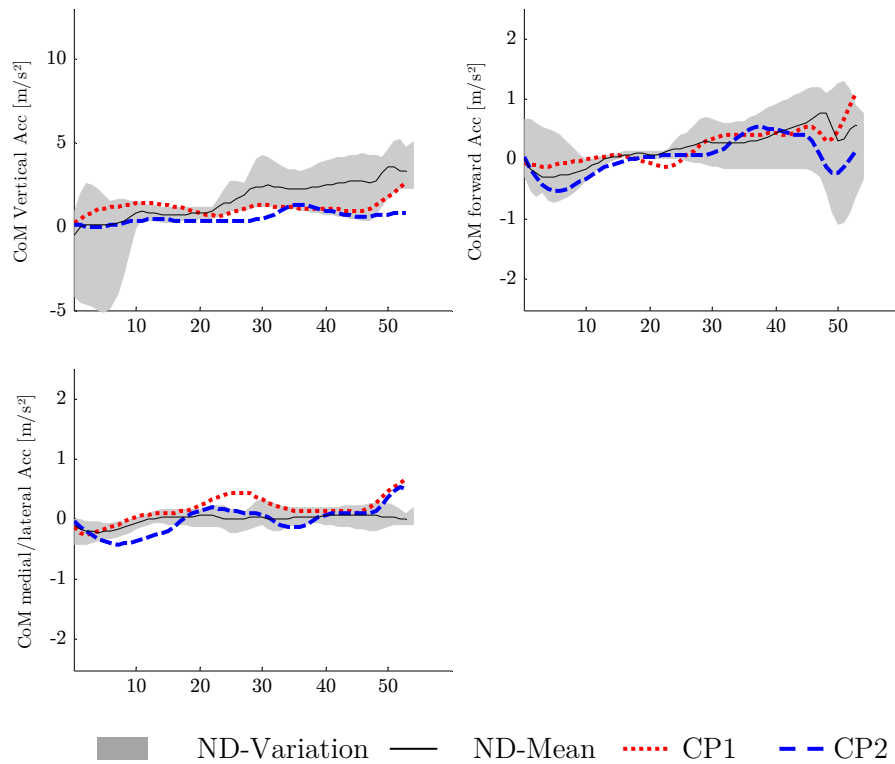
Figure B.2.30 Vastus: Accelerations in gait - Contribution to hip (e,f), knee (g) and ankle joint (h) angular acceleration as well as fore-aft (i) and vertical (j) acceleration of the centre of mass (CoM) in the CP-children (CP1,CP2) and the control group (ND) in stance phase

B.3 Additional Accelerators in Gait

B.3.1 Contribution of inertia on CoM accelerations

Figure B.3.1 Inertia: Accelerations in gait - Contribution to hip (e,f), knee (g) and ankle joint (h) angular acceleration as well as fore-aft (i) and vertical (j) acceleration of the centre of mass (CoM) in the CP-children (CP1,CP2) and the control group (ND) in stance phase